Volcanic Perturbations of Stratospheric Ozone in Contemporary and Future Atmospheres

HARVARD UNIVERSITY
Graduate School of Arts and Sciences

DISSERTATION ACCEPTANCE CERTIFICATE

The undersigned, appointed by the

Department of Chemistry & Chemical Biology

have examined a dissertation entitled:

Volcanic Perturbations of Stratospheric Ozone in Contemporary and Future Atmospheres

presented by : J. Eric Klobas

candidate for the degree of Doctor of Philosophy and hereby certify that it is worthy of acceptance.

Signature _____
Typed name: Professor James G. Anderson

Signature _____
Typed name: Professor Steven C. Wofsy

Signature _____
Typed name: Professor Frank N. Keutsch

Date: 25 April 2018

Volcanic Perturbations of Stratospheric Ozone in Contemporary and Future Atmospheres

A DISSERTATION PRESENTED
BY
J. ERIC KLOBAS
TO
THE DEPARTMENT OF CHEMISTRY AND CHEMICAL BIOLOGY

IN PARTIAL FULFILLMENT OF THE REQUIREMENTS
FOR THE DEGREE OF
DOCTOR OF PHILOSOPHY
IN THE SUBJECT OF
CHEMICAL PHYSICS

HARVARD UNIVERSITY
CAMBRIDGE, MASSACHUSETTS
APRIL 2018

Thesis advisor: Professor James G. Anderson J. Eric Klobas

Volcanic Perturbations of Stratospheric Ozone in Contemporary and Future Atmospheres

Abstract

Volcanic eruption columns possess the potential to transport great quantities of reactive gases to the stratosphere where they might subsequently interact with ozone. While explosive volcanic eruptions currently increase rates of ozone-loss catalysis due to an enhancement in the availability of reactive chlorine following the stratospheric injection of sulfur, future eruptions are expected to enhance total column ozone as halogen loading approaches pre-industrial levels.

In this thesis, the sensitivity of the ozone layer to future Pinatubo-like volcanic eruptions is explored in the context of the Representative Concentration Pathway (RCP) greenhouse gas emission trajectories. Heterogeneous chemical effects following large eruptions are evaluated in a variety of future atmospheres spanning contemporary times to the year 2100. Differences between the models become evident following an analysis of vertical profile response and total column response. Sensitivity studies are performed to evaluate the effect of stratospheric temperature, methane burden, and hemispheric mass loading.

A predictive random forest regression model is developed and employed to account for the difference between prescribed RCP and World Meteorological Organization (WMO) halocarbon decay rates. While the ozone layer is found to be more sensitive to volcanic perturbation under WMO

halocarbon trajectories, the difference between WMO and RCP scenarios is not extreme and does not represent a modal shift in behavior for any of the RCP storylines.

Heterogeneous chemical processing is found to produce net ozone depletions until the 2070's for all RCP scenarios, and significant depletions of greater than 1 % ozone loss until the 2060's. These dates occur later than prior estimates due to the inclusion of 4 pptv bromine from short-lived bromocarbons in the chemical model. Using the WMO EESC correction, slight ozone losses are observed following eruptions until the end of the century, though in some cases these losses are smaller than expected ozone contributions from radiative-dynamical causes.

Additionally, tremendous quantities of volcanic halogens are occasionally transported to the stratosphere in the eruption column of a large, explosive volcanic eruption. Volcanic co-injections of sulfur dioxide and hydrogen chloride are evaluated for simulated Pinatubo-scale eruptions with HCl:SO_2 molar ratios corresponding to recent MLS results and the ice core record. Halogen-rich eruptions produce global ozone depletion regardless of the halogen background from long-lived anthropogenic halocarbons. In cases of more severe halogen partitioning, 9-year global average losses exceed 8% with more extreme zonal losses predicted over a shorter time horizon. Additionally, it is demonstrated that perturbations of stratospheric ozone by halogen-rich eruptions have significantly longer lifetimes than perturbations of ozone by Pinatubo-like eruptions due to differential decay trajectories of volcanic SO_2 and HCl. The stratospheric ozone response to co-injections of HCl with SO_2 is shown to scale non-linearly in comparison to individual injections of each component.

Contents

Listing of figures

Listing of tables

To my teachers

Acknowledgments

Second chances have defined the different phases of my life so far. Most individuals on this planet aren't afforded the luxury of doing "it" again, whatever "it" may be; "It" in my case has taken on many forms and I want to thank those individuals who have facilitated my second chances or otherwise took risks which contributed to my personal and technical development– those who inexplicably decided to hire teenage me as a chemist in the quality control laboratory at ALZA Corporation, those who supported me when I left ALZA to enroll in college for the first time at the age of 25, and those who assisted me in completely switching my research discipline in the middle of my graduate studies. I will always be deeply indebted to you.

I want to explicitly acknowledge my scientific mentors and tutors, Professor Jim Anderson, Dr. David Wilmouth, Dr. Martin Schmid, Dr. Till Cremer, Professor Sergey Nizkorodov, and Professor Barbara Finlayson-Pitts – who have all contributed to my professional development through consultation and/or training. From each of you, in different ways, I have learned how to ask and answer questions.

My time at Harvard was metered by the weekly meetings of ASAASA, a scientific journal club. I want to thank everyone involved in its production – especially Noam Prywes, Anders Sejr Hansen, and James Kath. Additionally, I acknowledge my former housemates at Nashton Estate and the

extended community for providing a dynamic environment: Eli Cohen, Molly Klaisner, Miriam Huntley, Dougal MacLaurin, Melissa Lefkowitz, Chris Rondinelli, among notable others. Greg Boursalian – our weekly backgammon sessions were invaluable. Guglielmo Lockhart – for the weekly standing bar hours. Thanks to Andrei Levin, Tamas Szalay, Jarrod McClean, and Reem Hannun. Thanks to my colleagues, Jordan Wilkerson, Jessica Smith, David Sayres, Debra Weisenstein, and Corey Clapp. Acknowledgements to the barbeque crew for making CCB great again – especially the weekly standard-bearers – Cédric Barroo, Matthijs van Spronsen, Andrew Crampton, Christopher O'Connor, and Christian Reese, among others. Special appreciation to Fanny Hiebel for keeping me sane and well-fed.

I hope to make many more mistakes necessitating second-chances, as there is no joy to be found in improvement if an individual does not err.

Winning does not tempt that man.

This is how he grows:

by being defeated, decisively

by constantly greater beings

Ranier Maria Rilke, 1906

0

Introduction

The stratospheric ozone layer exists as an abstraction for most, manifesting itself in thought only in relation to its absence in the Antarctic springtime. Though the ozone layer serves as an essential shield of ultraviolet radiation for surface life, due to its apparent permanence and distance from the surface those living beneath the stratospheric ozone layer's screen may easily forget it even exists. It is only when the ozone layer is perturbed that the general public takes notice.

Thankfully – by virtue of its nonproximity to the surface, the extreme coincidence of properties of fluid mechanics and photochemistry, and the oxidizing power of the troposphere – the stratospheric ozone layer is remarkably robust to perturbation; however, as will be discussed in the following chapters, the ozone layer is not immune to perturbation. Deterministic factors dictating the steady-state balance between ozone production and ozone loss are changing as a result of the anthropogenic emission of greenhouse gases. As the troposphere is expected to warm, so too is the stratosphere expected to cool – and the ozone layer is projected to thicken in the middle stratosphere resultantly. Simultaneously, long-lived halocarbons released in massive quantities to the atmosphere during the 20th century will continue to perturb ozone chemistry throughout the remainder of the 21st century during their slow decay, though to an ever-lessening extent.

Upon this changing background, factors related to the emission, transport, and chemical fate of trace gases are predicted to vary. Very short-lived halocarbons, discussed in chapter 5, are projected to partition to the stratosphere with greater efficacy due to enhanced chemical lifetimes and convection under certain climate change scenarios[1] – and in greater quantity as marine sources proliferate.[2–4] Also changing are the efficiency of the chemical cycles contributing to the steady state of the ozone layer. Bimolecular ozone-destroying reaction rates are expected to decline with stratospheric temperatures while heterogeneous processing rates accelerate. Increased inventories of stratospheric water due to warming of the tropical tropopause[5,6], enhanced convection[7,8], and increasing troposphere-stratosphere exchange[1,9,10] may significantly perturb stratospheric ozone via chemical processes discussed in chapter 1.

The Intersectionality of Climate Change and Stratospheric Ozone

Clearly, changes to the stratospheric ozone layer and the Earth's climate are not orthogonal. Radiative feedbacks from changes in ozone may dictate changes in climate patterns, chemical feedbacks resultant from changes in radiative forcing from greenhouse gases dictate changes in stratospheric ozone inventories, and elective feedbacks – measures enacted by humans to mitigate symptoms of the changing climate – may perturb both the thermal and chemical structure of the atmosphere. These feedbacks may manifest in profound ways. For example, the abrupt 17.7 kya southern hemispheric deglaciation is postulated to have been caused by large-scale perturbations in atmospheric circulation triggered by long-lasting halogen-catalyzed ozone depletion of volcanic origin.[11] As discussed in chapter 4, climate trajectories demonstrate that future stratospheric ozone layers are likely to be very different in vertical profile than the preindustrial stratospheric ozone layer, resulting in an ozone "super-recovery" as anthropogenic halocarbons decay.[12,13] Meanwhile, as detailed in chapter 7, human interventions in the changing climate – such as the deliberate seeding of the stratosphere with short-wave scattering aerosols – may both catalyze the chemical conversion of inactive trace gas reservoirs to their ozone-destroying form and boost the rates of ozone loss processing via radiative heating of their immediate environment.

A primary concern lies in the possibility of an irreversible transition in the climate state resulting in a loss of the equator-to-pole temperature gradient as a consequence of greenhouse gas forcing. A shift toward a climate monopole is predicted to have far-reaching effects on both stratospheric chemistry and dynamics and would perhaps resemble the dominant climate state during the Eocene

period, 40 million years ago.[14] This is notable for countless reasons including: (a) during this period, all landmasses and oceans were free of permanent ice, (b) the stratosphere was likely far more moist than it is today. For reasons discussed in section 1.7 and section 7.2.1, a moister stratosphere is likely to perturb the steady-state solution of coupled chemical reactions and dynamical factors that dictates the spatio-temporal distribution of the ozone layer.[15–17]

The Importance of the Ozone Layer

The stratospheric ozone layer has existed in some form since the emergence of the oxidizing atmosphere 2.3 billion years ago, its origin a consequence of metabolism.[19] Because column ozone density grows nonlinearly with molecular oxygen concentration, the surface of the Earth was likely screened from UV radiation nearly as soon as molecular oxygen first appeared.[20]

The top-of-the-atmosphere solar spectrum, illustrated in figure 1 (blue trace), extends from the vacuum ultraviolet to the near infrared, maximizing near 500 nm. The same spectrum recorded at the surface of the Earth (red trace: figure 1) spans a shorter wavelength range, with significant intensity from the near-ultraviolet to the near-infrared. Between the top of the atmosphere and the surface of the Earth lies the stratospheric ozone layer, which is responsible for the majority of the difference between these two spectra. The absorbance spectrum of ozone, traced in black in figure 1, manifests as a broad continuum maximizing at 253 nm in the ultraviolet.

This wavelength spectrum coincidentally aligns with the regions of maximum DNA-base absorbance (230 – 260 nm)[21], and the exposure of an organism to this radiation is directly correlated

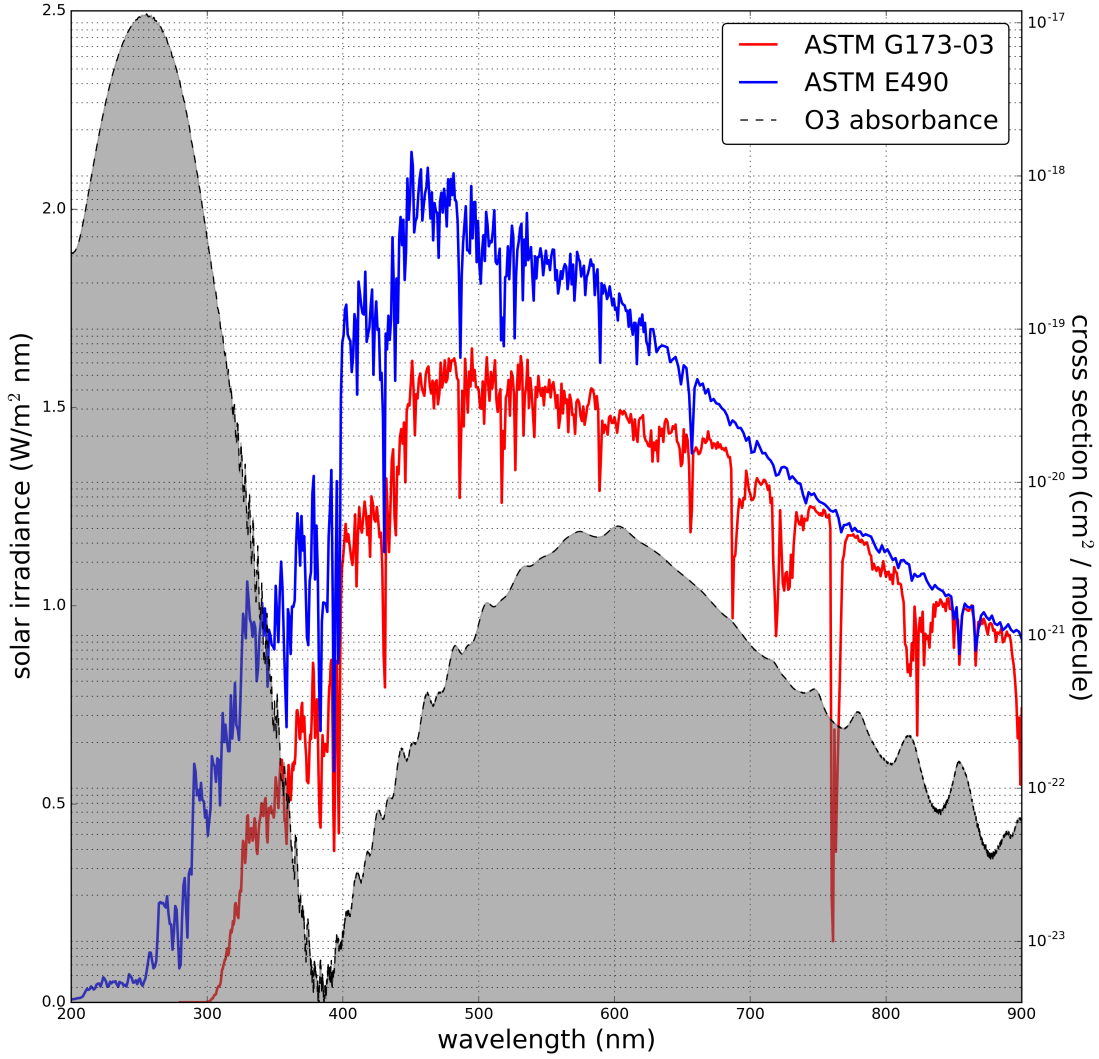

Figure 1: Left axis – blue: the solar spectrum recorded at the top of the atmosphere, ASTM standard E490, as a function of wavelength. red: insolation as recorded at sea level, ASTM standard G173-03, as a function of wavelength. Right axis – black (shaded): the absorbance cross section of the ozone molecule as a function of wavelength (log scale). Ozone cross sections from Serdyuchenko et al. (2014). [18]

with the development of erythema (sunburn), melanomas, and other cancers.[22,23] Perhaps less familiar are the ecological consequences of enhanced surface ultraviolet radiation: the lethality of UVB radition to plants doubles following a fifty percent reduction in column ozone.[24] Stratospheric ozone thus provides the essential screening of ultraviolet radiation to allow for the existence of surface life on Earth.

Ozone Response to External Forcing in a Changing Atmosphere

A variety of natural and anthropogenic phenomena may induce changes in the spatiotemporal distribution of ozone. As the climate and the stratospheric trace gas burden evolve, the nature of the response of the ozone layer to such phenomena is likely to evolve as well. The external forcing may take the form of frequent, small perturbations – for example, accelerations in ozone loss caused by emissions from a booming privatized space launch market[25] – extremely rare stratospheric catastrophes – such as the injection of massive quantities of water, chlorine, bromine, and nitrogen into the stratosphere following the impact of a 250 m asteroid into the ocean (a 25,000 year event, refer to chapter 7)[26] – or something in-between the two scenarios in recurrence frequency and severity – such as large, explosive volcanism.

The interaction between the stratospheric ozone layer and large, explosive volcanic eruptions provides a highly interesting system to study because the modality of stratospheric ozone response is expected to change as the atmosphere evolves throughout the 21st century. Though the eruption of Mount Pinatubo was demonstrated to cause ozone depletion, it is believed that chemical reac-

tions occuring on volcanic sulfate aerosols following future volcanic eruptions will result in an increase in the thickness of the ozone layer. The date at which the ozone response mode switches from depletion to accretion is highly unconstrained, with predictions ranging between the years 2015 – 2050.[27–29] These eruptions occur frequently – there exists a 20% chance of a Pinatubo-sized eruption during any given decade[30] – so it is imperative to constrain expected levels of ozone response and provide hazard response authorities with an adequate assessment of the associated risks.

Structure of the Thesis

In the following chapters, I shall discuss how stratospheric ozone can be disturbed with a focus on explosive volcanism. This thesis is composed of two parts. The first portion, comprising chapters 1 – 4, provides the essential background required to approach this interdisciplinary topic:

- In chapter 1, I will describe the thermal structure of the natural atmosphere, the major circulation patterns of air in the troposphere and stratosphere, and the primary chemical reactions governing the production and loss of ozone. In combination these properties dictate the spatiotemporal distribution of the ozone layer.
- Changes in the burden of stratospheric aerosols produce outsized responses in stratospheric chemistry and transport. Chapter 2 discusses the origin of stratospheric aerosols, their chemical properties, and how they perturb the ozone steady-state as discussed in chapter 1.
- The character and quantity of gases emitted during a volcanic eruption have a complex origin. Moreover, volcanic eruptions exhibit great variation in the composition of emitted volcanic gases. In chapter 3, I outline the chemical and physical processes influencing the evolution of volcanic gases from the magma reservoir, past the crater rim, and to the umbrella cloud.
- It is a common belief that the phenomena of ozone layer depletion and climate change are noncovariate. In fact, the complex chemical reactions governing the production and loss rates of stratospheric ozone are highly dependent on the physical state of the stratosphere and

the physical state of the stratosphere is influenced by the presence of the ozone layer. Along with this feedback, projections of future climates and emissions of greenhouse gases will be described in chapter 4.

The second half of this work consists of case studies from my research. These case studies will synthesize concepts from each of the first four chapters as new conclusions are developed. Two case studies and a broad-reaching literature review will be presented, concluding with a discussion on directly-related follow-up work:

- Consensus indicates that future large volcanic eruptions will enhance, rather than deplete the thickness of the ozone layer; however, the date at which such a shift in the mode of ozone layer response to volcanic perturbation will occur is uncertain. Additionally, when the stratospheric burden of anthropogenic halogen emissions has returned to its preindustrial level, small changes in the mixing ratio of very short-lived bromocarbons will dictate whether or not the net ozone layer response to a volcanic eruption is one of increasing or decreasing thickness. In chapter 5, I outline similarities and differences in longitudinal ozone response to explosive volcanism in four different climate futures, exploring the different parameters which govern ozone sensitivity.
- An emerging consensus of evidence indicates that some explosive volcanic eruptions inject not only sulfur dioxide, but also inorganic halogen gases, to the stratosphere. In chapter 6, I outline the state of the art, and present model simulations of the impact of such an eruption on the stratospheric ozone layer.
- There exist many natural and anthropogenic scenarios by which the ozone layer may be perturbed (e.g., asteroid impact, various geoengineering schema, solar flares, etc.). I present a literature review on these other, non-volcanic mechanisms in chapter 7.
- The scenarios presented in chapters 5 and 6 are highly specific to the tropical eruption. The characteristics of extratropical and subpolar volcanic eruption aerosol clouds vary greatly. In addition to exploring how eruption latitude may modulate climate and ozone response, I discuss the necessity for further study of volcanic clouds containing multiple halogen species in chapter 8.

Quantitative Hedges on Prognostications of Stratospheric Ozone Response to External Perturbation

It is important to mention that contemporary climate models do not yet reliably reproduce synoptic changes in stratosphere-tropopause exchange dynamics and long-term forecasts of the stratospheric response of trace gas species to perturbation in such future climate systems are poorly constrained. I do not even attempt to address this deficiency in this thesis, instead I focus on changes in the rates of heterogeneous processing of halogen reservoir species following a volcanic eruption in various parameterizations of future climate and chemical states within a chemical transport model with prognostic aerosol evolution. The conclusions presented should be considered with this in mind: a far more comprehensive understanding of stratosphere-tropopause exchange (including constraints on the frequency and intensity of convective transport of troposheric moisture and halogenated compounds) must be included for a quantitative depiction of ozone response to external pertubation. Additionally, as discussed in chapter 4, the climate system currently exists in a state of instability with regard to climate-related stratospheric ozone loss and production. Though many excellent groups are currently dissecting this problem (e.g. Austin and Wilson, 2006[31]; Waugh et al., 2009[13]; and Li et al., 2009[12], among others), the model employed in this thesis work cannot predict changes from radiative-dynamical factors as a result of greenhouse forcing: all predicted deviations of ozone following volcanic perturbation only reflect changes in the heterogeneous processing rate of halogen reservoir species as a result of varying, prescribed thermal and chemical conditions.

Prognostications of the future are inevitably bounded by error, and the bounds of this error tend

to increase nonlinearly with amplification of the complexity of the modeled system. This thesis does not purport to predict the ozone response to any particular future volcanic eruption, in time or space. In fact, as discussed in chapters 6, 7, and 8, an extraordinarily dynamic range of stratospheric injection efficiency for volcanic halogen species has been reconstructed from the paleorecord and the factors controlling this are poorly understood. Though declining stratospheric halogens as a result of the eminently successful Montreal Protocol (and subsequent amendments) are a near-certainty – barring some sort of global industrial-political calamity, future changes in the transport and oxidation of very-short lived halogenated substances from the marine and continental boundary layer are extremely uncertain and may produce significant structural variation in the vertical distribution and thickness of the ozone layer. Again, this work did not attempt to address these uncertainties beyond a simple investigation of short-lived bromine compounds.

That said, the conclusions presented in the following were produced from over 300 carefully constructed experiments and provide the first quantitative examination of how halogen-rich volcanic eruptions might interact with the climate system in either contemporary or future atmospheres. Though several prior works have examined the sensitivity of the future ozone layer to Pinatubo-like volcanic eruptions, as defined and discussed in chapter 5, this work provides a much-needed update to the literature by exploring such a situation while including the effects of short-lived halocarbons while within the context of the Representative Concentration Pathways emissions scenarios. Finally, it must be noted that future work addressing some of the uncertainties noted above have already been initiated and are discussed in chapter 8.

1

The Natural Atmosphere and Ozone Layer

It seems appropriate that a thesis about perturbations to the atmosphere begin with a discussion on the unperturbed atmosphere. In the following section, I will briefly describe the structure of the atmosphere, its constituent layers, and the key factors governing the transport of air parcels within them. Then, I will outline the spatiotemporal structure of the natural ozone layer, both as a function of latitude and vertical profile. Following this, the key photochemical reactions governing the

production and loss rates will be illustrated for each of the prominent ozone-depleting chemical families. Finally, a short discussion on the relative reactivity of various halogen species will clarify why even small quantities of bromine or iodine may have significant impact on stratospheric ozone.

Structure of the Atmosphere

The Earth's atmosphere is composed of several zones of differing meteorology and chemistry. These are the *planetary boundary layer*, the *troposphere*, the *stratosphere*, the *mesosphere*, the *thermosphere*, and the *exosphere*. Though the pressures, temperatures, and chemical composition of each region are unique, their boundaries can be defined by a single convenient metric, the *lapse rate*. While the majority of the topics and processes discussed in this thesis are stratospheric phenomena, a brief description of the structure of the entire atmosphere follows.

The Barometric Equation, Lapse Rate, Potential Temperature, and Convection

The atmosphere is a fluid layer of gases of decreasing density as altitude increases. At the surface of the Earth, the pressure is on average, 985 hPa. Note that this value differs from the mean sea level pressure of 1013 hPa due to orography – the majority of the Earth's surface is well above sea level. Pressure may be related to altitude by means of the *Barometric Equation* as presented in equation 1.1, where P_0 is the mean sea level pressure, z is vertical distance between the point of measurement and sea level, and H is the *scale height* of the atmosphere. Atmospheric scale height, the distance over which atmospheric pressure decreases by a factor of e, is related in equation 1.2 as a function of k_b, the Boltzmann constant, T, temperature, M, molecular mass, and g, the gravitational constant.

From this, one can deduce that altitude scales with the natural logarithm of atmospheric pressure. Altitude and pressure will be used interchangeably throughout this thesis as the context dictates.

$$P = P_0 \exp^{-\frac{z}{H}} \tag{1.1}$$

$$H = \frac{k_b T}{Mg} \tag{1.2}$$

The lapse rate, Γ, is the measure of the change in air temperature, T, as a function of z, altitude, and in the most general sense is defined per equation 1.3. In the troposphere, the average lapse rate, the *environmental lapse rate*, is about $6.5 \frac{K}{km}$

$$\Gamma = -\frac{dT}{dz} \tag{1.3}$$

The transfer of heat in the troposphere is largely mediated through the process of *convection*. Convection occurs as a result of the adiabatic expansion and contraction of air masses. Warm surface air masses expand, rising and cooling in the process. As they approach the region of neutral bouyancy, they cease to rise. Conversely, cold air masses may contract as a result of nearby expanding hot air masses. These parcels will descend while heating. In any dry air mass, the rate at which a parcel will cool (or heat) as a result of adiabatic processes is given by the *dry adiabatic lapse rate*, equation 1.4, in which g is the constant of gravitational acceleration and C_p is the constant pressure heat capacity of dry air. While it is useful to know the change in the temperature of a parcel as it as-

cends or descends, in order to determine whether or not a parcel will rise a metric that relates the properties of two air masses to one another is needed.

$$\Gamma_d = -\frac{g}{C_p} = -9.81\frac{K}{km} \tag{1.4}$$

It can be shown from the ideal gas law that there is a relation between the ratio of any two pressures and the ratio of their temperatures, as given in equation 1.5. From this relation, a value known as the *potential temperature*, Θ, can be derived, as in equation 1.6. The potential temperature of an air mass indicates whether or not it will rise or sink and in the absence of exchange processes, is a conserved quantity. If the potential temperature decreases with altitude (e.g., actual lapse rate is greater than the dry adiabatic lapse rate), convection is likely to occur, with the mass rising to its bouyancy point.

$$\frac{P_1}{P_0} = \frac{T_1}{T_0}^{\frac{C_p}{R}} \tag{1.5}$$

$$\Theta = T_0 = T_1\frac{P_0}{P_1}^{\frac{R}{C_p}} \tag{1.6}$$

Thermal Classification of the Atmosphere's Layers

Planetary Boundary Layer

Closest to the Earth's surface, terminating at a few hundred meters, lies a region called the planetary boundary layer (PBL) where the atmosphere interfaces with topography. Surface-air radiative cou-

pling is strong here and the dynamics of the PBL is subject to diurnal variation. Daytime heating tends to induce instability in vertical structure of the PBL (e.g., $\frac{d\Theta}{dz} < 0$), producing strong vertical mixing. Conversely, at night air masses radiate heat to space at a faster rate than they are heated from the surface. Resultantly, a stratified air mass is produced (e.g., $\frac{d\Theta}{dz} > 0$) and convection is suppressed.

The Troposphere

Above the PBL lies the *free atmosphere* (that is, those regions of the atmosphere which are not subject to topographical friction). The lowest level of the free atmosphere is the troposphere, which when including the PBL, spans from the surface to about 10 – 16 km depending on the latitude. The troposphere is defined by a positive lapse rate and thus has a maximum temperature at the surface (global yearly average of 288 K). As altitude increases the temperature reaches a minimum at the *tropopause* (around 180 – 200 K, depending on latitude and time of year). Because of the positive lapse rate, the troposphere is a region of extensive vertical mixing and is home to the bulk of Earth's weather phenomena, such as cloud formation and precipitation. As convecting air parcels rise, they will eventually cool to the *dew point* at which point clouds may condense. Precipitation occurs when the gravitational settling of cloud condensation nuclei exceeds the rate of upward vertical transport and re-evaporation. The tropopause is defined by its lapse rate. In a general sense, it is the lowest region of the atmosphere in which the lapse rate does not exceed $2\frac{K}{km}$. The tropopause forms a 'cold trap' at the top of the troposphere, effectively condensing out most condensible gases. Because geological and anthropogenic activities generally occurs on the surface of the Earth, any

trace gases emitted at the surface which will perturb the chemical balance of the stratosphere must, to some degree, partition favorably through the tropopause.

The Stratosphere

The stratosphere lies immediately above the troposphere between 200 hPA – 1 hPa. As the tropopause is defined by an inflection in the lapse rate, the stratosphere is characterized by a negative lapse rate resultant from photochemical heating. This stratified layer of the atmosphere is very stable ($\frac{d\Theta}{dz} > 0$) and vertical transport is suppressed. The stratosphere terminates at its temperature maximum (typically between 240 – 270 K, depending on latitude and season), some 50 km above the surface of the Earth. This region is called the *stratopause*. Because of the high vertical stability of stratospheric air masses, trace gases contained within these air masses tend to persist within the stratosphere for many years. The *mean age of air* in the stratosphere, the required amount of time for an air parcel to travel from a source region (e.g, the tropical tropopause) to a destination region (e.g., exit the stratosphere at the poles), is on the order of 5 years. The *photochemical lifetime* of a molecule in the stratosphere is a property of the electronic structure of the molecule and varies greatly, ranging from totally inert (e.g., SF_6, $\tau \approx 800 - 3000$ years[32,33]) to extremely photolabile (e.g., NO_3 radical, $\tau \approx 10$ s[34]) and ranges in between (e.g., CFC-11, $\tau \approx 50$ years[32,35]). The overall lifetime of a molecule in the stratosphere is thus a convolution of the properties of stratospheric transport and molecular photochemistry.

The Mesosphere

The mesosphere extends from the temperature maximum at about 50 km above the surface of the Earth to another temperature minimum, the *mesopause*, at an altitude of about 80 km (spanning approximately 1 hPa – 0.01 hPa). The lapse rate, again positive, is driven by the decreasing density of shortwave-absorbing molecular species and radiative cooling from carbon dioxide. This region of the atmosphere possesses great chemical complexity. HO_x radicals dominate the chemical landscape at lower levels, but also interface with molecular and atomic ions produced from energetic particle precipitation processes as discussed in section 7.2.4. Additionally, the mesosphere is where the bulk of infalling meteors and grains vaporize due to frictional heating – a process resulting in the accumulation of 5.5 $\frac{\text{Mg}}{\text{day}}$ of meteoric material.[36]

The Thermosphere

Above the mesopause, the increasingly diffuse air increases in temperature as a result of atomic ionization from unscreened solar UV radiation. The mean free path of atoms, ions, and molecules in the thermosphere is sufficiently large that molecular diffusion dominates and stratification occurs in homogeneous layers as a function of molecular mass. The thermosphere terminates at the *thermopause*, which is defined as the point above which variations in solar insolation do not appreciably influence the physicochemical state of the surrounding medium – typically between 400 – 1000 km above the surface of the Earth. The solar constant is thus measured at the thermopause.

The Exosphere

The exosphere is a region of gradually declining density of mainly helium and hydrogen ions. It has no clear boundary, being the interface between the Earth's atmosphere and interplanetary space. Depending on space weather conditions and the metric employed, the exosphere may extend as far as 10,000 km from the surface of the Earth.

Compositional Classification of the Atmosphere's Layers

It is sometimes convenient to refer to layers of the atmosphere by their compositional structure rather than by their thermal structure. Common classiffiers are briefly presented in the following:

The Homosphere

The lowest compositional layer of the atmosphere is sometimes referred to as the *homosphere*, in which the average molecular mass of the atmosphere remains constant, around 29 g/mol. This layer extends from the surface to about 100 km. The *homopause* terminates the homosphere.

The Heterosphere

The heterosphere extends outward from the homopause toward interplanetary space. In this layer, molecules and ions are segregated in altitude by molecular mass, those species with greatest mass accumulating at the bottom and those with the lowest mass at the top.

The Chemosphere

The layer of the atmosphere in which photochemical reactions dominate is also known as the *chemosphere*. This region extends from about 10 km upward, generally encompassing the region of the upper troposphere to the mesopause.

The Ionosphere

The *ionosphere* is characterized by the presence of atomic and molecular ions produced from the harsh ultraviolet environment 60 km above the surface. Heavier molecular ions such as NO^+ and O_2^+ are prevalent at the lower altitudes, comprising the so-called *D layer*. Above this, at about 100 – 150 km, lies the *E layer*, comprised of atomic oxygen ions. The ions in these layers are quickly collisionally quenched, via reactions similar to those discussed in section 7.2.4, and thus these layers are only daytime phenomena. The *F layer* of the ionosphere is comprised of atomic ions of helium and hydrogen, which occur at much higher altitudes. The mean free path of these ions is sufficient that the F layer does not extinguish with the passage of the solar terminator.

Transport-Circulation

The topics discussed in this thesis require some description of the movement of air masses in both the troposphere and the stratosphere.

Geostrophic Flow, Cell Circulation, and Prevailing Winds

When one balances a the force exerted on a parcel of air as a result of a pressure gradient with the *Coriolis force*, *geostrophic winds* result. Briefly, because the Earth is a sphere, insolation will vary as a function of latitude, producing a latitudinal surface temperature gradient and air parcels near the surface will subsequently expand, per the ideal gas law. Additionally, the heat capacity of land and water differ greatly – as does their albedo, producing thermal heterogeneity within latitudes. The sum of these factors results in the establishment of pressure gradients. A stationary air parcel placed in a pressure gradient will experience a force, accelerating it toward the region of lower pressure. On an irradiated homogeneous spherical body, this acceleration is normally antipoleward. If the spherical body is also rotating, this parcel will begin to experience a deflecting motion resultant from the virtual Coriolis force. This force, originating from the conservation of angular momentum, is exerted in the opposite direction of the pressure gradient force. When both the pressure gradient force and the Coriolis force are equal, the air parcel will flow normal to the direction of the pressure gradient, in what is known as geostrophic flow. If the Earth were a homogeneous sphere, this would result in one band of *zonal* winds in each hemisphere with very little *meridional* mixing. Reality is clearly more complex. As the Earth's surface is heterogeneous, so too is the distribution of *cyclones*, *anticyclones*, *troughs*, and *ridges*. In a generalized conception of the Earth's pressure gradient, one may imagine a belt of low pressure centered about the equator. This equatorial trough originates mainly from the thermal gradient. At the poles lie the polar anticyclones, also resultant from the thermal gradient. In between the equatorial trough and the polar anticyclone lie a subtropical ridge

and a subpolar trough which originate due to the *overturning circulation*, a dynamical cause. At the equatorial low, air parcels are heated and are transported vertically, following the pressure gradient upward and then poleward. Because angular momentum is conserved, as the parcel moves poleward the air mass subsides, and the momentum of the parcel must increase to compensate. This results in strong easterly winds, which as the parcel moves ever farther poleward, eventually lose their poleward vector entirely. At this point (about 30 lats from the equator), the parcel subsides to the surface and forms the midlatitude ridge. Surface air then flows antipoleward, producing the westerly trade winds, completing the circuit. Such a cell is known as the *Hadley Cell*. Two more overturning circulation cells, the *Ferrel Cell* and the *Polar Cell*, account for circulation between the midlatitude ridge and the subpolar trough and the subpolar trough and the polar anticyclone. Because of the general eastward/westward directionality of these wind patterns, zonal mixing occurs on much faster timescale than meridional mixing. As a rule of thumb, zonal mixing occurs on the time scale of several weeks while meridional mixing requires several months.

Upper Air Westerlies and Easterlies and Stratospheric Zonal Winds

The zonal wind situation is much simpler at high altitudes due to reduced drag (resulting in higher wind speeds) and reduced significance of radial distance on total angular momentum (due to higher wind speeds). In the upper troposphere there exist the *upper air easterlies* between about 20°S and 20°N and the *upper air westerlies* poleward from 20° in both hemispheres. Similarly, in the stratosphere, winds are mainly geostrophic, with westerly flows in the midlatitudes.

Brewer-Dobson Circulation

The *Brewer-Dobson circulation* (BDC) is characterized by the ascent of air parcels through the tropical tropopause and subsequent subsidence in the midlatitudes and poles. During ascent, water is condensed out and trapped in the troposphere, producing the characteristically dry stratosphere and latitudinal distribution of ozone as discussed in section 1.3. A detailed description of the mechanism behind the BDC is beyond the scope of this thesis (see reference[37,38] and references therein). The tropical branch of the BDC is the primary means by which tropospheric material is transported to the stratosphere. Of the air that transits to the stratosphere, 90% subsequently mixes meridionally before it reaches 32 km in altitude[37], subsiding once it reaches 30°N or 30°S. These parcels are remixed into the troposphere. Long-lived chemical species contained within these parcels, such as anthropogenic halocarbons, will largely remain intact due to their limited exposure to UV radiation in the lower stratosphere. The remaining 10% of the material entering the BDC are injected much higher, and remain in the stratosphere for a much longer time. The BDC is perhaps best illustrated by the transport of ozone, as discussed in section 1.3.

The Quasi-Biennial Oscillation

The stratosphere, like the troposphere, possesses strong zonal winds; however, the directionality of the equatorial zonal winds oscillates with a periodicity of about 29 months in what is known as the *quasi-biennial oscillation* (QBO). Total ozone variation between peaks of the QBO varies by about 10%.[39]

Spatiotemporal Distribution of Stratospheric Ozone

Between about 20 and 30 kilometers above the surface of the Earth, depending on the latitude, the mixing ratio of ozone (O_3) reaches a maximum. This region is known as the *ozone layer* and provides the critical screening of ultraviolet radiation required to sustain surface life on Earth. Even small reductions in its thickness are demonstrated to produce significant impacts on human health, agricultural yield, and the lifetime of manufactured materials.[22,40–42]

Despite its incredible importance, if condensed to a pure layer at surface pressure, the ozone layer would on average only be three millimeters thick (300 Dobson units). Even at its most concentrated point in the middle stratosphere, the ozone layer is extremely diffuse, existing in mixing ratio quantities of a few parts per million.

Figure 1.1 illustrates the vertical profile of the so-called *natural ozone layer*, which is the ozone layer prior to anthropogenic perturbation of stratospheric chlorine inventories. Notably, we see that the concentration of equatorial ozone begins to increase in the lower stratosphere between 80 and 50 hPa and maximizes in the middle stratosphere. Because its steady state concentration is dependent on photochemical processes, production and loss rates of ozone are highest over equatorial regions. The tropics, where isolation is greatest, are the source region for most ozone production. Brewer-Dobson circulation tends to move this ozone-rich air poleward as it subsides in altitude. Consequently, equatorial ozone columns are thinner than midlatitude ozone columns, especially in the lower stratosphere where photolysis of ozone is suppressed due to reduced insolation. This trend is illustrated in figure 1.2.

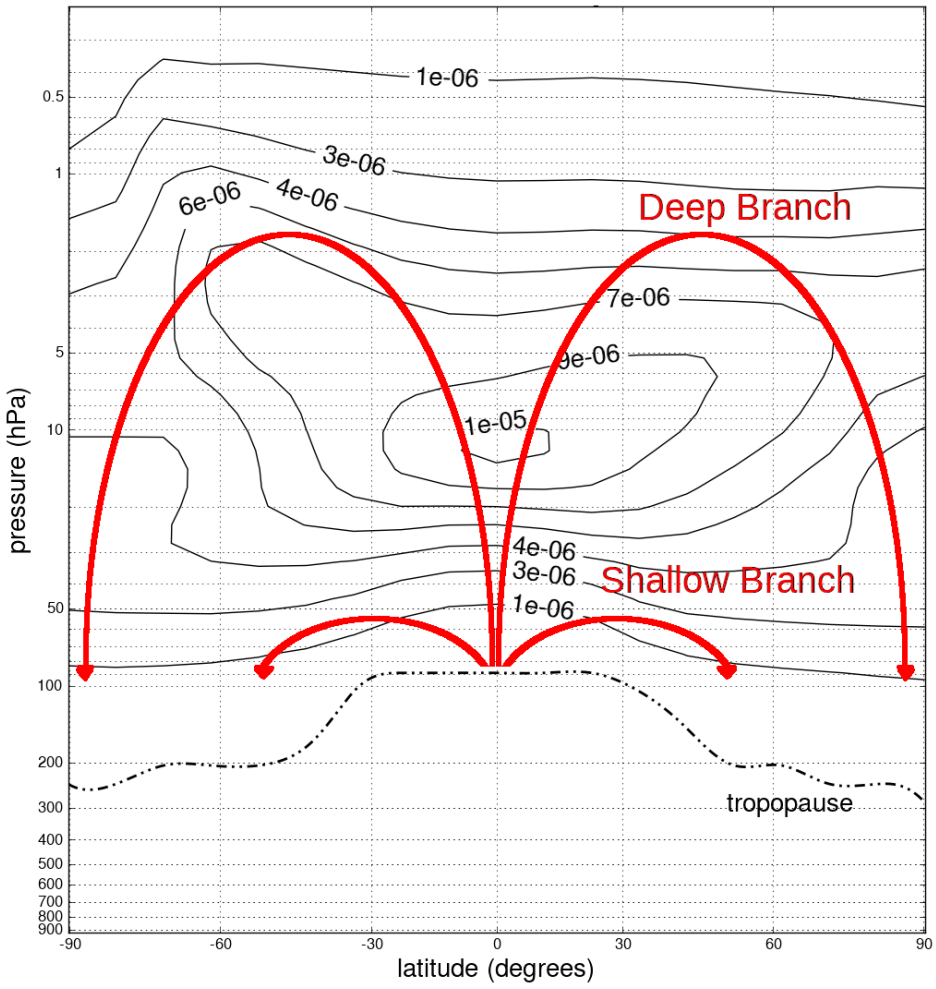

Figure 1.1: The ozone layer (isopleths: mixing ratio) as a function of pressure and latitude. Profile generated using historical emissions fields for the year 1950 in the AER-2D chemical transport model. Red arrows indicate general branches of the Brewer-Dobson Circulation.

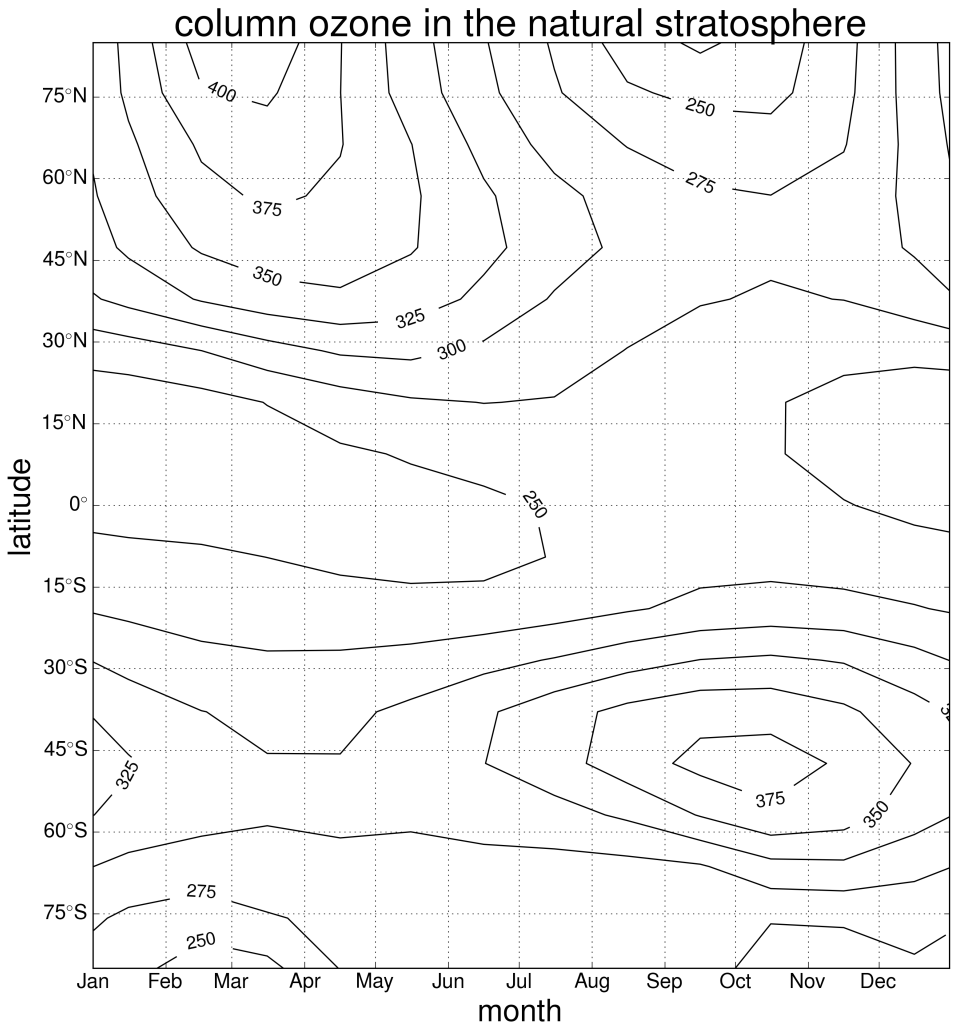

Figure 1.2: Temporal variation of column ozone (in Dobson Units) as a function of latitude. Profile generated for the year 1950 within the AER-2D model. Despite high tropical insolation leading to high rates of production, poleward transport and subsequent reduction in photochemical loss rates due to variation in the solar zenith angle leads to an accumulation of column ozone at higher latitudes.

O_x Chemistry: The Chapman Cycle

The vertical distribution of ozone in the atmosphere, depicted in figure 1.1, is primarily resultant from several interconnected photochemical processes known collectively as the Chapman cycle. A graph theory representation of this reaction cycle is illustrated in figure 1.3. Here, and in similar figures that follow, fast-cycling catalytic species are presented in the color green. Reservoir species are presented in the color red.

The production of ozone via the Chapman cycle begins with the photolysis of molecular oxygen by ultraviolet light as indicated in reaction 1.7.

$$O_2 + h\nu\,(\lambda{>}240\text{ nm}) \rightarrow 2O\left(^3P\right) \tag{1.7}$$

The oxygen atoms rapidly react with molecular oxygen (O_2) to form ozone.

$$O\left(^3P\right) + O_2 + M \rightarrow O_3 + M^* \tag{1.8}$$

The molecule M is any non-reactive third-body, but usually N_2 or another molecule of O_2. Reaction 1.8 results in a net heating of the environment, as indicated by the asterisk for the excited M species. Upon absorption of ultraviolet light, ozone photolyzes to form molecular oxygen and atomic oxygen.

$$O_3 + h\nu\,(\lambda{>}320\text{ nm}) \rightarrow O_2 + O\left(^1D\right) \tag{1.9}$$

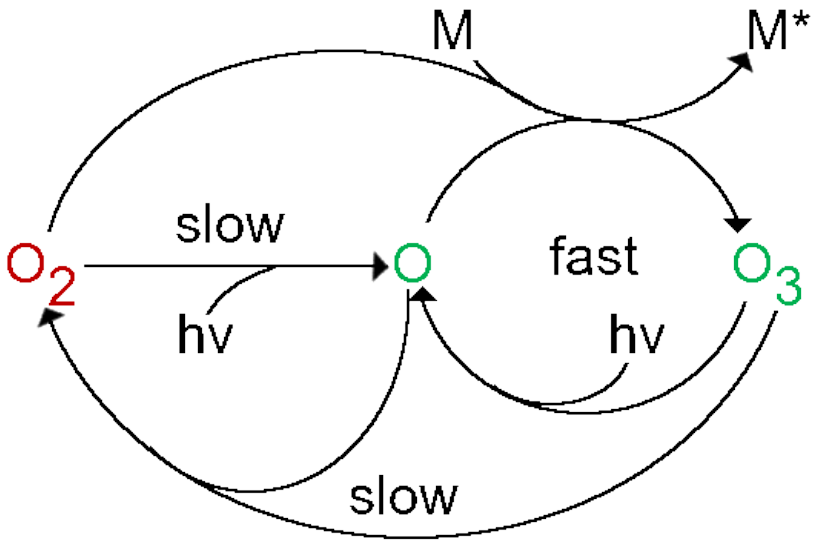

Figure 1.3: Graph theory depiction of the Chapman cycle ozone. Oxygen atoms, produced from the photolytic activation of molecular oxygen (λ < 200 nm), recombine with molecular oxygen to form ozone in a ternary reaction. Ozone photolyzes (λ < 250 nm) to regenerate atomic oxygen and molecular oxygen. This scheme, colored green, cycles rapidly, terminating upon the reaction of the oxygen atom with ozone to reform two molecules of molecular oxygen.

This atomic oxygen quickly relaxes to the triplet state. The cycle is completed by the reaction of ozone with atomic oxygen per reaction 1.10.

$$O_3 + O \rightarrow 2O_2 \tag{1.10}$$

A General Motif for Ozone Loss Catalysis

The ozone layer can be thought of as the steady-state solution to the Chapman cycle and a series of simultaneous photocatalytic loss reactions. A general motif for loss reactions in the middle and upper stratosphere, where oxygen atoms are prevalent, is detailed in reactions 1.11 - 1.13. This cycle, depicted in figure 1.4, begins upon stratospheric activation of precursor species Y, which is a molecular entity robust to tropospheric oxidative processes. Upon activation, usually photolytic or oxidative, reactive radical species X is produced. This radical will react quickly with ozone to form radical species XO and O_2. XO will react with O to form another molecule of O_2 and regenerate radical species X. Termination of the chain reaction and formation of a long-lived reservoir will occur in a manner idiosyncratic to the identity of species X.

$$X + O_3 \rightarrow XO + O_2 \tag{1.11}$$

$$XO + O \rightarrow X + O_2 \tag{1.12}$$

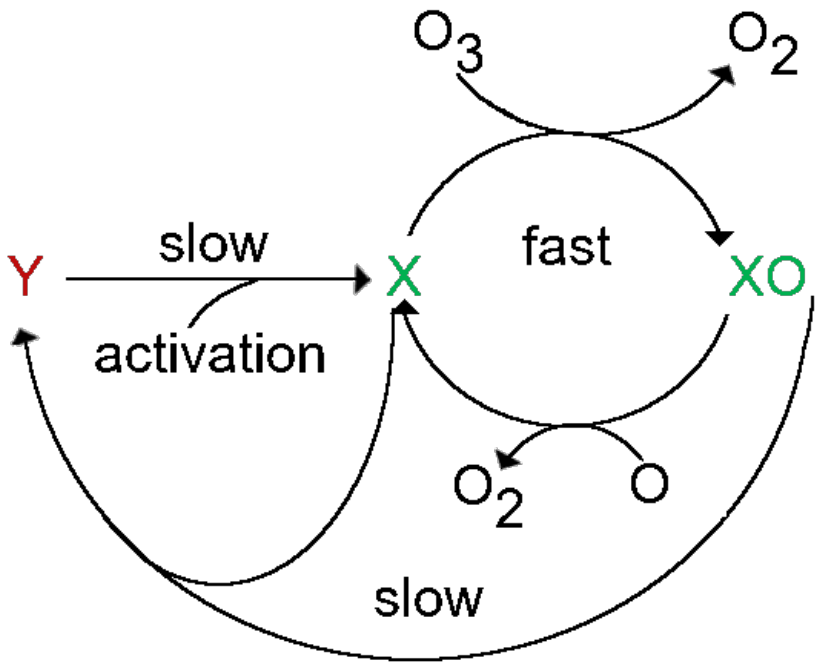

Figure 1.4: Graph theory depiction of generalized middle/upper stratospheric catalytic ozone loss cycling. Precursor species Y (here both a reservior species and a precursor species, though this is not always the case) is activated to form catalytically active species X. Bimolecular reaction with ozone produces species XO and molecular oxygen. Species XO subsequently reacts with atomic oxygen to regenerate species X in the net reaction: $O_3 + O \rightarrow 2O_2$.

$$\text{Net: } O_3 + O \rightarrow 2O_2 \tag{1.13}$$

in which X = H, NO, Cl, Br, and I.

The steady state solution to the ozone system is perturbed when physicochemical processes produce changes in the stratospheric availability of the various participants, X. Reductions in the quantity of X will result in increases in column ozone. Conversely, enhancements in the quantity of X will reduce the thickness of the ozone layer.

In the natural atmosphere, the odd-nitrogen cycle (NO_x) constitutes the primary non-Chapman sink of ozone and is most important in the middle stratosphere, as indicated in Figure 1.5a. Close behind in importance as a sink of ozone, the odd hydrogen cycle (HO_x) is a major sink of ozone in the lower stratosphere. The odd-halogen cycles are relatively unimportant in the natural stratosphere. The vertical profile of ozone is illustrated in Figure 1.5b.

NO_x Chemistry

A graphical depiction of the NO_x cycle is presented in figure 1.6. In notable contrast to the general motif depicted in figure 1.4, the precursor species, nitrous oxide (N_2O), does not also serve as a reservoir species. The odd-nitrogen cycle is initiated when nitrous oxide interacts with singlet oxygen, producing two equivalents of nitric oxide (NO).

$$N_2O + O\left(^1D\right) \rightarrow 2NO \tag{1.14}$$

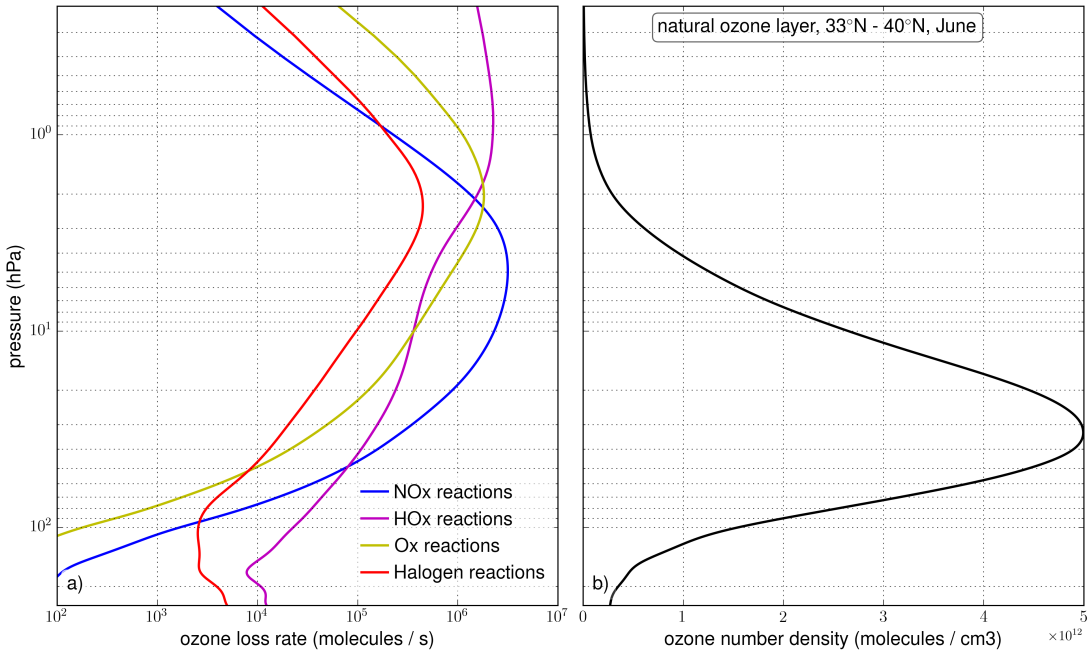

Figure 1.5: The natural stratosphere in June, 33°N - 42°N: a) photochemical ozone loss rates by chemical family. b) vertical profile of ozone. Note that NO_x processing dominates over all other loss rates at pressure levels where ozone number density is greatest. HO_x processing of ozone is the most significant process in the lower stratosphere. Halogen species contribute minimally to ozone loss rates in the natural stratosphere.

Once initiated, rapid cycling of nitric oxide and nitrogen dioxide (NO_2) via reactions 1.15 and 1.16 provides for the efficient conversion of ozone to molecular oxygen.

$$NO + O_3 \rightarrow NO_2 + O_2 \tag{1.15}$$

$$NO_2 + O\left(^3P\right) \rightarrow NO + O_2 \tag{1.16}$$

$$\text{Net: } O_3 + O \rightarrow 2O_2$$

A secondary catalytic pathway for the destruction of ozone, involving the photolysis of the nitrate radical (NO_3), may also occur:

$$NO + O_3 \rightarrow NO_2 + O_2 \tag{1.17}$$

$$NO_2 + O_3 \rightarrow NO_3 + O_2 \tag{1.18}$$

$$NO_3 + h\nu \rightarrow NO + O_2 \tag{1.19}$$

$$\text{Net: } 2O_3 \rightarrow 3O_2$$

Termination of these cycles occurs via one of two pathways: in the nighttime, reactions 1.20-1.21 dominate, forming the dinitrogen pentoxide reservoir (N_2O_5) from reaction of nitrogen dioxide with the nitrate radical (NO_3).

$$NO_2 + O_3 \rightarrow NO_3 + O2 \tag{1.20}$$

$$NO_3 + NO_2 + M \rightarrow N_2O_5 + M^* \tag{1.21}$$

In the presence of sunlight, due to the rapid photolysis of the nitrate radical, reaction 1.22 is the primary radical terminator.

$$NO_2 + OH \rightarrow HNO_3 \tag{1.22}$$

Finally, when aerosol loading is high, reactive hydrolysis and uptake of dinitrogen pentoxide provides a sink – the hydroxynitrate product remains adsorbed and/or solvated.

$$N_2O_5 + H_2O \xrightarrow{\text{aerosol}} HONO_{2(aq)} \tag{1.23}$$

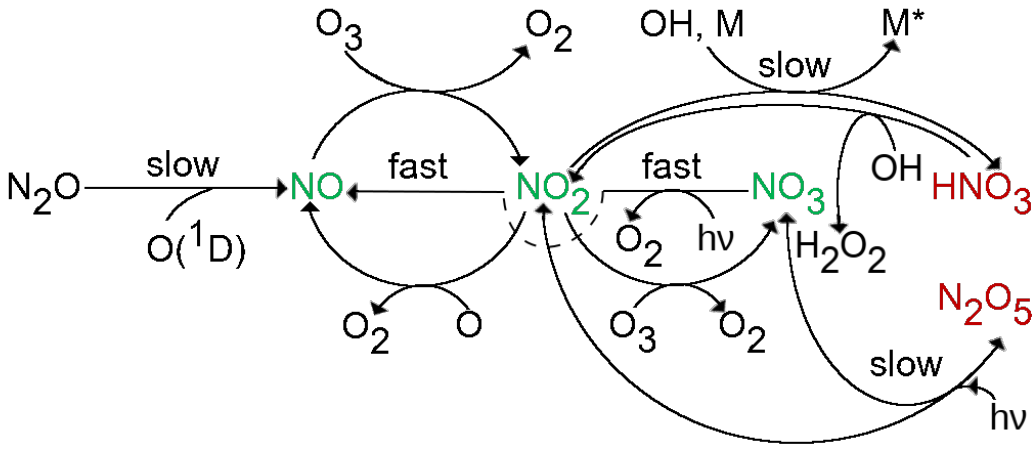

Figure 1.6: Graph theory depiction of the odd-nitrogen cycle. Nitric oxide, formed from the reaction of atomic oxygen with nitrous oxide, rapidly reacts with ozone to form nitrogen dioxide and molecular oxygen. Nitrogen dioxide may then react with oxygen atom to reform nitric oxide to complete a catalytic cycle, or may react with another molecule of ozone to form the nitrate radical. When nitrate photolysis produces nitric oxide and molecular oxygen, another catalytic cycle is completed. Termination and formation of reservoir species occurs according to two pathways. In the daytime, nitrogen dioxide reacts with hydroxyl radical to form hydroxyl nitrate. At night, when photolysis of the nitrate radical is suppressed, the recombination of nitrogen dioxide with nitrate produces dinitrogen pentoxide.

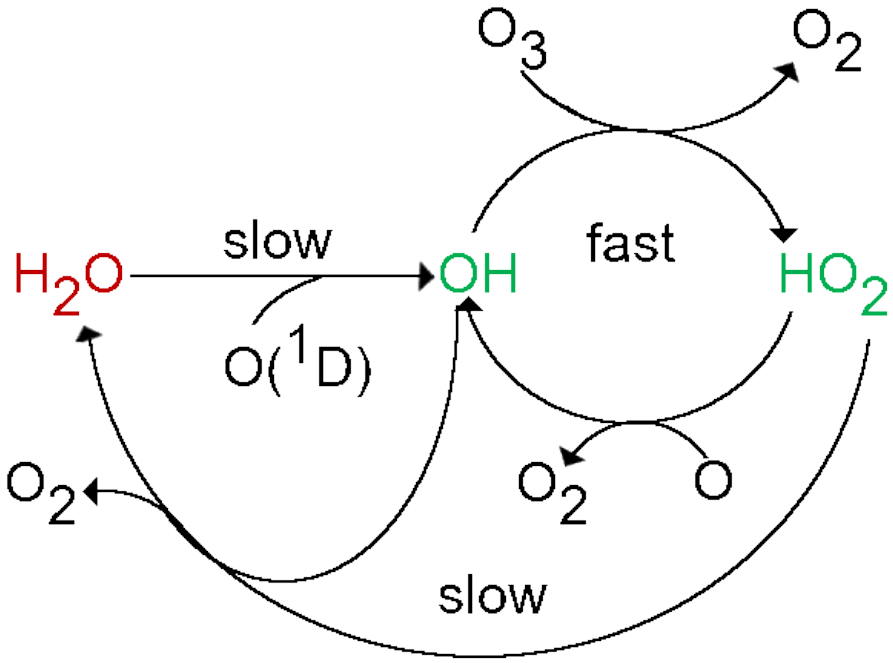

Figure 1.7: Graph theory depiction of the odd-hydrogen cycle. Hydroxyl radical, formed from the reaction of atomic oxygen with water vapor, rapidly reacts with ozone to form the hydroperoxy radical and molecular oxygen. This species will then react with an oxygen atom to reform the hydroxyl radical to complete a catalytic cycle. The recombination of hydroxyl radical and hydroperoxy terminates the cycle with the reformation of water vapor

HO_x Chemistry

HO_x-mediated catalytic ozone, depicted in figure 1.7, begins with the conversion of water vapor to two hydroxyl (OH) radicals. This cycle plays a major role in the lower stratosphere, where water vapor mixing ratios are elevated.

$$H_2O + O\left(^1D\right) \rightarrow 2OH \tag{1.24}$$

The hydroxyl radical rapidly cycles with hydroperoxy radical (HO_2), consuming ozone in the process, as indicated in reactions 1.25 and 1.26.

$$O_3 + OH \rightarrow O_2 + HO_2 \tag{1.25}$$

$$HO_2 + O \rightarrow OH + O_2 \tag{1.26}$$

$$\text{Net: } O_3 + O \rightarrow 2O_2$$

This reaction cycle terminates typically through self-reaction of the two radicals to form water and molecular oxygen.

$$OH + HO_2 \rightarrow H_2O + O_2 \tag{1.27}$$

ClO_x Chemistry

The majority of inorganic stratospheric halogen species contain chlorine. Hydrogen chloride (HCl) and chlorine nitrate ($ClONO_2$) account for the bulk of these. These species could be activated via the following homogeneous pathways:

$$ClONO_2 + h\nu \rightarrow Cl + NO_3 \tag{1.28}$$

$$HCl + OH \rightarrow Cl + H_2O_{(aq)} \tag{1.29}$$

$$ClONO_2 + HCl \rightarrow Cl_2 + HONO_2 \tag{1.30}$$

The rates of equations 1.28 – 1.30 are too slow to be of stratospheric significance. Heterogeneous processing of the chlorine reservoir species on natural sulfate aerosols is rapid, but dependent on the spatiotemporal stratospheric burden of aerosols:

$$ClONO_2 + H_2O \xrightarrow{\text{aerosol}} HOCl + HONO_{2(aq)} \tag{1.31}$$

$$HCl + HOCl \xrightarrow{\text{aerosol}} Cl_2 + H_2O \tag{1.32}$$

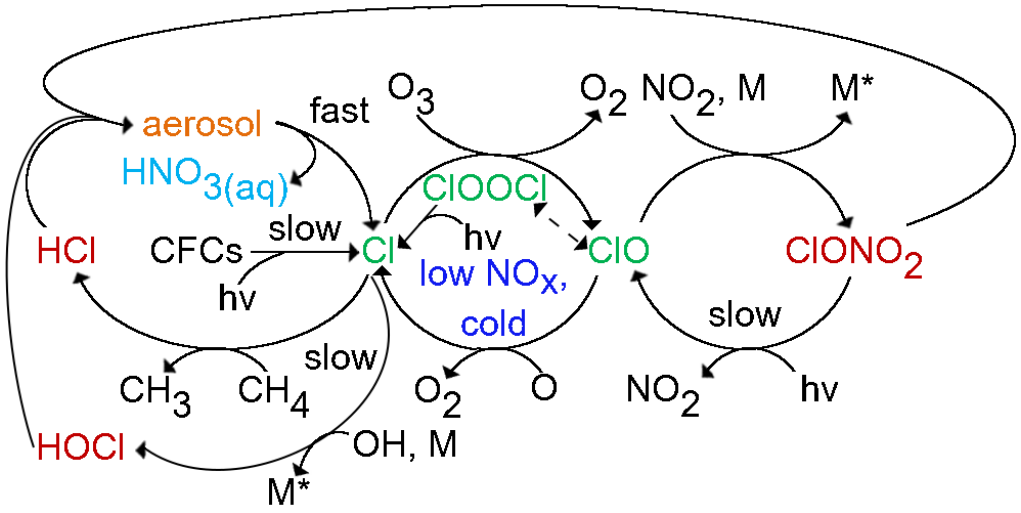

Figure 1.8: Graph theory depiction of the odd-chlorine cycle. The cycle initiates in the natural stratosphere via either the rapid heterogeneous conversion of chlorine nitrate, hypochlorous acid, and hydrogen chloride to molecular chlorine, which subsequently photolyzes, or through slow gas-phase photolysis and oxidation reactions (not depicted). The resultant chlorine radical reacts with ozone to produce chlorine monoxide and molecular oxygen. Chlorine monoxide may then complete the catalytic cycle via one of two ways: (1) chlorine monoxide reacts with an oxygen atom to produce molecular oxygen and regenerate the chlorine radical. (2) chlorine monoxide may dimerize in cold, denitrified environments, producing the chlorine peroxide molecule. This molecule rapidly photolyzes and decomposes to form two equivalents of chlorine radicals. Termination of the cycle occurs upon reformation of the reservoir species.

$$\mathrm{ClONO_2 + HCl \xrightarrow{aerosol} Cl_2 + HONO_{2(aq)}} \tag{1.33}$$

Molecular chlorine is rapidly photolyzed in the stratosphere to form the chlorine radical species.

$$\mathrm{Cl_2 + h\nu \rightarrow 2Cl} \tag{1.34}$$

Once activated, the chlorine radical quickly reacts with ozone to produce the chlorine monoxide radical (ClO) and molecular oxygen. In warmer environments (e.g., outside the polar vortex) this chlorine monoxide radical can react with atomic oxygen to produce molecular oxygen and regenerate the chlorine radical.

$$\mathrm{Cl + O_3 \rightarrow ClO + O_2} \tag{1.35}$$

$$\mathrm{ClO + O \rightarrow Cl + O_2} \tag{1.36}$$

$$\text{Net: } \mathrm{O_3 + O \rightarrow 2O_2}$$

The chlorine monoxide radical exists in thermal equilibrium with its dimer. When the lifetime of chlorine monoxide is sufficiently large and the temperature is sufficiently low (e.g., following denitrification of a stationary wintertime polar air mass), high quantities of chlorine peroxide (ClOOCl)

may form. This species rapidly photolyzes to produce two chlorine radical species in the following catalytic cycle:

$$2ClO + M \leftrightarrow ClOOCl + M^* \tag{1.37}$$

$$ClOOCl + h\nu \rightarrow Cl + ClOO \tag{1.38}$$

$$ClOO + M^* \rightarrow Cl + O_2 + M \tag{1.39}$$

$$2\left(Cl + O_3 \rightarrow ClO + O_2\right) \tag{1.40}$$

$$\text{Net: } 2O_3 \rightarrow 3O_2$$

Termination of the catalytic mechanism can result from several different pathways:

$$Cl + OH + M \rightarrow HOCl + M^* \tag{1.41}$$

$$Cl + CH_4 \rightarrow HCl + CH_3 \tag{1.42}$$

$$\mathrm{ClO} + \mathrm{NO_2} + \mathrm{M} \rightarrow \mathrm{ClONO_2} + \mathrm{M^*} \tag{1.43}$$

Other Halogens and Interfamily Reaction Cycles

In the lower stratosphere, small quantities of bromine and iodine are produced from the reactive oxidation of *very short-lived substances* (VSLS), halocarbons of mostly natural, biogenic origin. These compounds are vulnerable to hydroxyl radical attack or photolysis in the troposphere and subsequently undergo depositional processes, resulting in small, pptv (Br) or ppqv (I) stratospheric mixing ratios.

The lower stratosphere is largely screened of UV radiation, substantially enhancing the photochemical lifetime of ozone. Resultantly, the mixing ratio of atomic oxygen is very low and the catalytic reaction cycle presented in figure 1.4 is not efficient. Instead, interfamily chemical reactions dominate, especially reactions with much more concentrated $\mathrm{ClO_x}$ and $\mathrm{HO_x}$ radicals, as depicted in figure 1.9. Activation of bromocarbons and iodocarbons proceeds in the stratosphere via hydroxyl radical reaction or via photolytic pathways, as in reaction 1.44.

$$\mathrm{R[I/Br]} + \mathrm{OH,h}\nu \rightarrow \mathrm{R} + \mathrm{I/Br} \tag{1.44}$$

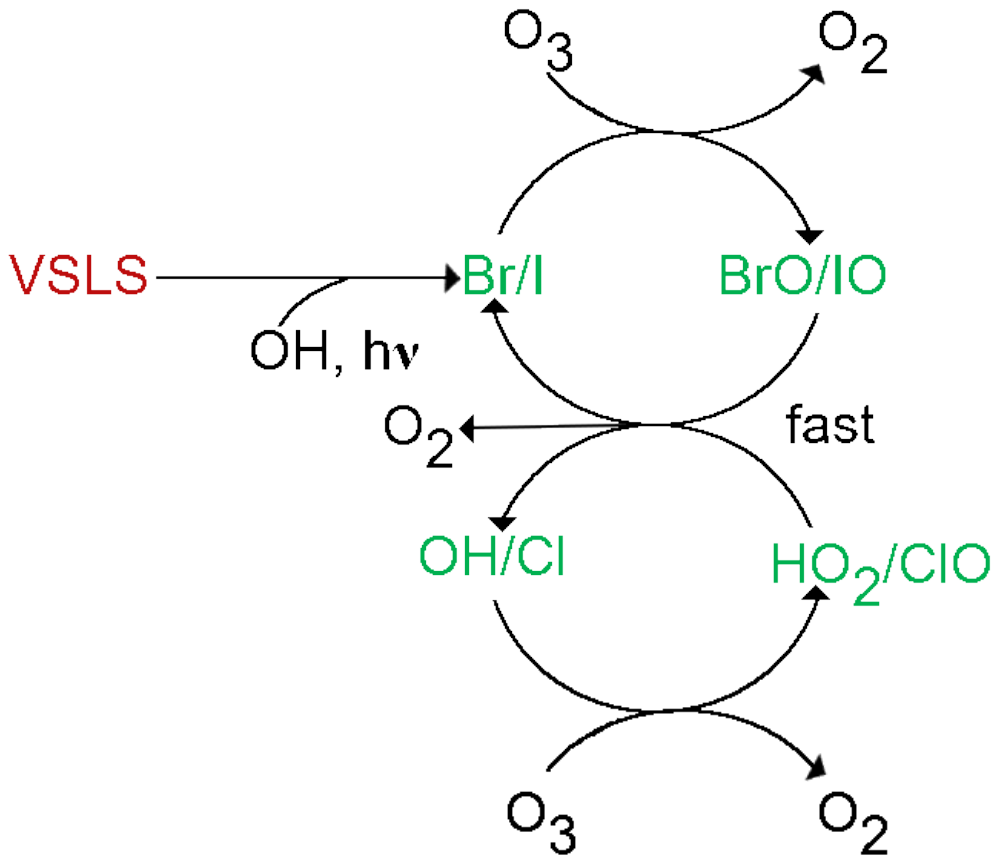

Figure 1.9: Graph theory depiction of lower stratospheric interfamily halogen cycles. The cycle initiates via rapid oxidation or photolysis of very short-lived halocarbons to produce bromine or iodine radicals. These radicals react with ozone to produce a halogen monoxide radical and molecular oxygen. Subsequent reaction with the much more abundant chlorine monoxide or hydroperoxy radical regenerates the halogen radical (a fast intermediate process is not depicted). The net reaction converts two ozone molecules to three molecules of dioxygen.

Bromine-Chlorine Interhalogen Cycling

Bromine radicals produced from the reactive stratospheric oxidation of short-lived bromocarbons (reaction 1.44) rapidly react with ozone to form bromine monoxide radicals and molecular oxygen.

$$Br + O_3 \rightarrow BrO + O_2 \tag{1.45}$$

In the lower stratosphere, chlorine monoxide is significantly more abundant than bromine monoxide and thus serves as a dominant reaction partner for bromine monoxide. Three product channels dominate this bimolecular reaction as indicated in equations 1.46 – 1.48.[43]

$$Cl + O_3 \rightarrow ClO + O_2 \tag{1.35}$$

$$BrO + ClO \rightarrow Br + ClOO \tag{1.46}$$

$$BrO + ClO \rightarrow BrCl + O_2 \tag{1.47}$$

$$BrO + ClO \rightarrow Br + OClO \tag{1.48}$$

For reactions 1.46 and 1.47, these intermediate products are rapidly converted in the daytime to

regenerate the chlorine and/or bromine radicals in order to complete the catalytic cycle. Reaction channel 1.48 mostly leads to a null cycle as in reaction 1.52, though a small proportion of photolyzed chlorine dioxide will complete the cycle per reaction 1.51.

$$\mathrm{ClOO} + \mathrm{M} \rightarrow \mathrm{Cl} + \mathrm{O_2} + \mathrm{M} \tag{1.49}$$

$$\mathrm{BrCl} + \mathrm{h}\nu \rightarrow \mathrm{Br} + \mathrm{Cl} \tag{1.50}$$

$$\mathrm{OClO} + \mathrm{h}\nu \rightarrow \mathrm{Cl} + \mathrm{O_2} \tag{1.51}$$

$$\text{Net: } 2\mathrm{O_3} \rightarrow 3\mathrm{O_2}$$

$$\mathrm{OClO} + \mathrm{h}\nu \rightarrow \mathrm{ClO} + \mathrm{O(null)} \tag{1.52}$$

Chlorine/Odd-Hydrogen Catalytic Ozone Processing

The bulk of halogen-catalyzed lower-stratospheric ozone loss is resultant from the coupling of the chlorine-mediated destruction of ozone with the hydrogen-mediated destruction of ozone. Chlorine monoxide will form per reaction 1.35 and hydroperoxy per reaction 1.25. The species then react in

the following cycle:

$$Cl + O3 \rightarrow ClO + O_2 \tag{1.35}$$

$$OH + O3 \rightarrow HO_2 + O_2 \tag{1.25}$$

$$ClO + HO_2 \rightarrow HOCl + O_2 \tag{1.53}$$

$$HOCl + h\nu \rightarrow OH + Cl \tag{1.54}$$

$$\text{Net: } 2O_3 \rightarrow 3O_2$$

Bromine/Odd-Hydrogen Catalytic Ozone Processing

Besides reaction with other halogen species, lower stratospheric bromine will also engage odd-hydrogen. Following activation per reaction 1.44, bromine will rapidly react with ozone to form bromine monoxide, as in reaction 1.45. This species will then react with the hydroperoxy radical (formed according to reaction 1.25 as discussed in section 1.7. The catalytic cycle proceeds per reactions 1.55 and 1.56.

$$Br + O_3 \rightarrow BrO + O_2 \tag{1.45}$$

$$OH + O_3 \rightarrow HO_2 + O_2 \tag{1.25}$$

$$BrO + HO_2 \rightarrow HOBr + O_2 \tag{1.55}$$

$$HOBr + h\nu \rightarrow OH + Br \tag{1.56}$$

$$\text{Net: } 2O_3 \rightarrow 3O_2$$

Iodine-Interfamily Cycling

Iodine, once partitioned to the lower stratosphere, will behave similarly to bromine. After initiation (see reaction 1.44), iodine radicals rapidly react with ozone to form iodine monoxide radicals and molecular oxygen. Though iodine monoxide will react with bromine monoxide and hydroperoxy radicals, these reaction partners will not be discussed in this section due to the insignificance of these pathways relative to reaction with chlorine monoxide.[44]

$$I + O_3 \rightarrow IO + O_2 \tag{1.57}$$

$$Cl + O_3 \rightarrow ClO + O_2 \tag{1.35}$$

Iodine monoxide will then react with chlorine monoxide to reform the iodine and chlorine radical. Note that all significant reaction channels lead quickly to reform I and Cl, unlike the case with bromine.[44]

$$IO + ClO \rightarrow \text{Products} \rightarrow I + Cl + O_2 \tag{1.58}$$

$$\text{Net: } 2O_3 \rightarrow 3O_2$$

Relative Halogen Reactivity: Alpha Factors

The vast majority of inorganic chlorine in the lower to middle stratosphere is present in the reservoir forms HCl and ClONO2. Typically, only a few percent of inorganic chlorine in the lower stratosphere is present in active forms, such as ClO. Active, halogen radical species may participate in catalytic ozone-destroying chemical reaction cycles, such as the interfamily cycles presented in section 1.9. The gas-phase conversion of inorganic chlorine reservoirs to their active, ozone-destroying forms, reactions 1.28 – 1.30, in the atmosphere is too slow to be of atmospheric relevance; however, heterogeneous reactions on the surfaces of stratospheric aerosols[45,46], as indicated in reactions 1.31 – 1.34, are sufficiently fast to enable significant engagement of ClO_x ozone-depletion cycling. BrO_x and IO_x mechanisms are much less dependent on the surrounding environment than ClO_x. This is because inorganic reservoirs of bromine and iodine are significantly less stable, enhancing the quantity of reactive halogen available for ozone processing. Though the ratios of active chlorine, bromine,

and iodine to their reservoir forms are a function of environmental conditions, bromine and iodine are up to several orders of magnitude more likely to be found in their active form than chlorine.[47] Quantification of the ozone-depleting efficiency of a bromine or iodine atom relative to chlorine provides a metric known as an *alpha factor*, α. These efficiency factors are especially useful in determining parameterized estimates of the *Effective Equivalent Stratospheric Chlorine* (EESC, refer to section 4.3.4), which is a quantity expressing the ozone-depleting power of a mixture of stratospheric trace gases.[48,49] Uncertainties in future values of α contribute to the uncertainty in predictions of future stratospheric ozone recovery.[12,13,49] Alpha factors are calculated either as a function of ozone loss rates from different catalytic cycles[48,50] (equation 1.59) or as a function of the overall change in ozone abundance[48,51] (equation 1.60), where x is either Br or I:

$$\alpha_x = \frac{\text{bromine (iodine) catalyzed ozone loss rate per reactive bromine (iodine) atom}}{\text{chlorine catalyzed ozone loss rate per reactive chlorine atom}} \tag{1.59}$$

$$\alpha_x = \frac{\delta O_3/\delta x_y}{\delta O_3/\delta Cl_y} \tag{1.60}$$

Values of α vary depending on the physicochemical environment. Globally-averaged values for α_{Br} are typically estimated between 45 – 80, while α_I is estimated to be between 150 – 300.[44,48,50–54] Values of α tend toward a minimum at the equator, maximizing at the poles and exhibiting very little seasonal variation outside the polar vortex. Likewise, α is enhanced in the lower stratosphere where reactive chlorine is less prevalent than in the middle stratosphere.[48] Values of α for future

climates are unknown and are likely to be different than the values computed for the contemporary atmosphere due to significant changes in the physicochemical environment of the stratosphere.

2

Stratospheric Aerosols

Atmospheric aerosols appear in the most unexpected places: the Antarctic ozone hole, the red sunsets following a temperature inversion, in the formation processes of clouds, the chemical effects of large volcanic veils, primary culprits in the toxicity of air pollution, and even in some proposed geoengineering schemes to reduce surface insolation. Indeed, they appear to be involved in some shape or form in nearly every atmospheric phenomenon.

Aerosols are defined as two-phase systems consisting of condensed particles and the gas in which they are suspended. In the context of the Earth's atmosphere, these particles may range in size between a few nanometers to several microns, composed of solid inorganic salts and metals, complex organic molecules, liquids formed from condensed atmospheric gases, and mélanges of the aforementioned types. Once formed, aerosols exert outsized effects on the rates of chemical reactions and on the scattering of sunlight.

Distribution

Peaking near 24 km in altitude at the equator and 17 km at the poles, stratospheric aerosol forms a distinct layer, known as the *Junge layer*, between approximately 15 – 25 km.[55,56] The upper terminator of the Junge layer is controlled by rising stratospheric temperatures with altitude – as temperatures increase, stratospheric aerosols tend to evaporate – while the lower terminator is governed via sedimentation processes into the tropopause.[57,58] Figure 2.1 presents AER-2D model output of the stratospheric background of sulfate aerosol mixing ratio.

Stratospheric aerosols are frequently reported as a function of their *aerosol optical depth* (AOD) at specific wavelengths. Typical non-volcanic backgrounds hover around 0.004 OD, 0.002 OD, and 0.001 OD at 525 nm, 750 nm, and 1020 nm respectively.[59] Multichannel reporting of AOD allows for the determination of number density and median distribution radius simultaneously.[60]

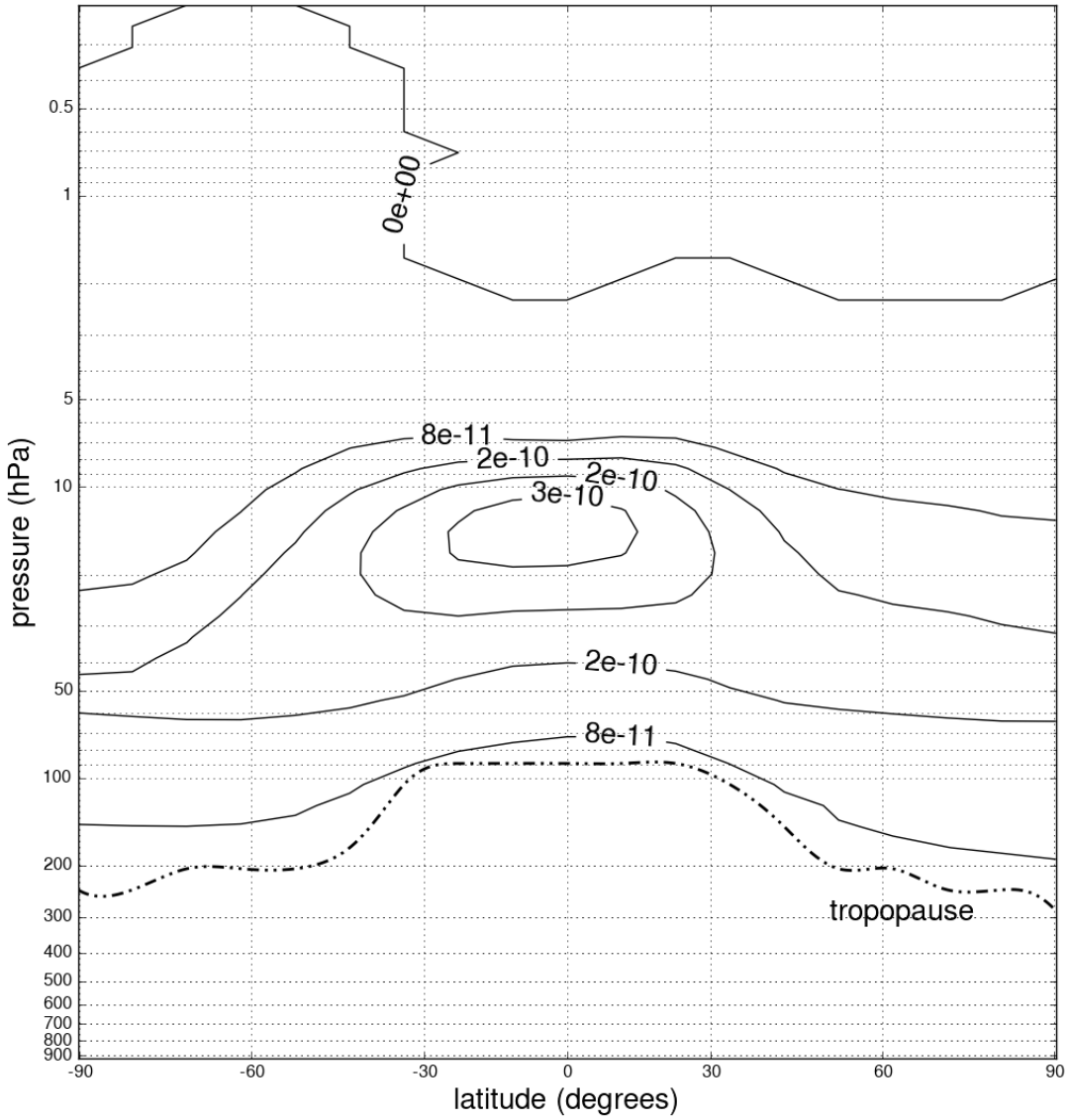

Figure 2.1: 2-D contour map of the May stratospheric sulfate aerosol mixing ratio produced using the AER-2D CTM. Sulfate aerosol is most concentrated in the middle equatorial stratosphere.

Characterization of Stratospheric Aerosols

Stratospheric aerosols may be characterized according to their number density (N) , particle diameter (DP), mass density (M), surface area density (A), or volume density (V). Aerosols of different origins will frequently exhibit different density distributions with respect to their particle diameter. For example, meteoric particles from bolides will exhibit high mass density across all size modes while particles formed from in situ nucleation and coagulation processes will exhibit a peaked mass distribution favoring fine particle sizes. Aerosols are categorized by three size modes: nucleation (Aitken), accumulation, and coarse-particle.

Nucleation mode aerosols, as their name implies, are formed from homogeneous and heterogeneous nucleation processes. They feature particle diameters smaller than 0.1 μm and are subdivided into ultrafine (diameter < 0.01 μm) and fine mode (0.01 μm < diameter < 0.1 μm).

Accumulation mode particles range between 0.1 μm and 1 μm in diameter. They are so named because removal mechanisms for particles of this size are slow. Aerosols of this size tend to accumulate in the stratosphere.

Coarse mode particles feature diameters greater than 1μm and sediment rapidly out of the stratosphere.

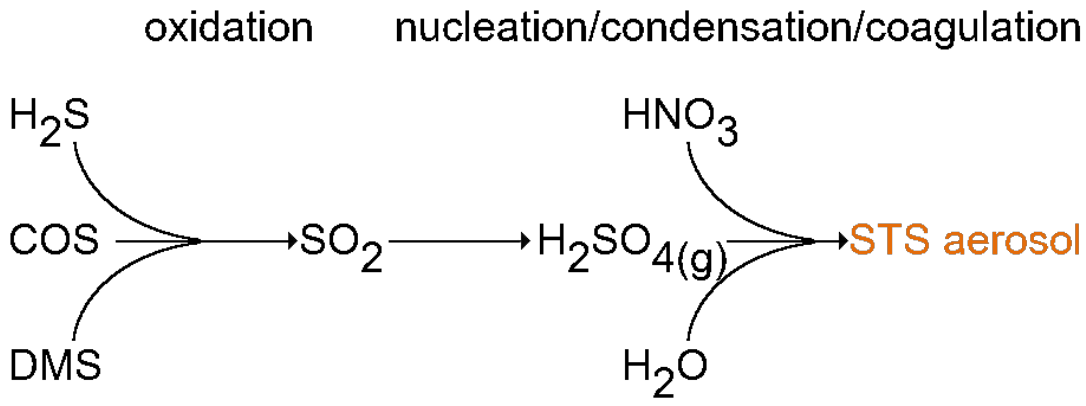

Figure 2.2: Production of sulfate aerosol. Sulfur-bearing compounds transported into the stratosphere are oxidized, producing SO_2. Further oxidation (through many pathways) results in the formation of H_2SO_4. Nucleation, coagulation, and reactive uptake with water vapor and/or hydroxynitrate produces the aerosolized supercooled ternary solution.

Chemical Origin/Composition of Stratospheric Aerosols

Supercooled Ternary Solution (STS)

Sulfate aerosols comprise the bulk of all stratospheric aerosols and typically form following the progressive oxidation of sulfur-bearing compounds. Figure 2.2 provides a schematic of sulfate oxidation to form a sulfate aerosol. Oxidation steps are diverse and many pathways exist; regardless of the original species, most reduced sulfur compounds are highly reactive with respect to the hydroxyl radical and very quickly are transformed to oxidized species such as SO_2 and subsequently H_2SO_4. This species then coagulates/condenses to form a droplet of H_2SO_4, H_2O, and HNO_3 known as a supercooled ternary solution (STS). Heterogeneous reactions, such as equation 1.23 and equations 1.31 – 1.33 further contribute to the formation of STS aerosols.

Polar Stratospheric Clouds

Polar Stratospheric Clouds (PSCs) form at depressed temperatures typically associated with the polar winter and are classified according to their physical properties.[61,62] Type I clouds form at temperatures above the frostpoint while type II clouds exclusively form below the frost point (e.g., 188 K at 5 ppmv H_2O / 60 hPa). PSCs are especially associated with *lee-waves*, a topographical effect in which parcels are forced to rise due to underlying geography, cooling adiabatically.[63]

Type Ia Polar Stratospheric Clouds

Nucleating below 195 K, type Ia PSCs are non-spherical solid particles composed of nitric acid trihydrate and/or nitric acid dihydrate. If cooling rates are low (e.g., < 5 K / day), type Ia PSCs will grow to large sizes (diameter > 1 μm). When cooling rates are higher than this – e.g., during lee-wave expansion – smaller particles are formed in more numerous quantities, enhancing surface area and rates of heterogeneous chemistry.[64–66]

Type Ib Polar Stratospheric Clouds

Problems rectifying the LIDAR backscatter depolarization ratios of PSCs with microphysical models of aerosol formation elucidated a second type of PSC which formed above the frost point. Like type Ia PSCs, type Ib PSCs also nucleate below 195 K; however, type Ib PSCs are composed of spherical liquid droplets composed of H_2O, H_2SO_4, and HNO_3 – supercooled ternary solutions as in section 2.3.1.

Type II Polar Stratospheric Clouds

Water-ice clouds form in the stratosphere below the frost point – typically around 190 K. These particles can grow to large sizes of up to 100 μm diameter, with correspondingly large sedimentation rates.

Minor Stratospheric Aerosols

Volcanic Ash

Volcanic ash, also known as tephra, is a silicate material which may rapidly scavenge volatile gases by physical and chemical processes during ascent in the eruption column.[67] Following an explosive volcanic eruption, the initial size distribution of volcanic ash particles injected to the stratosphere will be large, spanning the millimeter scale to the nanometer scale; however, sedimentation processes will rapidly favor smaller particles. Though particles between 1 μm and 15μm possess stratospheric lifetimes on the order of days, their outsized effect on heating, producing up to 20 K anomalies, has been attributed to deterministic perturbations of volcanic cloud evolution.[68]

In addition, volcanic ashes may facilitate the transport of halogen species to the stratosphere – and enable bromine-explosion chemistry (refer to section 6.2.2) within the eruption column.[69,70]

Estimates of volcanic ash deposition masses are largely unconstrained and idiosyncratic to the chemicophysical conditions of the volcanic eruption. Pinatubo-scale eruptions may produce tens of Tg of stratospheric volcanic ash.[71]

Black Carbon and Organic Aerosols

Aerosols of tropospheric origin comprise a significant fraction of total aerosols 2 km above the tropopause, the relative fraction decreasing with height as sulfate aerosol production increases.[72] Anthropogenic factors, such as biomass burning and incomplete combustion of fossil fuels, were found to contribute up to 50 % of the number of particles between 0.25 and 2 μm diameter in the UTLS over midlatitude North America and Asia.[72–74]

Meteoric Material

Estimates in the mass of extraterrestrial dust input to the atmosphere range from 3 – 300 t/d.[75] The uncertainty in that estimate is large due to limitations in the different instrumental and analytical techniques used to obtain meteoric mass fluxes — and the fact that no single technique can provide an integrated estimate over the entire size distribution. Recent estimates of mass fluxes seem to be biased toward the lower quartile of this quantity (e.g., 40 — 50 tons per day) — and this estimate contains both contributions from meteorite and cosmic dust infall.[76] In the case of cometary dust, the average velocity of an incoming meteorite is less than 15 km/s (though greater than 11 km /s — Earth's escape velocity), and some 20% of the infalling mass is converted to meteoric smoke[76,77] (nanometer-scale metallic particles of meteoric origin) via ablative processes (whose efficiency increases as a function of velocity). This accounts for roughly 10 tons meteoric smoke per day.

These particles subsequently sediment toward the poles during their 4-year lifetime, serving as mesospheric and stratospheric cloud nuclei and possibly participating directly in ozone chem-

istry.[78,79] Meteoric material is largely non-carbonaceous – e.g., chondrites ($FeMgSiO_4$). Meteoric iron and magnesium particles have been implicated removal processes of gas-phase H_2SO_4 via nucleation of sulfate aerosols, accounting for up to 1 % by mass of mid-latitude stratospheric sulfate.[80]

Heterogeneous Chemical Reactions

Chemical reactions in which at least one of the elementary transformations occurs between two different phases of matter, such as the reaction of a trace gas on an aerosol, are called heterogeneous reactions.

Very often, only the first and last elementary steps in a heterogeneous reaction scheme are truly heterogeneous, the intermediate steps occuring entirely on the surface. Such multi-step mechanisms are initiated by adsorption, during which a liquid- or gas-phase molecule impinges on a surface and thermally accommodates (physisorption), and terminated by desorption. An adsorbed species may also transport to the bulk of a solid or liquid – or incorporate into a reconstruction of the surface – in a process called mass accommodation.

On solid surfaces, a region of perturbed electronic density known as the surface state projects outward and may interact with the electronic structure of the adsorbed molecule, forming a bond in a process known as chemisorption. Depending on the strength of the bond, which is modulated by surface temperature, among other factors, the molecule may be stuck in place at a specific adsorption site, it may hop between neighboring adsorption sites, or it may diffuse freely across the surface as a 1-D or 2-D gas. This confinement of translational motion to only one or two degrees of freedom

produces significantly enhanced collision rates between adsorbates and thus accelerates fundamental reaction steps in which diffusional collision is the rate-limiting factor – such as the low-temperature desorption of chemisorbed molecular oxygen on silver surfaces following collision with hot oxygen adatoms as was demonstrated by Klobas et al., 2014.[81] Additionally, the perturbed electronic structure of an adsorbate may enable reaction pathways which are not available in the gas phase such as photodissociation at lower frequencies of light or previously unfavored molecular attack. For example, Klobas and coworkers determined that certain formulaic alloys of silver and gold perturbed the stability of adsorbed oxygen adatoms such that they reacted with significantly greater probability to form surface carbonate upon exposure to carbon dioxide than on the pure silver or gold surface alone.[82]

Heterogeneous Chemistry in the Stratosphere

In the atmosphere, heterogeneous reactions are primarily between the gas and liquid phases and to a lesser extent, between gases and an (often wetted) solid phase. Unlike the metal surface reactions described above in which diffusional collision controlled the recombination reaction rates, mass accommodation often dictates the rate of atmospheric reactions.

A net uptake coefficient, γ, describes the probability that an impinging gas-phase molecule will be accommodated by a liquid and is a function of the concentration of the gas-phase molecule (n_g, cm^{-3}), the molecule's mean molecular velocity ($\bar{c}$, cm s^{-1}), and the flux rate of the molecule into the

liquid surface (J, $cm^2\ s^{-1}$), as given in equation 2.1

$$\gamma = \frac{4J}{n_g \bar{c}} \tag{2.1}$$

The flux rate, J, is modulated by the mass accommodation coefficient α_{ma} – valued between 0 and 1 – per equation 2.2.

$$J(\alpha) = \frac{n_g \bar{c} \alpha_{ma}}{4} \tag{2.2}$$

α_{ma} represents the probability that an impinging molecule will enter the bulk of the liquid aerosol. The net flux into the bulk (k_{sol}, set equal to equation 2.2) is defined by the difference between the adsorption rate (k_{ads}) of the gas phase species (n_g) and the desorption rate (k_{des}) of the surface species (n_s), per equation 2.3.

$$n_s k_{sol} = \frac{\alpha_{am} n_g \bar{c}}{4} = n_g k_{ads} - n_s k_{des} \tag{2.3}$$

The adsorption rate is modulated by the sticking coefficient, S, which represents the fraction of impinging molecules which are thermally accommodated by the surface (e.g., have lost memory of their past momentum) vs those that are not (e.g., scatter off the surface at peaked angular distributions). Solving for n_s in terms of k_{sol} ($n_s = \frac{\alpha_{am} n_g \bar{c}}{4}$) and incorporating the sticking coefficient, the flux into the bulk is then:

$$\frac{\alpha_{am} n_g \bar{c}}{4} = \frac{n_g S \bar{c}}{4} - \frac{\alpha_{am} n_g \bar{c} k_{des}}{4 k_{sol}} \tag{2.4}$$

which can be rearranged to provide a definition of α_{am}:

$$\frac{1}{\alpha_{am}} = \frac{1}{S} + \frac{k_{des}}{Sk_{sol}} \tag{2.5}$$

Thus the mass accommodation coefficient, which modulates the total reactive uptake of the aerosol, is the branching ratio of solvated impinging gas molecules.

Relevant Reactions

The activation of chlorine reservoirs on aerosols, such as reactions 1.32 – 1.34, is of extraordinary importance in the lower stratosphere. Figure 2.3 presents γ values for these reactions on stratospheric sulfate aerosol as a function of temperature and acid weight percent. Notably, γ for reactions 1.33 and 1.32 increases by five orders of magnitude as temperatures decrease from 210 K to 190 K (and the sulfate fraction of the aerosol correspondingly decreases). Reaction 1.31 exhibits less temperature dependence over typical mid-latitude lower stratospheric temperatures.

$$ClONO_2 + H_2O \xrightarrow{\text{aerosol}} HOCl + HONO_2 \tag{1.31}$$

$$HCl + HOCl \xrightarrow{\text{aerosol}} Cl_2 + H_2O \tag{1.32}$$

$$ClONO_2 + HCl \xrightarrow{\text{aerosol}} Cl_2 + HONO_2 \tag{1.34}$$

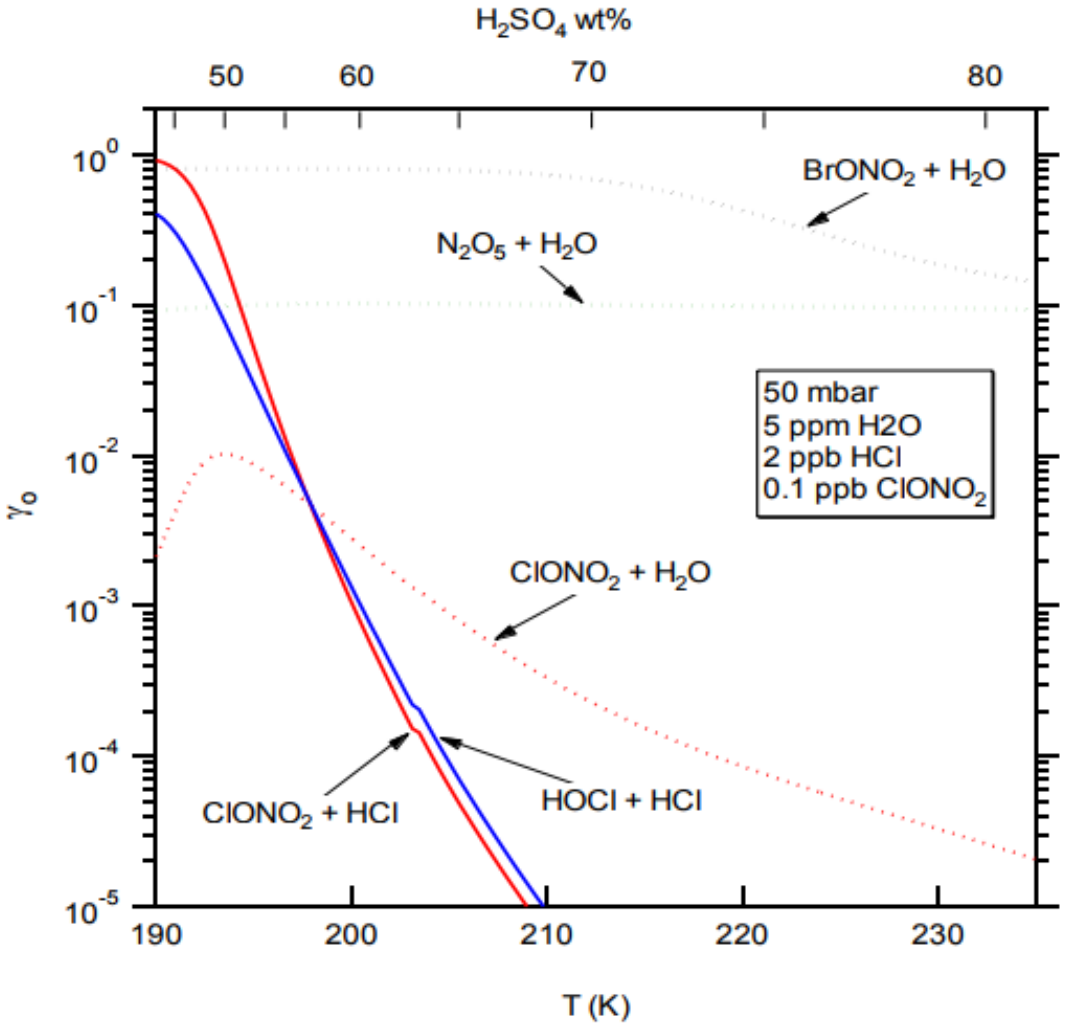

Figure 2.3: Reactive uptake coefficients for several stratospherically relevant reactions as a function of temperature and acid weight percent at the conditions noted. Figure adapted from the JPL Data Evaluation.[43]

Additionally, figure 2.3 presents γ values for reaction 1.23, the hydrolysis of N_2O_5. This reaction occurs with high efficiency across all relevant temperatures and aerosol acid compositions. The combination of reactions 1.31 – 1.33 with reaction 1.23 can lead to the massive enhancement of $\frac{Cl_x}{Cl_y}$ ratios as a result of atmospheric denitrification.

$$N_2O_5 + H_2O + M \xrightarrow{\text{aerosol}} 2HONO_{2(a)} + M \tag{1.23}$$

The heterogeneous reaction of bromine nitrate with water, 2.6 demonstrates little variance at all relevant temperatures with an uptake coefficient about 1000 times greater than the analogous chlorine reaction and a mass accommodation coefficient of about 0.8.[83] The corresponding reaction with iodine is also expected to be highly favored, in keeping with the alpha efficiency factor scaling of the halogen species.[84]

$$BrONO_2 + H_2O \xrightarrow{\text{aerosol}} HOBr + HONO_2 \tag{2.6}$$

Though the actual γ value of a given reaction is complicated function of the specific environmental parameters which dictate the aerosol acid-fraction composition and temperature, the general trend indicated in figure 2.3 holds across the relevant temperature and pressure ranges discussed later in this thesis with respect to processing rates on volcanic aerosols.

3

Volcanism

Tectonics and Volcanic Zones

The continents of the Earth float atop tectonic plates. These plates are in constant motion, moving apart from one another in some places, called a divergent plate boundary, and colliding with each other in other places, known as convergent plate boundaries. Volcanism occurs at both types of plate boundary; however, the character of this volcanism is highly specific to plate boundary type.

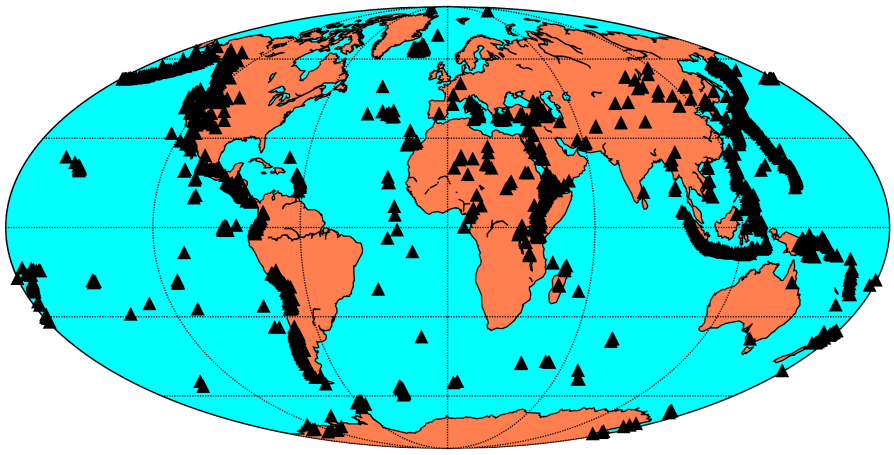

Figure 3.1: Map projection of 1551 volcanoes known to have erupted in the prior 500 years. Data courtesy of Global Volcanism Project. [85]

Mid-Ocean Ridges (MORs) form at divergent plate boundaries. There, basaltic magma rises to the surface and cools, forming new oceanic crust known as Mid-Ocean Ridge Basalt (MORB). Most MOR volcanism is effusive in character due to the combination of low viscosity, high-temperature basaltic magma and low interfacial pressure differentials between the subsurface and the ocean floor, though MOR explosive eruptions have been observed when the magmatic carbon dioxide loading is very high.[86] Regardless, because MORs are situated below a 3.6 km column of water (on average), neither effusive nor explosive MOR volcanic eruptions are capable of directly influencing the state of the stratosphere under normal circumstances.

Subduction Zone (SZ) volcanism occurs at convergent plate boundaries, wherein one plate subducts beneath another forming a trench. The crust of this plate carries water and hydrated minerals along with it, and this water is released to the mantle above, reducing the melting point of the magma. By this process, high-melting point silicic minerals such as andesite may begin convecting to the surface. As the silicic magma ascends, it encounters lower pressures. This has several effects: (1) lower pressure enhances the melt fraction of magma, and (2) dissolved trace gases begin to exsolve, forming bubbles. As the pressure further decreases, water also exsolves from the magma, producing a very brittle and extremely viscous magma prone to explosive fragmentation.

Because of its explosive character and interface with the atmosphere (e.g., high pressure differential), SZ volcanism is responsible for the overwhelming majority of stratospherically relevant eruptions. Figure 3.1 illustrates over 1500 known volcanic eruptions occuring within the prior 500 years. With few exceptions these eruptions trace out the SZ boundaries, forming what is known as 'the ring of fire'. Linear chains of islands, called island volcanic arcs, tend to form at these locations when

they are undersea (e.g., Sunda Arc, Aleutian Islands, Lesser Antilles). Beneath continental shelves, SZ volcanism produces continental arcs (e.g., Cascade Volcanic Arc, Kamchatka, Central America Volcanic Arc).

When volcanoes are formed outside of plate boundaries they are known as Hot-Spot (HS) volcanoes. Islands formed from HS volcanism are readily identified – they characteristically develop in linear chains exhibiting age progression from one end to another as is famously the case in Hawaii and Tahiti. HS volcanoes are typically basaltic in character and rarely explosive.

Classification of Eruptions

Table 3.1: Comparison of VEI and Magnitude, Sulfur Yield, and Column Height

Eruption	Year	VEI	Magnitude	Sulfur Yield (Tg S)	Column Height (km)
Taupo	$\approx$ 181	7	6.9	6.5	51
Baitoushan	$\approx$ 969	7	6.8	2	25
Samalas[a]	1257	7	>7	79	40
Kuwae?	1452	7	6.9	40	>20
Huaynaputina	1600	6	6.3	23	46
Tambora	1815	7	7.1	28	43
Krakatau	1883	6	6.5	15	25
Santa Maria	1902	6	6.3	11	34
Katmai	1912	6	6.4	10	32
Agung[b]	1963	5	5	6	>20
Mt St Helens	1980	5	4.9	0.5	19
El Chichón	1982	5	5.4	3.5	32
Pinatubo	1991	6	6.3	10	34

Table entries adapted from Oppenheimer (2003) unless otherwise noted.[87]
[a]Lavigne et al. (2013)[88], Vidal et al. (2015)[89], Vidal et al. (2016)[90]
[b]Rampino and Self (1982)[91], Self and King (1996)[92]

Eruptions may be classified according to the mechanism of their initiation, the categorical type they resemble (named after archetypical volcanoes), or by metrics of intensity and magnitude. These are briefly described in the following.

Of the mechanisms of volcanic initiation, there exist three main types: magmatic, phreatic, and phreatomagmatic. Magmatic eruptions originate from magmatic processes – typically the explosive fragmentation of magma as it nears the surface from exsolved gases. Magmatic eruptions can be of very long duration, lasting months-to-years as magma continuously transports toward the surface. Phreatic eruptions occur when groundwater intrudes on a magma plume and vaporizes. These eruptions are transient and explosive in character. Phreatomagmatic eruptions combine attributes of both phreatic and magmatic eruptions.

Volcanic eruptions are qualitatively classified according to six named types (listed in order of increasing explosivity): Hawaiian, Strombolian, Vulcanian, Peléan,Plinian, and Ultra-Plinian. Hawaiian eruptions are basaltic, effusive, of long duration, and with little-to-no eruption column. Strombolian eruptions feature frequent small explosions. Vulcanian eruptions are highly explosive and low in intensity. Peléan eruptions are explosive and ashy, producing pyroclastic flows. Plinian and ultra-Plinian eruptions are more explosive, with tall eruption columns penetrating into the stratosphere, frequently collapsing to form pyroclastic flows.

There exist two primary classifications of the intensity of a volcanic eruption: The Volcanic Explosivity Index (VEI) introduced by Newhall in 1982 and the scaling of eruption magnitude in-

troduced by Pyle in 2000.[93–95] Both types feature logarithmic scaling with intensity; however, VEI expresses the total volume of material displaced while the magnitude scaling expresses total mass of material displaced. This is a nuanced but important distinction, magmatic materials and displaced rock dominate the VEI scale while volcanic gases are largely neglected. The chemical and climate impact of a volcanic eruption is thus correlated with, but slightly agnostic toward, VEI. On the other hand, the magnitude scaling more appropriately scales with potential stratospheric impact.

The VEI scale spans between 0 – 8. Hawaiian-type eruptions are typically rated between 0 and 1, Strombolian eruptions are frequently VEI 1 – 2, Vulcanian eruptions span 2 – 3, Plinian eruptions feature explosivity indices between 4 – 5, and ultra-Plinian eruptions exceed 6. For indices greater than 3, VEI scales logarithmically with ejecta volume. A VEI 3 eruption produces 0.01 km^3 ejecta, a VEI 4 eruption 0.1 km^3, a VEI 5 eruption 1 km^3, an so on.

The eruption magnitude scale is defined per equation 3.1, in which m is the mass of erupted materials in kg. The offset of 7 generally aligns the eruption magnitude scale with VEI, with some distinction. Table 3.1 indicates the correspondance between VEI and magnitude scaling for several historical events.

$$M_e = \log_{10}(m) - 7 \tag{3.1}$$

Figure 3.2 provides explosive volcanic eruptions as a function of latitude and date before the present. Because the historical record is incomplete and because geological records are compromised by subsequent volcanic activity, bias toward larger eruptions is evident farther in the past. While

VEI 7+ events are relatively infrequent, as indicated by the maroon stars, smaller VEI 5 and VEI 6 eruptions are expected to occur multiple times a century. High latitude explosive eruptions are observed to be relatively infrequent, though this is likely due to a combination of (a) reduced surface area in high latitude zones, (b) reduced land area in high latitude zones, (c) a paucity of historical record from inhabitants at high latitudes, (d) reduced rates of magmatic melt formation due to compressional forces from glaciation, and (e) difficulty in obtaining geological records in high latitude environments. Panel (b) provides the same data as in panel (a), except for only eruptions in the common era. VEI 4 and VEI 5 eruptions are seen to be exceedingly common. Records of high-latitude eruptions begin to appear around the era of polar exploration.

Trace Gas Constituents of Volcanic Gas Inventories

It is apparent in Table 3.1 that eruptive stratospheric sulfur yield does not necessarily scale with eruption size. Some volcanic eruptions are comparatively small, with very rich stratospheric sulfur gas components, as was the case during the 1963 eruption of Gunung Agung while other eruptions are quite depleted relative to the total mass ejected.

The major volatile components of magma – H_2O, CO_2, S, F, Cl – and important trace components – such as Br, I, Hg – vary greatly between magmas of different composition. For example, subduction zone andesites and rhyolites tend to be highly enriched in halogen species relative to mid-ocean ridge basalts (MORB) likely due to (a) the subduction of halogen-enriched crust in crustal recycling processes, (b) differential sequestration of Cl in magmatic fluids.[96] Similarly, due to geolog-

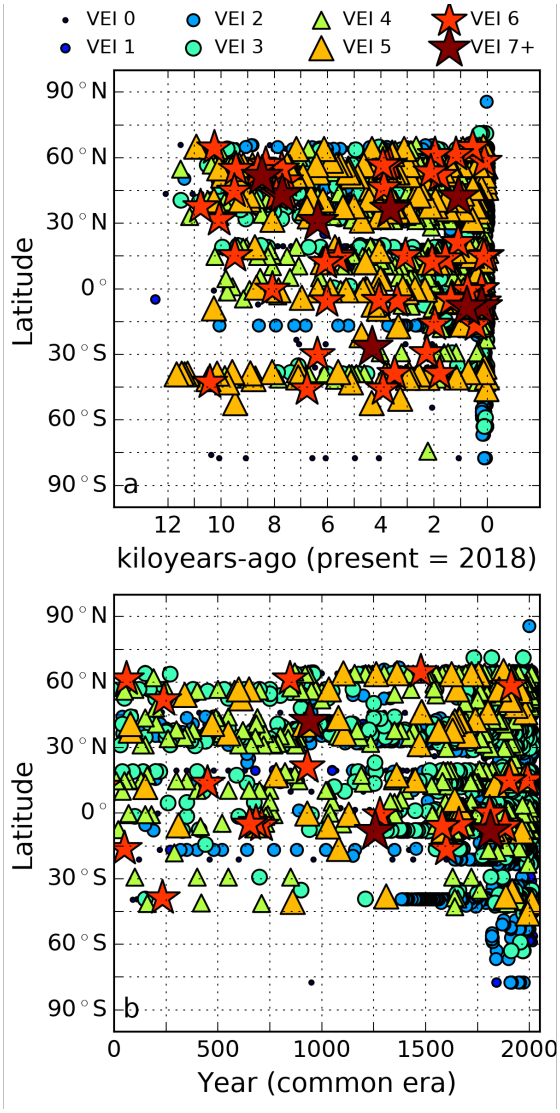

Figure 3.2: (a) Known volcanic eruptions for which VEI indices have been calculated are presented as a function of date and time (kya). Incomplete historical records and compromised geological records result in a detection bias toward larger volcanic eruptions for historical eruptions. (b) The same as in panel (a), except only eruptions occurring between 0 C.E. and the present are shown. Data courtesy of the Global Volcanism Project.[85]

ical, geochemical, and geographical reasons, SZ island-arc basalts tend to be greatly enriched in sulfur relative to MORBs.[97]

Complex processes of exsolvation and fractionation of volatile gas components can enhance the relative concentrations of volatile species as magma rises. A frequently encountered phenomenon is the so-called "excess sulfur problem" in which masses of sulfur released to the atmosphere cannot be rectified with quantities estimated to have been released from petrological analysis. This problem is likely produced by the long term, pre-eruptive storage of degassed volatiles in the magma chamber. Small eruptions from sulfur-poor magma can, via this process, produce large releases of sulfur compounds. Similar processes have been invoked to account for excesses released volcanic halogens.[90,98]

The Eruption Column

When gases, ash, and debris are ejected from a volcano, they form an eruption column, composed of several characteristic regions: the gas thrust region, the convective thrust region, and the umbrella region.

Volcanic gas carries with it some momentum as it expands from the high pressure magma chamber to the atmosphere. The mass ejection rate is given in equation 3.2 in which ρ_0 is the bulk density, R_0 is the vent radius, and U_0 is the exit velocity. At some point, gravity and friction with (and entrainment of) the surrounding atmosphere counters this momentum. Depending on the strength of the eruption, this region of zero gas thrust momentum may occur immediately at the crater rim to several km above the crater rim. At this point, convective thrust drives vertical transport within

the eruption column. Air parcels within the eruption column are considerably buoyant and will convect to their point of neutral buoyancy where the parcels will diffuse horizontally, forming the umbrella cloud.

$$M_0 = \pi \rho_0 R_0^2 U_0 \tag{3.2}$$

The maximum height of an eruption column is limited by the amount of heat transferred to the atmosphere per unit time. Individual eruptions may be classified in a logarithmic scaling by their mass ejection rate (alternatively magma eruption rate) per equation 3.3 in kg / s, where M_0 is the mass ejection rate from the previous equation. A simple and approximate metric provides the maximum height (in meters) as a function of power (in Watts) as in equation 3.4.[95] And thus a 15 km eruption column must be fed by a sustained 11 TW volcanic input of heat.

$$\text{Intensity} = \log_{10}(M_0) + 3 \tag{3.3}$$

$$H = 8.2 \times Q^{0.25} \tag{3.4}$$

A more sophisticated treatment indicates that the maximum height of an eruption column is a function of the mass ejection rate (kg / s) and the Brunt-Väisälä frequency, N, per equation 3.5, where $k_1 + k_2 = 1$.[99] The Brunt-Väisälä frequency itself is a function of temperature lapse rate, Γ, the Earth's gravitational acceleration, g, and the specific heat capacity of the air, c_p, as expressed in

equation 3.6.[99]

$$H \propto N^{-k_1} M_0^{k_2} \tag{3.5}$$

$$N^2 = \frac{g}{T}\left(\frac{g}{c_p} - \Gamma\right) \tag{3.6}$$

Maximal eruption height is thus a product of many factors which will vary according to geography, geology, and meteorology.

The Pinatubo Eruption as a Case Study

The VEI 6, magnitude 6.3 eruption of Mount Pinatubo remains the largest volcanic eruption of the satellite era and is the canonical case study for investigations of the interaction of volcanoes with the stratosphere.

Date, Location and Meteorology

Mount Pinatubo is situated on the island of Luzon at 15.1°N and 120.3°E in the country of the Phillipines and produced a series of eruptions in June 1991. The volcano was thought to be dormant prior to its 1991 activity. The paroxysmal eruption coincided with the simultaneous landfall of a tropical cyclone, Yunya, producing prodigious lahar flows.[100,101]

1991 Eruptive Sequence

A magnitude 7.8 earthquake centered 60 miles to the northeast of Mount Pinatubo on July 16, 1990 provided the first indications that the volcano was no longer dormant. Following the earthquake, steam emissions were observed and small phreatic explosions followed in March and April of 1991.[102] Seismic monitors were placed on the mountain in April of 1991 following reports of increased seismicity by locals and volcanologists were able to successfuly forecast the escalating eruptive potential prior to the onset of explosive eruptive activity.[103] Magma first reached the surface on June 7th; however, it was pre-degassed and effusive. Lava flows continued for 6 days, producing a large lava dome.[104] The first explosive eruption at Mount Pinatubo occured on June 12, the eruption column reaching a height of 20 km. Further stratosphere-penetrating eruptions occured on June 13th and June 14th. On June 15th, the largest eruption occurred, ejecting some 1.3×10^{13} – 1.8×10^{13} kg of material over the course of 9 hours at an average rate of up to 550 kt of ejecta per second.[87,102] The eruption terminated with a caldera collapse.

Enhancement in Stratospheric Sulfate Aerosol

Of the 1.3 – 1.8 $\times 10^{16}$ g of material ejected from the volcano, approximately 2×10^{13} g SO_2 and 1×10^{15}g H_2O were emitted to the tropical stratosphere.[105–108] Subsequent oxidation rapidly produced 32 Tg of sulfate aerosol.[109,110] Figure 3.3 demonstrates the extraordinary enhancement in aerosol number density from El Chichón and Pinatubo aerosols which persisted for several years.

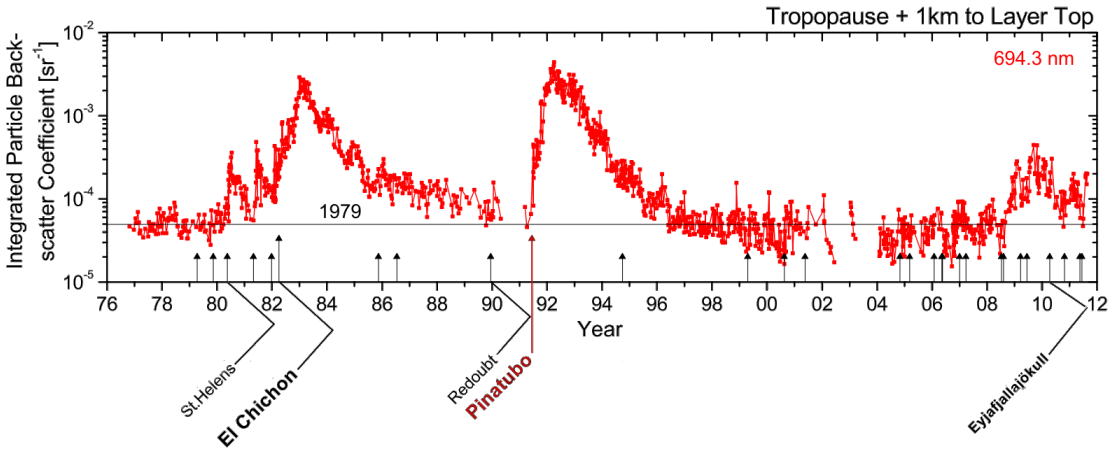

Figure 3.3: Longitudinal aerosol backscatter at 700 nm. Figure adapted from WMO 2014.[29]

Radiative Impact of a Volcanic Aerosol Veil

The Pinatubo aerosol cloud quickly spread to produce a zonal band. Within months, the veil mixed meridionally, forming a global stratospheric aerosol veil. Figure 3.4 provides the temporal evolution of the Pinatubo aerosol veil as a function of latitude. It is evident that the aerosol cloud traversed the equator with nearly equal distribution. Reconstructed aerosol enhancement following historical volcanic eruptions are also depicted in figure 3.4 spanning the years 1850 – 2000. Notably, not every eruption produced a global aerosol veil. Askja (1875), Bandaisan (1888), Kyudach (1907), and Novarupta (1912), high latitude northern hemisphere volcanoes, produced hemispherically-confined volcanic aerosol veils. Of the confirmed eruptions that perturbed aerosol in both hemispheres, all lay within the tropics.

Figure 3.5 demonstrates the growth and decay of aerosol effective radius as a function of time following a volcanic eruption. It is seen that, following a large volcanic eruption, the effective radius in-

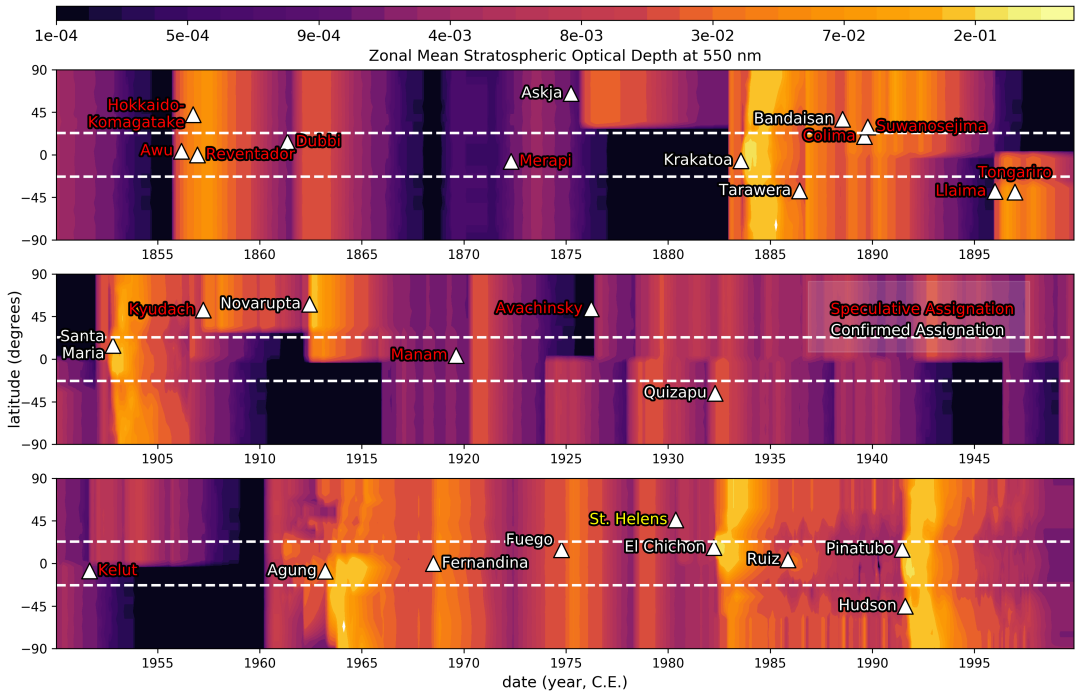

Figure 3.4: Zonal mean stratospheric Optical Depth at 550 nm. Optical depths are plotted as a function of latitude and year: 1850 – 1900 (top), 1900 – 1950 (center), and 1950 – 2000 (bottom). Tropical bands are indicated by dashed white lines. Volcanic eruptions are indicated by white triangles. Identity of volcanic eruptions producing the subsequent aerosol enhancement are indicated as speculative (red) or confirmed (white). Data obtained from NASA GISS. [111,112]

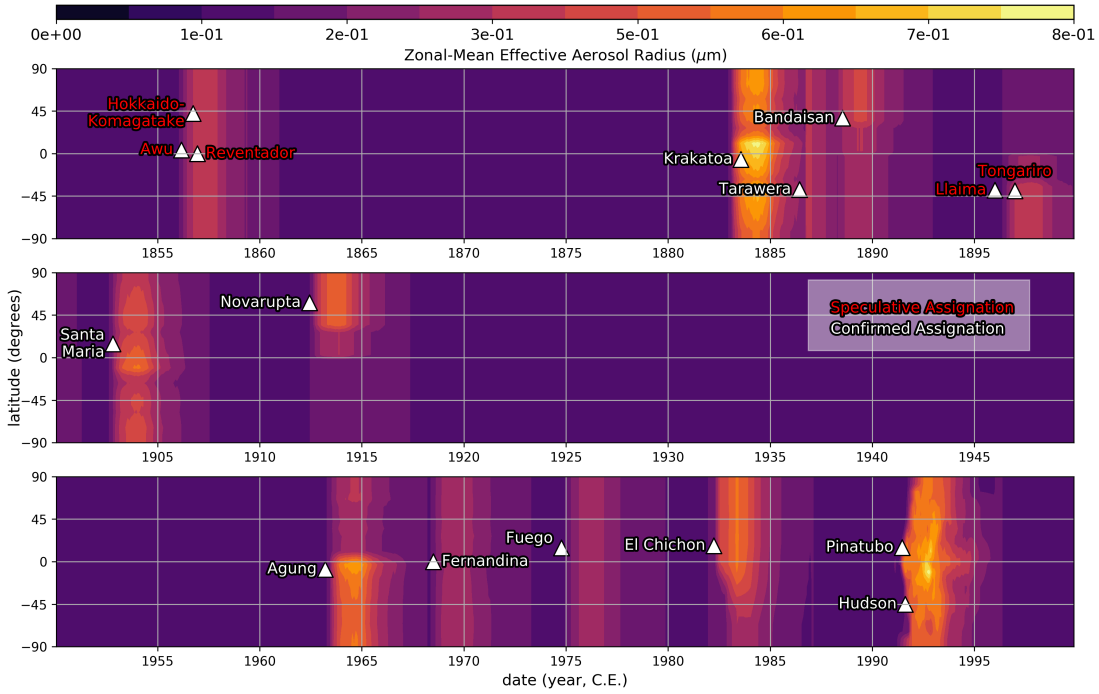

Figure 3.5: Zonal mean aerosol effective radius between years 1850 – 2000. Aerosol effective radius is plotted as a function of latitude and year: 1850 – 1900 (top), 1900 – 1950 (center), and 1950 – 2000 (bottom). Volcanic eruptions are indicated by white triangles. Identity of volcanic eruptions producing the subsequent aerosol enhancement are indicated as speculative (red) or confirmed (white). Data obtained from NASA GISS. [111,112]

creases by up to 8-fold over the background. The aerosol effective radius provides a metric by which the radiative perturbation of an aerosol distribution can be measured – the area of a particle is proportional to the amount of incident radiation scattered. Aerosols with effective radius smaller than 2 μm are expected to cool the surface while aerosols with effective radius greater than this value are expected to warm the surface due to increased reradiation to the surface of buffered infrared.[113;] From this figure one can see that radiative perturbations from volcanic aerosol clouds varied between (a) volcanic eruptions, (b) hemispheres, and (c) temporally. Following the eruption of Pinatubo, the aerosol effective radius slowly grew to about 600 – 800 nm over two years, after which removal processes resulted in a decay back to the background levels. In all cases, aerosol remained at an effective radius smaller than 2 μm.

The effect of stratospheric aerosol on the radiative balance of the surface is drawn in a schematic in figure 3.6. Shortwave radiation incident on the aerosol cloud is scattered to some degree, upwards of 20% following the eruption of Mount Pinatubo in some locations.[100,114,115] Half of this light is directed downward as diffuse radiation, producing a whiter sky.[116] A portion of this light is scattered back to space. The planetary albedo is enhanced, and as a result, the surface forcing from shortwave radiation is reduced. The surface cools. Meanwhile, outgoing infrared radiation is trapped in the aerosol veil, producing local stratospheric heating. Following Pinatubo, this effect was large and resulted in an enhancement in the equator-to-pole temperature gradient. Following high-latitude eruptions, this effect is likely to reduce the equator-to-pole temperature gradient, with corresponding impact on corresponding large-scale circulation patterns.[116–118]

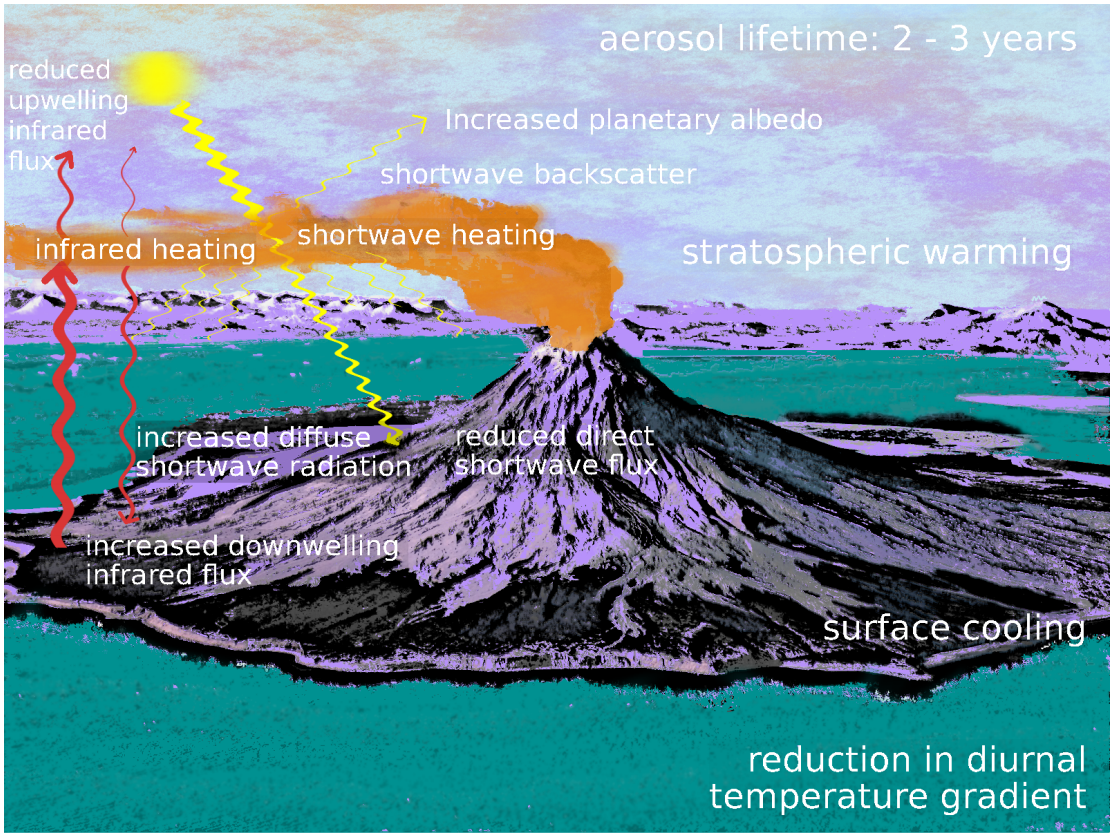

Figure 3.6: Cartoon schematic of the interaction of volcanic aerosol with the radiative balance of the Earth.

Stratospheric Ozone Impact of Mount Pinatubo

Ozone inventories are perturbed by both radiative-dynamical and heterogeneous chemical factors: while negative zonal ozone anomalies exceeding 10% were observed over populated northern mid-latitude regions during the two years following the eruption of Mount Pinatubo, no similar ozone loss was observed in the Southern Hemisphere due to changes in stratospheric circulation – despite similar levels of aerosol loading in the southern hemisphere.[119–125] Figure 3.7 depicts the change in column ozone between 35°N – 60°N. Temperature increases of up to 3 K in the Northern midlatitude stratosphere were observed, resulting in the upwelling of ozone-poor air, accounting for some of the characterized ozone column losses.[120,126]

The majority of the Mount Pinatubo ozone anomaly is ascribed to halogen chemical processing. Volcanic sulfate aerosol enhances the partitioning of chlorine radicals from their stable reservoirs, HOCl, HCl, and ClONO2, while simultaneously suppressing the rate of reservoir recombination. Notably, this mechanism only occurs when substantial stratospheric chlorine reservoirs exist. While there was no detectable stratospheric enhancement of HCl due to Mount Pinatubo, the eruption occurred near the period of peak long-lived anthropogenic halocarbon loading, ensuring ample available stratospheric chlorine for the initiation of ozone depletion catalysis.[127]

Pinatubo-Like / Pinatubo-Scale Eruptions

The meteorological conditions accompanying the paroxysmal explosion of Mount Pinatubo were highly unusual and resulted in the total tropospheric hydrometeor scavenging of volcanic hydro-

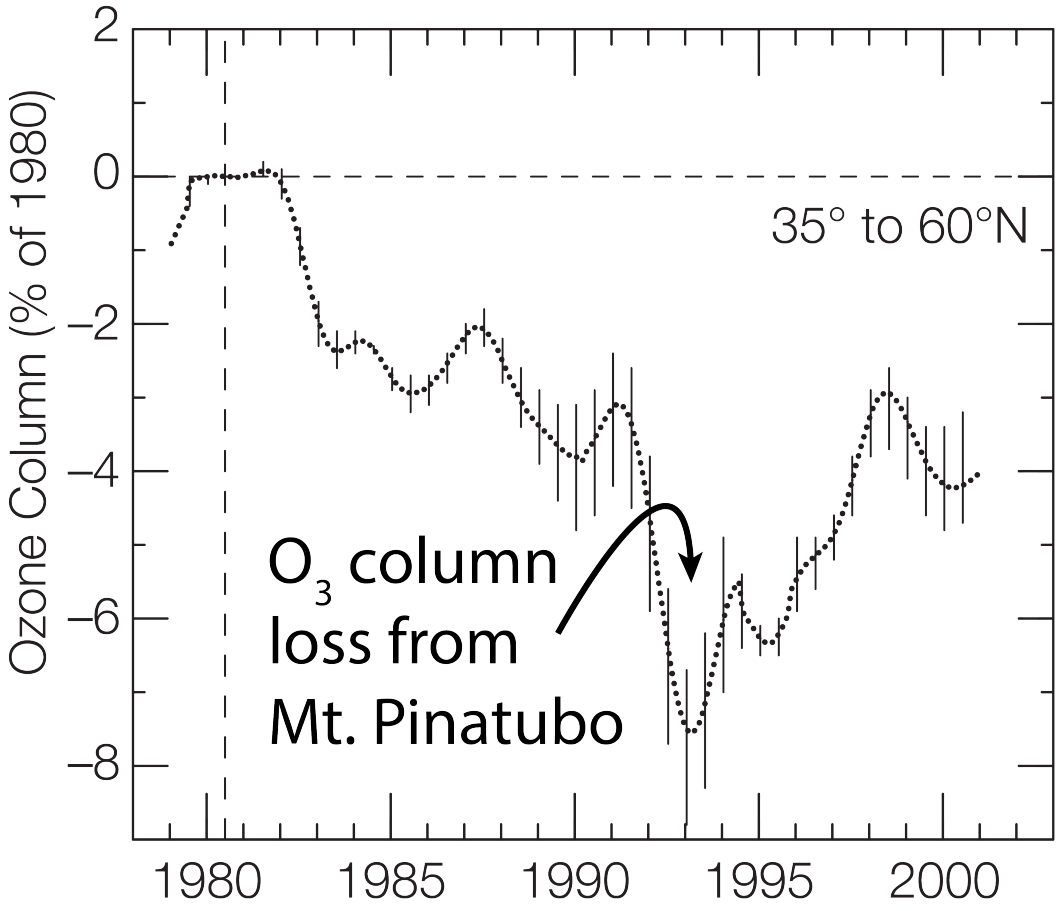

Figure 3.7: QBO-corrected northern mid-latitude ozone column deviations (TOMS) from 1980 levels as a function of year. Enhanced stratospheric aerosol loading following the 1991 eruption of Mt. Pinatubo produced marked ozone losses the two years following. Figure adapted by author from Salawitch, et al. [119]

gen halide species. Specifically, in a great coincidence, tropical cyclone Yunya directly transited the Mount Pinatubo volcanic plume, significantly enhancing the moisture content of parcels within the eruption column entrainment zone and essentially completely removing the inorganic halogen species before they could reach the stratosphere.[101]

For the following chapters, eruptions during which the stratospheric injection of halogens is negligible are referred to as *Pinatubo-like eruptions*. A Pinatubo-like eruption will, by definition, input SO_2 to the stratosphere; however, the amount of SO_2 injected does not have to be Pinatubo-scale – defined as matching the estimated 14 - 21 Tg SO_2 stratospheric injection mass of Mount Pinatubo.

Thus human beings are now carrying out a large scale geophysical experiment of a kind that could not have happened in the past nor be reproduced in the future. Within a few centuries we are returning to the atmosphere and oceans the concentrated organic carbon stored in sedimentary rocks over hundreds of millions of years. This experiment, if adequately documented, may yield a far-reaching insight in to the processes determining weather and climate.

Roger Revelle and Hans E. Suess (1957)

4

The Changing Climate and Stratosphere

Radiative Equilibrium and the Greenhouse Effect

The Earth is a system that exists in radiative equilibrium with its surroundings. Shortwave solar forcing provides an energy input resulting in surface heating, as indicated in equation 4.1, where R is the radius of the Earth, F is the solar constant (Wm^{-2}), and M is the albedo. The surface subsequently emits an equal amount of longwave radiation according to the Stefan-Boltzmann law, equation 4.2,

in which σ is the Steffan-Boltzmann constant, A is the surface area of the Earth, and T is the temperature of the surface.

$$\text{Energy absorbed} = \pi \mathrm{R}^2 \mathrm{F}(1 - \mathrm{M}) \tag{4.1}$$

$$\text{Flux} = \mathrm{A}\sigma \mathrm{T}^4 \tag{4.2}$$

From these two relations, one can determine the effective temperature of the planet, T, as demonstrated in equation 4.3. For the Earth, this value is about 253 K, much cooler than the average surface temperature of the planet of 288 K. This residual, the observed temperature minus the effective temperature, is an effect of the Earth's atmosphere. Some amount of heat is partitioned and re-emitted to the surface. Thus, the surface can have a temperature greater than the effective temperature produced from solar heating alone; however, because the Earth is in radiative equilibrium with the Sun – an observer in space would observe the mean thermal temperature of the Earth to be the effective temperature of the planet. That is, there is a layer of the atmosphere above the surface from which escaping infrared radiation originates.

$$\mathrm{T} = \sqrt[4]{\frac{F\,(1 - \mathrm{M})}{4\sigma}} \tag{4.3}$$

Greenhouse Gases

This phenomenon, an atmosphere translucent to incoming solar radiation and opaque to outgoing infrared radiation, is known as the greenhouse effect. Those gases which are opaque to infrared radiation are known as greenhouse gases. Molecular absorption of radiation follows the Lambert-Beer law – for unsaturated transitions, the opacity of the atmosphere scales linearly with number of absorbers.

A number of important greenhouse gases are presented in figure 4.1. From top-to-bottom: carbon dioxide, perhaps the most notorious greenhouse gas, exhibits a very strong absorbance between 2400 – 2200 Kayser. In the Earth's atmosphere, this absorbance is saturated, and scales with the order $\ln(CO_2)$ from collisional-broadening effects. Methane features a sharp C-H stretch at 3020 K and a deformation mode at 1305 K. Water is a strong absorber of IR, with many rotational lines between 4000 – 3500 K and 2000 – 1000 K. Like carbon dioxide, nitrous oxide also absorbs strongly between, 2300 – 2100 K. HFC-41 (fluoromethane) is an extremely strong greenhouse gas with very strong C-H transitions. Likewise, HCFC-22 (Chlorodifluoromethane) presents strong C-F and C-Cl stretches at 1100 and 800 K in addition to slight C-H activity. CFC-11, representative among the CFCs, also absorbs IR radation; however, for obvious reasons, the absorbance is confined only to the C-F and C-Cl stretches.

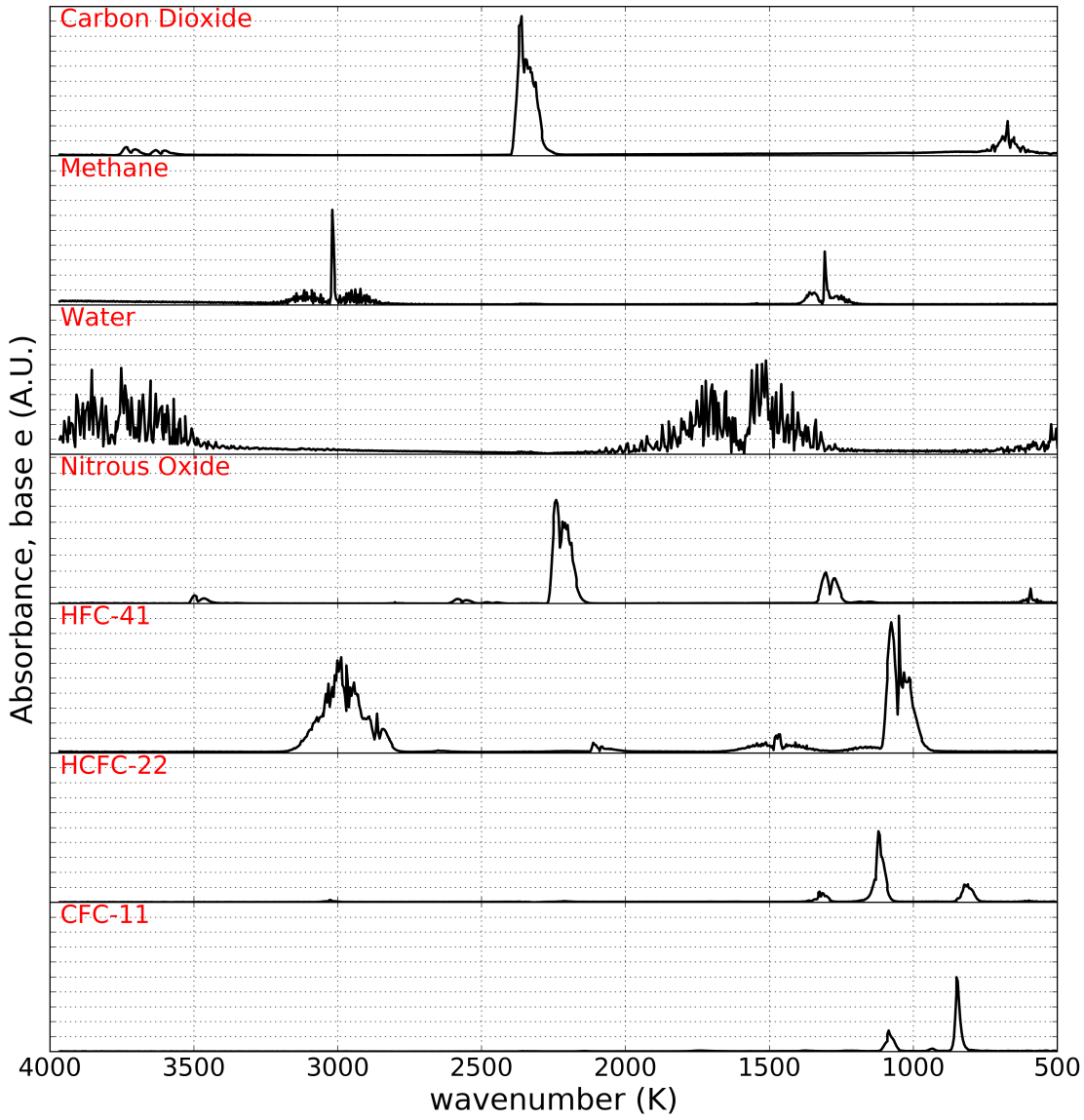

Figure 4.1: Infrared absorbance spectra of important trace gas atomspheric absorbers. Data obtained from the NIST Webbook. [128]

Table 4.1: Atmospheric Lifetime, Ozone Depletion Potential, Global Warming Potential of Selected Molecules

Species	Lifetime (years)	ODP (CFC-11 eq.)	GWP (20 year)	GWP (100 year)	GTP (20 year)	GTP (100 year)
Miscellaneous Trace Gases						
Carbon Dioxide	5 – 200[a]	0	1	1	1	1
Methane	12.4	0	84	28	67	4
Water[b]	1×10^{-3}	–	–	–	–	–
Nitrous Oxide	121	0.017	264	265	277	234
Sulfur Hexafluoride	3,200	0	17,500	23,500	18,900	28,200
Selected Hydrofluorocarbons						
HFC-23	222.0	0	10,800	12,400	11,500	12,700
HFC-41	2.8	0	427	116	177	16
HFC-125	28.2	0	6,090	3,170	5,800	967
Selected Hydrofluorochlorocarbons						
HCFC-22	12	0.05	5,160	1,810	4,200	262
HCFC-123	1.3	0.06	292	79	98	11
HCFC-141b	9.2	0.11	2,550	782	1,850	111
Selected Chlorofluorocarbons and (Hydro)chlorocarbons						
CFC-11	45	1	6,730	4,750	6,890	2,340
CFC-113	85	0.85	6,490	5,820	6,730	4,470
CFC-115	1,020	0.5	5,860	7,670	6,310	8,980
Carbon Tetrachloride	26	0.82	3,480	1,730	3,280	479
Methylene Chloride	0.4	0.4	33	9	10	1
Chloroform	0.4	0.2[c]	60	16	18	2
Selected Halons and Bromocarbons						
Methyl Bromide	0.8	0.7	9	2	3	<1
Methylene Bromide	0.3	0.2[d]	4	1	1	<1
Halon-1211	16	6	4,590	1,750	3,950	297
Halon-1301	65	12	7,800	6,290	7,990	4,170
Halon-2402	20	8.6	3,440	1,470	3,100	304

Table entries compiled from IPCC AR5 (2013) (GWP) and WMO Ozone Assessment Report No. 55 (2014) (ODP) unless otherwise noted.[52,129]

[a] The atmospheric lifetime of carbon dioxide is complex and governed by biogeochemical equilibria. Refer to Archer et al. (2009) for an excellent review of the topic.[130]

[b] Though it is a strong greenhouse gas, water vapor participates in a complicated climate change feedback cycle and its GWP is not calculated. Refer to Held and Soden (2000) for more information[131]

[c] Hossaini et al. (2015)[132]

[d] Zhang et al. (1997)[133]

Metrics for Perturbations of Greenhouse Gases on Ozone and Climate

Global Warming Potential

The total impact of a greenhouse gas perturbation on the heat partitioning of the atmosphere is a function of the atmospheric lifetime of the species, usually defined as the e-folding time of that species. The Global Warming Potential (GWP) provides a metric for quantifying the impact of the superposition of a molecule's radiative efficiency and its chemical lifetime over a specified time period. By definition (equation 4.4), the GWP of species x is always normalized to carbon dioxide, which has a value of 1, where a_x is the radiative efficiency, TH is the time horizon of the integration, and x(t) is the instantaneous value of species x at time t, given an impulse perturbation of x_0 at time t=0.

$$GWP_{(x)} = \frac{\int_0^{TH} a_x \times [x(t)]\, dt}{\int_0^{TH} a_{CO_2} \times \left[CO_{2(t)}\right] dt} \tag{4.4}$$

Global warming potentials for various trace gas species, including those species depicted in figure4.1, are given for 20-year and 100-year time horizon in table 4.1.

Global Temperature-Change Potential

An alternative metric to the GWP, known as the Global Temperature-Change Potential (GTP), relates the expected change in Absolute Temperature Change Potential (ATCP, expressed in K kg^{-1}) resulting from an impulse of a gas relative to the ATCP resulting from the same mass impulse

of CO_2 at the defined time horizon and is presented in equation 4.5 for species x. A derivation of ATCP is beyond the scope of this thesis, but may be found in Shine et al. (2005).[134]

$$GTP_x = \frac{AGTP_x(t)}{AGTP_{CO2}(t)} \tag{4.5}$$

This metric provides an understanding of future behavior that is agnostic to the lifetime of various chemicals, unlike GWP, which uses time-integrated radiative forcing for comparison. For example, identical mass impulses of nitrous oxide (100-year GWP: 265 / lifetime 121 years) and HCFC-123 (100-year GWP: 292 / lifetime 1.3 years) would produce wildly different changes in surface temperature at the time horizon due to their different lifetimes despite their similar GWP values. In this example, the GTP for nitrous oxide is 234 while for HCFC-123 it is 11. GTP values for selected gases are presented in table 4.1.

Ozone Depletion Potential

Many greenhouse gases are also involved in ozone-depletion catalysis. A useful metric for quantifying the relative depletion in ozone produced from an impulse of a gas is the Ozone Depletion Potential (ODP). ODP presents a numeric value for gas x normalized to the expected perturbation from an equivalent impulse of CFC-11, as indicated in equation 4.6. ODP values range from 0 (e.g., HFCs) to the tens (e.g., halons). ODP values for selected molecules are presented in table 4.1.

$$ODP_i = \frac{\delta\,[O_3]_i}{\delta\,[O_3]_{\text{CFC-11}}} \tag{4.6}$$

This value is then multiplied by the mass of the gas impulse, m_i to derive the equivalent mass of CFC-11 (kg), per equation 4.7.

$$\text{Ozone Depletion } [\text{kg CFC-11}]_{eq} = \text{ODP}_i \times m_i \tag{4.7}$$

Equivalent Effective Stratospheric Chlorine

The stratospheric burden of halogenated gases is frequently quantified according to the Equivalent Effective Stratospheric Chlorine (EESC) representation. EESC formulations account for the alpha efficiency of the different halogen species (generally chlorine and bromine, to a lesser extent iodine) and the rate at which halogen species are liberated from the source chemical. Equation 4.8 relates EESC as a function of time, in which c is a scaling constant, α_x is the appropriate alpha factor, n_x is the number of halogens of species x in source gas i, f_i is the fractional decomposition of the source gas i at time t-Γ, and p_i is the surface mixing ratio of the source gas at time t-Γ, where Γ is an offset representing the age of air.[49]

$$\text{EESC}(t\text{-}\Gamma) = c \left(\sum_{i} \sum_{x = \text{Cl/Br/I}} \alpha_x n_x f_i(t\text{-}\Gamma) p_i(t\text{-}\Gamma) \right) \tag{4.8}$$

As described in section 1.10, alpha factors for bromine and iodine are normalized to chlorine, such that $\alpha_{Cl} = 1$. Globally-averaged α_{Br} and α_I are commonly estimated to be 60 and 300, respectively.[52] The fractional dissociation of a halogen-bearing gas is a function of the environment to which the molecule is exposed and the length of time it was exposed to that environment. This is

commonly parameterized to a zonal or global average decomposition rate and the generalized age of air for a parcel at that pressure level and latitude. It is assumed that all halogens are liberated upon decomposition (e.g, for multi-halogen source species the rate limiting step is the first halogen abstraction).

Representative Concentration Pathways and Shared Socioeconomic Pathways

The prognostication of future trends carries inherent uncertainty which increases as the time horizon of prediction widens. The Representative Concentration Pathways (RPCs) attempt to encompass the uncertainty envelope of future greenhouse gas emissions by exploring four storyline scenarios.[135] Scenario end-of-century radiative forcing are 2.6, 4.5, 6.0, and 8.5 W/m^2. The individual storylines are coded according to the end-of-century radiative forcing (e.g., the scenario leading to 2.6 W/m^2 end-of-century forcing is known as RCP2.6).

Each scenario contains emission, concentration, and land-use trajectories.

RCP2.6 is the most optimistic: the end-of-century mean temperature increases by only 2 K. This limitation is achieved via the adoption of transformational bioenergy and renewable energy sources.[136] Carbon-Capture-and-Storage technology (CCS) is deployed in the year 2020 and by the year 2100, nearly all energy is produced via either renewable means or with CCS. Agricultural land conversion is conservative, favoring highly-efficient vegetable crops rather than meat. The world population starts to decrease in the year 2050.

RCP4.5 stabilizes radiative forcing at 4.5 W/m^2 by the year 2100.[137] Like RCP2.6, the global pop-

ulation begins to decrease, though now around the year 2070. Per capita energy use declines from present day values, and energy sources shift from fossil fuels to nuclear and renweable supplies. CCS technology is deployed around the 2030's. Globally, cropland increases, but about 5% of contemporary pasture land is converted to forest.

RCP6.0 presents a scenario of increasing global demand for energy.[138] Greenhouse gas emissions peak in the year 2060, when renewable energy solutions are implemented in response to climatic catastrophe. Renewable energy is rapidly introduced in the year 2060 alongside the deployment of CCS. Population growth continues until the year 2100 and beyond, albeit at a slower rate than present – eastern Europe and Russia experience significant declines in population by the year 2060 while Africa and the Middle East grow at contemporary growth rates.. Pasture land decreases marginally in favor of forestation.

RCP8.5 is the most severe of the modeled storylines, representing a world in which no climate directives guide policy.[139] Populations and economies grow along with energy demand, which is supplied by fossil fuel technologies. In particular, coal utilization represents a 10-fold increase over contemporary rates by the end of the century. Even so, oil use declines slowly over the course of the century. Forests are cleared for cropland, significantly so in Latin America and Africa. The world grows to 12 billion inhabitants by 2100, and the majority of the growth is centered in Sub-Saharan Africa and portions of Asia.

Figure 4.2 presents calculated lapse rates for each RCP scenario in the year 2100. Notably, and expectedly, RCP2.6 resembles most closely the 1979 – 1995 average value while increasing radiative forcing scenarios diverge ever more greatly. All scenarios diverge from the plotted 1979 – 1995 aver-

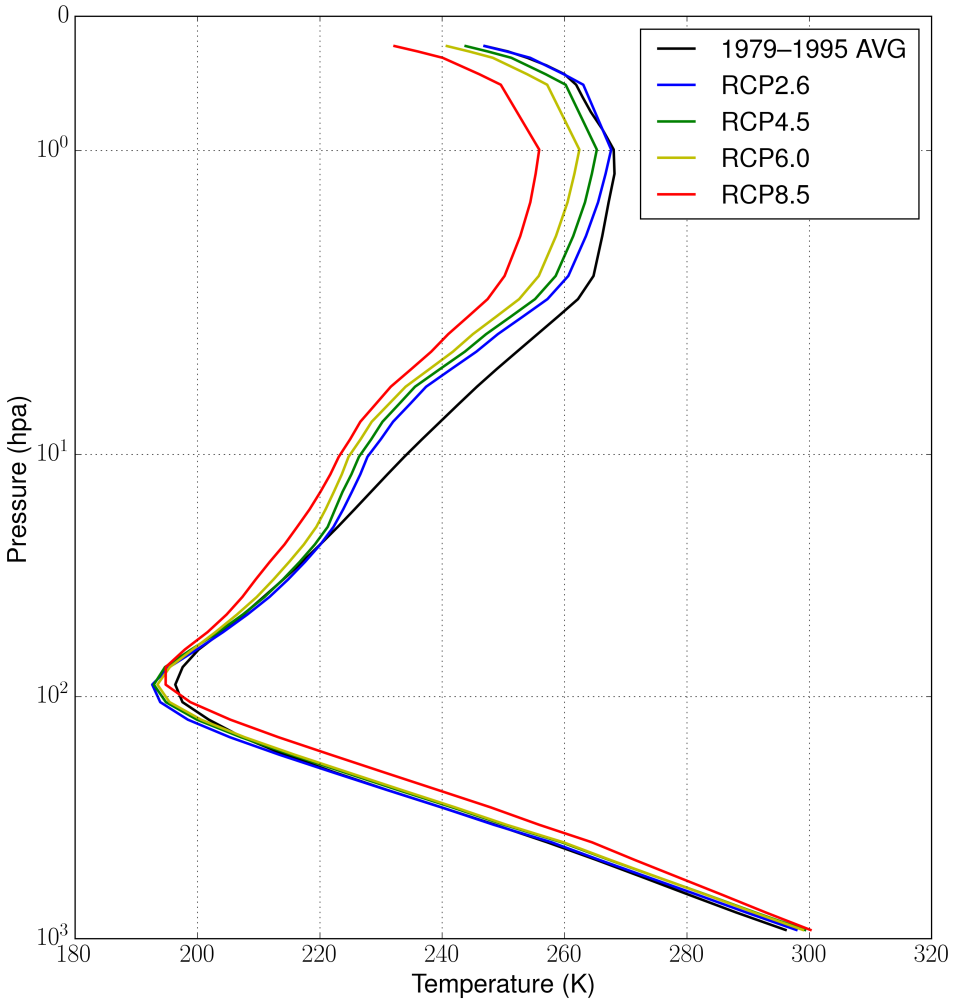

Figure 4.2: Vertical profile of midlatitude summertime temperatures as a function of RCP scenario for the year 2100. RCP Temperature fields recovered and adapted from Watanabe et al. (2011).[140] Climatological average fields from Fleming et al. (1999).[141]

age due to data treatment differences between the two sources.[140,141]

For the purposes of the work performed in this thesis, RCP concentration trajectories were employed, as parameterized by Meinshausen et al. (2011).[142] These trajectories will be explored for each storyline in the following section. It is important to note that the RCP emissions trajectories do not account for speculative releases of greenhouse gases – including releases of carbon dioxide, methane, ethane, and nitrous oxide from thawing permafrost.

Trends in the Emissions of Stratospherically Relevant Gases

Carbon Dioxide

Though CO_2 does not directly participate in chemical reactions, trends in the future emission of CO_2 significantly impacts the future thermal structure of the stratosphere. Figure 4.3a) demonstrates the trend in CO_2 as a function of RCP scenario. All storylines feature increases in CO_2 mixing ratios relative to the year 2000; however, RCP2.6 peaks in mid-century due to the adoption of clean energy technology combined with decreasing energy demand from a declining world population. Carbon emission under RCP4.5 plateaus to around 500 ppmv by the end of the century. In both RCP6.0 and RCP8.5 carbon emissions continue to increase by the century's end; however, in RCP8.5, CO_2 mixing ratios exceed an astonishing 900 ppmv.

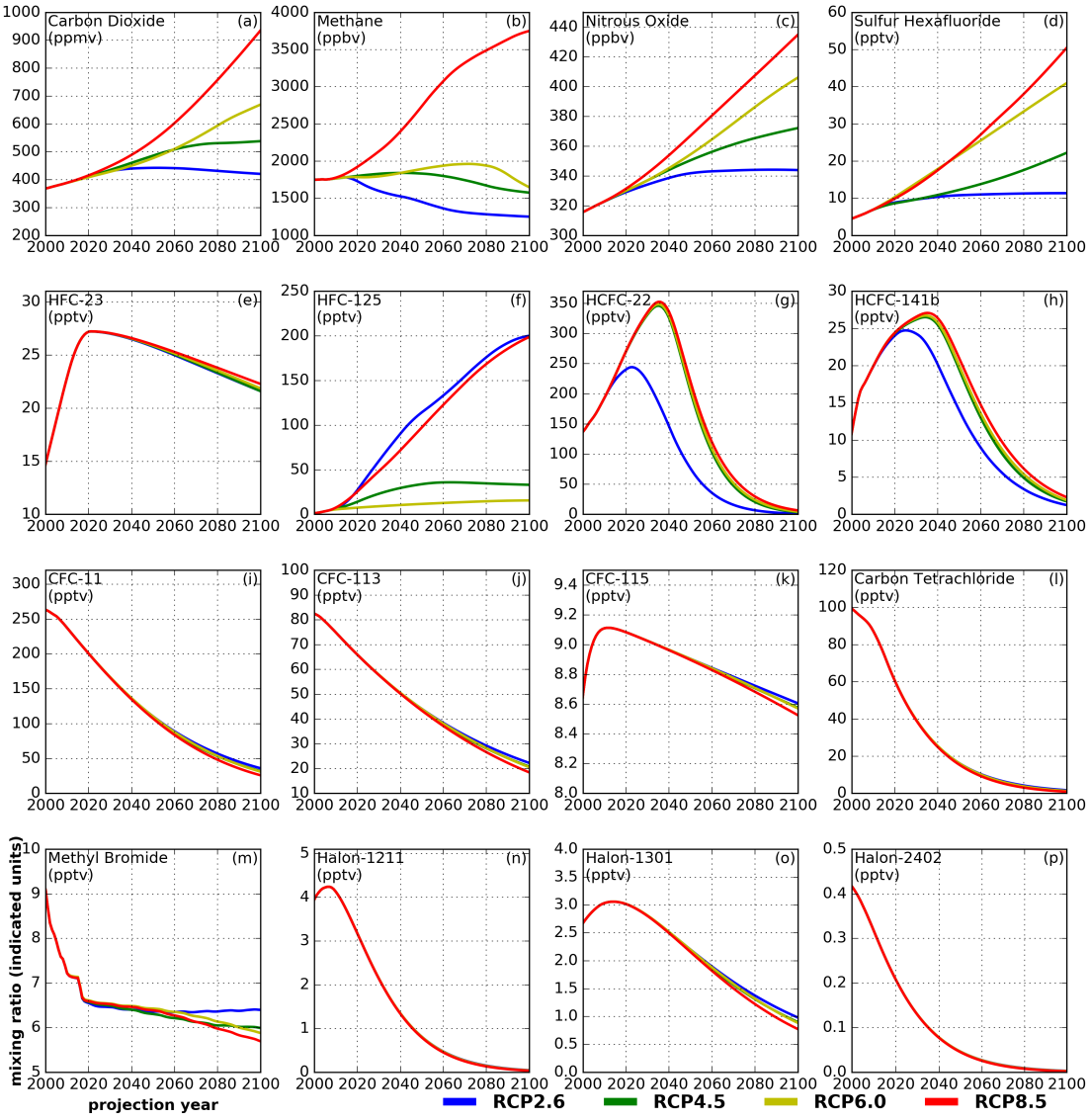

Figure 4.3: RCP emissions trends for many of the gases listed in table 4.1. Data from Meinshausen et al. (2011) [142]

Methane

CH_4 is both a greenhouse gas and a chemically active stratospheric trace gas. As discussed in chapter 1, abstraction of a proton from CH_4 serves to sink Cl_x (and to a lesser extent Br_x), slowing down the overall rate of ozone destruction, per equation 1.42 below.

$$Cl + CH_4 \rightarrow HCl + CH_3 \tag{1.42}$$

RCP trends in CH_4 are plotted in figure 4.3b). For RCP scenarios 2.6, 4.5, and 6.0, future CH_4 will decline below year 2000 levels because of changes in land-use and energy sourcing. In the most optimistic case, CH_4 plateaus at 1200 ppbv. RCP4.5 and RCP6.0 trajectories settle near 1500 ppbv by 2100. CH_4 mixing ratios continue to climb in the RCP8.5 scenario, reaching a staggering 3700 ppbv by the year 2100.

Nitrous Oxide

Like CH_4, N_2O is both a greenhouse gas and a chemical participant in the stratosphere as a precursor source of ozone-destroying NO, as indicated in equation 1.14.

$$N_2O + O(1D) \rightarrow 2NO \tag{1.14}$$

N_2O emissions rather closely mimic CO_2 in trend, as indicated in figure 4.3c). In the RCP2.6 storyline, N_2O stabilizes at 340 ppbv due to more efficient use of land and conservative agricultural

choices. RCP8.5 continues a linear increase with no sign of abatement, ending the century at 430 ppbv.

Sulfur Hexafluoride

SF_6 follows the same secular trend with regard to RCP emissions – figure 4.3d). RCP2.6 features stabilization, and subsequent RCP storylines feature ever-increasing emissions. SF_6 is a potent greenhouse gas because of its very long lifetime as a result of its chemical stability in the troposphere and stratosphere. Primary atmospheric loss mechanisms result from interactions with secondary particles produced from energetic particle precipitation, as discussed in section 7.2.4.

Hydrofluorocarbons

Hydrofluorocarbons (HFCs) are compounds composed of C, H, and F. Because they possess C-H bonds, they are vulnerable to tropospheric oxidation by OH especially. As indicated in table 4.1, these compounds carry a hefty GWP. RCP estimates of HFC emissions demonstrate a worldwide decrease in employment of longer-lived species such as HFC-23 – figure 4.3e) – and continued use of shorter-lifetime species in some scenarios – HFC-125, figure 4.3f). The adoption of the Kigali Amendment to the Montreal Protocol in 2016 will phase out the use of these substances on a much shorter timeframe than simulated in the RCP storylines.

HFCs, HCFCs, and CFCs are numbered according to their chemical structure in the following manner: for a given XFC numbered as XFC-abc, a = number of carbon atoms - 1, b = number of hydrogen atoms + 1, and c = number of fluorine atoms. Because these compounds are saturated

compounds, the remaining number of chlorine atoms can be determined by subtraction.

Hydrochlorofluorocarbons

Hydrochlorofluorocarbons (HCFCs) are both ozone-depleting substances and greenhouse gases. They are regulated by the Montreal Protocol and are scheduled for phaseout beginning in the year 2020. Figure 4.3g),h) provides trajectories for two of the most commonly used HCFCs.

Chlorofluorocarbons

CFCs are regulated by the Montreal Protocol and were phased out in the 1990s for most use cases. The RCP scenarios uniformly show CFC mixing ratios decline throughout the 21st century, as depicted in figure 4.3i) – k).

One interesting feature of the RCP CFC trajectories is the differential rates of CFC decay as a function of storyline. Beginning around the year 2040, CFC concentrations skew lower for storylines with greater radiative forcing. This is possibly an effect of modeled enhanced Brewer-Dobson circulation resulting in greater transport of halocarbons to the stratosphere in such scenarios.

Halons

Halons are fluorocarbons with at least one bromine atom and are regulated by the Montreal Protocol. Figure 4.3 demonstrates the significant decline in halon mixing ratios as the 21st century progresses. Note, however, that in the case of long-lived halons, again, storylines with greater radiative forcing also have greater rates of halon decay.

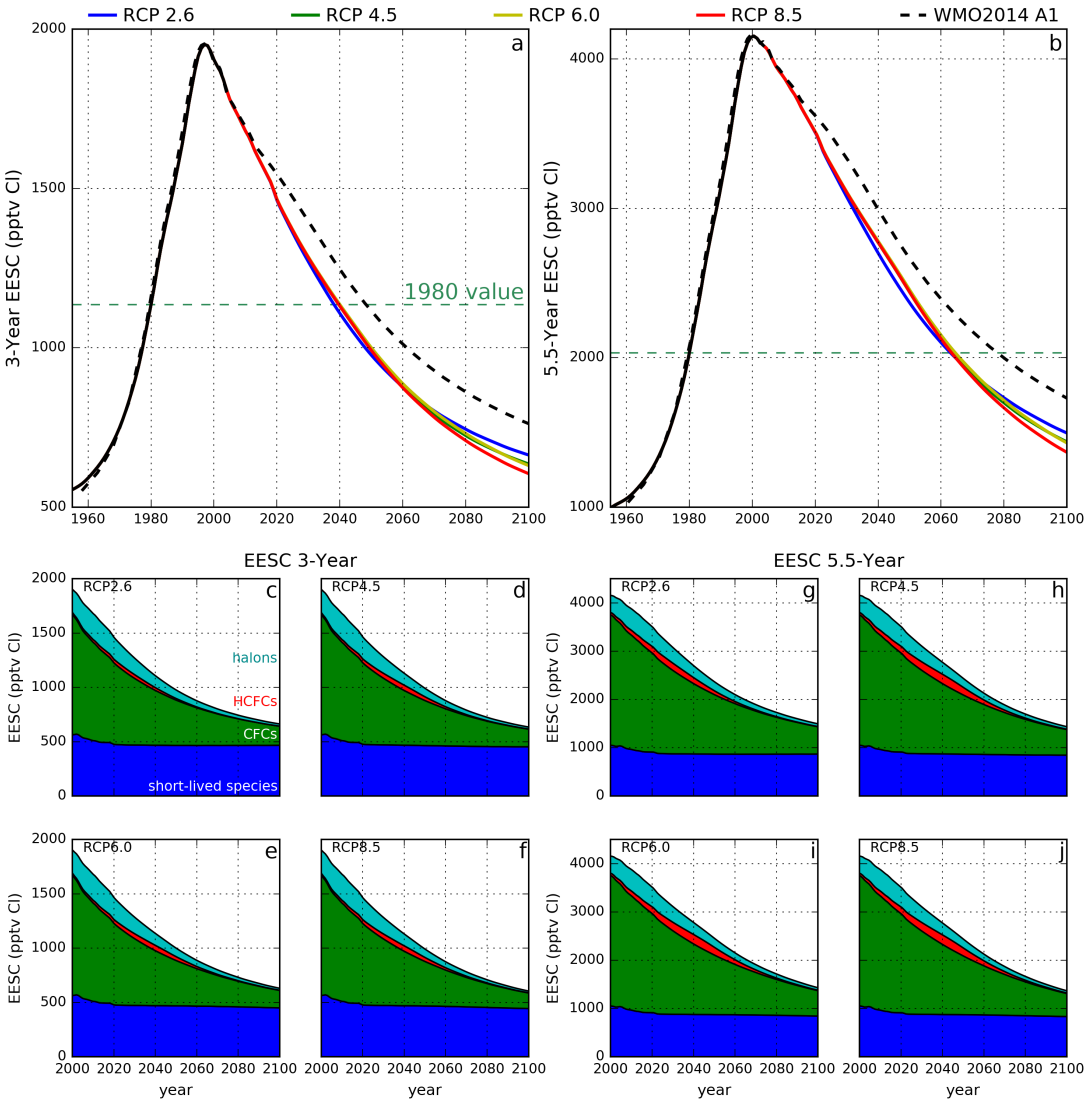

Figure 4.4: EESC calculated as a function of year per Newman et al. (2007)[49]. a,b) comparison of sum total EESC (3-year/5.5-year) for each RCP scenario. Dashed green line indicates 1980 value. c – f) componentwise contribution to 3-year EESC for each RCP scenario. g – j) same, except for 5.5-year EESC. Note that VSL contributions are neglected in this calculation. Also note that RCP halocarbon decay recovers significantly sooner than WMO projections. Data from Meinshausen et al. (2011)[142]

Each halon compound is numbered in accordance with the following standard: for a given halon numbered as Halon-abcd, a = number of carbon atoms, b = number of fluorine atoms, c = number of chlorine atoms, and d = number of bromine atoms.

Temporal Trends in EESC

From figure 4.3 it is evident that EESC is declining, regardless of the scenario; however, differences do exist between the storylines. Figure 4.4a,b) presents a comparison of 3-year and 5.5-year EESC for the various RCP scenarios. In the RCP framework, scenarios in which more radiative forcing occurs tend to result in enhanced decay of stratospheric halogens. This is true for both 3-year EESC calculations and 5.5-year EESC calculations and is likely the result of enhancements in Brewer-Dobson circulation as radiative forcing increases. Chemical effects from stratospheric temperature differences may also play a role in the differences between RCP scenarios.

Very few differences are discernable between the individual RCP scenarios in figure 4.4c-f) and g-j). HCFC use appears to perturb mid-century EESC for the RCP4.5 and RCP6.0 scenarios, while halon decay seems to be enhanced in the RCP8.5 scenario. This produces about a 100 pptv difference in year 2100 EESC between the RCP2.6 and RCP8.5 scenarios.

Also notable is that RCP scenario EESCs recover to their 1980 values far quicker than expected by the WMO 2014 A1 estimates, although the same parameters (e.g., chemical identity and fractional activation) employed by Newman et al. (2007) were used in this analysis. Per the WMO 2014 A1 scenario EESCs recover to 1980's levels a full decade later than RCP estimates[49] – and the origin of these differences is likely due to different treatments of stratospheric chemistry in the various

models used to produced these future values. It is very likely that the results originating from the RCP projections are less accurate than WMO estimates.

While the results discussed in later chapters of this thesis are contingent on stratospheric halogen loading, the RCP framework appears to underestimate this parameter – and thus the reported values must be understood within this uncertainty. End of century EESCs for the RCP scenarios deviate from WMO 2014 A1 estimates of 3-year EESC of 735 pptv by -11 – -19 % and estimates of 5.5-year EESC of 1650 pptv -11 – -21 %. In both cases, RCP2.6 more closely matches WMO 2014 A1 trajectories, RCP scenarios with increasing levels of radiative forcing progressively deviating downward. For parameters of ozone column sensitivity to perturbation, as presented in the following sections, the ozone response should be considered a conservative estimate.

Future Spatiotemporal Distribution of Stratospheric Ozone

As discussed in chapter 1, the spatiotemporal distribution of stratospheric ozone is a result of both chemical and dynamical factors. Ozone is primarily produced in the tropics and it is subsequently transported poleward, producing the characteristic polar and subpolar ozone maxima in wintertime, as depicted in figure 1.2. Stratospheric temperatures are expected to decrease as a result of increased greenhouse gas loading, and this will in turn contribute to changes in stratospheric circulation.

Future climate models unilaterally agree that post-CFC stratospheric ozone distributions will not be identical to pre-CFC stratospheric ozone distributions.[143] Most models converge on an expected super-recovery, in which changes to the thermal structure of the stratosphere produce enhancements

in total column ozone relative to pre-1980 levels.[144] Feedbacks limit the precision of model results on future ozone distributions. For example, increasing water vapor from enhanced troposphere-stratosphere exchange and increasing methane concentrations will influence the radiation balance, while increased rates of ozone photolysis will produce heating.

Li et al., (2009) find that year 2100 lower tropical stratospheric ozone will increase by several DU at pressures below 15 hPa while simultaneously decreasing at pressures above 15 hPa.[12] In the midlatitudes, ozone is predicted to increase at all stratospheric pressure levels. They attribute the middle-stratospheric enhancements in ozone to chemical processes and the lower-stratospheric tropical depletion to strenghtening advection and Brewer-Dobson transport. Akiyoshi et al. (2009) and Shepherd (2008) provide similar results and conclusions.[145,146]

Expected Chemical Response to Temperature

The work performed in this thesis did not include radiative-dynamical feedbacks due to model limitations. Instead, changes in future ozone are solely of chemical origin. Figure 4.5 illustrates vertical profiles of ozone for various RCP scenarios in the (a) lower tropics and (b) in the mid-latitudes. In all far-future scenarios, middle-atmospheric ozone columns have increased by large margins as a result of stratospheric cooling and, in the cases of RCP6.0 and RCP8.5, elevated methane mixing ratios. In all cases, the lower stratosphere remains depleted in ozone relative to 1950's levels (e.g., natural stratosphere). The production of stratospheric ozone via the recombination of atomic oxygen and molecular oxygen proceeds through a complexed bimolecular intermediate state whose lifetime is shorter than any intramolecular relaxation process, as indicated in equation 1.8. Resultantly, a

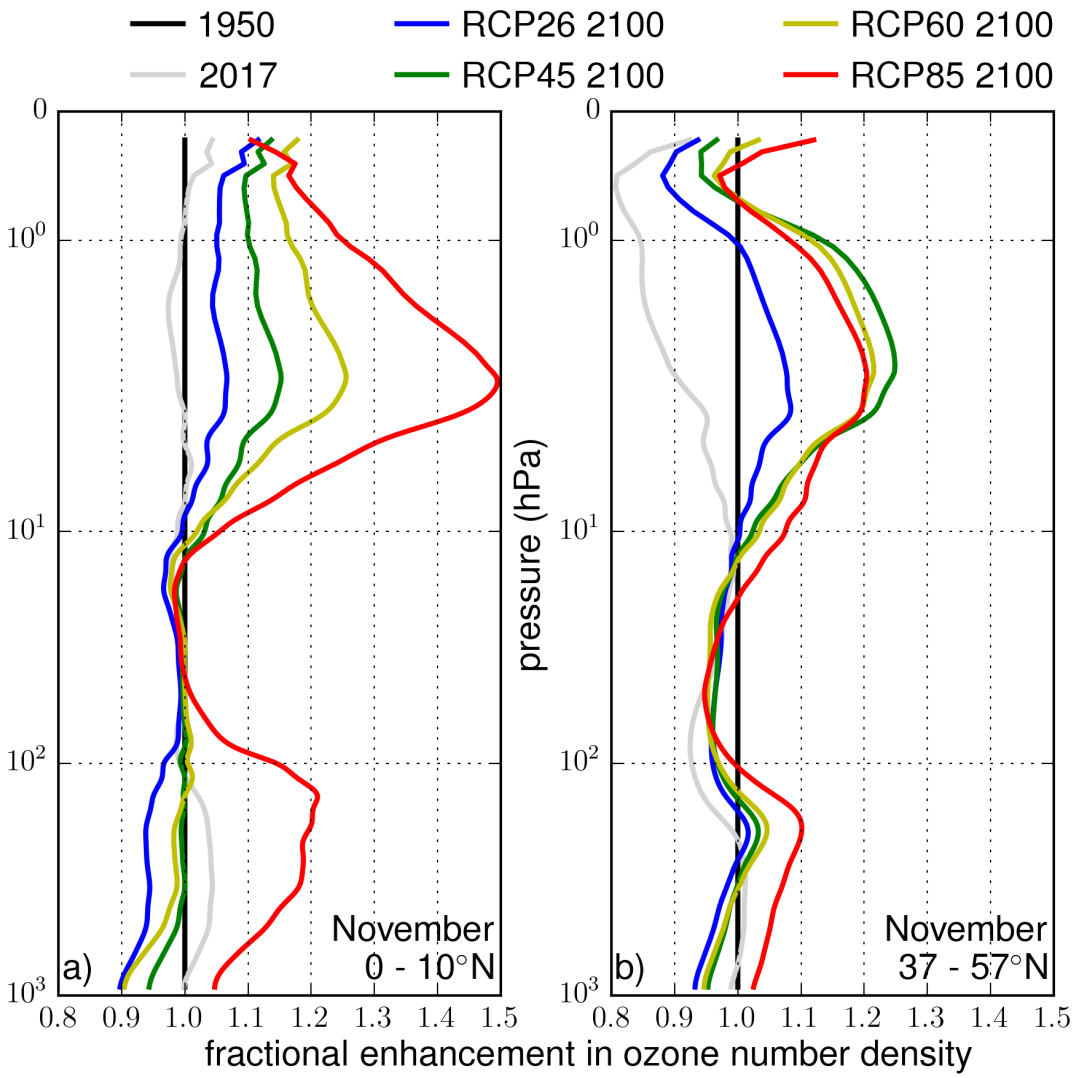

Figure 4.5: Projections of fractional change in ozone number density relative to 1950 levels as a function of pressure from the AER-2D model. (grey) year 2017, (blue) RCP 2.6 year 2100, (green) RCP 4.5 year 2100, (yellow) RCP 6.0 year 2100, (red) RCP 8.5 year 2100. (a) lower tropical ozone vertical profile. (b) mid-latitude ozone vertical profile.

third-body collision partner – a chaperone – is required to dampen the system and absorb excess energy. The frequency of successful recombinations scales inversely with atmospheric temperature due to a) an increased number density of third body reaction partners, resulting in a higher chaperone collision rate with the activated bimolecular complex and b) lower average energies of the reactants producing intermediates with proportionately longer lifetimes, also increasing the third-body collisional rate. Ozone production rates are thus enhanced as stratospheric temperatures decrease. Catalytic ozone destruction processes, on the other hand, are bimolecular as in equations 1.11 and 1.12. Bimolecular reaction rates increase exponentially with temperature (e.g., Arrhenius scaling). Resultantly, ozone destruction rates decrease as stratospheric temperatures decline. The sum of these two processes: enhanced production and suppressed destruction contributes to the chemical enhancement terms in ozone as a result of stratospheric cooling.

$$O\left(^3P\right) + O_2 + M \rightarrow O_3 + M^* \tag{1.8}$$

$$X + O_3 \rightarrow XO + O_2 \tag{1.11}$$

$$XO + O \rightarrow X + O_2 \tag{1.12}$$

$$\text{Net: } O_3 + O \rightarrow 2O_2$$

Projected Changes in Volcanic Eruption Column Height

The maximum height of a volcanic eruption column was related in terms of the mass ejection rate, M_0 and the Brunt-Väisälä frequency, N, in chapter 3. The Brunt-Väisälä frequency is a function of temperature lapse rate, Γ, which is expected to vary according to the climate scenario realized.

$$H \propto N^{-k_1} M_0^{k_2} \tag{3.5}$$

$$N^2 = \frac{g}{T}\left(\frac{g}{c_p} - \Gamma\right) \tag{3.6}$$

Aubry et al., 2016 explore how the frequency of stratosphere-penetrating eruption columns will change as a function of RCP scenario and eruption location.[99] Because the Brunt-Väisälä frequency is expected to decrease, they find that the volcanic input of stratospheric SO_2 is expected to decline by 2 – 12 % over the next century. This will result in a positive temperature feedback.

5

Volcanism in the Changing Climate

Abstract

The sensitivity of the ozone layer to future Pinatubo-like volcanic eruptions is explored in the context of the RCP storylines. Heterogeneous chemical effects following large eruptions are evaluated in a variety of future atmospheres spanning contemporary times to the year 2100. Differences between the models become evident following an analysis of vertical profile response and total col-

umn response. Sensitivity studies are performed to evaluate the effect of stratospheric temperature, methane burden, and differences in hemispheric mass loading. A predictive random forest regression model is developed and employed to account for the difference between RCP and WMO halocarbon decay rates as discussed in chapter 4. While the ozone layer is found to be more sensitive to volcanic perturbation under WMO halocarbon trajectories, the difference between WMO and RCP scenarios is not extreme and does not represent a modal shift in behavior. Heterogeneous chemical processing is found to produce net ozone depletions until the 2070's for all RCP scenarios, and significant depletions of greater than 1 % ozone loss until the 2060's. These dates occur later than prior estimates due to the inclusion of 4 pptv VSLS bromocarbons in the chemical model. Using the WMO EESC correction, slight ozone losses are observed following eruptions until the end of the century, though in some cases these losses are smaller than expected ozone contributions from radiative-dynamical causes.

Introduction

Eruption columns from explosive volcanism provide conduits for the efficient transport of massive quantities of degassed volatiles to the lower-to-middle stratosphere over very short time periods.[147] Although explosive volcanic events of stratospheric significance are relatively infrequent, occurring every 5.5 years on average,[148] they are remarkable in their impact on the trace gas composition of the stratosphere. The enhanced loading of stratospheric sulfuric acid aerosol, produced from the oxidative processing of volcanic SO_2, provides surface area for the conversion of catalytically inactive

halogen species to their active form and can also induce global climatological changes in radiative forcing and atmospheric dynamics.[126,149–152]

Chemical Mechanisms

Volcanic perturbations of stratospheric aerosol exert contrasting effects on ozone in different chemical environments.[27,29,109,153–155] In the middle stratosphere, enhancement in the rate of heterogeneous reactive uptake of N2O5 results in a suppression of the catalytic odd-nitrogen destruction of ozone. Conversely, in the lower stratosphere, enhanced activation rates of halogen reservoirs such as chlorine nitrate and hydrogen chloride produce an intensification in reactive halogen-induced ozone destruction. The net impact on column ozone is a function of many factors, including halogen availability (equivalent effective stratospheric chlorine – EESC, which includes chlorine and weighted bromine contributions), halogen sink abundance, aerosol injection mass distribution, and stratospheric temperature.

As a result, in the contemporary stratosphere, lower stratospheric chemistry dominates the chemistry of the middle stratosphere and forces net reduction of total column ozone in response to enhanced surface area following a major volcanic eruption. In future scenarios of low anthropogenic halogen loading, Pinatubo-like eruptions, defined here as volcanic eruptions in which only SO_2 is injected into the stratosphere, are expected to cause net increases in total column ozone as middle stratospheric effects on odd-nitrogen outweigh lower stratospheric halogen chemistry.[27,28,156,157]

VSLS Bromocarbons

Recently, it has been shown that small changes in the concentrations of Very Short-Lived Substances (VSLS) – such as the bromocarbons CH_3Br and CH_2Br_2 – may produce significant changes in ozone loss rates.[29] Current inventories of stratospheric bromine assign a stratospheric mixing ratio between 16 – 23 pptv or which 2 – 8 pptv originates from VSL bromocarbons.[29,158,159]

The large uncertainty in the present day measurements of bromine propagates to future assessments of ozone sensitivity, when biological production of bromocarbons is likely to be greater than in the present. Yang et al. (2014) investigate how a doubling of VSL Br (from 5 pptv to 10 pptv) might perturb total ozone in a world with a preindustrial halocarbon burden, finding reduced sensitivity relative to a world with an enhanced halocarbon burden.[160] Regardless of the reduced sensitivity, an additional 5 pptv is predicted to delay stratospheric ozone recovery by up to a decade.[160,161] In such a scenario, bromine-mediated processing of ozone is expected to produce an expansion in the ozone hole magnitude by about 14%.[161]

VSLS bromine is produced by microplankton and bromocarbon emissions trajectories are resultantly influenced by ocean temperatures. Future projections of VSL Br production estimate between 10 – 30 % increases depending on the RCP scenario[162,163] – and that increasing ocean acidification is unlikely to reduce production rates.[164] Additionally, future changes in (a) troposphere-stratosphere exchange[165] and (b) tropospheric HO_x[1] may significantly enhance the chemical lifetime of VSLS compounds and enhance the lower stratospheric bromine burden.

Iodocarbons, like bromocarbons, are primarily produced and emitted to the atmosphere by ma-

rine microplankton. VSL I is much more susceptable to tropospheric oxidation than most bromocarbons and partition to the stratosphere with much lower efficiency. Upper limits on stratospheric I are established at 0.15 pptv by compendial sources[29]; however, recent observations indicate this value may be underestimated by a factor of four or more.[166] Given that α_I is estimated in excess of 250, even extremely small perturbations in the production and lifetime of VSL I might exert outsized impacts on the chemistry of the lower stratosphere. Iodine inventories and chemistry were not included in the following work, but should be considered for future evaluations.

In the following chapter, scenarios of ozone response to Pinatubo-like volcanism – eruptions in which only volcanic SO_2 is partitioned to the stratosphere in significant quantities – are evaluated as a function of future climate scenario. Though particular emphasis is placed on the RCP 6.0 scenario, all RCP storylines are considered. Unless otherwise noted, VSL bromine mixing ratios are computed at 4 pptv Br and 100 pptv Cl.

Model

2D Chemical Transport Model

The AER-2D chemical-transport-aerosol model[167,168] was selected for the work described in the following chapters due to its extensive prior use in studies of the 1991 Mt. Pinatubo eruption[106,108,119,169] and its benchmark performance treating stratospheric aerosol of volcanic origin in model intercomparison studies[169]. The model is fully prognostic with regard to aerosol evolution, employing 40 sectional size bins along with nucleation, coagulation, condensation/evaporation, sedimentation,

and heterogeneous chemical interactions. I simulate the transport and chemistry of volcanic clouds of varying composition using prescribed temperature and transport fields with a focus on the effects of heterogeneous chemistry on total column ozone over a grid of 19 latitudes (90S -90°N) and 51 pressure levels (1000 – 0.2 hPa). Initial conditions for each eruption experiment were established after spin-up to model stability at the relevant boundary conditions for the specified simulation years. A total of 264 model scenarios were evaluated over 2600 model years. All column ozone deviations reported were calculated as percentage differences from scenarios in which no volcanic input was allowed, but all other conditions were identical; i.e., the reported changes in ozone are due only to the volcanic perturbation, as indicated by equation 5.1.

$$\Delta_{\text{column O3}}(\%) = \frac{\text{column O3}_{\text{volc}} - \text{column O3}_{\text{no volc}}}{\text{column O3}_{\text{no volc}}} \times 100 \tag{5.1}$$

Greenhouse gas and long-lived halocarbon chemical boundary conditions were obtained from the RCP emissions projections of Meinshausen et al. (2011).[142] Historical average climatological transport fields were employed in all cases.[141] Temperature fields were obtained from MIROC-CHEM-ESM, an Earth Simulator Model (ESM) with stratospheric chemistry, and employed for the RCP future and contemporary scenarios.[140] Unless otherwise noted, short-lived halocarbons were parameterized at 4 pptv bromine and 100 pptv chlorine according to common VSLS mixing ratio estimations.[49]

Volcanic Input Parameters and Mass Sensitivity Validation

For experiments in which volcanic input occurred, SO_2 vertical mass distribution was parameterized according to the optimal distribution of Sheng et al. (2015).[108] Using this vertical distribution, I performed a sensitivity study to determine the mass input required to reproduce the observed 1991 Mt. Pinatubo northern midlatitude ozone anomalies[119,120,124] under prescribed climatological fields representative of the historical 1990s.[141] SO_2 injections between 7 – 17 Tg provided acceptable matches; the lowest eruption mass, 7 Tg SO_2, was selected for further experimentation as our Pinatubo-scale injection mass as it provides good agreement with the observed response within the model framework and minimizes the impact of radiative dynamical effects discussed below.

Figure 5.1 provides diagnostic information relating the total simulated ozone losses as a function of SO_2 injection mass in a simulated 1991 stratosphere, employing 1979 - 1995 average climatology and temperatures.[141] SO_2 masses are titrated upward from (a) – (d). 3-year northern midlatitude averages are reported in the top right corner of each panel, ranging from -5.2 % to -7 %, scaling with injection mass. Solomon et al. (1996) report northern midlatitude column anomalies (compared to 1978 – 1979 average) of $\approx 5 - 6$ % over a three year period.[120] The 7 Tg SO_2 injection most closely matches this value.

Radiative-Dynamical Corrections

Volcanic clouds may perturb the Brewer Dobson Circulation in addition to repartitioning chemical inventories. This effect can either enhance or reduce column ozone thickness, depending on latitude

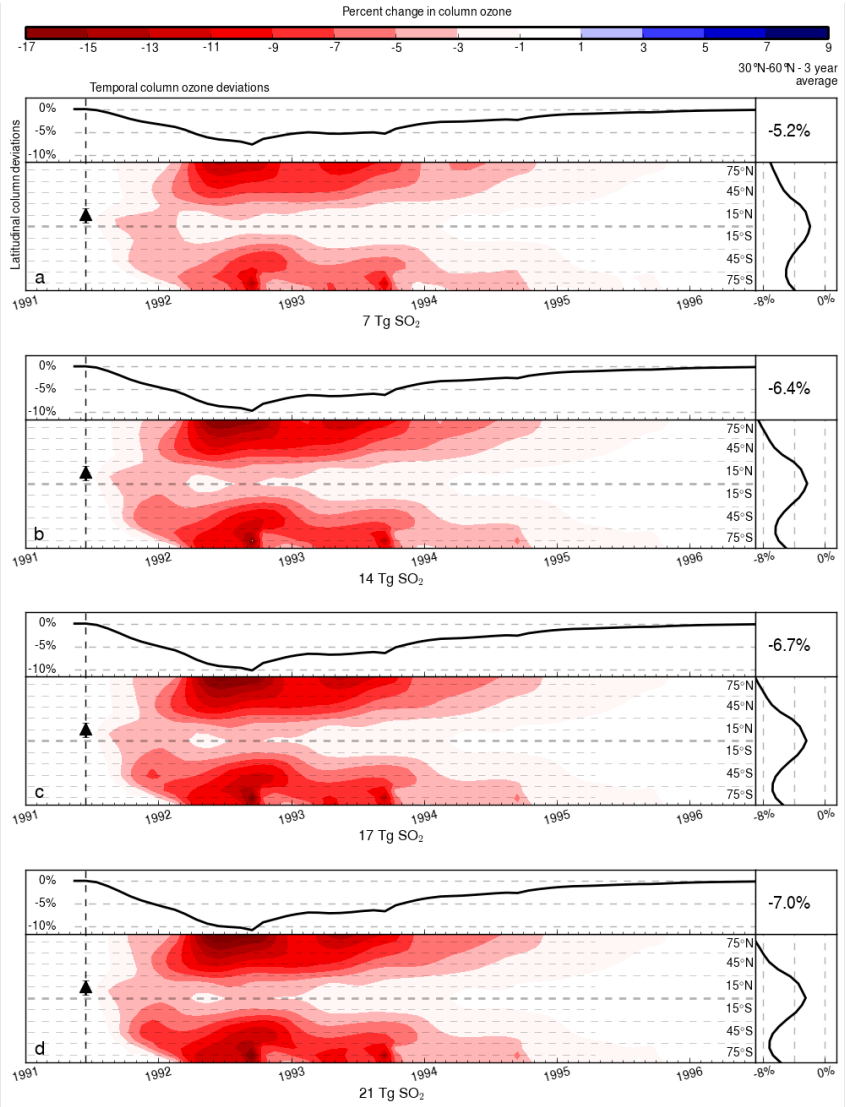

Figure 5.1: Simulated response of column ozone to eruptions of Mount Pinatubo in the year 1991. For each panel: (main) response of column ozone as a function of time. The simulated eruption occurs at the time and latitude denoted by the black triangle. (top) Global-average ozone response as a function of time. (right) Temporal-average ozone response as a function of latitude. (top right) Northern midlatitude-temporal average ozone response. (a) 7 Tg SO_2, (b) 14 Tg SO_2, (c) 17 Tg SO_2, (d) 21 Tg SO_2.

and climatological conditions.[126,151,170,171] The magnitude of the radiative-dynamical perturbation on the ozone anomaly has been demonstrated to be proportional to the mass of the stratospheric injection of SO_2 [107,125]; larger, more explosive injections tend to induce more pronounced dynamical changes resultant from radiative heating. Though the AER-2D model does not capture these volcanically-induced modifications to atmospheric transport effects, it provides a comprehensive analysis of the chemical response.

Because this model does not include online climatology, care must be taken to minimize the expected role of radiative-dynamical processes (as opposed to heterogeneous chemical processes, which AER-2D quantifies) from any physical perturbation on column ozone. Figure 5.2 demonstrates the aerosol injection mass sensitivity of column ozone following tropical eruptions in a) pre-industrial atmospheres (year 1814) and b) contemporary greenhouse-gas loaded (year 1990) atmospheres, digitized from Muthers et al. (2015).[125] Notably, radiative-dynamical effects in both climate scenarios are expected to produce net enhancements in column ozone following a volcanic eruption; however, this effect appears to dampen as greenhouse gas loading increases, presumably due to enhanced Brewer-Dobson circulation.[125] Figure 5.2 provides the projected temporally-averaged anomaly as a function of SO2 injection mass. Dashed lines indicate a linear fit, which represents the upper limit for a nonlinear, unsaturated system. For all AER-2D simulations of volcanic eruption, injection masses were limited below 7 Tg SO2 (yielding a worst-case +1.5 DU temporally-averaged error) in order to minimize the contribution of errors arising from neglected radiative-dynamical effects. This value is less than the reported global-temporal average ozone anomalies for all simulated eruptions in this work except for the year 2100 RCP 6.0 scenario with 4 ppt VSL bromine.

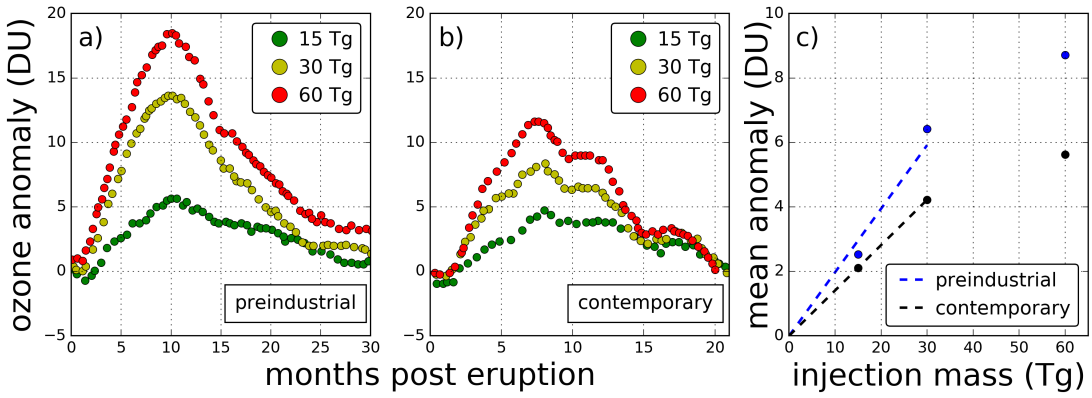

Figure 5.2: Global ozone anomaly as a function of time after a tropical volcanic eruption with SO2 mass injection in a) preindustrial and b) contemporary atmospheres – data taken from Muthers, et al. (2015). [125] In both cases, radiative-dynamical effects are expected to increase column ozone, and this effect will scale with injection mass. c) 20-month, time-integrated global ozone anomaly as a function of mass. An injection of 7 Tg SO2 is expected to produce a positive ozone anomaly of 0.9 DU.

Impact of Pre-Industrial Pinatubo-Like Volcanic Eruptions on Ozone

The climatological impact of Pinatubo-like volcanic eruptions occuring prior to the massive-release of chlorofluorocarbons is considered more important than the chemical impact of eruptions during the same time period.[125,172] Model results of Pinatubo-sized to Tambora-sized eruptions in pre-industrial atmospheres found enhanced ozone columns as a result of the heterogeneous reactive uptake of N_2O_5 and enhancements in Brewer-Dobson circulation.[125]. The magnitude of the enhancement was slight, on the order of several percent, and scaled with SO_2 injection quantity. One should note that pre-industrial atmospheres differ from far-future atmospheres: while both share low burdens of EESC, pre-industrial stratospheres are much warmer than future stratospheres and the chemical effects of enhanced aerosol are not expected to map onto one another exactly. Prehistoric eruptions will be discussed in more detail in the context of halogen-injection, in chapter 6.

Contemporary and Future Pinatubo-Like Volcanic Eruptions

The contemporary atmosphere is marked by high – but declining – burdens of stratospheric halogen, as depicted in figure 4.4. Additionally, atmospheric temperatures deviate from preindustrial values as a result of the emission of large quantities of greenhouse gases. In the future, these temperatures will continue to decline, the magnitude dependent on the future emissions trajectory of greenhouse gases, as indicated in figure 4.2.

Many important heterogeneous chemical reaction rates in the stratosphere are highly dependent on temperature. This temperature dependence is depicted in figure 2.3. Notably, the rate of chlorine activation from HCl, the principle reservoir of inorganic chlorine in the stratosphere, increases exponentially as temperature declines. Other reactions, such as the hydrolysis of N_2O_5 and $BrONO_2$, are generally agnostic to temperature changes.

The differential extent of ozone loss following future Pinatubo-like volcanic eruptions as a function of emissions trajectory then becomes a function of EESC, reactive gas burden, and temperature. From figure 4.4, it is evident that EESCs do not differ significantly between RCP storylines. On the other hand, figure 4.3 indicates large differences in N_2O and CH_4 emissions trajectories between scenarios. These effects will be explored in the following sections.

Vertical Profile Response: Contemporary Pinatubo-Like Eruption

Figure 5.3 visualizes the vertical profile of ozone response to a Pinatubo-like eruption which injects 7 Tg SO_2 in a contemporary atmosphere. In the tropics (panel a), rapid transport of aerosol mass is

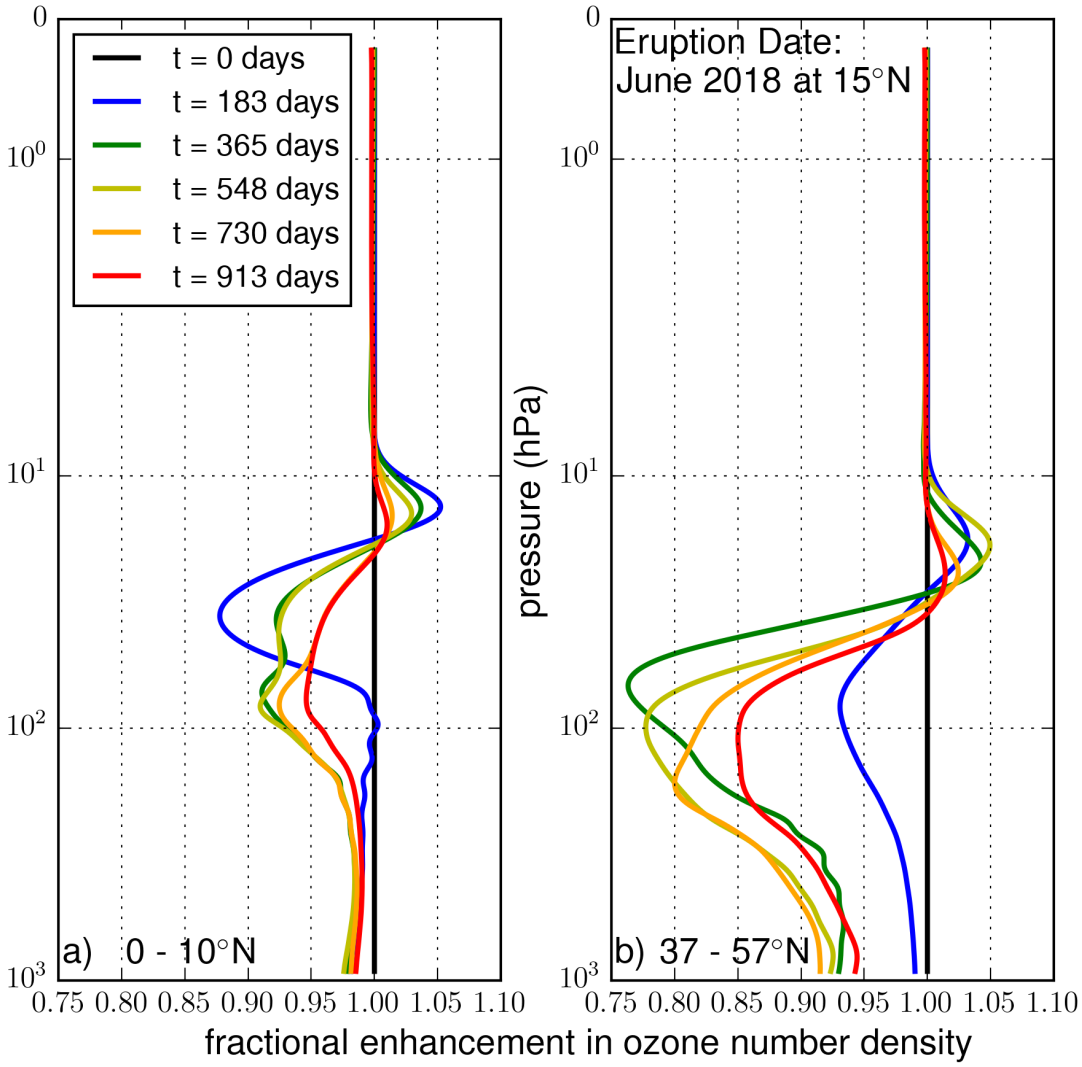

Figure 5.3: Vertical profile response of ozone in a contemporary atmosphere to an injection of 7 Tg SO_2 on June 16th 2018, at 15°N. Zonal vertical profiles are presented for various dates after the eruption (colors) in (a) the tropics and (b) the northern midlatitudes.

demonstrated by the rapid attenuation of lower stratospheric losses and middle stratospheric ozone enhancements. In the northern midlatitudes (panel b), lower stratospheric losses from halogen activation slowly grow in, also with transport, and maximize one year after the eruption.

Vertical Profile Response: Future Pinatubo-Like Eruptions

As EESC burdens decline, so too does lower stratospheric response to Pinatubo-Like volcanism. Figure 5.4 demonstrates the progressively decreasing sensitivity of ozone to eruption as the years progress. Tropical profiles, as depicted in panel a, exhibit less variation with time than midlatitude profiles (b) due to reduced availability of halogens from long-lived halocarbons as the age of air is comparatively small. Especially notable is the enhancement in middle-stratospheric midlatitude N_2O_5 hydrolysis as EESC declines – not only is ozone enhanced in the middle stratosphere, but the domain in which the enhancement occurs increases by 10 hPa between 2017 and 2100. This effect is present, but attenuated in in the tropics.

Though figure 4.4 indicates very little variation in EESC as a function of RCP scenario, significant variation in ozone response to volcanic eruption as a function of RCP storyline emerges, as demonstrated in figure 5.5. The response trend in lower stratospheric ozone destruction does match the hierarchy in EESC values (EESC declines as RCP scenario increases from RCP 2.6 – RCP 8.5), but in some cases, the vertical profile hardly changes between the thirty year period, which would not be expected if EESC alone were the driving factor in variation between the models.

Figure 5.6 demonstrates the change in northern mid-latitude ozone loss rates by chemical family 12 months after a Pinatubo-like eruption in the year 2017 and 2100 under the RCP 8.5 emissions

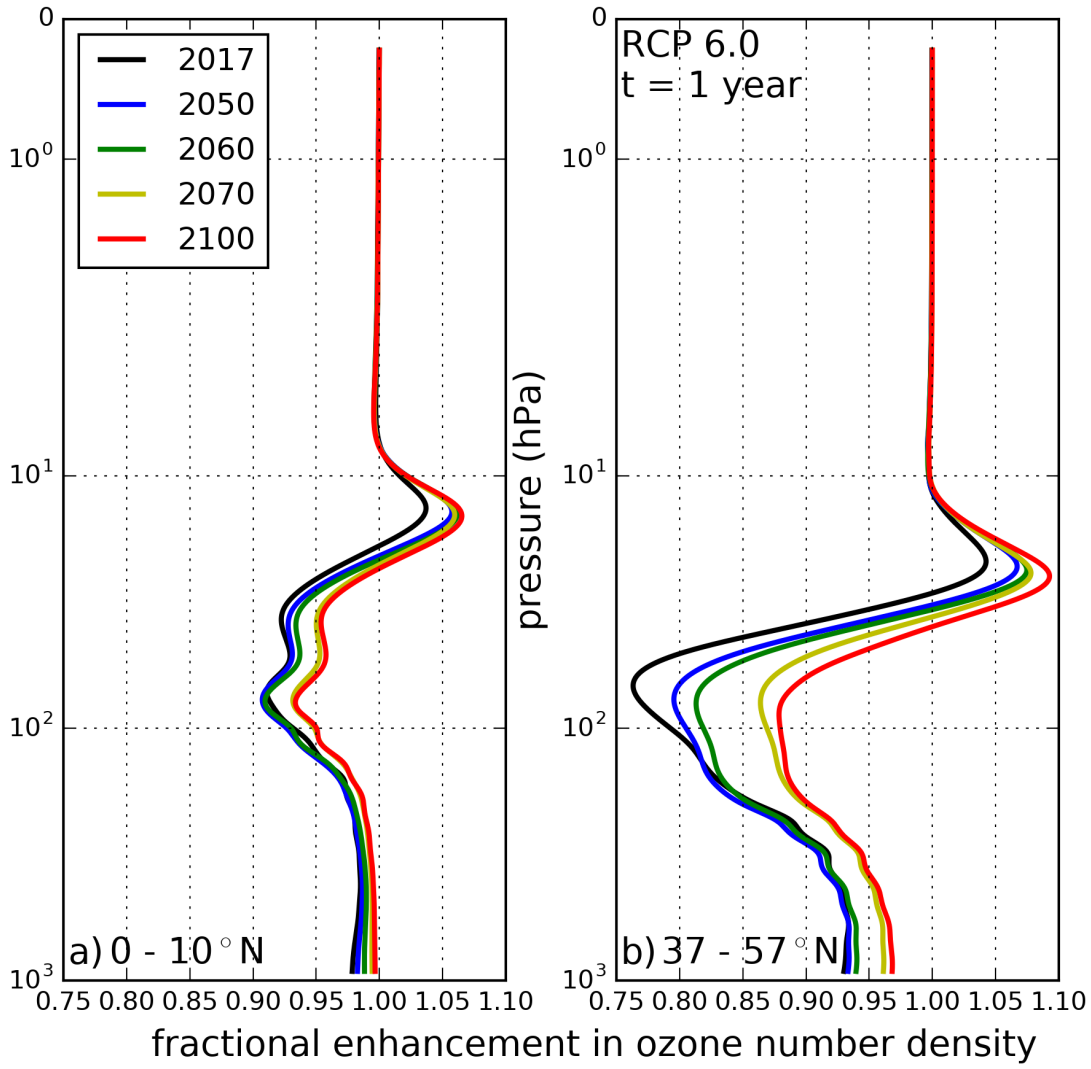

Figure 5.4: Vertical profile response of ozone to an injection of 7 Tg SO_2 – one year after eruption. Zonal vertical profiles are presented for various years of eruption (colors) within the RCP 6.0 scenario in (a) the tropics and (b) the northern midlatitudes.

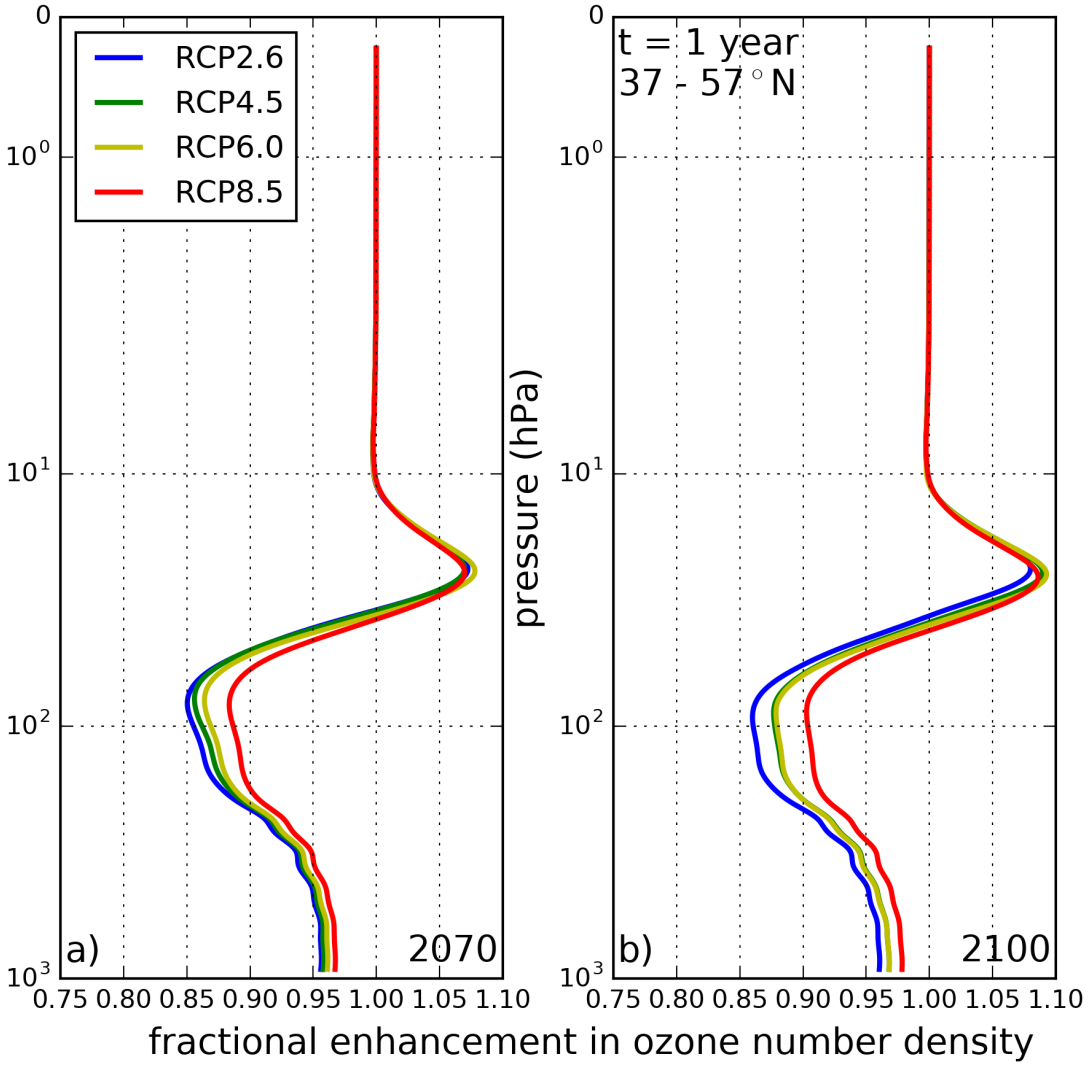

Figure 5.5: Vertical profile response of ozone to an injection of 7 Tg SO_2 – one year after eruption. Zonal vertical profiles are presented for the four RCP storylines (colors) in the northern midlatitudes in (a) the year 2070, (b) the year 2100.

storyline. Panels (a) and (b) correspond to a contemporary eruption and panels (d) and (e) correspond to an end-of-century eruption. Dashed lines indicate the values of the respective processing rates in the non-volcanic baseline scenario. Shaded regions visualize the enhancement (or suppression) of these rates following a Pinatubo-like eruption – changes toward the left signify accelerations in chemical processing rates and changes toward the right signify reductions in chemical processing rates. For eruptions in the year 2017 and 2100, NO_x-mediated ozone loss is suppressed significantly in the middle stratosphere. The domain in which NO_x suppression occurs expands slightly in the year 2100 – likely due to decreased rates of $ClONO_2$ formation as anthropogenic chlorine inventories decline. ClO_x processing rates are slightly reduced in the future scenario, especially in the middle stratosphere; however, the rate of bromine-mediated processing of ozone is mostly the same. A stark difference appears comparing the interhalogen processing rates, which are an order of magnitude lower at the end of the century due to the decreased availability of chlorine. The net result of the changes in chemical family processing rates is presented in panels (c) and (f), in which the ozone number density is plotted. For Pinatubo-like eruptions occuring in the present, significant loss is predicted in the lower-to-middle stratosphere. Only above 30 hPa does the ozone layer thicken following an eruption. For eruptions occuring at the end of the century, within the RCP 8.5 emissions trajectory, this transition instead occurs at 50 hPa, and losses of ozone below this pressure level are markedly attenuated.

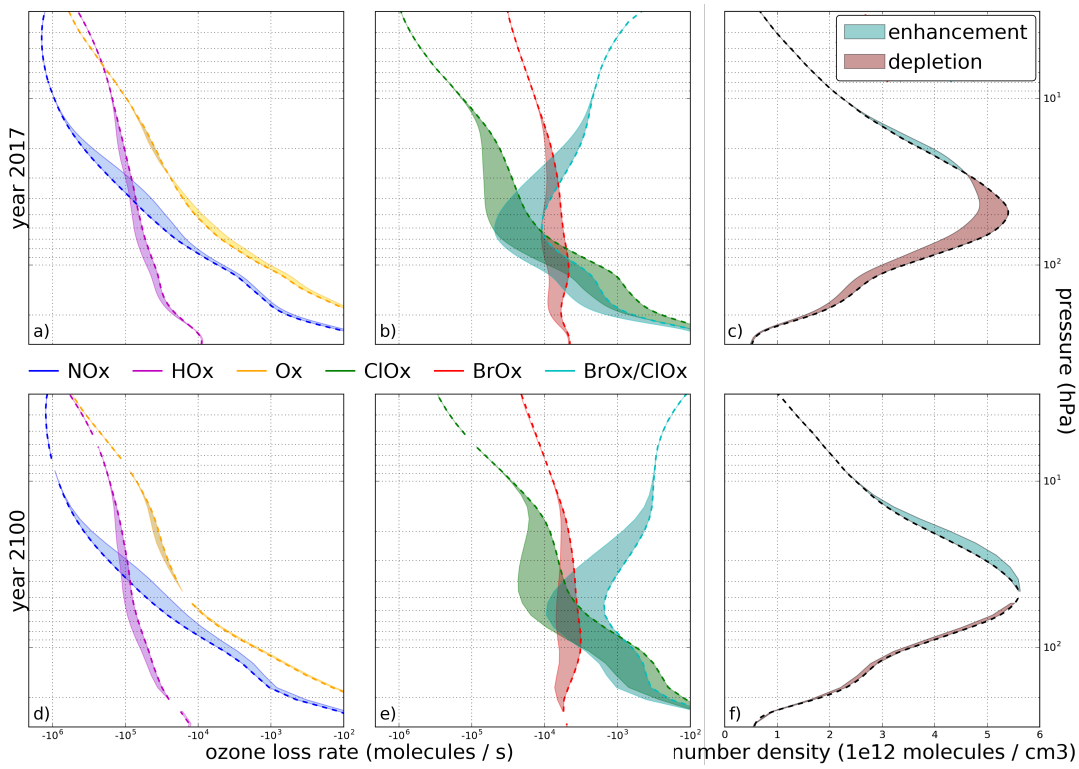

Figure 5.6: (a,b,d,e) ozone loss rates as a function of pressure by chemical family. Dashed lines indicate the non-volcanic baseline rate. Shaded areas present the change in chemical family ozone processing rate after a Pinatubo-like eruption in the appropriate year under the RCP 8.5 emissions trajectory. Changes toward the left are accelerations in ozone-loss rates. (a,b) for contemporary eruptions, note the large role played by interhalogen chemical reactions in the lower stratosphere. (d,e) toward the end of the century, interhalogen reactions are an order of magnitude less important, despite bromine processing rates remaining very similar to contemporary levels. (c,f) Ozone number density as a function of pressure. Lower stratospheric losses outweigh middle stratospheric enhancement in the present day; however, in the future, suppression of NO_x reactions will dominate lower stratospheric halogen-mediated ozone loss.

Trend in Column Ozone

The temporal trend in ozone sensitivity, presented in the following section, provides some clues regarding the cause of the differences in ozone sensitivity between RCPs. Table 5.1 provides a summary of important diagnostic parameters.

The RCP 6.0 Time Series of Pinatubo-Like Volcanism

Figure 5.7 presents the modeled progression of total column ozone sensitivity following a Pinatubo-like eruption in contemporary and future scenarios as a function of latitude and time (main panels), as a function of latitudinal averages and time (top subpanels), as a function of time averages and latitude (right subpanels), and as a single four-year global-temporal average (top right boxes). For each panel, atmospheric conditions are defined by RCP 6.0 projections[142] of anthropogenic halogen and GHG mixing ratios, supplemented with 4 pptv bromine from very short-lived sources; VSL bromocarbons are known to contribute 4–10 pptv to stratospheric inorganic bromine loading.[119,159,173,174] The values of EESC are shown below each panel, determined per Newman et al. (2007).[49] As EESC decreases due to the decay of anthropogenic halogen sources over the remainder of this century, the sensitivity of column ozone to volcanic aerosol attenuates, as would be expected. Modest regional enhancements in column ozone begin to appear in 2061, with the inter-hemispheric differences in ozone response primarily because the simulated volcanic injection occurred in the northern tropics and produced an aerosol mass asymmetry across the hemispheres. Globally, there is still significant

Table 5.1: Column Ozone Response by RCP Storyline

Year	CH_4 (ppbv)	EESC (pptv)		T_{AVG} – 90°S – 90°N (K)			ΔO_3
		3-Year	5.5-Year	115 – 97 hPa	59 – 50 hPa	11 – 9 hPa	
Contemporary							
2018	1786	1991	3733	211.2	213.2	225.1	-3.5 %
RCP 6.0							
2051	1900	1304	2592	211.2	213.2	223.4	-2.4 %
2061	1943	1199	2327	211.0	212.8	222.4	-1.2 %
2071	1963	1104	2117	211.0	212.7	221.7	-0.7 %
2101	1636	944	1699	211.1	212.9	220.3	-0.2 %
RCP 2.6							
2071	1307	1117	2124	211.1	213.1	223.4	-1.3 %
2101	1252	991	1777	211.6	213.7	224.1	-1.3 %
RCP 4.5							
2071	1738	1103	2099	211.4	212.9	221.9	-1.4 %
2101	1573	961	1713	211.1	213.0	222.4	-0.7 %
RCP 8.5							
2071	3341	1091	2071	211.6	212.7	219.8	-0.5 %
2101	3758	928	1633	211.6	212.5	217.8	+0.17 %

Global-temporal changes (4-year average) in total column ozone following a Pinatubo-Like eruption of 7 Tg SO_2 in the years and RCP scenario indicated relative to identical conditions in which no eruption occurred. EESC contributions calculated per Newman et al. (2007) with additional contributions from 4 pptv VSL bromine and 100 pptv VSL chlorine.[49] Temperatures are presented as yearly, global averages at the pressure level indicated.

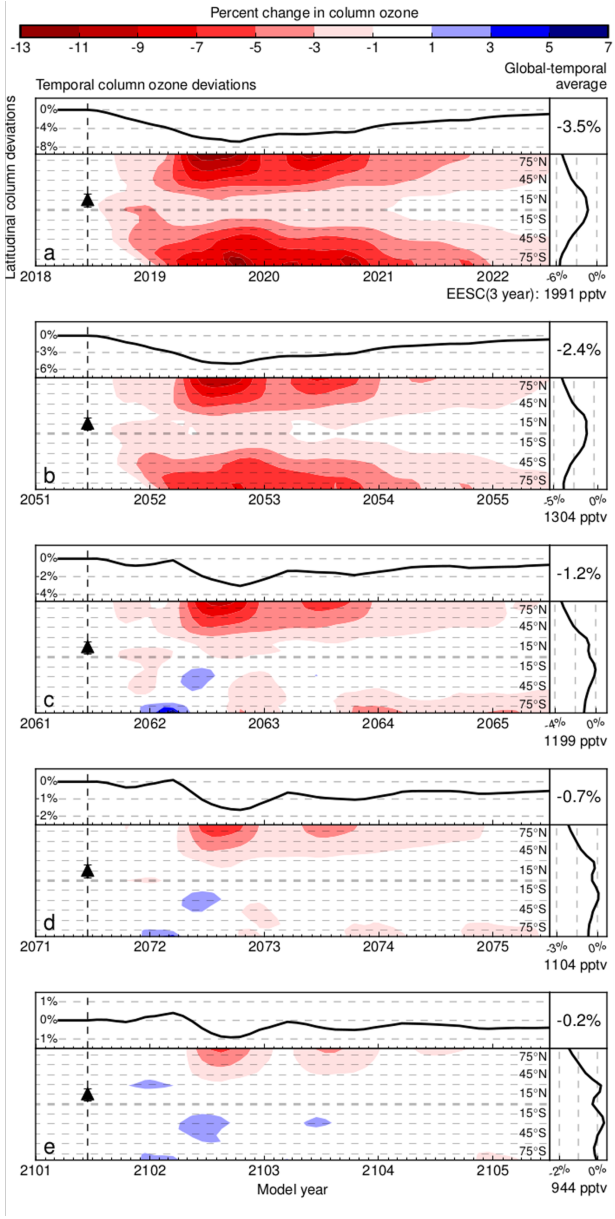

Figure 5.7: Ozone response to Pinatubo-like eruptions in contemporary and future atmospheres. RCP 6.0 scenarios including 4 pptv VSL bromine are simulated for: a. 2018, b. 2051, c. 2061, d. 2071, and e. 2101. Global averages (90°S – 90°N) of total column ozone perturbation are traced atop each panel as a function of time. Temporal average ozone anomalies are traced right. Global-temporal averages are enumerated in the top right. Black triangles indicate injection latitude and time. Red colors indicate column ozone depletion, and blue colors indicate column ozone enhancement. EESC values are presented for 3-year-old air parcels.

net loss of total column ozone beyond modeled year 2071.

The RCP 2.6 Time Series of Pinatubo-Like Volcanism

Figure 5.8 presents future column ozone response to volcanism within the RCP 2.6 storyline for eruptions in the years 2071 and 2101. Immediately, a large difference is observed between RCP 2.6 and RCP 6.0 (figure 5.7). Not only are column ozone losses greater in both the years 2071 and 2101 within RCP 2.6 than RCP 6.0, but they also do not appear to decline significantly as time progresses. Though background EESC continues to decline between the years 2071 and 2101 (refer to figure 4.4), the 4-year global-temporal average stays the same. Greater losses are observed in the subpolar northern regions in the year 2071 than in the year 2101, but only by 1 % at the most.

A quick look at figure 4.3a–d may provide some insight into the origin of the differences between the two scenarios. In the RCP 2.6 storyline, CO_2, N_2O, and SF_6 emissions stabilize between the years 2070 and 2100. This is not the case in with RCP 6.0, in which the mixing ratios of these gases continue to increase. In both RCP 6.0 and RCP 2.6 CH_4 levels decline between the years 2070 and 2100, albeit, not by a large degree in the RCP 2.6 scenario. These factors together indicate that temperature differences resultant from greenhouse gas emission may be the principal factor contributing to differential ozone response between the two scenarios.

The RCP 4.5 Time Series of Pinatubo-Like Volcanism

The time series of RCP 4.5 total column ozone response to Pinatubo-like volcanic eruption, presented in figure 5.9, resembles a juxtaposition of RCP 2.6 and RCP 4.5. The magnitude of losses is

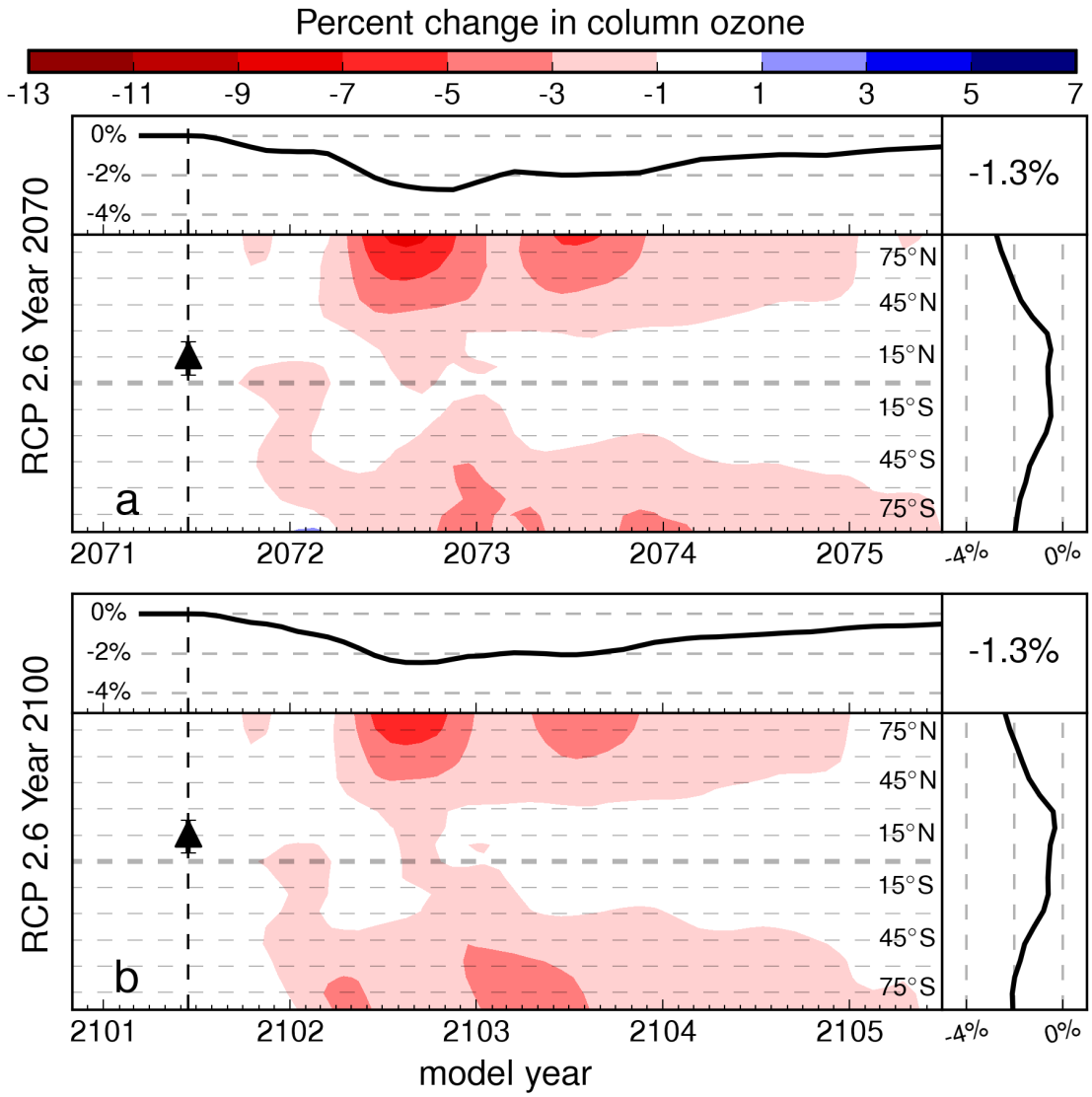

Figure 5.8: Ozone response to Pinatubo-like eruptions in contemporary and future atmospheres. RCP 2.6 scenarios including 4 pptv VSL bromine are simulated for: a. 2071 and b. 2101. Global averages (90°S – 90°N) of total column ozone perturbation are traced atop each panel as a function of time. Temporal average ozone anomalies are traced right. Global-temporal averages are enumerated in the top right. Black triangles indicate injection latitude and time. Red colors indicate column ozone depletion, and blue colors indicate column ozone enhancement.

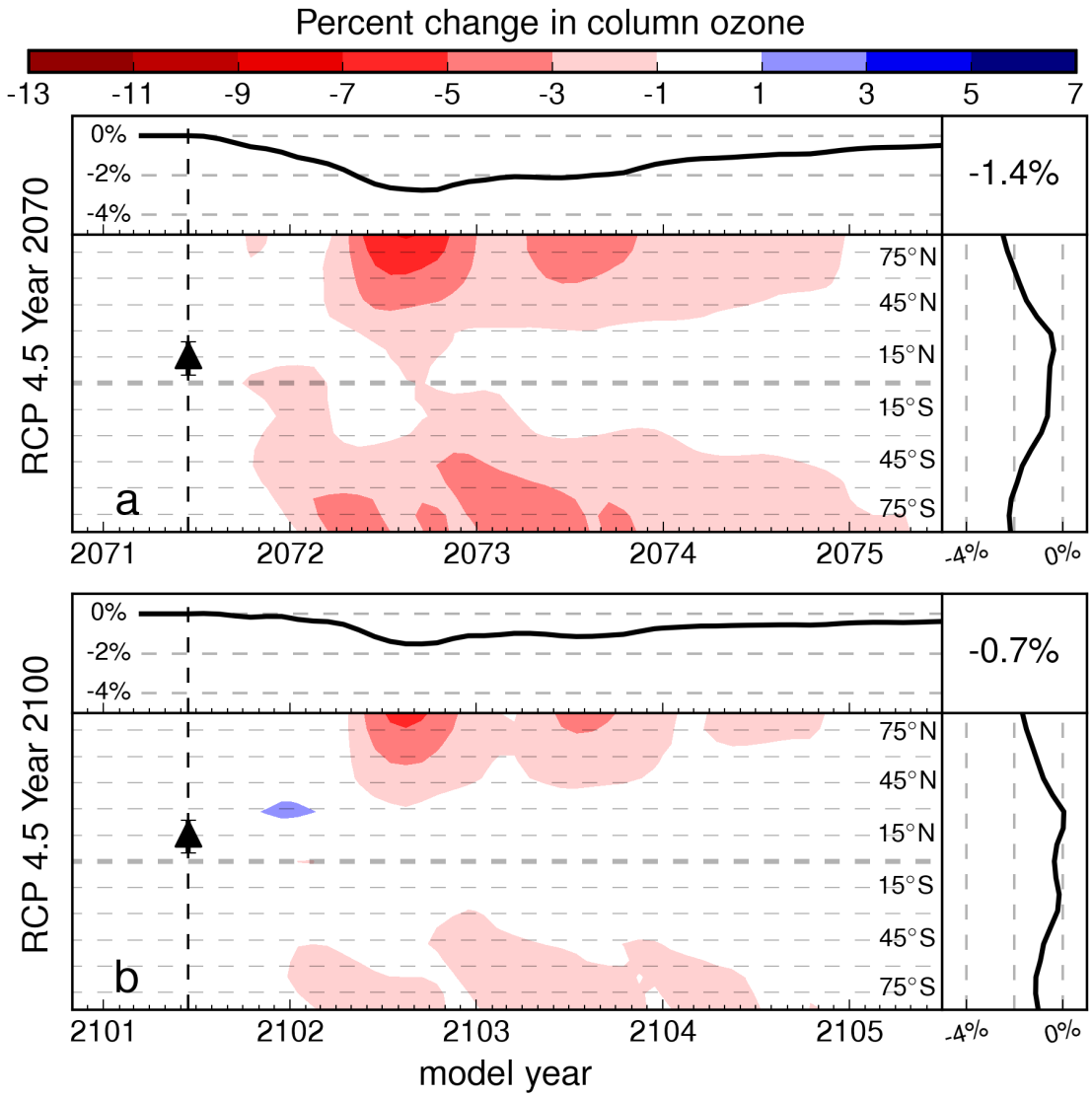

Figure 5.9: Ozone response to Pinatubo-like eruptions in contemporary and future atmospheres. RCP 4.5 scenarios including 4 pptv VSL bromine are simulated for: a. 2071 and b. 2101. Global averages (90°S – 90°N) of total column ozone perturbation are traced atop each panel as a function of time. Temporal average ozone anomalies are traced right. Global-temporal averages are enumerated in the top right. Black triangles indicate injection latitude and time. Red colors indicate column ozone depletion, and blue colors indicate column ozone enhancement.

greater than RCP 6.0 in both cases, as occurs in the RCP 2.6 scenario, but the difference in global-temporal losses between the year 2071 and 2101 is significant, as in the RCP 6.0 scenario. From figure 4.3, it is apparent that N_2O and SF_6 emissions continue to increase between 2070 and 2100 while CO_2 stabilizes and CH_4 declines. Resultantly, as depicted in figure 4.2, stratospheric temperatures are warmer than in RCP 6.0. Signficant stratospheric cooling of 0.5 K occurs between 2070 and 2100.

The RCP 8.5 Time Series of Pinatubo-Like Volcanism

RCP 8.5 is a scenario of runaway greenhouse gas emissions. Paradoxically, this produces both a super-recovery of ozone and an insensitivity of ozone to heterogeneous chemical perturbation. Figure 5.10 shows total column ozone response to Pinatubo-like eruptions in the year 2071 and 2101. In the decade of the 2070s, lower stratospheric halogen activation largely cancels out middle stratospheric nitrogen suppression, except at the midlatitude and subpolar regions. In the year 2101, only transient losses are observed in the northern subpolar regions, briefly. Production of ozone occurs elsewhere.

In the case of RCP 8.5, stratospheric temperatures are very cold – in the year 2100, 5 degrees colder than RCP 2.6. Simultaneously, CH_4 mixing ratios have reached an extraordinary 3700 ppbv, possibly further reducing the effect of heterogeneous chemistry.

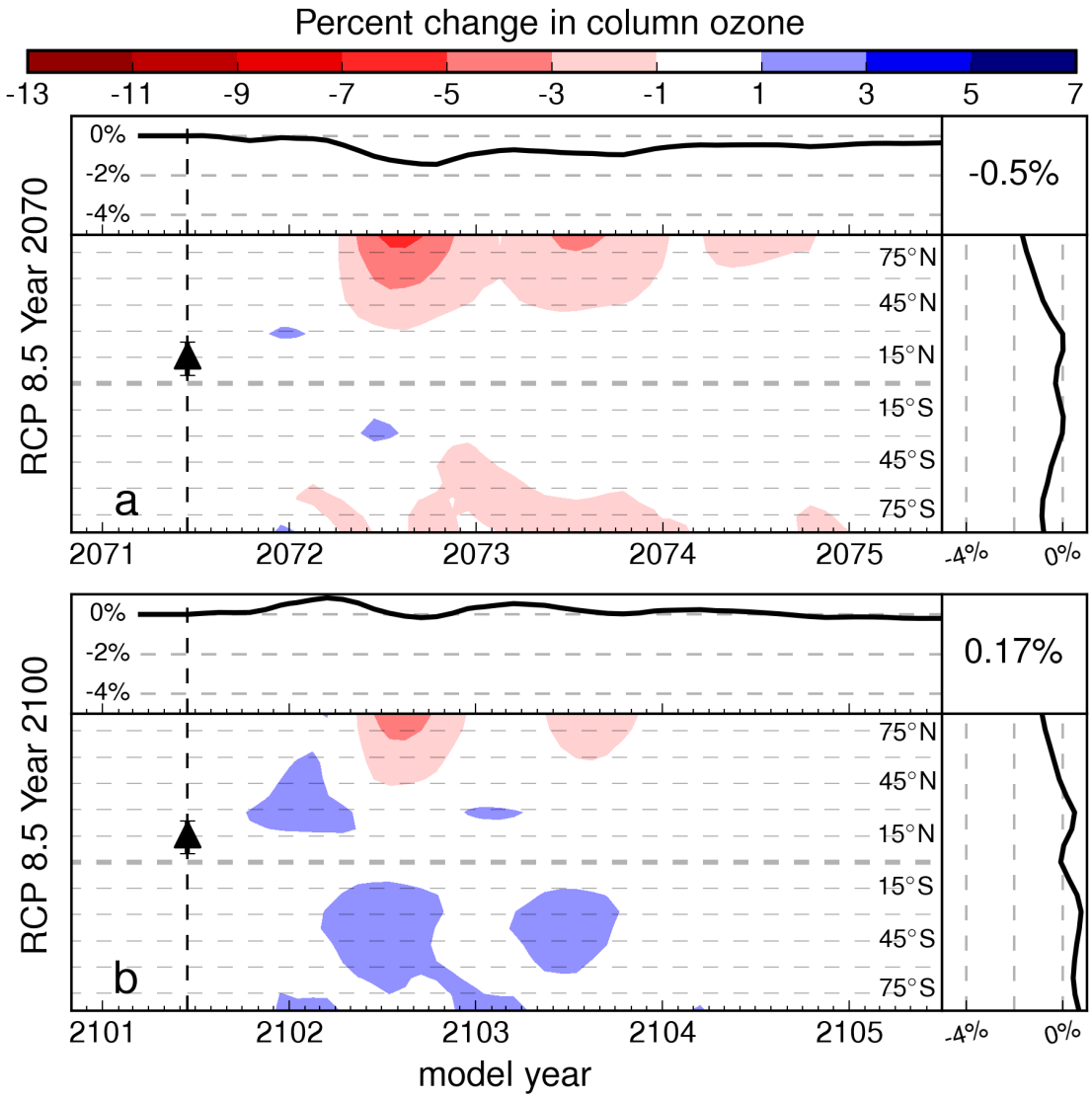

Figure 5.10: Ozone response to Pinatubo-like eruptions in contemporary and future atmospheres. RCP 8.5 scenarios including 4 pptv VSL bromine are simulated for: a. 2071 and b. 2101. Global averages (90°S – 90°N) of total column ozone perturbation are traced atop each panel as a function of time. Temporal average ozone anomalies are traced right. Global-temporal averages are enumerated in the top right. Black triangles indicate injection latitude and time. Red colors indicate column ozone depletion, and blue colors indicate column ozone enhancement.

Sensitivity Studies

There are several varying factors between the different RCP scenarios at each year. Primarily, as time progresses, stratospheric halocarbon loading decays toward its preindustrial levels – while at the same time, human emissions of greenhouse gases increase, producing enhancements in anthropogenic radiative forcing. Radiative forcing itself is a proxy for the vertical temperature distribution of the atmosphere. Within the set of greenhouse gases are gases which also participate in ozone chemistry, such as N_2O (indirectly) and CH_4 (directly). A series of sensitivity studies were performed to evaluate the impact these differences might have on column ozone response to Pinatubo-like eruptions and are described in the following.

Temperature Sensitivity Study

A sensitivity study was performed to determine the role of temperature differences in driving variation in ozone response between the four RCPs. Because the AER-2D model contains offline climatology the chemical and climatological parameters are separable and can be mixed between simulations. For the temperature sensitivity study, four model runs were conducted in which year 2100 RCP 6.0 chemical and transport parameters were conserved. Temperature fields corresponding to each of the RCP scenarios were then applied.

Figure 5.11 a – d visualizes how temperature impacts ozone response to volcanic perturbation. Panels a and b, in which the RCP 2.6 and RCP 4.5 temperature fields were allowed to interact with the RCP 6.0 chemical and transport fields, exhibit comparatively high levels of ozone depletion. In

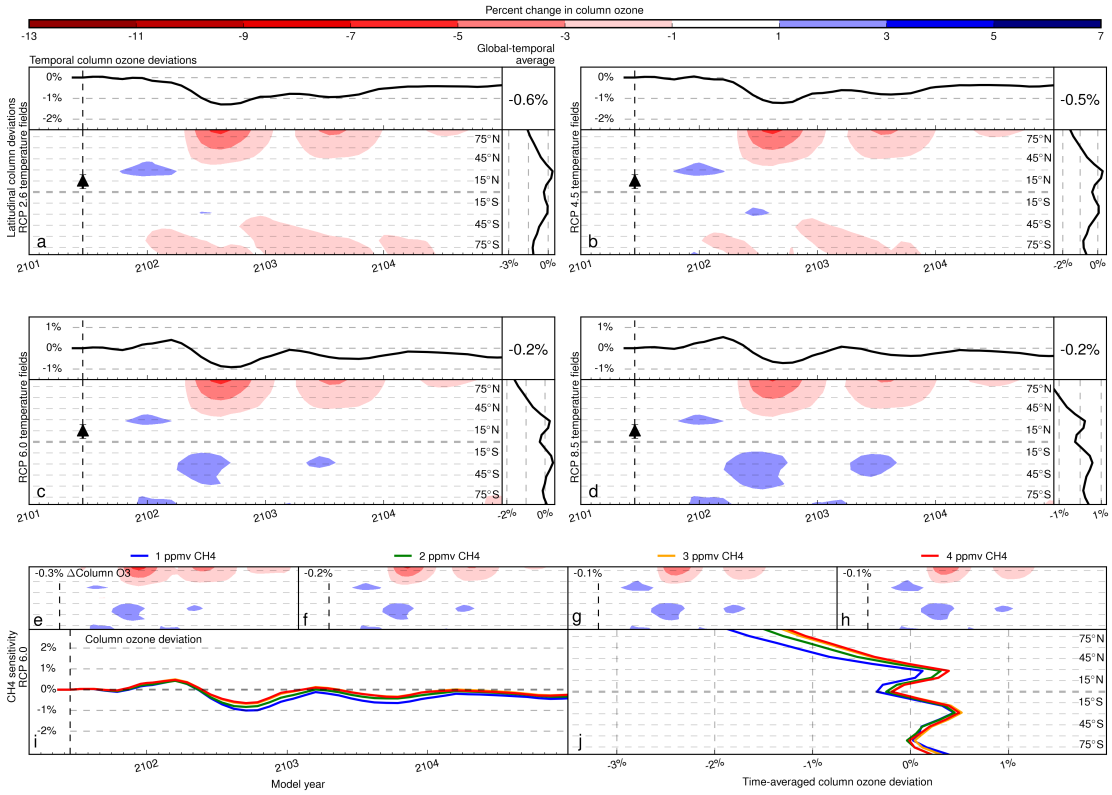

Figure 5.11: Diagnostic plot of temperature (a – d) and methane (e – j) sensitivity studies. a – d: Year 2100 RCP 6.0 chemical parameterizations are evaluated with the indicated year 2100 RCP temperature fields. e – i: Year 2101 RCP 6.0 simulations are evaluated with progressively increasing mixing ratios of CH_4 as indicated. i,j: temporal and latitudinal profiles of the methane sensitivity study.

colder stratospheres – panels c and d – total column ozone losses were reduced by a third relative to the RCP 2.6 temperature scenario. The differences between temperature scenarios are primarily manifest in the southern hemisphere, where aerosol loading is 1/3 the northern hemisphere quantity.

Methane Sensitivity Study

Because CH_4 mixing ratios vary significantly between RCP scenarios and by year within RCP scenarios, a sensitivity study to qualitatively evaluate its impact on column ozone was performed. RCP 6.0 year 2100 model scenarios were evaluated in which methane was titrated between 1 ppmv and 4 ppmv in four steps, as illustrated in figure 5.11(e) – (j). Increasing CH_4 resulted in small increases in O_3, the effect saturating around 3 – 4 ppmv.

Bromine Sensitivity Study

The primary determinant of future ozone response to a volcanic eruption within any specified RCP emission scenario in the year 2101 is VSL bromine from biogenic sources. This sensitivity mainly arises from the increasing fractional contribution of bromine to the overall halogen loading of the modeled lower stratosphere. Figure 5.12 illustrates the mode change induced when varying VSL bromine from 0 to 8 pptv within RCP 6.0. These scenarios are identical in all parameters except for VSL bromine. Global-temporal average column ozone depletions/enhancements are enumerated in each panel. Model runs in which VSL bromine is neglected or set to a small value result in volcanic enhancement of total column ozone, especially in the mid-latitudes, where the efficiency of N_2O_5

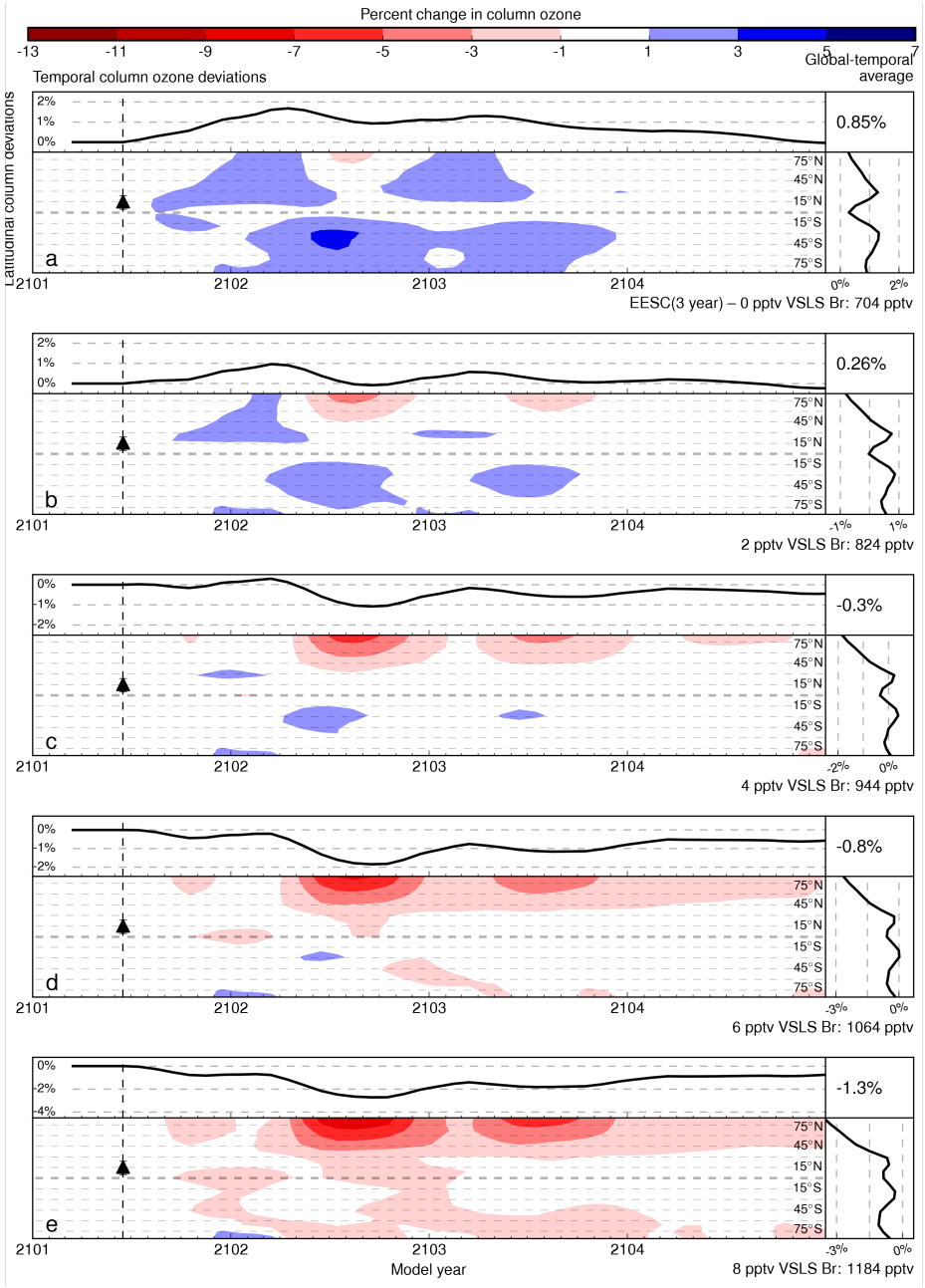

Figure 5.12: Evaluation of a Pinatubo-like eruption in the RCP 6.0 framework for the model year 2101 with varying quantities of VSLS-derived bromine. (a) 0 pptv VSLS Br, (b) 2 pptv VSLS Br, (c) 4 pptv VSLS Br, (d) 6 pptv VSLS Br, (e) 8 pptv VSLS Br.

hydrolysis is highest. Using more realistic values of VSL bromine in the stratosphere, however, column ozone remains susceptible to volcanic-aerosol-induced ozone depletion through the beginning of the next century.

Southern Hemisphere Mass Loading

Because the eruption is simulated in the northern tropics, total mass loading is asymmetric across the hemispheres. The initial injection quickly transports 5 Tg S northward and 2 Tg S southward and an asymmetry in heterogeneous chemical response emerges. To evaluate the the differential hemispheric ozone response in the temperature sensitivity study (depleting in RCP 2.6 / RCP 4.5 - enhancing in RCP 6.0 / RCP 8.5), an experiment was conducted to evaluate southern hemispheric response to larger masses of volcanic sulfate under the expectation that more southern hemispheric mass would produce greater southern hemispheric losses.

Figure 5.13 illustrates the results of this test, in which a northern-hemisphere eruption is simulated in panel a and a southern-hemisphere eruption is simulated in panel b. All input parameters besides the latitude of volcanic injection are held constant. Overall 4-year global response matches well between the two scenarios. The northern hemisphere features strong ozone loss regardless of the hemisphere of injection, though the hemispheric effects are nearly equal in magnitude when the eruption occurs in the southern hemisphere. This is partially because of enhanced transport northward of the equator for the southern hemispheric eruption, resulting in a northern hemisphere S burden of 3 Tg. Staggering the injection by six months would likely attenuate this effect.

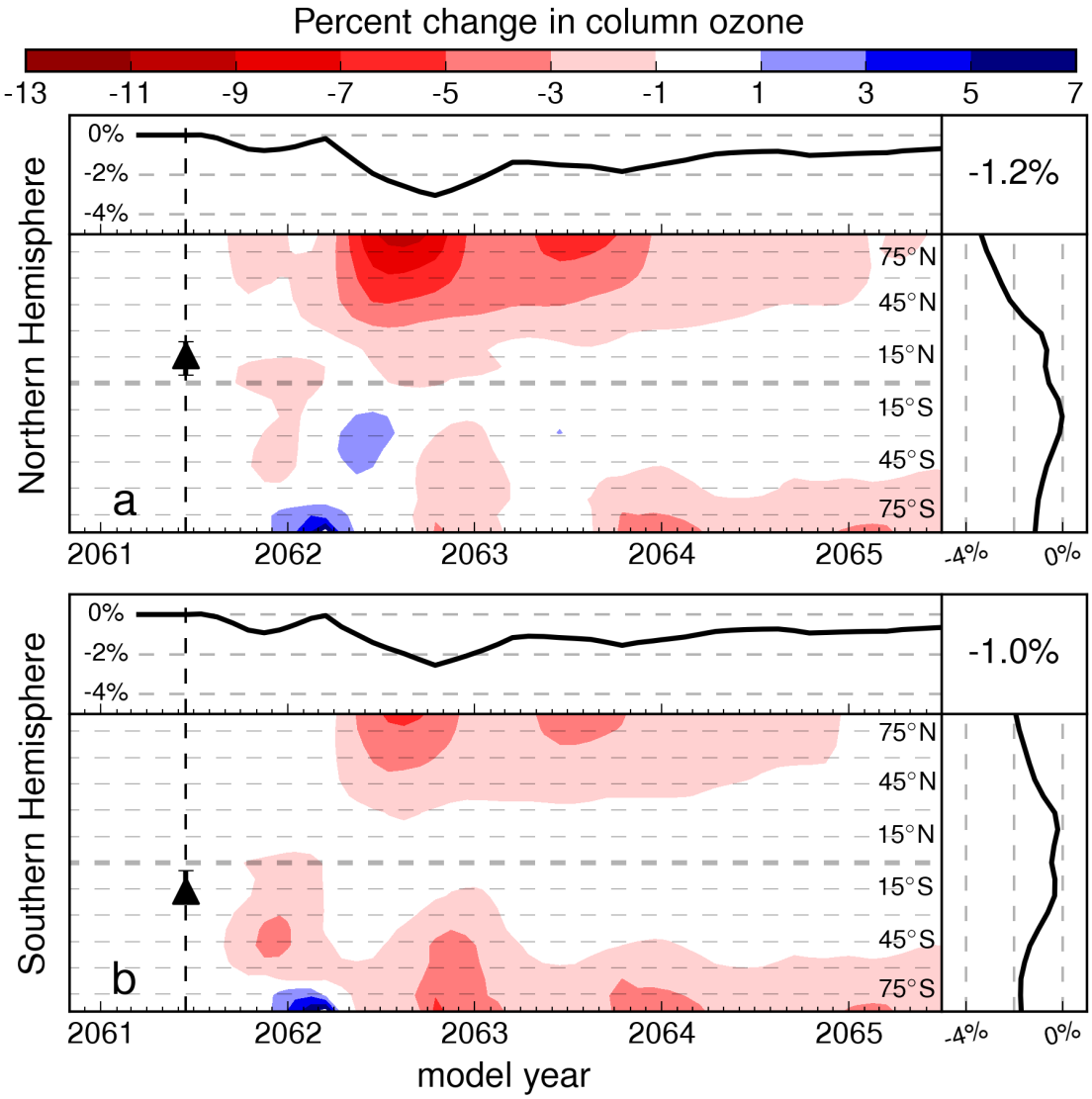

Figure 5.13: Evaluation of a Pinatubo-like eruption in the RCP 6.0 framework for the model year 2060. (a) Northern hemisphere Pinatubo-like eruption. (b) Plane-reflected Pinatubo-like eruption.

Statistical Model

A Simple Random Forest Regression Regression Model

Data were coded according to table 5.2 and fit to determine the role of the parameters as indicated in equation 5.2, the full model. Radiative forcing provides a convenient proxy by with stratospheric temperature may be parameterized.

$$\Delta O_{3i} = X_0 + X_1 RF_i + X_2 EESC_i + X_3 CH_{4i} \tag{5.2}$$

Dummy parameters were constructed to reduce covariance of EESC and CH_4 with radiative forcing: forcing from the explicitly treated greenhouse gases was subtracted from the total forcing. These corrections were first tested in a linear regression model. Methane mixing ratios were observed to wield small statistical power, as the chemical effects of added methane operate on ozone sensitivity to volcanic eruption in the same direction as radiative forcing. Further correction of the radiative forcing component by the radiative forcing imposed by EESC contributing gases slightly improved the fit due to the outsized chemical effect EESC has on stratospheric ozone. N_2O mixing ratios did not demonstrate a significant correlation with ozone response.

Random Forest linear regression modeling with full bootstrapping provides a powerful predictive framework for the exploration of a parameter space. Random samples, with replacement, of a training set are employed to construct trees composed of individual regression parameters. This

Table 5.2: A Predictive Model of Pinatubo-Like Volcanism

Chem.	Temp.	RF(tot) (W/m^2)	F(corrected)[a] RF (W/m^2)	EESC[b] 3-Y (pptv)	CH_4 (ppbv)	ΔO_3
RCP Analyses						
2018 RCP 6.0	RCP 6.0	2.31	1.52	1991	1786	-3.52 %
2051 RCP 6.0	RCP 6.0	3.48	2.75	1304	1900	-2.47%
2061 RCP 6.0	RCP 6.0	3.88	3.17	1199	1943	-1.26%
2071 RCP 2.6	RCP 2.6	2.69	2.26	1117	1307	-1.38%
2071 RCP 4.5	RCP 4.5	4.08	3.47	1103	1738	-1.41%
2071 RCP 6.0	RCP 6.0	4.42	3.74	1104	1963	-0.70%
2071 RCP 8.5	RCP 8.5	6.22	5.11	1091	3341	-0.59%
2101 RCP 2.6	RCP 2.6	2.60	2.24	991	1254	-1.32 %
2101 RCP 4.5	RCP 4.5	4.27	3.78	961	1576	-0.71 %
2101 RCP 6.0	RCP 6.0	5.53	5.01	944	1649	-0.28 %
2101 RCP 8.5	RCP 8.5	8.38	7.23	928	3751	+0.17 %
Temperature Sensitivity						
2101 RCP 6.0	RCP 2.6	2.60	2.24	944	1649	-0.58 %
2101 RCP 6.0	RCP 4.5	4.27	3.78	944	1649	-0.50 %
2101 RCP 6.0	RCP 6.0	5.53	5.01	944	1649	-0.28 %
2101 RCP 6.0	RCP 8.5	8.38	7.23	944	1649	-0.15 %
Bromine Sensitivity[c]						
2101 RCP 6.0	RCP 6.0	5.53	5.01	704	1649	0.81 %
2101 RCP 6.0	RCP 6.0	5.53	5.01	824	1649	0.24 %
2101 RCP 6.0	RCP 6.0	5.53	5.01	944	1649	-0.28 %
2101 RCP 6.0	RCP 6.0	5.53	5.01	1064	1649	-0.80 %
2101 RCP 6.0	RCP 6.0	5.53	5.01	1184	1649	-1.32 %
Methane Sensitivity						
2101 RCP 6.0	RCP 6.0	5.53	5.01	944	1000	-0.31 %
2101 RCP 6.0	RCP 6.0	5.53	5.01	944	2000	-0.19 %
2101 RCP 6.0	RCP 6.0	5.53	5.01	944	3000	-0.09%
2101 RCP 6.0	RCP 6.0	5.53	5.01	944	4000	-0.10 %

Global-temporal changes (4-year average) in total column ozone following a Pinatubo-Like eruption of 7 Tg SO_2 in the chemical and radiative forcing boundary conditions indicated relative to identical conditions in which no eruption occurred. Boundary conditions were informed by Meinshausen et al. (2011).[142] [a]Corrected RF values correspond to RF[Tot] - (RF[CH_4] + RF[EESC]). [b]EESC calculated using Meinshausen RCP global mixing ratios and the method of Newman et al. (2007) with the addition of 4 pptv Br and 100 pptv Cl from VSLS sources unless otherwise noted.[49] [c]Bromine from VSLS sources titrated between 0 – 8 pptv and added/subtracted from 3-Year EESC values.

sampling is repeated in a bootstrapping fashion (bagging) to construct a forest of coefficients. The predictor is then computed as the average of the entire forest.

For example, given a training set of X composed of entries x_0, x_1, x_2, ... x_n and responses Y composed of entries y_0, y_1, y_2, ... y_n, a random subset of n samples from X and Y are selected, with the possibility of selecting the same sample multiple times (replacement) to construct training predictor X_b and training response Y_b. This is done b = 1, 2, 3, ... B times to construct a forest. Subsequently, each tree, Y_b, is fit to obtain regression coefficients and generate a prediction. RFR was applied to the data in table 5.2 in a forest of 2000 trees using the dependent variables CH_4, EESC, and RF (corrected and uncorrected for CH_4 and EESC). The predictive model accounted for 96% of the variation between samples. 5.2. The RFR parameters were subsequently linearized to provide for extrapolation beyond the training dataset per the method of Song, et al., 2013.[175] The resultant linear coefficients are presented in table 5.3 along with bootstrapped confidence intervals.

For the Pinatubo-like volcanism dataset, EESC mixing ratios contribute 65% of the predictive power, radiative forcing contributes 32% of the predictive power, and methane mixing ratios contribute 2%. These variables are explored in figure 5.14. As expected, increasing EESC (a) results in increased rates of ozone destruction. Increased radiative forcing (b) and methane (c) produce slight decreases in column ozone response. The burgundy and blue lines trace predicted changes in ozone response only as a function of the indicated dependent variable.

A large slope is evident in the case of EESC and corrected RF; however, only a slight slope can be discerned in the case of methane mixing ratios between 1000 and 4000 ppbv. Inasmuch as methane mixing ratios have been separated from the radiative forcing component, the ozone response for

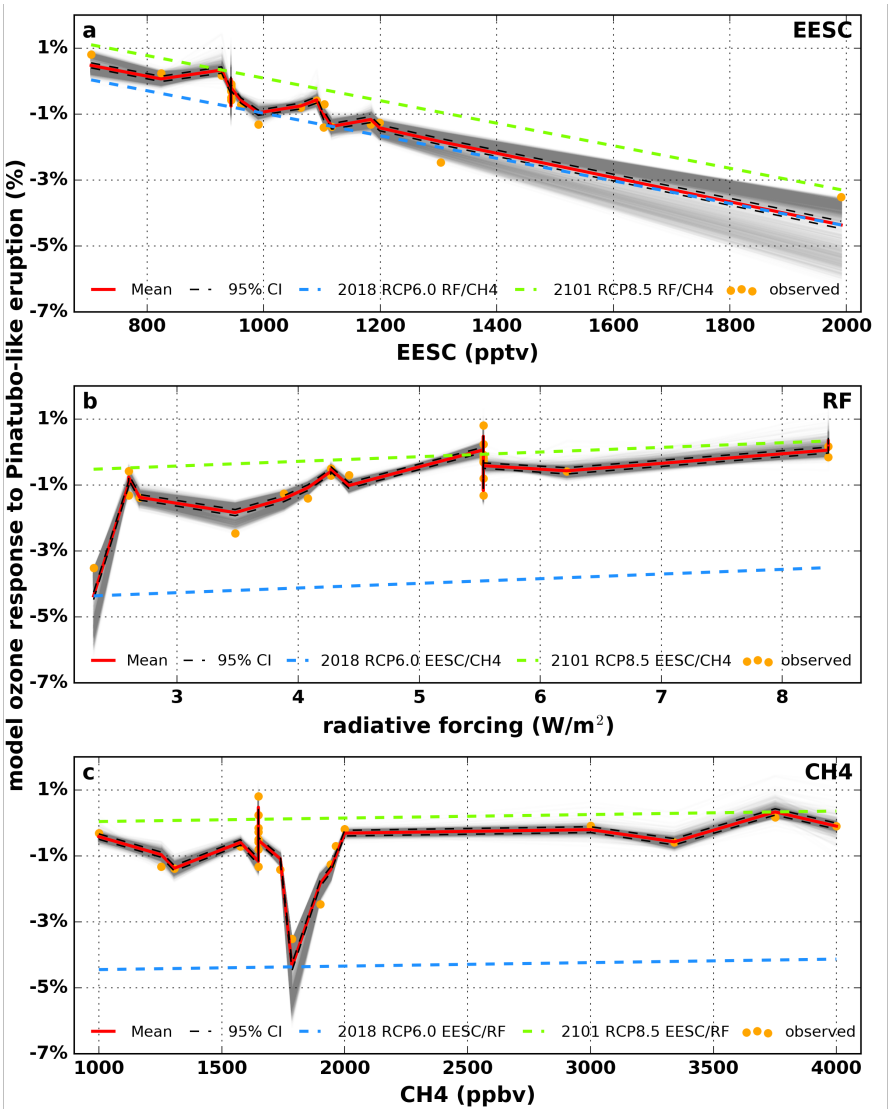

Figure 5.14: Evaluation of predictive model fit parameters as a function of dependent variables following n = 2000 bootstrap iterations. (orange) model output 4-year average ozone deviations following a Pinatubo-like volcanic eruption. (red) predicted model ozone response as a function ofall dependent variables via bootstrapped coefficients. (black) 95% bootstrapped confidence interval. (gray) individual bootstrap traces. (blue) evaluation of dependent variable with all other variables held constant to RCP 6.0 2018 levels (worst test-case scenario). (burgundy): evaluation of dependent variable with all other variables held constant to RCP 8.5 2101 levels (best test-case scenario). (a) Evaluation of model response as a function of increasing EESC. (b) evaluation of model response as a function of radiative forcing. (c) evaluation of model response as a function of methane mixing ratio.

any given change in methane is a superposition of the radiative forcing effect from methane and the participation of methane in stratospheric chemistry. Future changes in methane are unlikely to significantly alter the sensitivity of the ozone layer to Pinatubo-like volcanic eruptions absent extraordinary perturbations (e.g., abrupt clathrate shelf decomposition).

On the other hand, the sensitivity of ozone response to EESC coupled with the potential dynamic range of future EESC changes indicates that any future perturbation of ODS may significantly increase the sensitivity of the ozone layer to Pinatubo-like eruption.

Similarly, future enhancements in bromocarbons would produce enhancements in EESC which would increase ozone sensitivity to eruption. The inclusion of bromocarbons in the general category of EESC may not be appropriate as EESCs are parameterized to a stratospherically-averaged mixing ratio. In reality, Br enhancement from bromocarbons is concentrated in the lower stratosphere and their alpha factor values ($\alpha_{\mathrm{Br}} = 60$) are not constant with season, latitude, or pressure level. Indeed, future alpha factor values for bromine have not been quantified and the accepted value of 60 is derived from work in the 1990's studying 1990's atmospheres. Unfortunately, VSL Br scenarios did not encompass a large enough variation in the other parameters (RF, CH_4) to treat it as a separate variable. Minimal variation in the bootstrapped EESC parameter were observed when excluding the bromine sensitivity study from the analysis (on the order of 1%). Accordingly, though it is not of a large magnitude, the error resulting from this parameterization should be noted.

The positive slope in radiative forcing indicates that stratospheric cooling plays a strong role in slowing down the bimolecular reactions responsible for ozone destruction catalysis. Regardless of future EESC and methane scenarios, the ozone layer is expected to become less responsive to

Pinatubo-like volcanic eruptions as greenhouse gas forcing increases.

A single-point validation of the extrapolated ozone response can be performed by comparison of the AER-2D model output results corresponding to the year 1991 (5.15%, see figure 5.1) and that of the predictive model at the year 1991 (5.03%), as the predictive model training set did not include the 1991 data. The deviation of 0.12% results in a predictive model error of 2% at the prescribed conditions – though it should be noted that the 1991 AER-2D scenario employed time-dependent climatological fields while the predictive model was trained on AER-2D model runs employing 1978 – 2004 climatological average fields.

Prediction of Ozone Response with Corrected EESC Values

As discussed previously in chapter 4, RCP EESCs decay much more quickly than WMO projections. A comparison of WMO EESC with RCP 2.6 and RCP 8.5 is depicted in figure 5.15. Early 21st century EESCs are harmonized between emissions trajectories; however, a much slower decay in the WMO projections becomes apparent in the year 2011. The volcanic sensitivity reported in the previous sections are conservative estimates as a result of their employment of RCP emissions trajectories. As indicated in panel (a), 3-year EESCs recover to their 1980 values around the year 2050 according to the WMO 2014 A1 halocarbon trajectories; however, this recovery to 1980 values occurs much sooner in the RCP emissions projections – at around 2040. A similar story emerges in panel (b) for 5.5-year EESC mixing ratios – 1980 EESC mixing ratios are acheived in aged air masses around the year 2080 according to the WMO 2014 A1 projections, but around two decades earlier according to RCP guidelines.

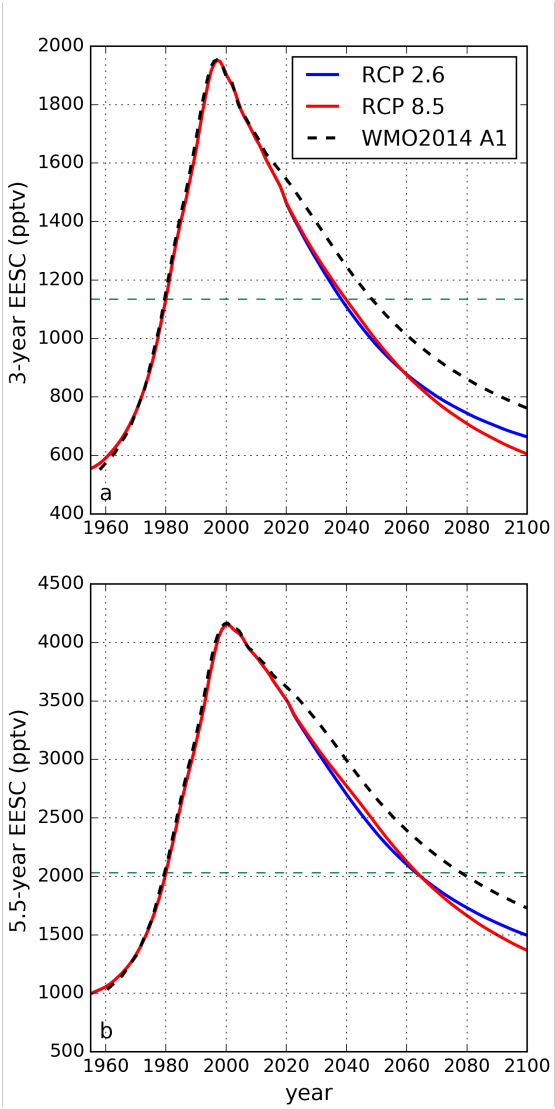

Figure 5.15: (a) Comparison of projected future 3-year EESC values determined using the (blue) RCP 2.6, (red) RCP 8.5, and (black) 2014 WMO Ozone Assessment A1 emissions trajectories of halogenated gases. Green dashed line projects 1980 EESC values. (b) Same as (a), except for 5.5-year EESC values. EESCs were computed according to Newman et al., 2007.[49]

Because the predictive framework prepared in the prior section is a function of corrected radiative forcing, EESC, and methane mixing ratios, it is possible to evaluate ozone response to volcanism within the WMO scenarios. EESCs for future scenarios, as reported in table 5.1 were substituted with respective WMO EESC quantities and fed into the linearized random forest predictors. Additionally, greenhouse gas RF quantities were corrected for the WMO2014 A1 EESCs. These revised results are reported in table 5.4. Universally, the model predicts an increase in ozone response with increasing EESC. The corrections are modest and do not change the conclusions of the analysis conducted using RCP emissions trajectories. Figure 5.16 illustrates the temporal trend in ozone response to a Pinatubo-like eruption for both the RCP GHG/ODS (solid lines) and the RCP GHG/WMO2014 A1 ODS (dashed lines) scenarios. Prior to the year 1955, ozone columns are predicted to thicken following a Pinatubo-like eruption; however, beginning in 1955, when anthropogenic halocarbon releases reached significant levels, the heterogeneous chemical response to a Pinatubo-like volcano is expected to reduce the thickness of the stratospheric ozone layer. The response function reaches a maximum in the year 1991 (coincidentally, the year Mount Pinatubo erupted), with a 4-year global-temporal average ozone loss of 5%. Following the adoption and implementation of the Montreal Protocol (and subsequent amendments – excluding Kigali, which is not included in the RCP storylines), heterogeneous chemical response of the ozone layer slowly recovers. Only in the case of the RCP 8.5 storyline does an expected positive ozone anomaly appear by the year 2100 when 4 pptv VSL bromocarbons are prescribed. After applying the WMO2014 A1 correction, it quickly becomes evident that the heterogeneous chemical component of ozone response remains negative regardless of the greenhouse gas emissions trajectory.

Table 5.3: Linearized Model Fit Parameters

coefficient	mean	lower 95% C.I.	upper 95 % C.I.
Intercept	1.92	1.89	1.96
EESC	-3.42e-3	-3.45e-3	-3.38e-3
RF	1.41e-1	1.39e-1	1.43e-1
CH4	1.06e-4	1.03e-4	1.09e-4

Linearized fit parameters obtained following RFR with 2000 bootstrap samples.

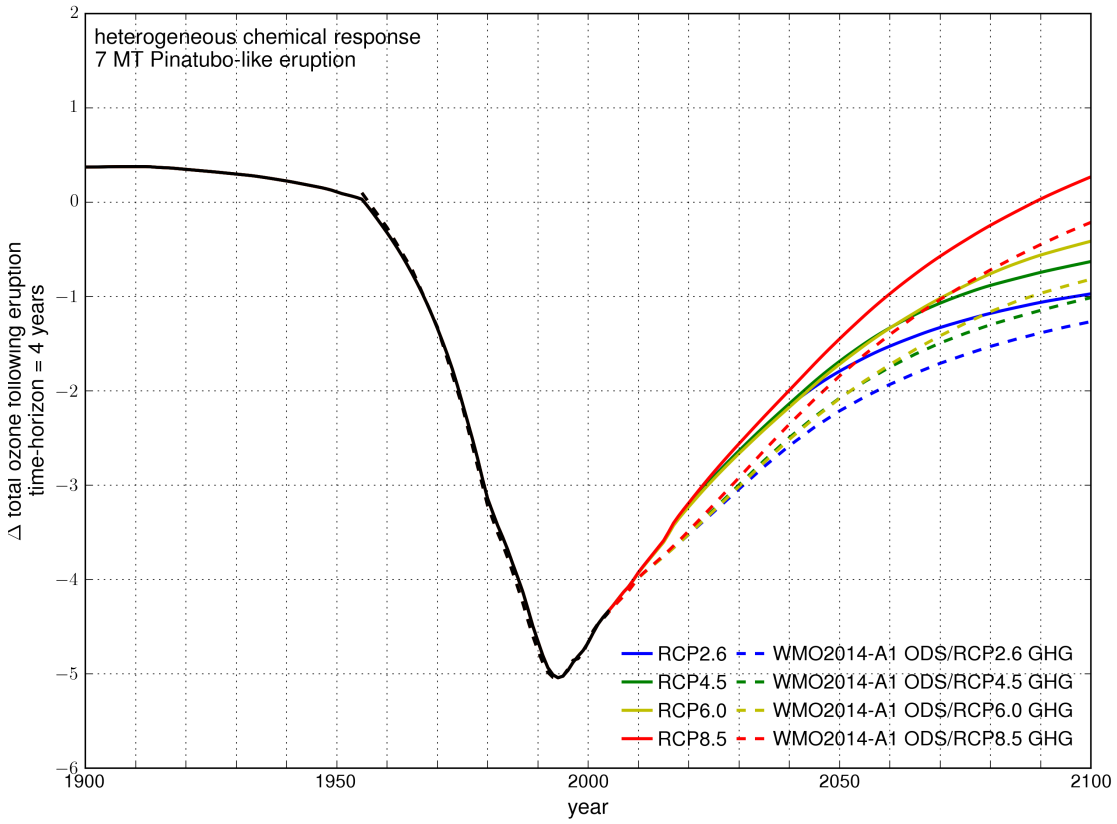

Figure 5.16: Model predictions of ozone response to 7 Tg SO_2 injection at 15.1°N as a function of year of eruption. (solid lines) RCP greenhouse gas and RCP ODS emissions trajectories. (dashed lines) RCP greenhouse gas trajectories (corrected for ODS radiative forcing using WMO2014 A1 ODS mixing ratios) and WMO2014 A1 scenario ODS emissions trajectories. Bromine from VSL bromocarbons fixed at 4 pptv.

Conclusions

Past attempts to identify the inflection point at which the response of total column ozone to heterogeneous chemistry on volcanic sulfate aerosol switches from net-depleting to net-enhancing are highly uncertain, ranging from 2015 to an indeterminate date after 2040.[27,28] However, these studies did not consider the supply of stratospheric bromine by VSL biogenic species, which are now known to play a significant role in the photochemistry of the lower stratosphere.[29] A more recent model intercomparison study of geo-engineering scenarios that does include VSL bromine determines that this shift may occur after 2050, but differs from our simulations of explosive volcanism with regard to total aerosol loading, temporal profile of mass injection, injection latitude, injection mass vertical distribution, and inclusion of radiative-dynamic effects.[156]

For late 21st century Pinatubo-like eruptions, after background chlorine loading is reduced, VSL bromine levels primarily dictate whether column ozone will be enhanced or depleted. This effect is dominant regardless of the projected RCP emissions scenario. Projections of bromocarbon production and stratospheric injection indicate that future scenarios with higher radiative forcing and methane mixing ratios will produce large enhancements of stratospheric bromine due to increased rates of production and chemical lifetime (from decreased HO_x and enhanced troposphere-stratosphere exchange). This trend occurs in the opposite direction of future ozone sensitivity to Pinatubo-like volcanism – possibly resulting in a smoothing of the differences between scenarios

as reported in this chapter. Regardless, perturbations of stratospheric EESC by bromine from VSL sources produced a large effect on ozone. When the strong sensitivity of the ozone response to small enhancements in bromine mixing ratios is juxtaposed with the large uncertainty in current and projected future lower stratospheric VSL bromocarbon fluxes, an investigational priority is evident.

I find that the vulnerability of the atmosphere to column ozone reductions following Pinatubo-like eruptions (SO2 only) will continue into the late 21st century, significantly later than prior estimates.[157] The magnitude of the expected ozone response is dependent on the GHG loading of the atmosphere, with the largest potential ozone losses occurring for future climate scenarios with the smallest increase in GHGs. The differences between the future climate scenarios (e.g., when the stratospheric halocarbon burden is no longer elevated) following a volcanic eruption are primarily driven by variations in projected stratospheric temperature, as well as future levels of methane. Presently, the burden of anthropogenic halocarbons provides the strongest control over the degree to which the ozone layer responds to a Pinatubo-like volcanic eruption.

Table 5.4: Adjusted EESCs and Ozone Response to Pinatubo-Like Volcanism

Scenario	RF(corrected) (W/m^2)	3-Year EESC RCP (pptv)	3-Year EESC WMO (pptv)	Methane (ppbv)	ΔO_3 RCP	ΔO_3 WMO
RCP Analyses						
2071 RCP 2.6	2.26	1117	1199	1307	-1.38%	-1.67%
2071 RCP 4.5	3.47	1103	1199	1738	-1.41%	-1.43%
2071 RCP 6.0	3.74	1104	1199	1963	-0.70%	-1.36%
2071 RCP 8.5	5.11	1091	1199	3341	-0.59%	-0.96%
2101 RCP 2.6	2.24	991	1064	1254	-1.32%	-1.22%
2101 RCP 4.5	3.78	961	1064	1576	-0.71%	-0.95%
2101 RCP 6.0	5.01	944	1064	1649	-0.28%	-0.77%
2101 RCP 8.5	7.23	928	1064	3751	+0.17%	-0.14%

Adjusted ozone response following EESC transform to WMO values using the random forest regression model. EESC calculated with the addition of 4 pptv Br and 100 pptv Cl from VSLS sources. [49]

6

Direct Volcanic Injection of Halogens to the Stratosphere

Abstract

Tremendous quantities of volcanic halogens are occasionally transported to the stratosphere in the eruption column of a large, explosive volcanic eruption. Significant and detectable quantities of

volcanic halogens partition to the stratosphere frequently. The stratospheric injection efficiency of volcanic halogen species is a function of geography, geology, meteorology, and the physicochemical environment of the eruption column. In this chapter, volcanic co-injections of sulfur dioxide and hydrogen chloride are evaluated in the AER-2D chemical-transport-aerosol model for simulated Pinatubo-scale eruptions with HCl:SO_2 ratios corresponding to recent MLS results and the ice core record. It is found that halogen-rich eruptions produce global ozone depletion regardless of the halogen background from long-lived anthropogenic halocarbons. In cases of more severe halogen partitioning, 9-year global average losses exceed 10% with more extreme zonal losses predicted over a shorter time horizon. Additionally, it is demonstrated that perturbations of stratospheric ozone by halogen-rich eruptions have significantly longer lifetimes than perturbations of stratospheric ozone by Pinatubo-like eruptions due to differential decay trajectories of volcanic SO_2 and HCl. The stratospheric ozone response to co-injections of HCl with SO_2 is shown to scale non-linearly in comparison to individual injections of each component.

Introduction

Explosive volcanoes often emit large quantities of hydrogen halides, particularly HCl, but these halogens can be removed by hydrometeors (e.g., rainwater and ice) in the troposphere before they can ascend to the stratosphere and lead to ozone destruction.[176] A number of recent publications, however, have shown that significant stratospheric halogen injection may accompany explosive volcanic eruptions.[11,90,98,177,178] Once dismissed as highly improbable, this effect is not considered in

current ozone assessments.[29] Despite highly efficient hydrometeor scavenging of hydrogen halides in volcanic eruption columns, the direct injection of significant quantities of volcanic halogens into the stratosphere is nonetheless predicted by theory[70,147] and has been confirmed via remote sensing[179–182], in situ observation[183–186], and ice-core analysis[11,187,188].

The Historical Case for Significant Volcanic Injection of Halogen Species to the Stratosphere

Estimates of volcanic hydrogen halide emissions from the historical record vary greatly, frequently exceeding several tens of Tg of HCl in addition to many hundreds of Gg of HBr following a large explosive eruption[90,98,177,178]. Although petrology cannot provide an estimate of stratospheric partitioning, these evaluations of volcanic halogen volatilization historical eruptions are of such a large magnitude that even a stratospheric injection efficiency of 1% would have a significant effect on column ozone. A lower boundary for the stratospheric injection efficiency of halogens within an eruption column is provided by the exceptional case of Mt. Pinatubo (15.1°N), in which the aforementioned tropical cyclone directly transited the paroxysmal eruption plume[101] and scrubbed nearly the entirety of the 4.5 Tg of HCl estimated to have degassed.[105,127] Conversely, case studies have quantified that the majority of the halogen mass emitted by an eruption of Hekla (64.0°N) in the year 2000 reached the stratosphere.[185,186] Moderate stratospheric inputs of HCl have often been observed; Aura MLS recorded stratospheric HCl:SO2 ratios of 0.01 – 0.03 (relative mixing ratios) for fourteen eruptions spanning the years of 2005 to 2014.[179] Additionally, ratios of 0.06 – 0.15 are estimated from the ice-core record of the much larger 7.7 kya eruption of Mt. Mazama (42.9°N).[187,189]

For perspective, the increase in stratospheric inorganic chlorine from Mt. Mazama was estimated to be 8.5 ppbv, a remarkable 4 times greater than the entire stratospheric mixing ratio of chlorine in 1980 (i.e., immediately prior to the major human-driven increase).[187]

Stratospheric Injection Implications of Active Halogen Partitioning Within a Volcanic Eruption Column

Volcanic eruption columns are complex and dynamic chemical environments. Along with sulfur dioxide and water, volcanic eruption columns may contain large quantities of the halogens chlorine and bromine, and to a lesser extent iodine.[69,190–195] Plume temperatures range from very hot at the crater rim to ambient in the umbrella region. Relative humidity and aerosol surface area are initially enhanced relative to the surrounding environment. Rapid adiabatic cooling during plume aging/ascent and simultaneous entrainment of neighboring air masses introduce chemicophysical perturbations that will repartition chemical inventories. Until recently, it had been assumed that volcanic halogen gases primarily existed in their hydrogen halide forms, i.e., hydrogen chloride, hydrogen bromide, and hydrogen iodide. This belief was founded on extrapolation from observations of chlorine, which is about 1000 times more abundant than volcanic bromine (and thus easily detected).[96] Hydrogen halides are extraordinarily soluble in water and water-soluble species are effectively screened from the stratosphere during eruption column ascent.[147,176]

If halogen chemistry is suppressed during eruption column ascent, the stratospheric injection efficiency of halogens is likely to be very low. Indeed, chlorine chemistry within the eruption column is largely suppressed and most chlorine remains bound as HCl with observations of reactive chlo-

rine oxides in plumes being sparse.[69,180,191,196–198] Conversely, volcanic emissions of bromine are frequently observed as bromine monoxide resultant from autocatalytic bromine explosion chemistry analogous to polar tropospheric bromine processing.[69,180–182,190,194–205] The oxidation of halogens in volcanic eruption columns has large implications in the halogenic stratospheric injection efficiency due to the very low solubility of these oxidized species in water.[206] In situ analysis of the Nyamulagira lava lake found that 18 – 35 % of total bromine and 8 – 18 % of total iodine were present in oxidized forms while only a negligible fraction of total chlorine existed as compounds other than hydrogen chloride.[207]

The autocatalytic oxidation of bromine within an eruption column is initiated by the production of bromine atoms from thermal dissociation, as indicated in equation 6.1 which subsequently react with entrained environmental ozone to produce the bromine monoxide radical (equation 6.2. A quantity of this bromine monoxide reacts with hydroperoxy, also produced in the volcanic eruption column, to produce hypobromous acid (equation 6.3). Hypobromous acid may then partition to an acidic aerosol (perhaps acidified by HCl and HBr) where it reacts with a bromine ion to produce the highly insoluble molecular bromine molecule, per equation 6.4 – and this bromine rapidly photolyzes in the daytime to react again with ozone (equations 6.5, 6.6). The net cycle thus produces two bromine monoxide radicals for every initial gas phase bromine atom, provided a supply of ozone and aqueous bromine ions, as illustrated in figure 6.1.

$$\mathrm{HBr} \xrightarrow{\Delta} \mathrm{H} + \mathrm{Br} \tag{6.1}$$

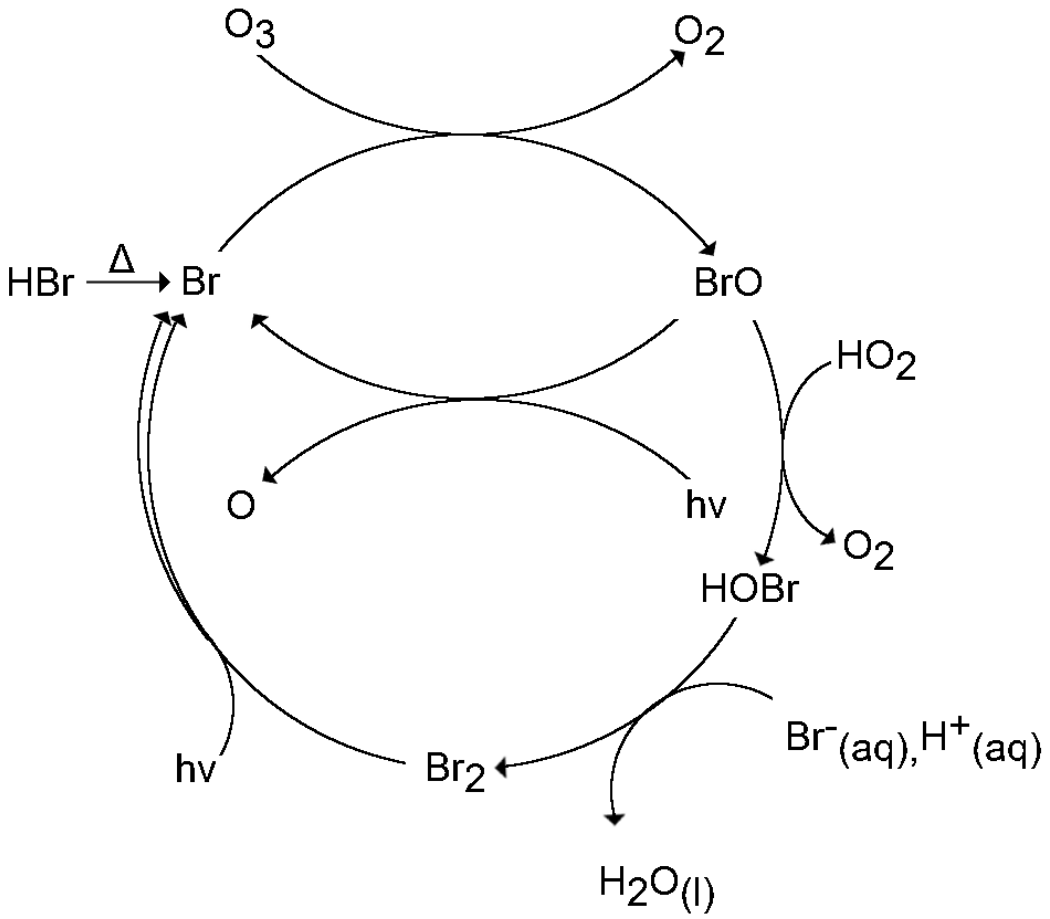

Figure 6.1: A graph theory depiction of the autocatalytic bromine explosion mechanism. Volcanic HBr is dissociated thermally and the bromine radical subsequently reacts with ambient ozone producing BrO. BrO then reacts with HO_2 to produce HOBr, which may then react in the aqueous phase with solvated bromine ions. The resultant Br_2 then photolyzes, producing two bromine radicals. Photolysis of BrO produces O atom which subsequently forms HO_2 and O_3, ensuring propagation of the cycle.

$$Br + O_3 \rightarrow BrO + O_2 \tag{6.2}$$

$$BrO + HO_2 \rightarrow HOBr + O_2 \tag{6.3}$$

$$HOBr_{(g)} + Br^-_{(aq)} + H^+_{(aq)} \rightarrow Br_{2(g)} + H_2O_{(l)} \tag{6.4}$$

$$Br_2 + h\nu \rightarrow 2Br \tag{6.5}$$

$$2\,(Br + O3 \rightarrow BrO + O_2) \tag{6.6}$$

$$\text{Net:} Br + 3O_3 + HO_2 + Br^-_{(aq)} + H^+_{(aq)} \rightarrow 2BrO + 4O_2 + H_2O_{(aq)}$$

Similar chemistry is proposed for the production of iodine and chlorine oxides via reaction with BrO.[198] Volcanic IO was observed in a volcanic eruption column for the first time as reported in 2017.[182] The observed IO was present within the 2008 Kasatochi (52°N) plume in 3 pptv (10 Mg) quantities, as detected in measurements made by both SCHIAMACHY and GOME-2. Within the same eruption column, BrO was quantified to be an order of magnitude more prevalent (100 Mg) than IO.[181,182] The majority of this BrO and IO are believed to have partitioned to the lower

stratosphere. An interdiction of the aged 2008 Kasatochi volcanic cloud during the CONCERT campaign indicated a 20% enhancement in local stratospheric HCl[208], and an extrapolation of Aura MLS HCl:SO2 ratios in the UTLS indicates a total additional stratospheric burden of about 10,000 Mg HCl from the eruption.[179] This relative halogen loading for stratospheric I: Br: Cl of 1: 16: 3611 matches well with expected volcanic halogen emission ratios[96], although it should be noted that uncertainties arising from differences in magma composition, degassing environment, and temporal evolution of the eruption in addition to meteorological perturbation of the stratospheric injection efficiency may significantly alter these values following a future eruption.

Model and Perturbations

Simulated volcanic injections of halogen species were evaluated with the AER-2D chemical-transport-aerosol model,[167,168] as described in section 5.3. Briefly, the model is fully prognostic with respect to aerosol evolution, featuring 40 sectional size bins to accommodate nucleation, coagulation, condenstation/evaporation, heterogeneous chemistry, and sedimentation microphysics. The model is two-dimensional, with 19 latitudinal zones spanning 90°S – 90°N. Pressure extends from the surface to the mesosphere, spanning 1000 – 0.2 hPa in 51 pressure levels, scaled equally in vertical distance (0 – 60 km). Transport and climatology are prescribed from external sources using late 20th century averages.[141] Initial conditions for each eruption experiment were established after spin-up to model stability at the relevant boundary conditions for the specified simulation years. All column ozone deviations reported were calculated as percentage differences from scenarios in which no volcanic

input was allowed, but all other conditions were identical; i.e., the reported changes in ozone are due only to the volcanic perturbation, as indicated by equation 5.1.

$$\Delta_{\text{column O3}}(\%) = \frac{\text{column O3}_{\text{volc}} - \text{column O3}_{\text{no volc}}}{\text{column O3}_{\text{no volc}}} \times 100 \tag{5.1}$$

For experiments in which volcanic input occurred, SO_2 vertical mass distribution was parameterized according to the optimal distribution of Sheng et al. (2015).[108] SO_2 injection quantities were fixed at 7 Tg to reduce the impact of radiative-dynamical perturbations as discussed in section 5.3. Halogen injection quantities were parameterized to encompass the range of HCl:SO_2 ratios observed via Aura MLS[179] (0.01 – 0.03 Moles HCl : Moles SO_2) and the estimate of Mount Mazama chlorine input as from the ice core record ($\leq$ 0.16 moles HCl : Moles SO_2).[187] For the halogen injection experiments, only chlorine injections, and not bromine/iodine injections, were simulated as reliable data for the stratospheric injection efficiency of bromine and iodine does not exist.

Greenhouse gas and long-lived halocarbon chemical boundary conditions were obtained from the RCP emissions projections of Meinshausen et al. (2011).[142] Historical average climatological transport fields were employed in all cases.[141] Temperature fields were obtained from MIROC-CHEM-ESM, an Earth system model with stratospheric chemistry, and employed for the RCP future and contemporary scenarios.[140] Short-lived halocarbons were parameterized at 4 pptv bromine and 100 pptv chlorine according to common VSLS mixing ratio estimations.[49]

Refer to section 5.3 for more information on model performance validation.

Halogen-Rich Eruptions in a Contemporary Scenario

A series of halogen-rich eruptions were simulated in an atmosphere corresponding to the year 2017, as predicted in the RCP 6.0 scenario. Halogen quantities were titrated between 0 – 3 Tg HCl. An injection of 1 Tg HCl corresponds to an approximate enhancement in global EESC by 1 ppbv by mass consideration. Figure 6.2 presents an overview of these eruptions for a period of 9 years following the eruption. In panel (a), the SO_2-only case, note that the ozone perturbation ends within five years of the eruption. Also note that the global-temporal average value of -1.7% total column O_3 is computed for a period of 9 years. In the previous chapter, these values were 4-year averages and the identical 2017 7 Tg SO_2 scenario reported a change of -3.5% total column O_3. Clearly, the time horizon matters.

Panel (b) presents an injection of 0.1 Tg HCl, corresponding to an injection ratio of 0.03:1 Cl:S, a ratio corresponding to the range of recent Aura MLS recoveries.[179] Note that though the ratio corresponds to Aura MLS recoveries, the injected SO_2 quantity is much greater than the recent historical eruptions from which those values were obtained. Slight increases in ozone response are evident following the injection of 0.1 Tg HCl, with slight Austral polar-vortex related enhancements until the year 2025 – two years later than the SO_2-only case.

As the amount of injected HCl is titrated higher, to 0.3 Tg HCl in panel (c), both intensity and longevity of response are observed to grow in. Now, signficant midlatitude losses extend until 2023 for the northern hemisphere and even later in the southern hemisphere. The differential duration of perturbation between the hemispheres is resultant from the asymmetric mass-loading of sulfate

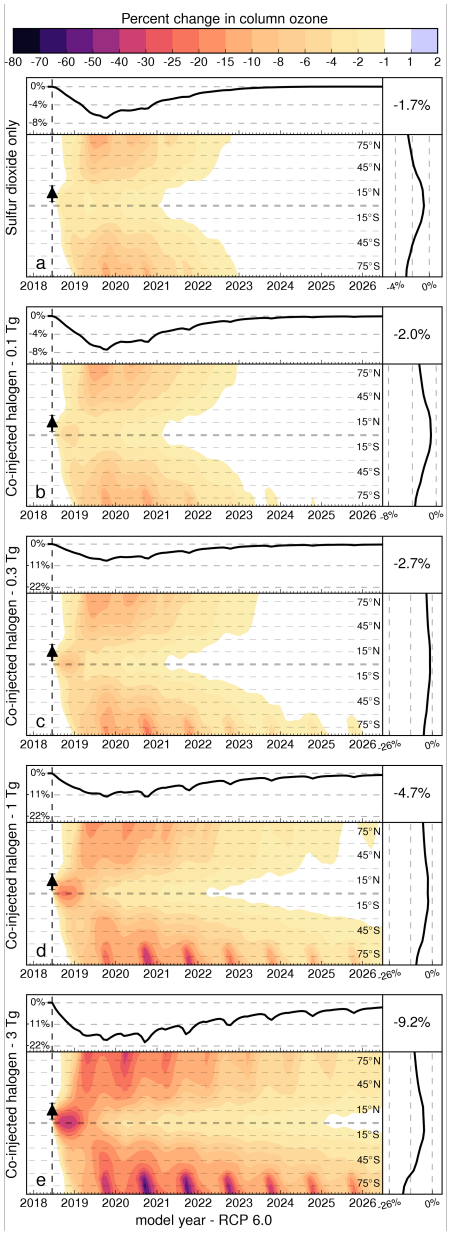

Figure 6.2: Simulated response of column ozone to eruptions of increasing halogen content in the year 2017. For each panel: (main) response of column ozone as a function of time. The simulated eruption occurs at the time and latitude denoted by the black triangle. (top) Global-average ozone response as a function of time. (right) Temporal-average ozone response as a function of latitude. (top right) Global-temporal average (9-year) ozone response. (a) 7 Tg SO_2, (b) 7 Tg SO_2 / 0.1 Tg HCl, (c) 7 Tg SO_2 / 0.3 Tg HCl, (d) 7 Tg SO_2 / 1 Tg HCl, (e) 7 Tg SO_2 / 3 Tg HCl.

aerosol following the simulated eruption at 15.1°N and the colder stratospheric temperatures in the southern hemisphere polar region. Enhanced surface areas in the northern hemisphere slightly enhance the decay rate of injected HCl via increases in the sedimentation trajectory while increased surface area from polar stratospheric clouds in the southern hemisphere interplay with elevated HCl burdens. A comparison of the far right subpanels between panel (b) and panel (c), latitudinal average losses over the entire9-year time period, indicates that much of the enhanced loss observed in panel (c) occurs in subpolar regions. The top panel, the temporal trend in total global ozone loss, is scaled for easy comparison with panels (d) and (e) below.

Panel (d) of figure 6.2 begins to demonstrate extreme ozone destruction over the entire 9 year simulation period. Enhancements in polar vortex processing result in 40 % losses in the 2020. 1 – 6% losses are observed in the northern hemisphere midlatitudes seven years after the eruption and for the first two years span 10 – 15 %. Note that the ratio of injected HCl:SO_2 corresponds to the ice core record of Mount Mazama, though the simulated eruption is about 10 times smaller in magnitude.

Mount Mazama produced between 3 – 8 Tg enhancements in the stratospheric HCl burden. Panel (e) explores an injection of 3 Tg HCl – the most severe case explored in this series of experiments. Immediately, shades of pink indicate profound ozone losses between 25 – 50 % in the immediate location of the eruption and later into the midlatitudes. Nearly-complete depletions of Antarctic ozone are observed as a result of volcanic processing alone. Total ozone nears recovery at the end of the 9 year experimental time horizon; however, a comparison to panel (c) provides indication that another three or four years may be required for complete recovery.

Future Halogen-Rich Eruptions in the RCP Framework

A series of experiments were conducted to evaluate the sensitivity of ozone in future climates to volcanic injections of halogen. Each RCP scenario was evaluated in the years 2071 and 2101 and subjected to volcanic injections of 0.3 Tg HCl and 3 Tg HCl.

Halogen-Rich Eruptions in the RCP 2.6 Framework

Figure 6.3 provides the ozone response to a halogen-rich eruption in the year 2071 under the RCP 2.6 emissions trajectory. Panel (a) corresponds to an eruption of only 7 Tg SO_2 in which the ozone perturbation is observed to disappear after four years, with a 9-year global loss of 0.7 % total column ozone. The addition of 0.3 Tg HCl, as demonstrated in panel (b) dramatically lengthens the longevity of the disturbance. Surface area effects are very evident, with the northern hemisphere recovering 5 years after the eruption while the southern hemisphere continues to suffer ozone depletion until the experiment ends in the year 2079. Panel (c), an injection of 3 Tg HCl, resembles closely the expected losses for an eruption in the year 2017. This will be the case for the following figures as well. In these future scenarios, the EESC perturbation fromthe injection of 3 Tg HCl is effectively a doubling of the pre-eruption stratospheric burden. That is to say, the volcanic eruption is the dominant perturbation and effects from the variation in RCP scenario radiative forcing and ozone-depleting substance mixing ratios are comparatively minor.

Figure 6.4 provides a similar story as the previous figure; while a Pinatubo-like eruption barely produces any loss in total column ozone over the 9-year time horizon, the injection of halogens re-

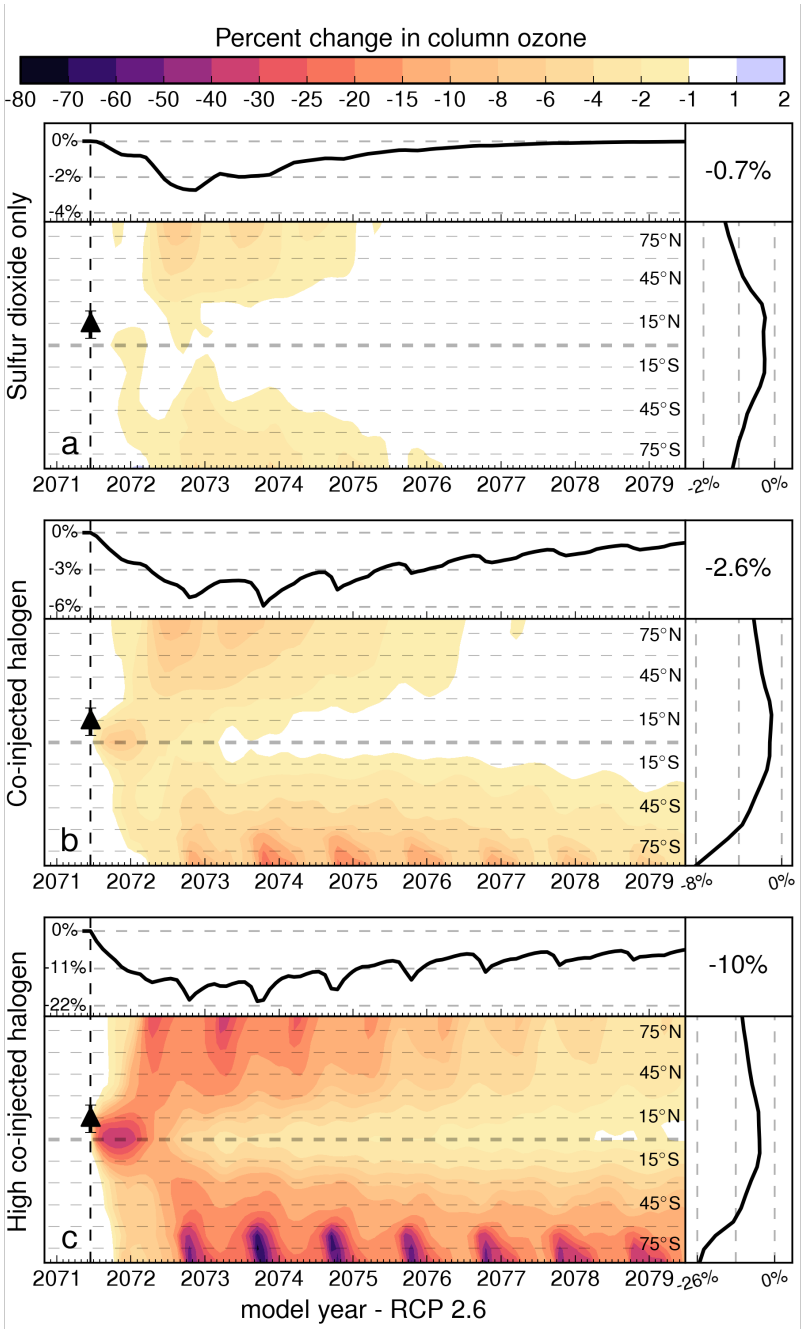

Figure 6.3: Simulated response of column ozone to eruptions of increasing halogen content in the year 2071 under the RCP 2.6 emissions framework. (a) 7 Tg SO_2, (b) 7 Tg SO_2 / 0.3 Tg HCl, (c) 7 Tg SO_2 / 3 Tg HCl.

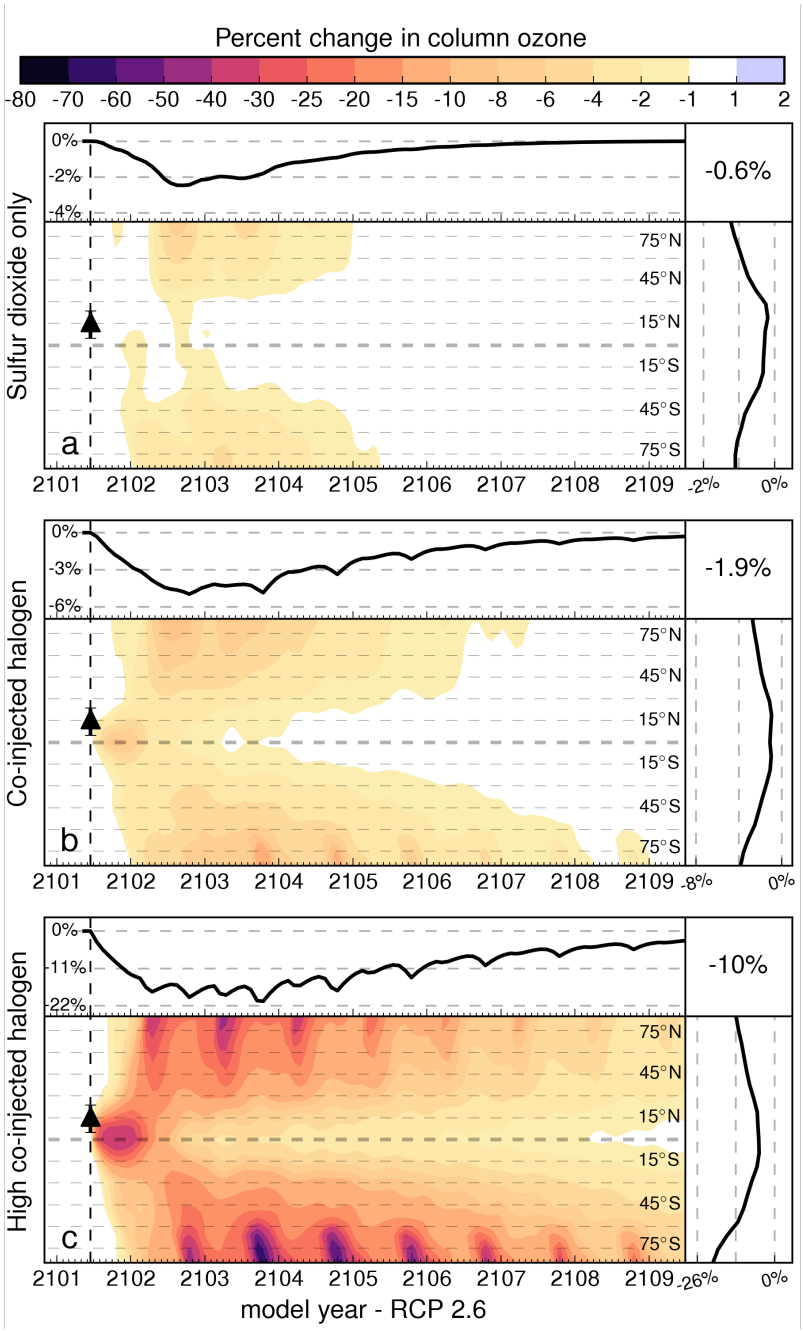

Figure 6.4: Simulated response of column ozone to eruptions of increasing halogen content in the year 2101 under the RCP 2.6 emissions framework. (a) 7 Tg SO_2, (b) 7 Tg SO_2 / 0.3 Tg HCl, (c) 7 Tg SO_2 / 3 Tg HCl.

sults in a significant enhancement in the duration of the perturbation. In panel (a), note that column ozone recovers in totality within four years of the eruption, whereas the injection of 0.3 Tg HCl, as in panel (b) produces column losses up to eight years later. Losses in panel (c) are essentially identical in quality and quantity to those observed in figure 6.3(c) except that very large losses in northern hemispheric ozone, rivaling those in the southern hemisphere, are observed in the year 2101 scenario. This is possibly because the radiative forcing declines from 2.69 W/m^2 to 2.60 W/m^2 between the years 2071 and 2101.

Halogen-Rich Eruptions in the RCP 4.5 Framework

Ozone response to halogenic eruptions in the RCP 4.5 emissions trajectory are very similar to eruptions under RCP 2.6. Figure 6.5 (a) depicts a SO_2-only eruption in the year 2071. Column ozone is slightly less perturbed than values predicted under RCP 2.6 and also return to pre-eruption values several months sooner. This earlier recovery is more evident in panel (b). In contrast to the RCP 2.6 scenario, complete recovery following an injection of 0.3 Tg HCl occurs within the experimental window of nine years in an RCP 4.5 year 2071 simulation. Figure 6.5 (c) initially looks nearly identical to figure 6.3 (c); however, the latitudinally-averaged temporal trace in the top subpanels exhibit a significant variation. In the RCP 4.5 scenario, there exist twice as many sharp seasonal dips in ozone. These dips correspond to wintertime processing of ozone within the polar vortex. In the case of RCP 4.5, this processing is significantly enhanced in the northern hemisphere as well as the southern hemisphere. Significant differences are evident when comparing figure 6.6 (a) with the corresponding RCP 2.6 scenario. Column ozone has recovered to pre-eruption values in about 3.5 years in both

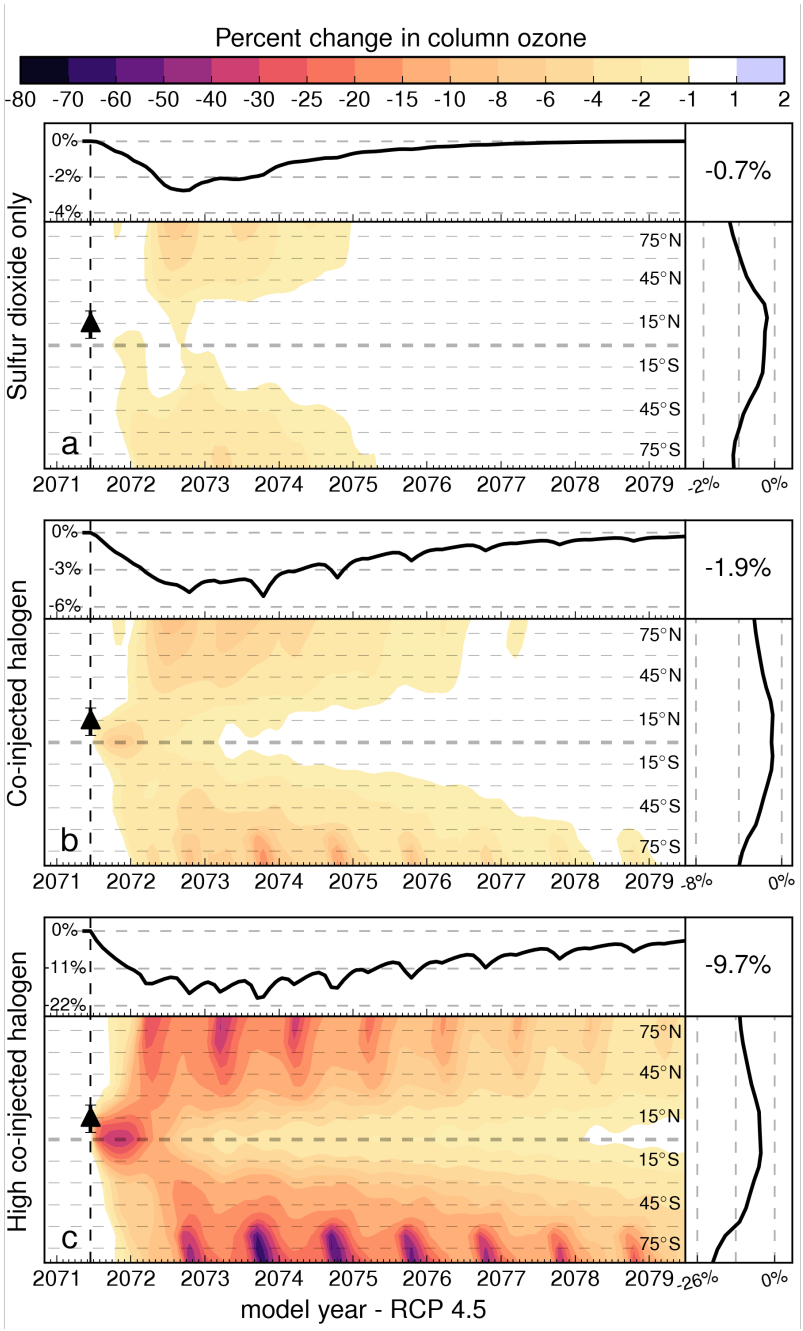

Figure 6.5: Simulated response of column ozone to eruptions of increasing halogen content in the year 2071 under the RCP 4.5 emissions framework. (a) 7 Tg SO_2, (b) 7 Tg SO_2 / 0.3 Tg HCl, (c) 7 Tg SO_2 / 3 Tg HCl.

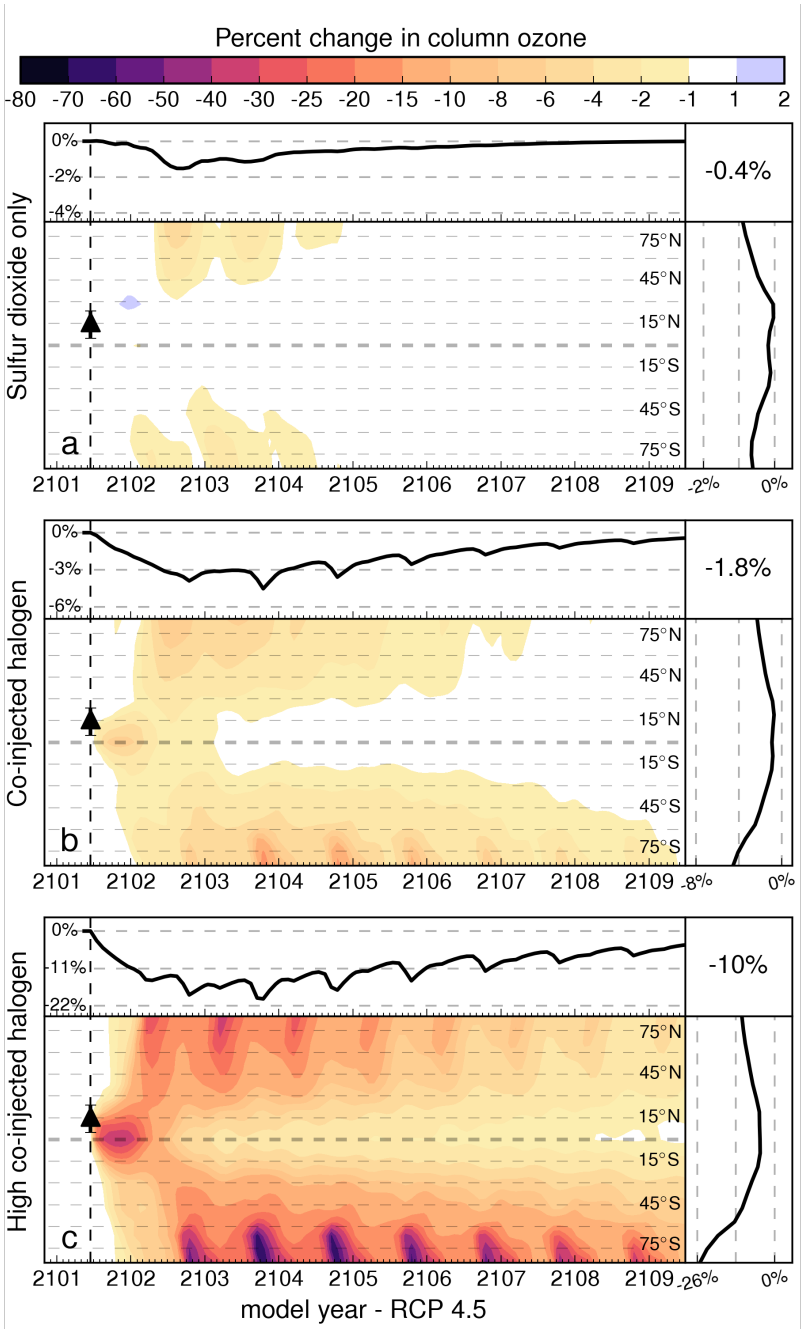

Figure 6.6: Simulated response of column ozone to eruptions of increasing halogen content in the year 2101 under the RCP 4.5 emissions framework. (a) 7 Tg SO_2, (b) 7 Tg SO_2 / 0.3 Tg HCl, (c) 7 Tg SO_2 / 3 Tg HCl.

hemispheres. A slight blue point is observed in the northern hemisphere, indicating that heterogeneous suppression of NO_x processing is beginning to outcompete lower-stratospheric enhancement in Cl_x. The addition of halogens to the eruption column induces ozone depletion averaging -1.8% over the 9 year time horizon. Recovery is evident immediately prior to the end of the simulation run in the year 2109. Again, panel (c) is quite similar to other injections of 3 Tg as the added halogens overwhelm other processes; however, it is apparent that enhancements in austral polar processing in response to a volcanic eruption are greater in RCP 4.5 than in RCP 2.6 – especially in the years 2105 and 2106. Interestingly, the boreal polar processing of ozone follows the opposite trend and is slightly weaker under RCP 4.5.

Halogen-Rich Eruptions in the RCP 6.0 Framework

RCP 6.0 shows significant differences in response to halogen-rich eruptions relative to the low-emissions RCP storylines. Figure 6.7 (a) depicts the expected response from a SO_2-only eruption. Several blue spots in the southern hemisphere indicate the suppression of NO_x-mediated depletion of ozone. While midlatitude ozone columns return to their pre-eruption levels within three years of the eruption, austral seasonal cycling is perturbed by the eruption for five years. When the eruption also injects 0.3 Tg HCl, as in panel (b), the perturbation in southern hemisphere ozone columns persists throughout the entire simulation period with no indications of recovery. If 3 Tg HCl are injected, significant ozone losses occur, mainly concentrated in the subpolar southern hemisphere. The same trends appear following an eruption in the year 2101, per figure 6.8. Minor reductions in the magnitude of column ozone loss are evident for the eruptions depicted in panels (a) and (b) in

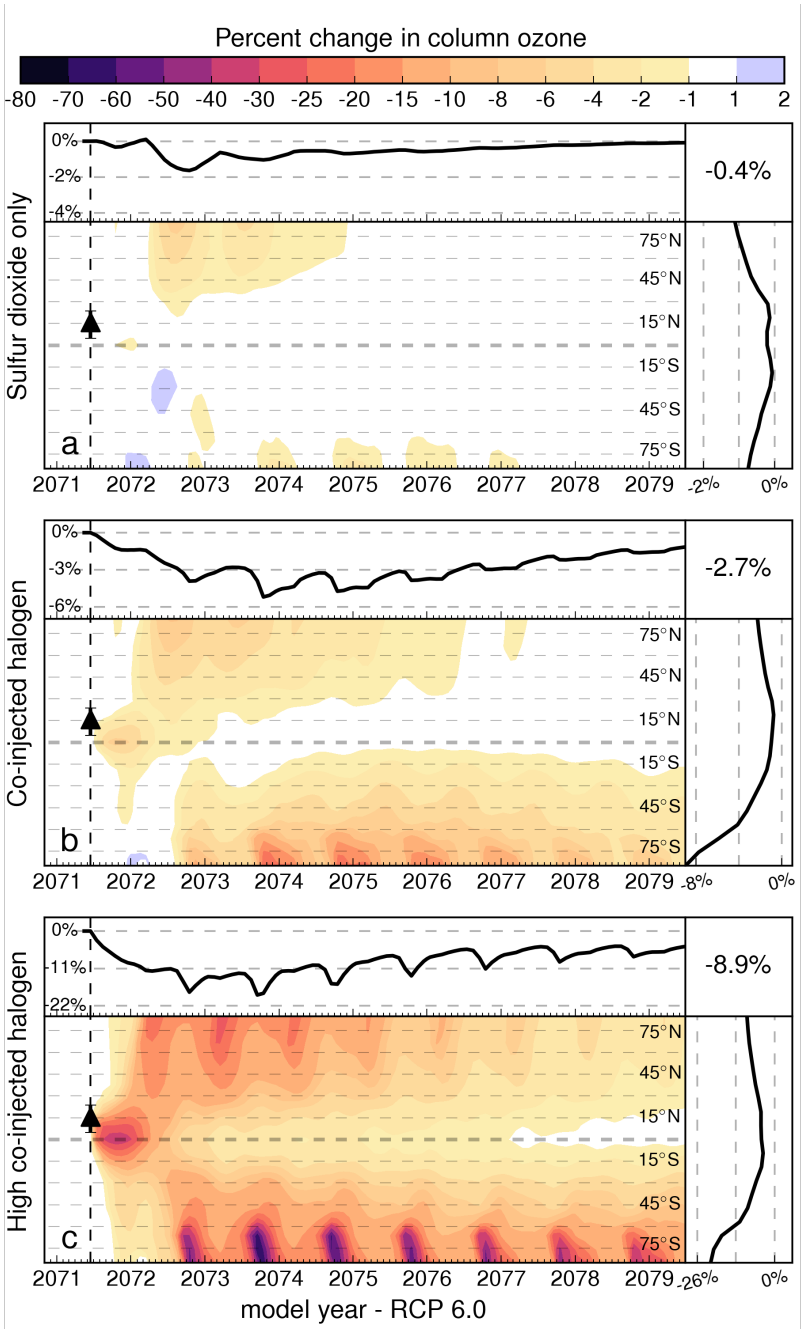

Figure 6.7: Simulated response of column ozone to eruptions of increasing halogen content in the year 2071 under the RCP 6.0 emissions framework. (a) 7 Tg SO_2, (b) 7 Tg SO_2 / 0.3 Tg HCl, (c) 7 Tg SO_2 / 3 Tg HCl.

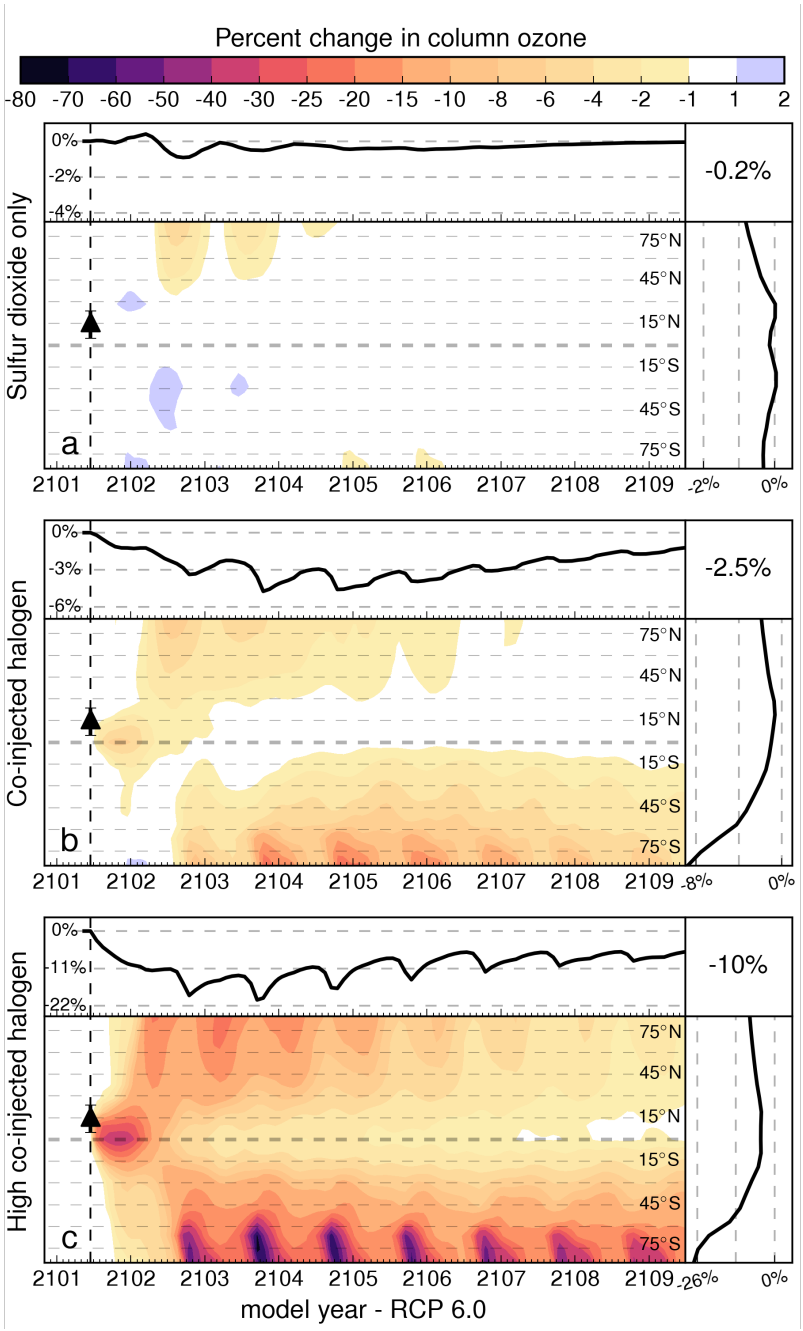

Figure 6.8: Simulated response of column ozone to eruptions of increasing halogen content in the year 2101 under the RCP 6.0 emissions framework. (a) 7 Tg SO_2, (b) 7 Tg SO_2 / 0.3 Tg HCl, (c) 7 Tg SO_2 / 3 Tg HCl.

2101 relative to the same eruptions in 2071; however, in the case of the 3 Tg injection, there is significatly more loss following an eruption in the year 2101 than in the year 2071. This loss is largely confined to the southern subpolar regions and is resultant from halogen concentrations passing a critical denitrification threshhold at which increasing zonal halogen increases $\frac{Cl_x}{Cl_y}$ rather than producing greater quantities of chlorine reservoir.

Halogen-Rich Eruptions in the RCP 8.5 Framework

Again, in the case of RCP 8.5, the trend is largely the same: attenuated ozone response following a Pinatubo-like eruption (figure 6.9 (a)) and increasing losses of column ozone following a halogen-rich eruption as a function of injected halogen quantity (e.g., figure 6.9 panels (b) and (c)). In the case of RCP 8.5, the Pinatubo-like eruptions only produce ozone perturbations in the high-midlatitudes and subpolar regions for the first 2.5 years following the eruption. In the case of the 0.3 Tg injection of HCl, complete recovery occurs within 9 years of the eruption. Strong enhancements in boreal polar processing of ozone follow an injection of 3 Tg HCl, as in panel (c).

For an eruption in the year 2101 under RCP 8.5 emissions trajectories, sulfate-only eruptions are expected to produce a coincidental 0.00% change in ozone over a globally-averaged 9-year time-horizon (figure 6.10 (a)). A small injection of halogens, as in panel (b), dramatically changes the situation, resulting in slight decadal losses of ozone. Larger injections of HCl, per panel (c) produce, again, dramatic losses – year-round averages of 25% loss in the southern subpolar regions for more than a decade.

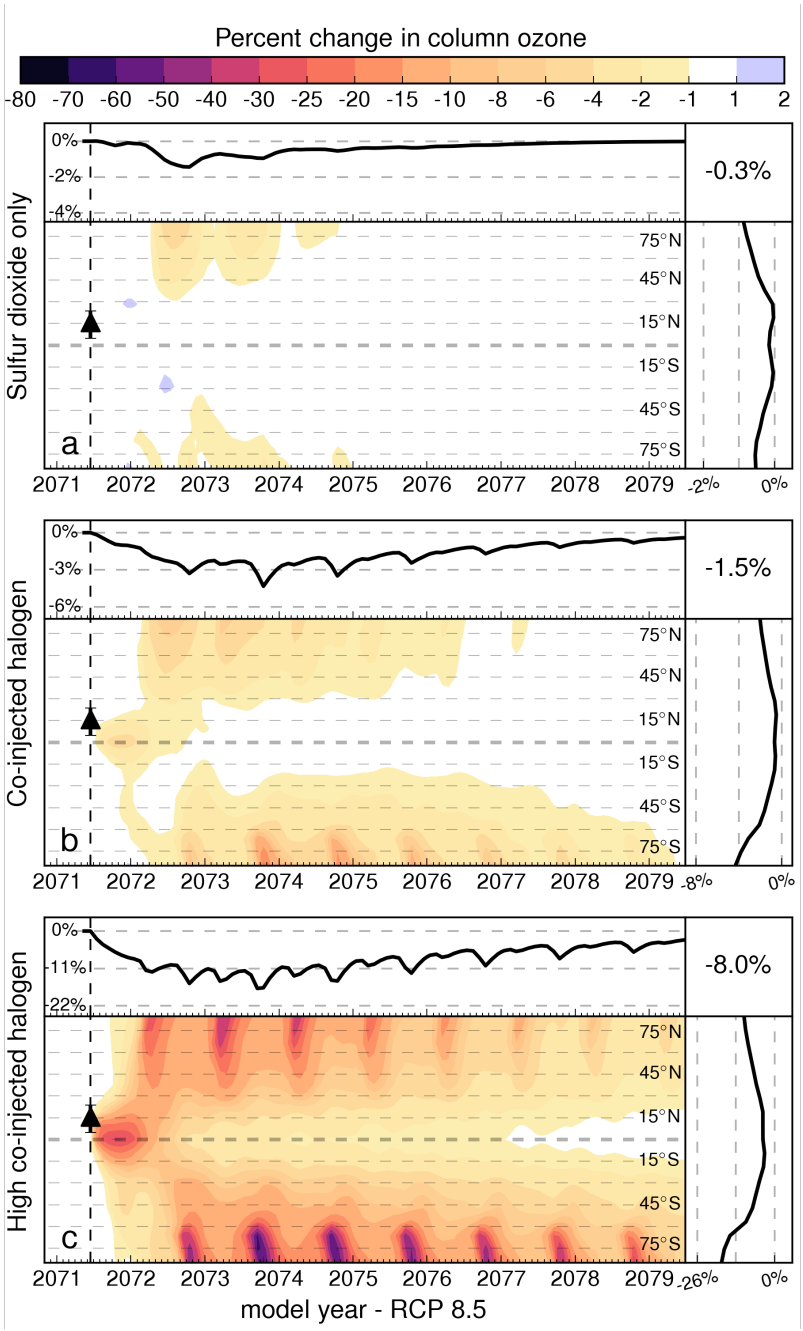

Figure 6.9: Simulated response of column ozone to eruptions of increasing halogen content in the year 2071 under the RCP 8.5 emissions framework. (a) 7 Tg SO_2, (b) 7 Tg SO_2 / 0.3 Tg HCl, (c) 7 Tg SO_2 / 3 Tg HCl.

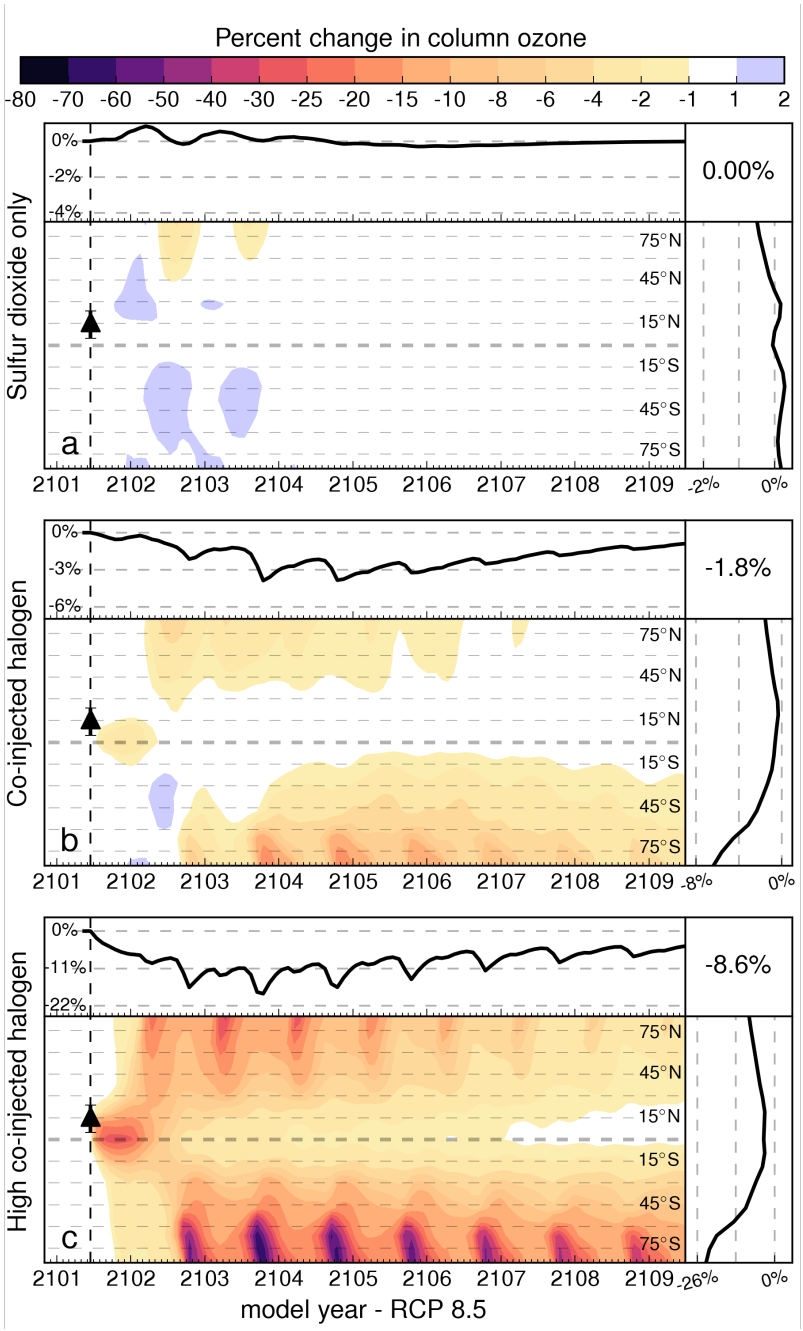

Figure 6.10: Simulated response of column ozone to eruptions of increasing halogen content in the year 2101 under the RCP 8.5 emissions framework. (a) 7 Tg SO_2, (b) 7 Tg SO_2 / 0.3 Tg HCl, (c) 7 Tg SO_2 / 3 Tg HCl.

Decay Trajectories of Halogens and Sulfate Aerosol

Figures 6.11 and 6.12 present the molar stratospheric anomaly for sulfate aerosol and HCl as defined in equation 6.7. Panel (a) presents the SO_2-only injection case. For both scenarios, a slight decline in background HCl is observed resultant from heterogeneous processing. The dashed lines indicate northern hemisphere averages. It is apparent that northern hemisphere sulfate inventories decline slightly faster in the first years of the eruption than southern hemisphere sulfate inventories due to increased rates of coagulation and sedimentation. Panel (b) presents the decay trajectory of HCl in the absence of SO_2 injection. It is apparent that some of the HCl initially injected has partitioned to other forms of Cl_x, but slowly repartitions back to HCl as it transports poleward. Even though unequal amounts of HCl were injected into each stratosphere, the anomalies quickly equalize and decay in tandem for both years explored. A difference emerges in panel (c) of figures 6.11 and 6.12. SO_2 is coinjected with HCl. In the case of the year 2017, it appears that enhanced surface area from aging SO_2 immediately repartions all of the injected HCl into Cl_x, while in the year 2101, this does not occur. The reason for this divergent behavior is not immediately apparent, but may be due to the very rapid reformation of HCl following activation in the year 2101 RCP 8.5 scenario due to very high methane mixing ratios. Panels (d) and (e) of both figures are nearly identical as injections of 3 Tg HCl overwhelm the entire stratosphere.

$$\text{Anomaly}_x = M_{x,\,\text{perturbation}} - M_{x,\,\text{no perturbation}} \tag{6.7}$$

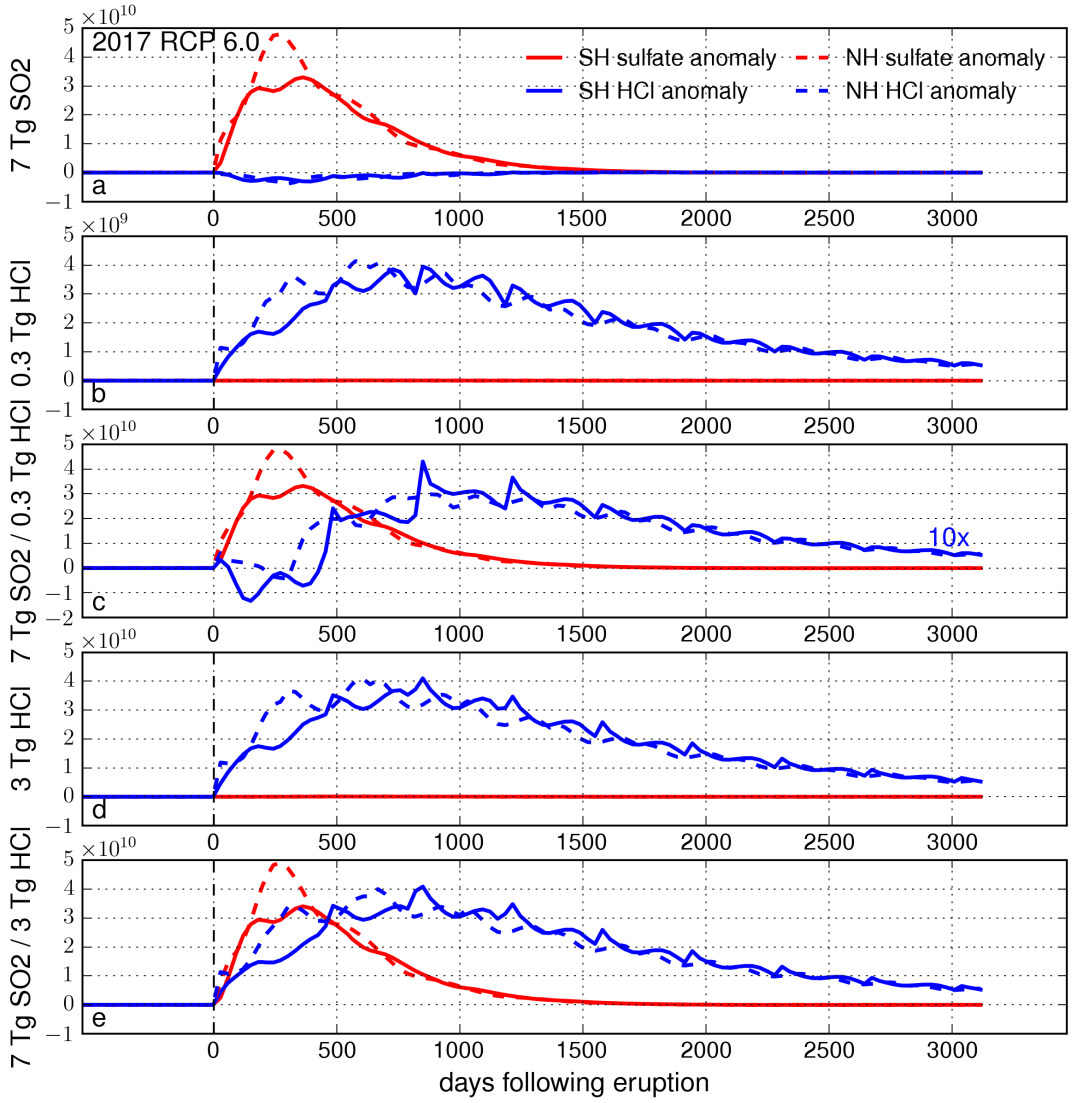

Figure 6.11: Decay trajectories for the molar stratospheric anomalies of (red) sulfate aerosol and (blue) HCl in the RCP 6.0 framework for the year 2017. Anomalies are calculated as the difference between a nonvolcanic baseline and the indicated perturbation. (a) 7 Tg SO_2, (b) 0.3 Tg HCl, (c) 7 Tg SO_2 / 0.3 Tg HCl, (d) 3 Tg HCl, (e) 7 Tg SO_2 / 3 Tg HCl.

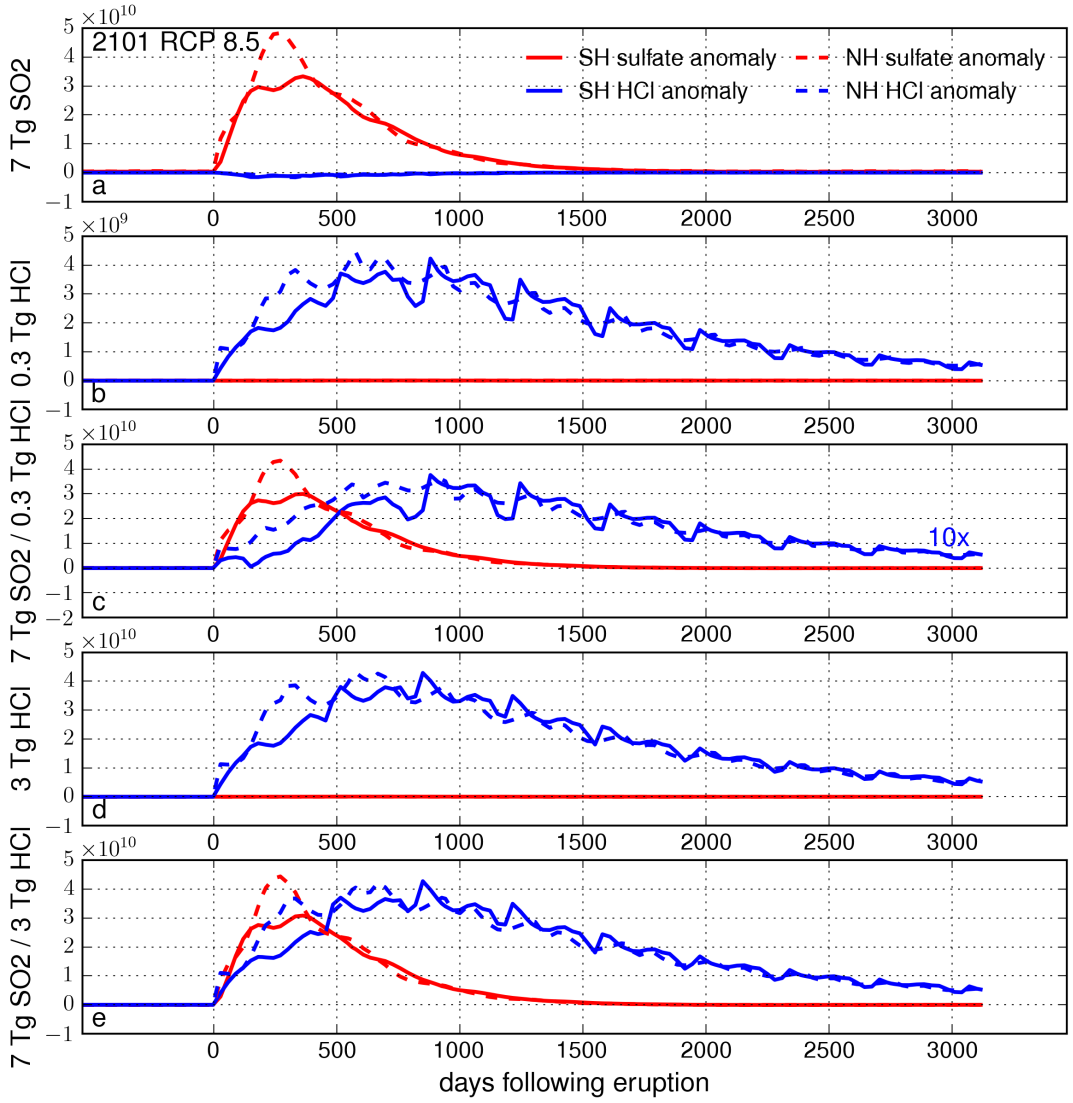

Figure 6.12: Decay trajectories for the molar stratospheric anomalies of (red) sulfate aerosol and (blue) HCl in the RCP 8.5 framework for the year 2101. Anomalies are calculated as the difference between a nonvolcanic baseline and the indicated perturbation. (a) 7 Tg SO_2, (b) 0.3 Tg HCl, (c) 7 Tg SO_2 / 0.3 Tg HCl, (d) 3 Tg HCl, (e) 7 Tg SO_2 / 3 Tg HCl.

Non-linear Enhancement in Ozone Depletion from Halogen Co-Injection

A comparison of the ozone anomaly produced from the co-injection of HCl and SO_2 relative to individual injections (equation 6.8) provides a measure of the activation of chlorine from heterogeneous reaction. A negative value indicates an enhancement in ozone-destroying species (e.g., an increase in $\frac{Cl_x}{Cl_y}$). Positive values indicate the opposite.

$$O_{3(\text{anomaly})} = \Delta O_{3\text{co-injection}} - \left(\Delta O_{3SO2\ \text{only}} + \Delta O_{3\text{HCl only}}\right) \tag{6.8}$$

This effect is plotted in figure 6.13 for an eruption occuring in the year 2018. Panel (a) presents the ozone anomaly following an eruption of 0.3 Tg HCl and 7 Tg SO_2 and appears almost featureless except for an additional 1 – 3 % loss over the equatorial regions immediately following the eruption. A much stronger anomaly is observed when 3 Tg HCl is co-injected, as in panel (b), in which a additional ozone losses of 5 –7 % are produced over northern midlatitude regions due to co-injection. Interestingly, the Antarctic ozone hole suffers less ozone depletion when HCl and SO_2 are co-injected than when they are individually injected. This results from the combination of (a) enhanced sedimentation of HCl on sulfate aerosol prior to transport to the austral polar vortex and (b) saturation effects. In the HCl-only injection case, volcanic HCl is less efficiently removed from the stratosphere due to interaction only with the stratospheric sulfate quiescent background and a greater proportion of the injection amount is subsequently activated by polar stratospheric clouds within the polar vortex.

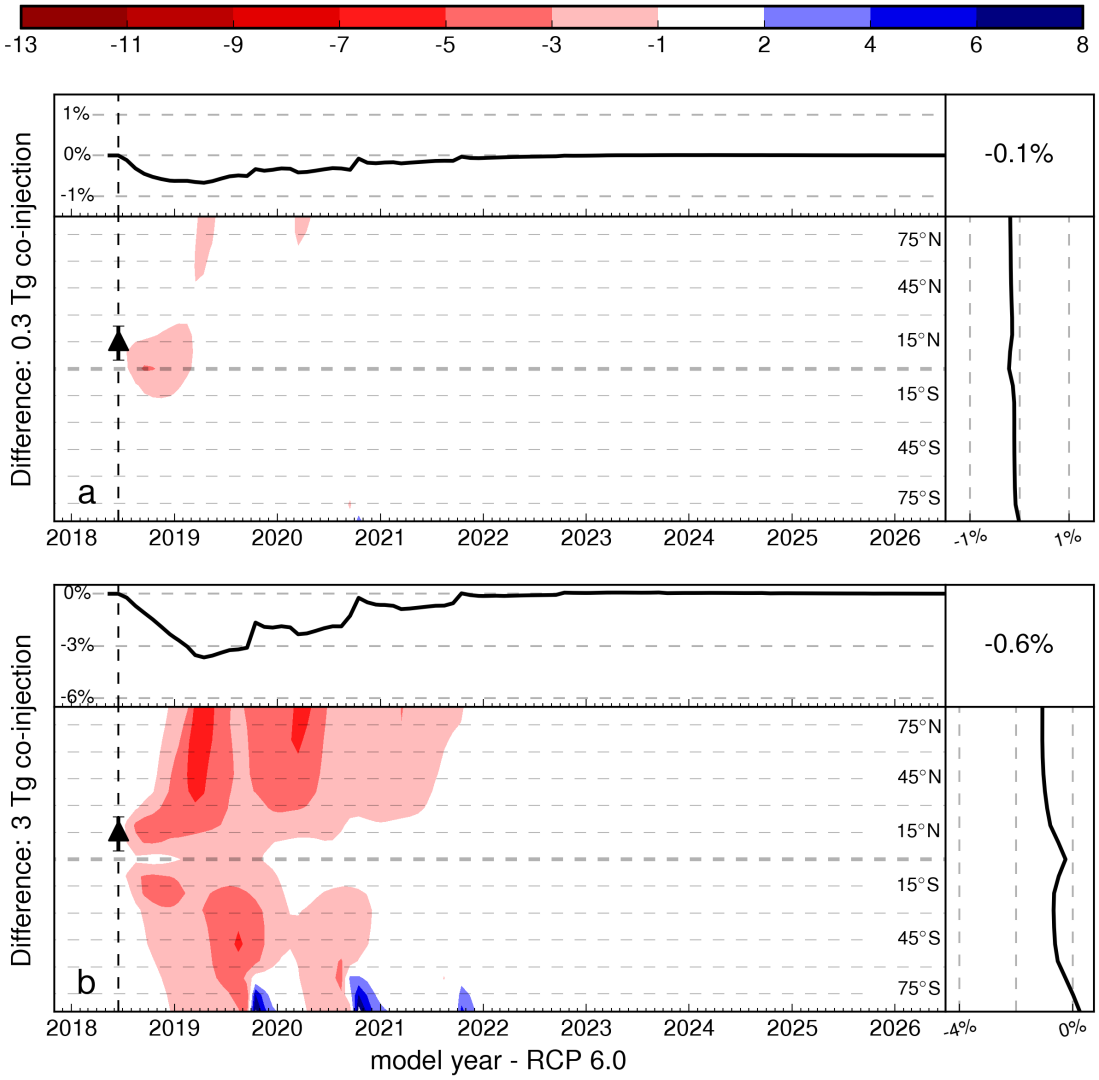

Figure 6.13: Differential response between co-injected SO_2 and HCl and the sum of individually injected SO_2 and HCl in the year 2018. The SO_2 and HCl are added in identical quantities in the co-injection and individual injection cases, corresponding to (a) 7 Tg SO_2/300 Gg HCl and (b) 7 Tg SO_2/3 Tg HCl.

Ozone anomalies for each of the RCP storylines in the years 2071 and 2101 are plotted in figures 6.14 – 6.21. The trend between RCP scenarios echoes the overall trend in expected ozone loss from Pinatubo-like eruptions: colder stratospheres are less responsive to co-injected halogens than warmer stratospheres.

Figures 6.14 – 6.17 present ozone anomalies following an eruption in the year 2071. Panel (a) of each figure corresponds to the 0.3 Tg HCl scenario. Global-temporally averaged anomalies range between -0.2% – -0.1%. All anomalies are negative except in the case of RCP 2.6, positive anomalies appearing due to the reasons discussed in the preceding paragraph. The 3 Tg HCl case is plotted in panel (b) of each figure and demonstrates a significantly greater anomaly. Note that anomalies do not scale linearly with HCl injection mass, though the scenario depicted in panel (b) involves an injection of 10 times more HCl than in panel (a), enhancements in ozone anomaly range from 3.5 – 7. Figure 6.16 merits particular attention. A comparison of high austral latitudes in panels (a) and (b) reveals a situation in which the anomaly is negative in the 0.3 Tg HCl scenario but positive in the same location in the 3 Tg HCl scenario. This is due to the aforementioned saturation effect affecting the HCl-only injection scenario, in which the heterogeneous processing rate of HCl at the superposition of the quiescent aerosol / trace gas burden and scenario-dependent stratospheric temperature is overwhelmed by the extreme addition of 3 Tg HCl.

Despite a colder end-of-century stratosphere, the magnitude of ozone anomalies from co-injection are reduced in the decade of the 2070's relative to the 2100's. This is the result of a threshhold effect in chlorine. Chlorine levels are sufficiently low in the decade of the 2100's that (a) injections of SO_2 alone hardly increase ozone loss rates and (b) enhancements in Cl_y are quickly converted

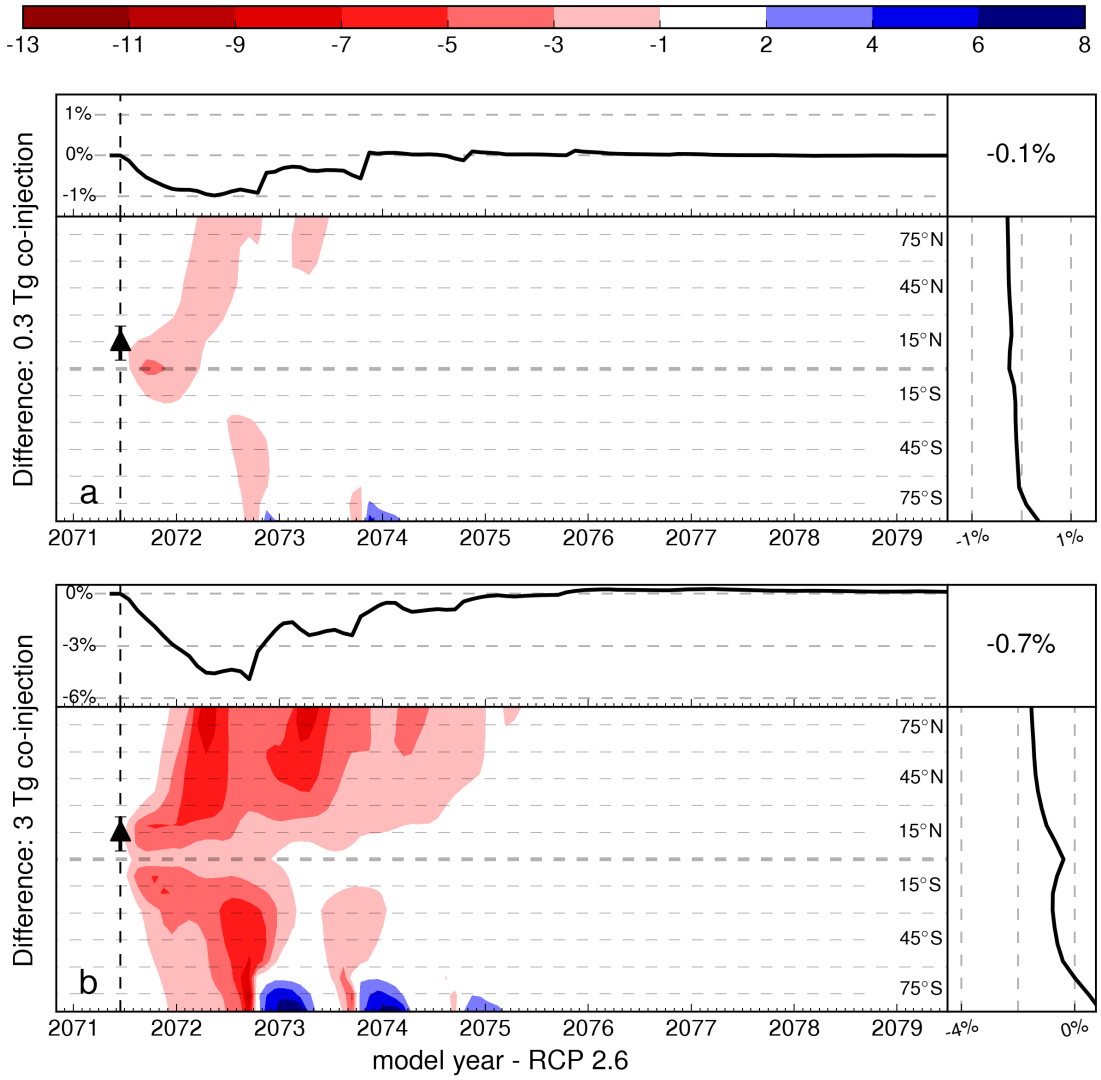

Figure 6.14: Differential response between co-injected SO_2 and HCl and the sum of individually injected SO_2 and HCl in the year 2071 under RCP 2.6 emissions projections. The SO_2 and HCl are added in identical quantities in the co-injection and individual injection cases, corresponding to (a) 7 Tg SO_2/300 Gg HCl and (b) 7 Tg SO_2/3 Tg HCl.

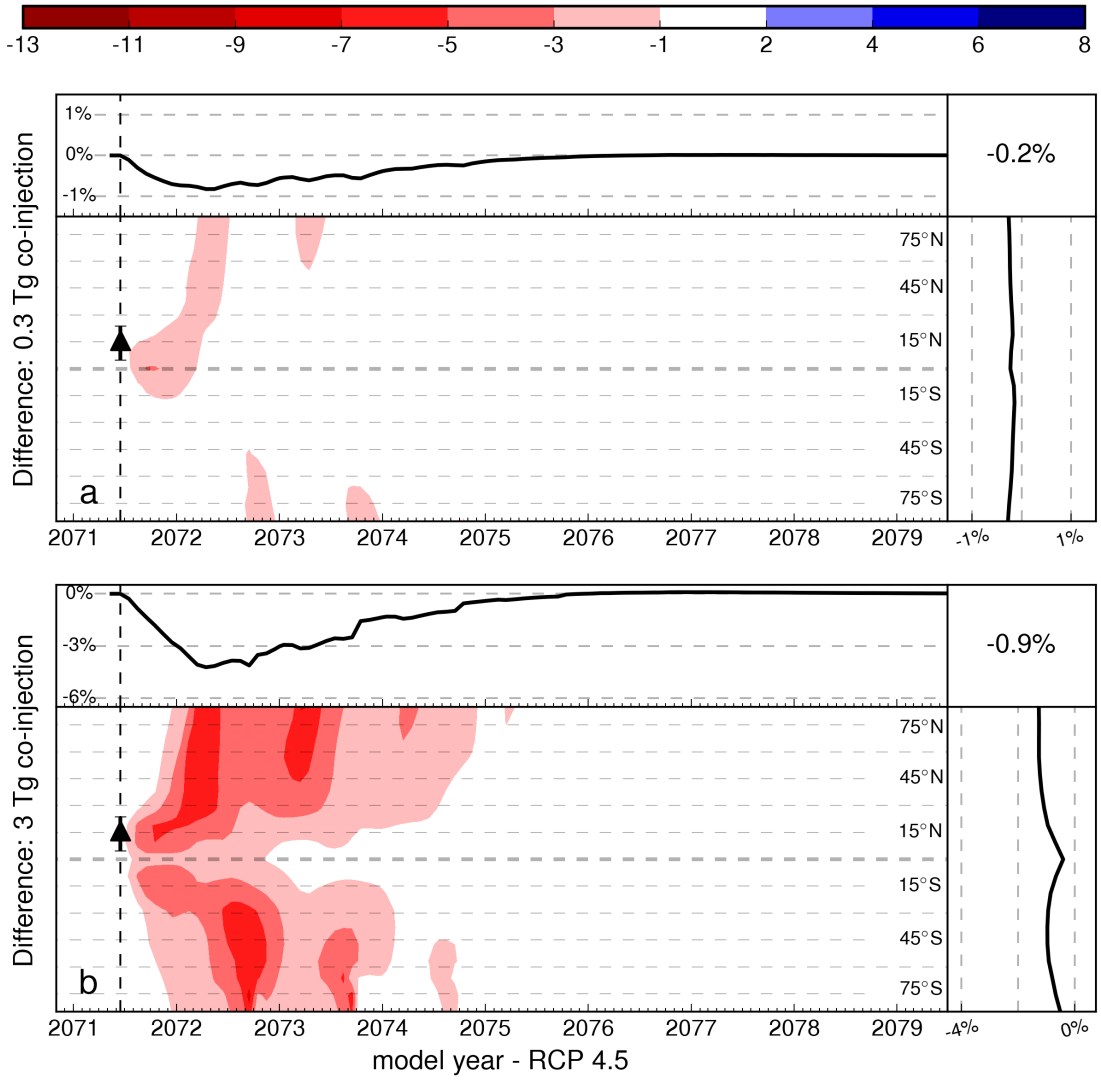

Figure 6.15: Differential response between co-injected SO_2 and HCl and the sum of individually injected SO_2 and HCl in the year 2071 under RCP 4.5 emissions projections. The SO_2 and HCl are added in identical quantities in the co-injection and individual injection cases, corresponding to (a) 7 Tg SO_2/300 Gg HCl and (b) 7 Tg SO_2/3 Tg HCl.

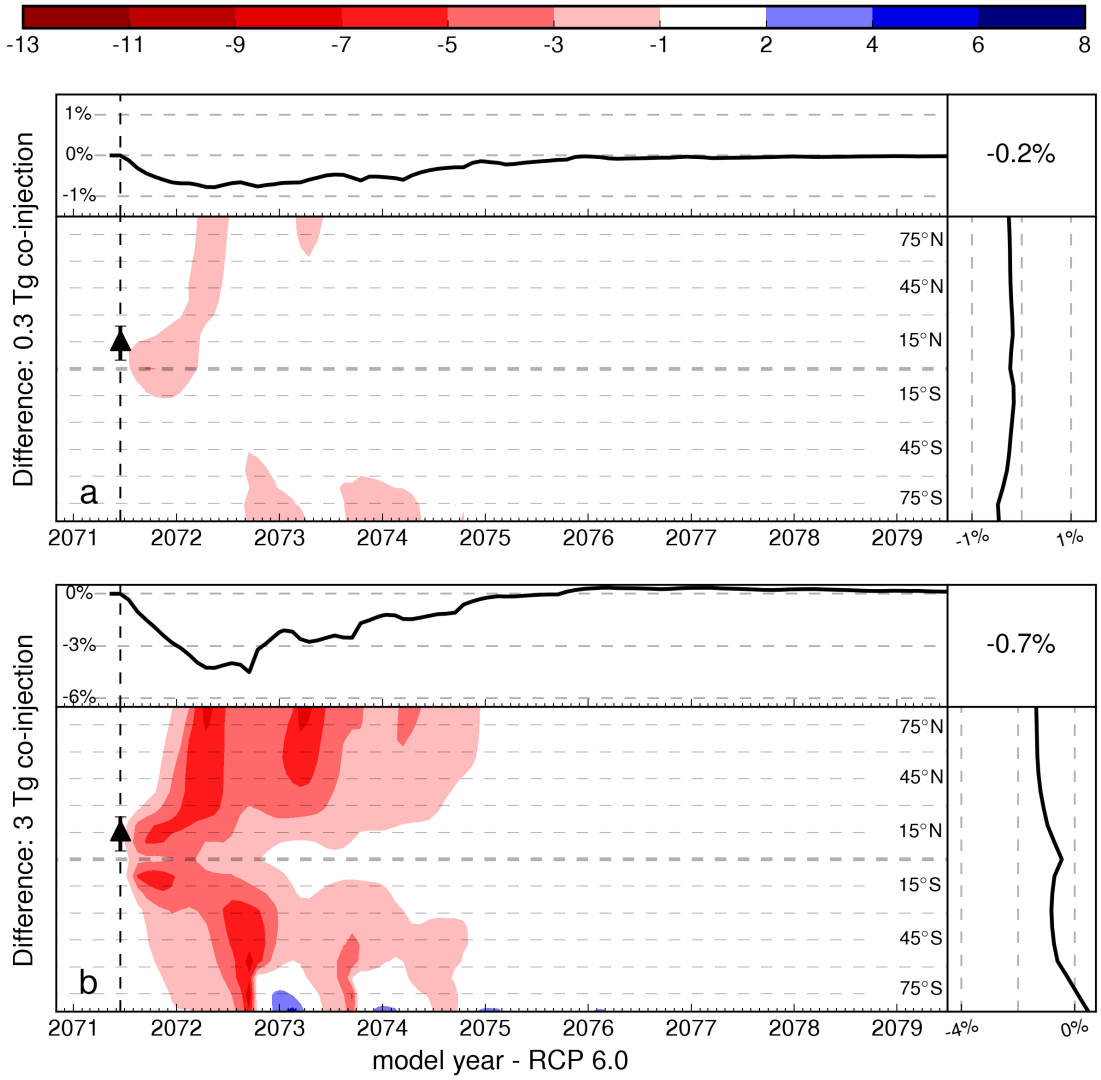

Figure 6.16: Differential response between co-injected SO_2 and HCl and the sum of individually injected SO_2 and HCl in the year 2071 under RCP 6.0 emissions projections. The SO_2 and HCl are added in identical quantities in the co-injection and individual injection cases, corresponding to (a) 7 Tg SO_2/300 Gg HCl and (b) 7 Tg SO_2/3 Tg HCl.

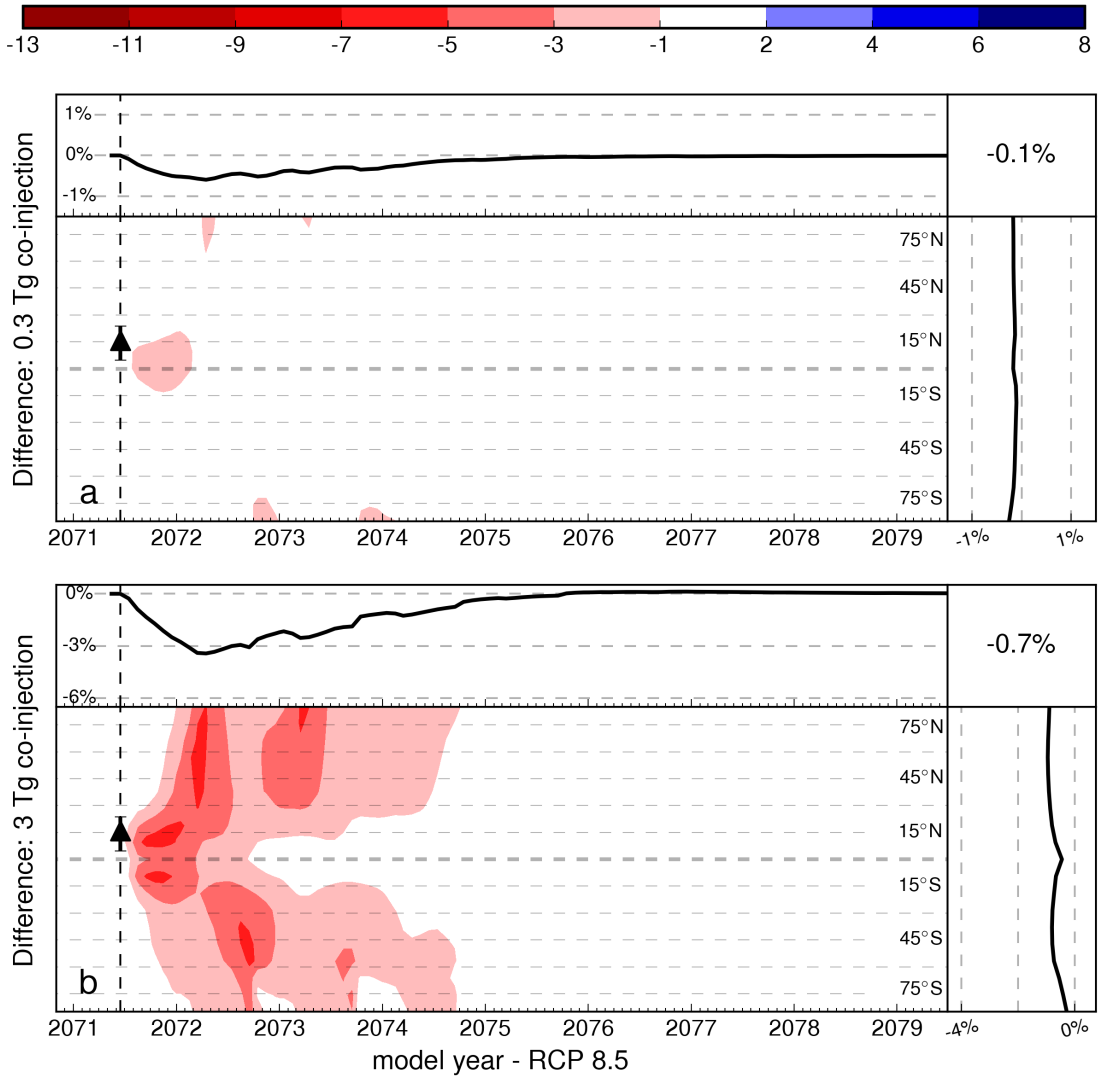

Figure 6.17: Differential response between co-injected SO_2 and HCl and the sum of individually injected SO_2 and HCl in the year 2071 under RCP 8.5 emissions projections. The SO_2 and HCl are added in identical quantities in the co-injection and individual injection cases, corresponding to (a) 7 Tg SO_2/300 Gg HCl and (b) 7 Tg SO_2/3 Tg HCl.

to their reservoir form due to the dominance of competing free radical species. Co-injections of HCl and SO_2 in year 2101 eruption scenarios counteract this effect to some degree, enhancing both the turnover frequency of Cl_y and the overall number density of Cl_y relative to the individual injection scenarios. Anomalies presented in panel (a) of figures 6.18 – 6.21 range between -0.3% – -0.1%. Significantly greater anomalies are predicted in panel (b) of the same figures, yielding magnitudes between -1.2% – -0.7%. Upon immediate inspection, one will notice far fewer positive anomalies, likely due to a combination of enhanced rates of surface processing of HCl on background aerosol in the colder stratosphere and chlorine threshhold effects as mentioned above.

Discussion and Conclusions

The stratospheric injection of significant quantities of volcanic halogens with volcanic SO_2 has been inferred from modeling/theory, ice core, remote sensing, and in situ records.[11,147,179–188] Petrological analyses of historical large, explosive eruptions reveals the potential for profound emissions of halogens to the stratosphere.[11,90,98,177,178] Indeed, a study of 42 eruptions within the Central American Volcanic Arc (CAVA) revealed that, given a 10% stratospheric injection efficiency, the average large CAVA eruption would result in an enhancement of EESC by 6 ppbv.[178]

This work is the first work to quantify the impact such a volcanic eruption would have on the contemporary and future ozone layer, finding significant reductions in column ozone regardless of background anthropogenic long-lived halogen loading or greenhouse gas emissions trajectory.[157] Column reductions averaging 10% or more over a 9-year time-horizon are predicted when HCl:SO_2

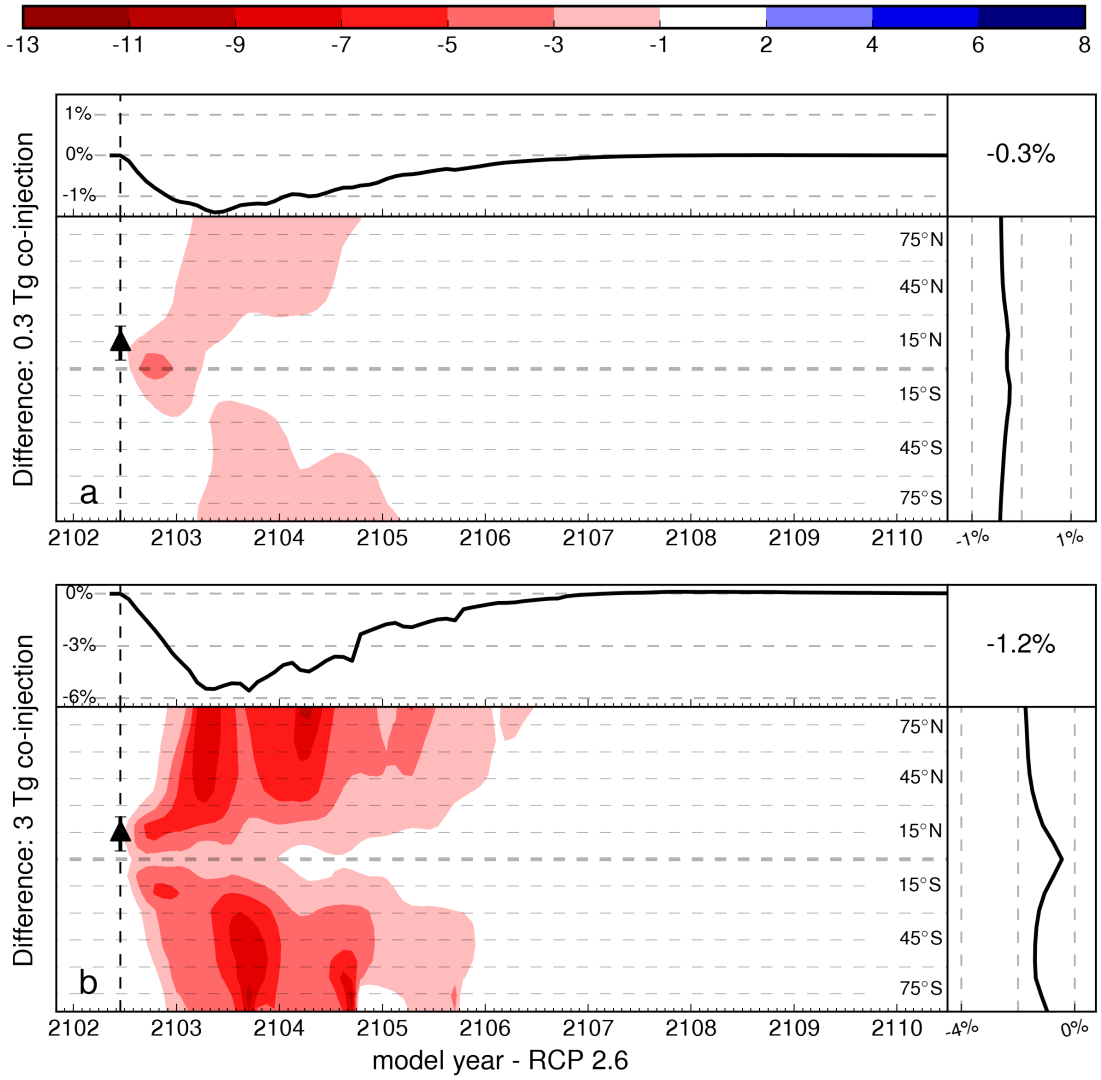

Figure 6.18: Differential response between co-injected SO_2 and HCl and the sum of individually injected SO_2 and HCl in the year 2101 under RCP 2.6 emissions projections. The SO_2 and HCl are added in identical quantities in the co-injection and individual injection cases, corresponding to (a) 7 Tg SO_2/300 Gg HCl and (b) 7 Tg SO_2/3 Tg HCl.

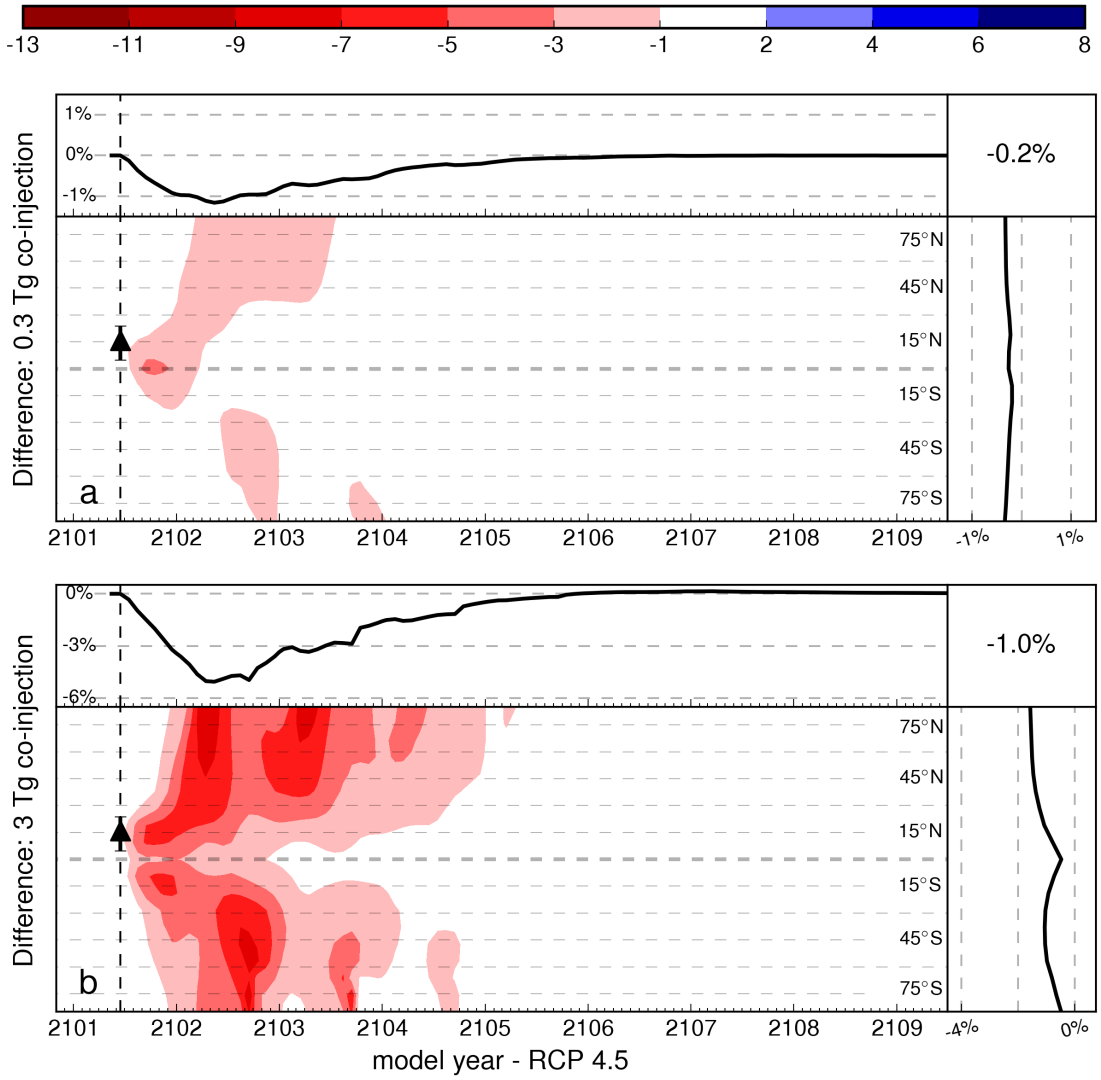

Figure 6.19: Differential response between co-injected SO_2 and HCl and the sum of individually injected SO_2 and HCl in the year 2101 under RCP 4.5 emissions projections. The SO_2 and HCl are added in identical quantities in the co-injection and individual injection cases, corresponding to (a) 7 Tg SO_2/300 Gg HCl and (b) 7 Tg SO_2/3 Tg HCl.

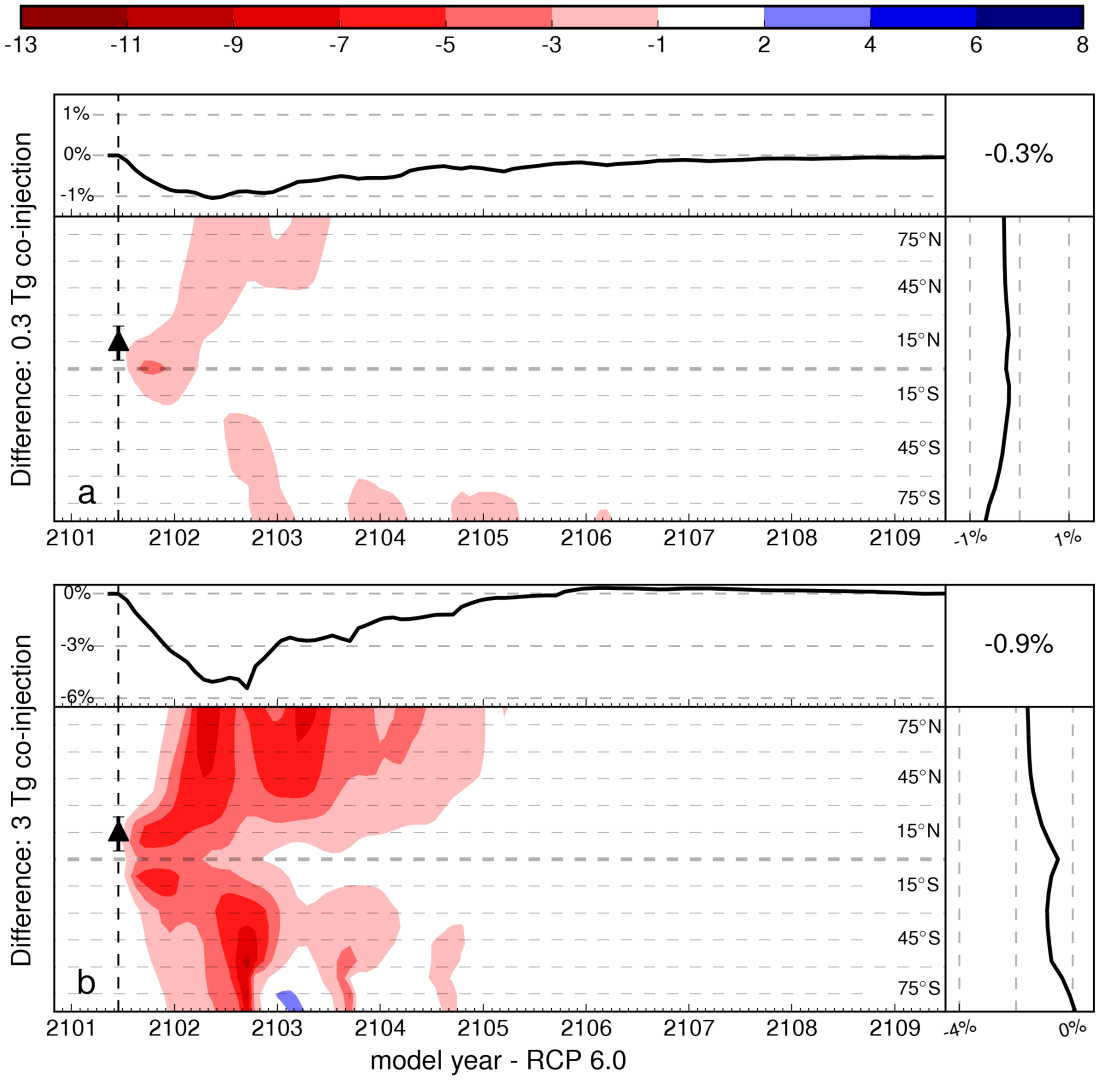

Figure 6.20: Differential response between co-injected SO_2 and HCl and the sum of individually injected SO_2 and HCl in the year 2101 under RCP 6.0 emissions projections. The SO_2 and HCl are added in identical quantities in the co-injection and individual injection cases, corresponding to (a) 7 Tg SO_2/300 Gg HCl and (b) 7 Tg SO_2/3 Tg HCl.

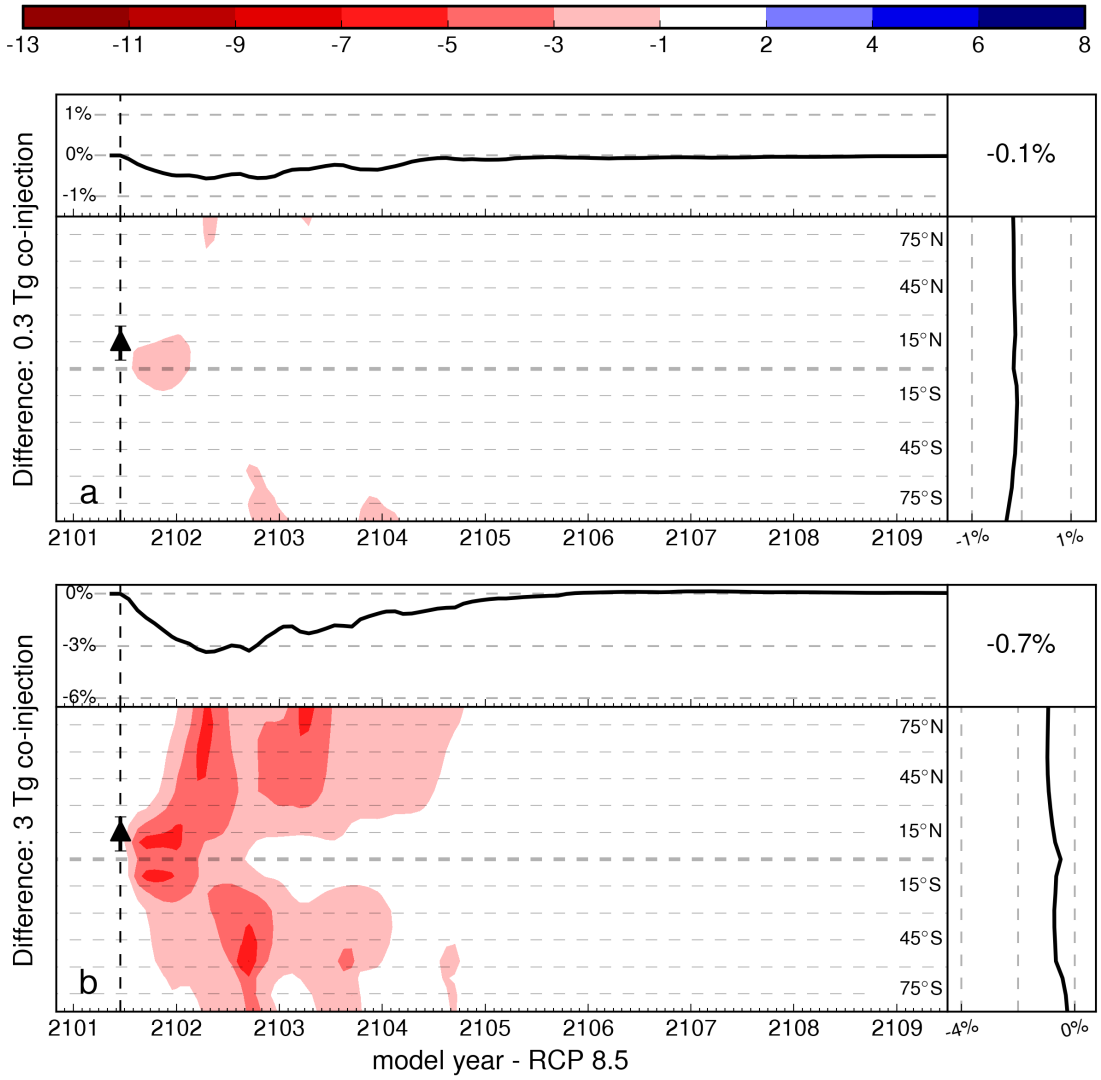

Figure 6.21: Differential response between co-injected SO_2 and HCl and the sum of individually injected SO_2 and HCl in the year 2101 under RCP 8.5 emissions projections. The SO_2 and HCl are added in identical quantities in the co-injection and individual injection cases, corresponding to (a) 7 Tg SO_2/300 Gg HCl and (b) 7 Tg SO_2/3 Tg HCl.

ratios are titrated to approximate stratospheric HCl:SO_2 signals recovered from the ice core record of the 7.7 kya eruption of Mount Mazama.[187,189] Less extreme injections of HCl, approximating the HCl:SO_2 injection ratios quantified in the last decade from MLS, though scaled to a much larger eruption, produce 2 – 3% globally-averaged depletions of ozone over a 9-year time horizon even toward the end of the century.[179]

This finding, in combination with the results of the previous chapter – that VSL halocarbons will provide a bromine source which will engage enhancements in chlorine in the lower stratosphere to produce significant ozone response to Pinatubo-like volcanism, demonstrates that the ozone layer will remain susceptible to perturbation by explosive volcanism in perpetuity. This is perhaps best illustrated by reviewing the vertical profiles of ozone processing rates by chemical family as in figure 6.22. Panels (a) – (c) correspond to eruptions in the year 2018, while panels (d) – (f) relate vertical profiles following an eruption in the year 2101 (RCP 6.0). Dashed lines in panels (a),(b),(d), and (e) correspond to the respective rates of each chemical family in the baseline non-volcanic scenario. Shaded lines denote the corresponding enhancement or suppression of the corresponding ozone processing rate following the indicated volcanic perturbation. In the Pinatubo-like eruption cases – panels (a) and (d) – modest increases in the halogen processing rates in the lower stratosphere are offset by reduced NO_x processing rates in the middle stratosphere. When halogens are co-injected with SO_2, as in panels (b) and (e), orders of magnitude increases in the chlorine-mediated ozone destruction rate are observed, along with a corresponding order-of-magnitude increase in the bromine-mediated ozone processing rate. The vertical spatial domain of halogen enhancement is significantly enhanced relative to the Pinatubo-like scenario as well, with increases in chlorine processing ob-

served as high as 2 hPa. Panels (c) and (f) provide the ozone number density for the baseline case (black, no volcano), the Pinatubo-like scenario (brown), a co-injection of 0.3 Tg HCl and 7 Tg SO_2 (green), and a co-injection of 3 Tg HCl and 7 Tg SO_2 (maroon). Clearly, large injections of HCl will deplete the ozone column regardless of year. In the present day scenario there exists very little difference between the Pinatubo-like eruption and the 0.3 Tg HCl co-injection; however, a much larger effect is observed for the two scenarios in the far future. Whereas the Pinatubo-like eruption would have produced a net-enhancement in ozone layer thickness (by increasing column thickness above 50 hPa), the halogen-rich eruption both reduces the extent of enhancement above 50 hPa and the total loss below 50 hPa. The net result is a reduction in column thickness.

The implications for surface life on Earth a future halogen-rich volcanic eruption could be profound regardless of anthropogenic halogen loading should such an eruption occur. Though I do not model the additional co-injection of bromine or iodine compounds with HCl and SO2, the sparse record of measurements indicates that the concentrations and fate of these halogens in volcanic gases could be of stratospheric significance.[96,177,178,209,210] The co-injection of chlorine with bromine and/or iodine would likely result in even more extreme ozone reductions following a halogen-rich eruption due to both the significantly greater ozone depletion efficiencies of bromine and iodine relative to chlorine and the complex intraplume oxidation chemistry of bromine and iodine which would likely increase the stratospheric injection efficiency of these compounds.[69,207]

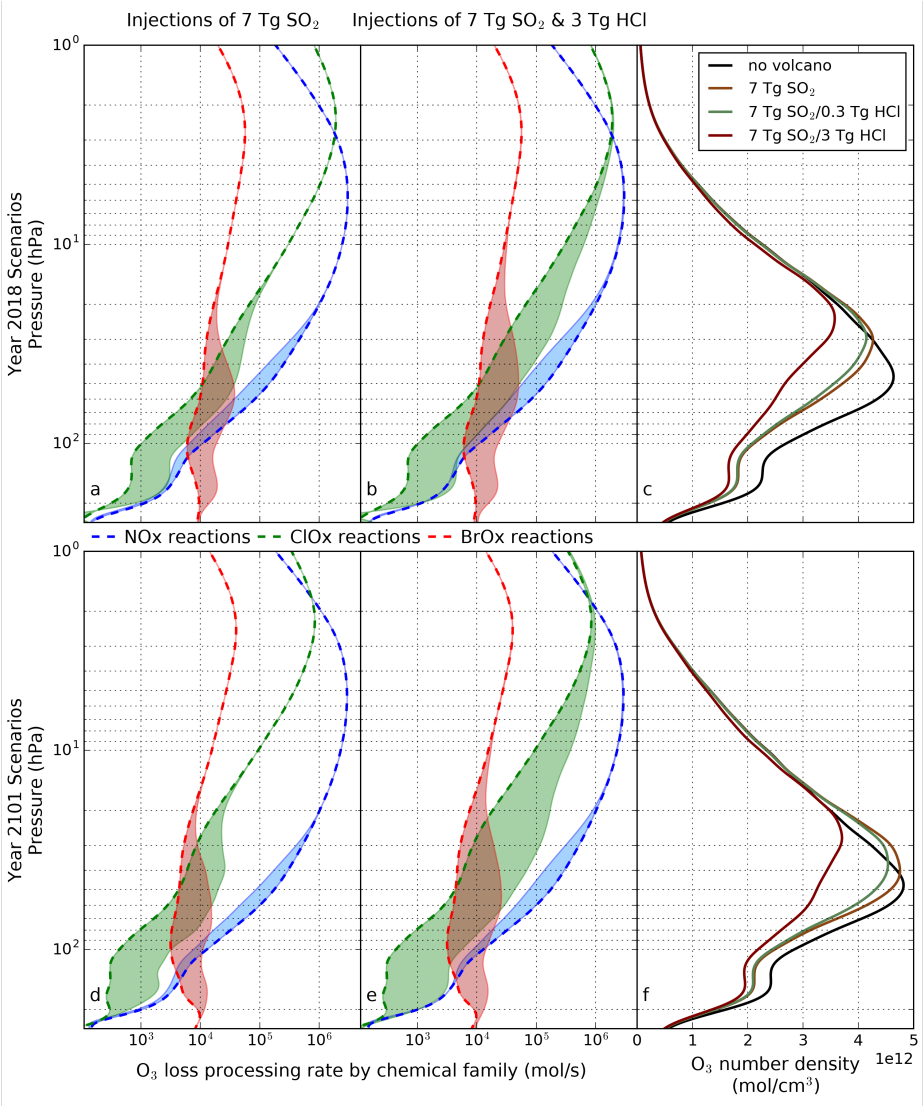

Figure 6.22: (a,b,d,e) Northern midlatitude vertical profiles of chemical family loss processing rates for eruptions occuring in the year 2018 (a,b) and 2101 (d,e) within the RCP 6.0 greenhouse gas emissions trajectory storyline one year after eruption. Dashed lines indicate the processing rate for each respective chemical family in the non-volcanic scenario. Shaded regions indicate the change experienced by each chemical family following the indicated volcanic perturbation. Pinatubo-like eruptions (a,d) demonstrate minor enhancements in halogen processing rates, especially in the lower stratosphere. Halogen-rich eruptions (b,e) are demonstrated to rapidly accelerate halogen processing rates and the domain in which halogen processing occurs. (c,f) Ozone number density corresponding to the indicated volcanic perturbations at the same latitude and date as (a,b,d,e).

7

Other Perturbations to the Stratospheric Ozone Layer

The Stratospheric Threat Matrix

The ozone layer is produced through photochemical processes and subsequently transported globally, as discussed in detail in chapter 1. These chemical and dynamical mechanisms are natural solu-

tions to the physicochemical state of the local environment.[211] Any perturbation to that condition will induce changes in the steady-state solution of the ozone layer's spatiotemporal structure.

Many phenomena are capable of inducing large-scale global changes in the manifestation of the ozone layer. Some are natural in origin, massive in scale, and have likely occurred many times since the formation of the ozone layer. Others are a consequence of human activity and consequently entirely preventable or mitigable given an adequate understanding of the threat and will to act.

Such phenomena must either, in the most simple sense:

- transport chemical species in massive quantity to the stratosphere via some mechanism –or
- significantly alter stratospheric circulation and/or insolation.

The following list of perturbative forces is not exhaustive, but constitute a stratospheric threat matrix – that is, they encompass those natural scenarios which are of reasonable likelihood to occur on historic timescales and those anthropogenic scenarios which appear increasingly probable. Brief descriptions of the phenomena and how they interact with the stratospheric ozone layer are presented.

Natural Phenomena

Deep Convection and Circulation within Structured Seasonal Storm Cycles

Water is the primary source of hydroxyl radical to the stratosphere, as outlined in section 1.7. The lower stratosphere is naturally dry due to the extremely cold temperatures of the tropical tropopause through which most troposphere-stratosphere exchange occurs;[212,213] however, deeply convecting

storms are known to inject large quantities of water vapor and ice directly into the extratropical stratosphere.[7,8,214–218] These deeply penetrating *overshooting tops* may also provide conduits for the transport of very short-lived halocarbons from the marine boundary layer to the extratropical lower stratosphere.[174] where they may participate in ozone loss catalysis.

Furthermore, the rate of heterogeneous activation of chlorine reservoir species on stratospheric sulfate aerosols is a function of several parameters – principally: aerosol surface area density, and local temperature.[219–221] This rate is additionally mediated by the composition of the aerosol itself. Sulfate aerosols with more aqueous character are more reactive. This relationship is presented in figure 7.1 in which the shaded region indicates the engagement of catalytic heterogeneous processing of halogen reservoir species as a function of background stratospheric water vapor and temperature. The red arrow provides an example of projected stratospheric background enhancements, matching prior in situ observations,[7,8,217], demonstrating that even small incursions of water to the stratosphere might shift the temperature range at which ozone loss processing is enabled. The green line provides an indication of further enhancement in halogen conversion expected if such a process were to occur in a Pinatubo-like aerosol background.

Future trends in the convective injection of water vapor are not well-defined; however, there are indications of a secular increase in volume and frequency of overshooting tops.[222] Such a trend, when coupled with long-lived summertime anticyclonic circulation patterns, may produce conditions leading to the enhancement of ozone loss catalysis rates over densely populated regions.[7,8]

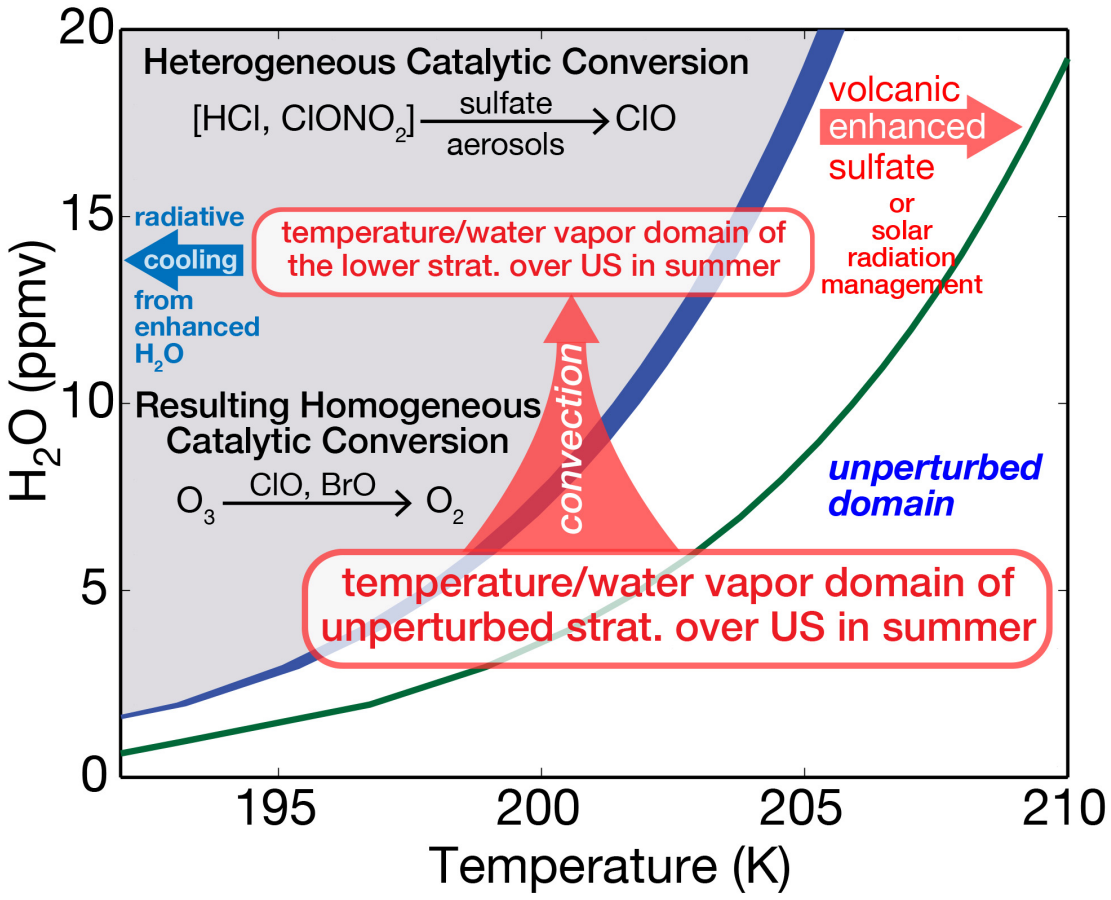

Figure 7.1: (shaded) regions in which the heterogeneous reactive conversion of halogen reservoir species to their photochemically active forms are enabled as a function of background stratospheric water mixing ratio and temperature. (green) the domain in which catalytic activation of halogen reservoir species occurs is enhanced greatly following a Pinatubo-like eruption. (arrow) indication of potential water vapor enhancements following seasonal convective injection and dynamical partitioning of water vapor.[8]

Comet/Asteroid Impact

The evolution of the Earth, and life on Earth, has been punctuated by periodic impacts with extraterrestrial bodies – some leading to mass extinction events.[223–227] Most famous among these is the 65 Mya Cretaceous-Tertiary (K-T) extinction, during which three quarters of all surface species were eliminated following the impact of a 15 km diameter asteroid at the Chicxulub site.[228]

Model simulations of the K-T event indicate catastrophic decadal reductions in surface and sea temperature following the injection of some 15 Pg soot and 10 Eg water vapor into the atmosphere.[229] Remarkably, the downwelling fraction of the solar flux was reduced one-billionfold for several months, recovering to one percent of the present flux value after two years. Extreme years-long lower stratospheric heating of 50 – 100 K allowed huge pptv increases in stratospheric water vapor. Subsequent odd-hydrogen chemical reactions as outlined in section 1.7 –and suppression of production of ozone from the extreme reduction in lower stratospheric insolation – result in the abrupt and near-total destruction of the ozone layer. After the recovery of surface solar forcing following sedimentation of soot, about 3 years after impact, incident UV flux increases by 300% until the abrupt reformation of the ozone layer, 6 years later.

Comet/asteroid impacts (CAI) occur frequently on a planetary timescale, with large dynamic range of energy release. Per equation 7.1, the recurrence interval t, the time between expected impacts, can be expressed as a power law function of impactor diameter, D (in meters).[230,231]

CAI will produce different chemical perturbations to the stratosphere depending on the environment of the impact. Ocean impacts will produce large amounts of vaporized water, halogens, and

nitrogen oxides while impacts on land will mostly produce nitrogen oxides and soot. Recurrence intervals can be scaled to reflect these events by means of equations 7.2, where $\alpha = 0.3$ for land impacts and 0.7 for ocean impacts. When impactors are larger than the average depth of the ocean (3.6 km), as was the case in the K-T event, $\alpha = 1$.

$$t_{\text{impactor}} = 3.71 \times 10^{-2} D^{2.377} \tag{7.1}$$

$$t_{\text{impact, land}} = \frac{t_{\text{impactor}}}{\alpha} \tag{7.2}$$

From this relation, it is evident that a recurrence of the catastrophic Chicxulub event is not a major concern, $t_{\text{impactor}} = 3.13 \times 10^{8}$ years. However, smaller CAI events are postulated to pose a threat especially to the ozone layer. Potential impactors are ranked from 0 - 10 on the Torino impact hazard scale, in which an increasing metric conveys both an increasing probability of impact and a higher potential destructiveness.[232] If the impactor is sufficiently energetic, the subsequent fireball will exceed the scale height of the atmosphere and the entirety of the volatilized material and entrained air within the fireball will "backfire" – rise quickly to the mesosphere and higher.[231,233–235]

Birks et al. (2007) explore CAI scenarios with impactors between 150 – 1200 m diameter (t_{impactor}: 5500 – 774,000 years), which are expected to produce this effect.[231] They quantify expected changes in stratospheric mixing ratios of NO_x, ClO_x, BrO_x, and HO_x for land and ocean impact cases, finding that an impactor would need to be greater than 450 m in diameter ($t_{\text{impactor}} = 75000$ years) to cause perturbations in stratospheric chemistry resulting in widespread ozone depletion – though

they do not include effects from the mesospheric injection of soot and the resulting reduction in stratospheric insolation into this calculation. A calculation of this effect in the upper mesosphere to middle stratosphere by the same workers concludes that this screening allows the majority of NO_x and HO_x injected into the mesosphere to survive long enough to subside into the stratosphere.

Pierazzo et al. (2010) evaluate the reduction in ozone and corresponding increase in surface erythemal radiation following the ocean impact of 500 m ($t_{impactor} = 96,500$ years) and 1000 m ($t_{impactor} = 500,000$ years).[26] Years-long reductions of ozone up to 30% (70%) at midlatitudes are expected following the 500 m (1000 m) impact with corresponding twofold (fivefold) increases in erythemal radiation.

Solar Variability

The production and loss reactions of stratospheric ozone are photochemical in nature, ebbing and flowing with any variation in the sun's radiation. The *sunspot cycle* is characterized by an 11-year periodicity with 6 – 7 % variation at 205 nm throughout.[236] The solar rotational cycle is much shorter and exhibits less variation, with 2 – 3 % changes observed at 205 nm over its 27 day period.[237] *Grand solar minima and maxima* are unpredictable, but occur frequently ($\approx$ 30 times in the last 10,000 years), often lasting a century or longer, with significant impact on column ozone.

Though total variation of the solar spectrum remains below 0.1% during the 11-year sunspot cycle, the ultraviolet region exhibits much higher volatility. Solar variation is higher at shorter wavelengths. While 6 – 7% variation is observed at 205 nm during the sunspot cycle, this variation increases to $\approx$ 68% at the Lyman-α wavelength (121.6 nm). At higher wavelengths, some variation is

observed at line emission intensities (e.g., 6% variation at Mg II lines between 279 – 282 nm), but in general, variability drops below 1% at wavelengths greater than 240 nm.[237]

During periods of high solar activity, molecular oxygen photolysis rates (and it follows, ozone production rates) are enhanced. Likewise, various photocatalytic ozone loss mechanisms are impacted by solar cycle variability; however, the relevant wavelengths tend to be red-shifted relative to the wavelengths responsible for molecular oxygen photolysis and are thus less volatile.

The ozone response to the sunspot cycle is latitude dependent. Model simulations find 1% changes in ozone abundance between solar minima and solar maxima conditions in the tropics, but about 2% changes near the poles.[237–239] These changes are accompanied by changes to the thermal structure of the stratosphere due to the close-coupling of ozone photolysis and stratospheric heating rates, and this feedback effect has been found to be nearly as strong as the photochemical effect in model studies.[240] Particularly, this alteration in stratospheric temperature fields modifies middle atmospheric circulation by impacting the propagation of planetary waves – the so-called top-down mechanism.[241] Variability resultant from solar rotation is found to be less than 0.5%, due mainly to these same dynamical forces and will not be discussed further.[237,238,242,243]

While interesting for modelers, climatologists, and other workers, these variations are liable to have very limited impact on human health at the surface. A strong decrease in solar activity corresponding to a grand solar minimum is predicted to reduce global ozone columns by up to 2% worldwide, with the strongest impact of up to 8% over midlatitudes.[244] Such an event, if it occurs before the decay of anthropogenic halocarbons to preindustrial levels, may interfere with stratospheric ozone recovery by up to a decade or longer.[244,245]

Energetic Particle Precipitation

Incoming energetic particles (EPs), primarily protons and electrons, mediate some chemical and physical processes in the Earth's atmosphere. Variations in the incoming flux of EPs can thus result in perturbations to the chemical partitioning of the stratosphere.

EPs arise from multiple origins and each source process produces a characteristic energy spectrum. Galactic cosmic rays (GCRs) are a highly energetic source of protons originating from outside the solar system, with characteristic energies between 10^{-12} J – 10^{2} J per nucleon. Solar cosmic rays (SCRs) originating from coronal mass ejections have energy spectra which typically peak around 10^{-7} J per nucleon. Fluxes of GCRs and SCRs are inversely correlated with 11-year periodicity. When the 11-year sunspot cycle is at a maximum, so too are SCR fluxes, while GCR fluxes are at a minimum due to pressure from solar winds.[246]

Regardless of their origin, sufficiently energetic EPs ($> 10^{-11}$ J) will collide with atmospheric gases and produce charged secondary products, classified by their soft (electrons, positrons, and photons) and hard (muons, pions, etc.) components.[247] These secondary products will then interact with atmospheric species in a variety of ways. Equations 7.3 – 7.13 present one such scheme resulting in the production of NO_x.

The reaction pathway is initiated following interaction with energetic secondary electrons, denoted e^*.[246,248,249]

$$e^* + N_2 \rightarrow N^+ + N + 2e^- \tag{7.3}$$

$$e^* + N_2 \rightarrow N + N + e^- \tag{7.4}$$

$$e^* + N_2 \rightarrow N_2^+ + 2e^- \tag{7.5}$$

$$e^* + O_2 \rightarrow O_2^+ + 2e^- \tag{7.6}$$

$$e^* + O_2 \rightarrow O + O^+ + 2e^- \tag{7.7}$$

Subsequent recombination/exchange chemistry further enhances atomic nitrogen.

$$N_2^+ + O \rightarrow NO^+ + N \tag{7.8}$$

$$N_2 + N^+ \rightarrow N_2^+ + N \tag{7.9}$$

$$N_2^+ + e^- \rightarrow N + N \tag{7.10}$$

$$NO^+ + e^- \rightarrow N + O \tag{7.11}$$

$$N^+ + O \rightarrow N + O^+ \tag{7.12}$$

Finally, reaction of atomic nitrogen with molecular oxygen produces nitric oxide.

$$N + O_2 \rightarrow NO + O \tag{7.13}$$

HO_x may also be produced following a solar proton event via ion chemistry, as presented in equations 7.14 and 7.15, but suffers a short lifetime in the mesosphere and exerts minimal impact on total column ozone.[248,250,251]

$$O_2^+ + H_2O \rightarrow O_2^+H_2O \tag{7.14}$$

$$O_2^+H_2O + H_2O \rightarrow H^+H_2O + OH + O_2 \tag{7.15}$$

Ozone depletion in the upper stratosphere and mesosphere is known to occur relatively frequently following a solar proton event and has been reported at least thirteen times since it was first observed in 1969.[252,253] Due to the sparse density of ozone in the upper stratosphere, the effect on total column ozone is attenuated[254], though decadal studies have demonstrated strong wintertime response of polar total ozone to EPP events.[255] Polar and subpolar stratospheres are susceptible to more significant ozone depletion episodes of up to 20% total column loss;[256–260] however, because

its strong seasonal and geographic dependency, most instances of SCR-mediated ozone depletion have a minimal impact on human health. Infrequent, large solar events may have a pronounced impact on midlatitude ozone, though perturbations to the halogen loading of the stratosphere will attenuate this effect.[261]

The influence of EPP on climate and chemistry are frequently categorized as ”direct” and ”indirect” effects. Direct effects are local implications of the enhanced production of HO_x and NO_x in the mesosphere. Indirect effects result from the subsequent transport of these products to the stratosphere.

Such changes in stratospheric ozone may have climate impacts. Meraner et al. (2018) quantify the expected change in dynamics and radiative forcing from both direct and indirect EPP effects, finding indication that EPP events may warm the polar stratosphere and weaken the polar vortex following indirect stratospheric ozone depletion.[262] Andersson et al. (2018) similarly investigate the changes imparted to radiative forcing from medium-energy electrons(300 – 1000 keV) and determine that indirect effects from medium-energy EPP is responsible for 5 – 7 % of the variability in austral stratospheric ozone columns.[263]

Thomas et al. (2007) use ice core records of nitrate enhancement to explore the atmospheric chemistry of one of the most intense solar flares in recorded history, which occured in 1859, finding large column reductions of up to 10% extending from the poles to about 20°, persisting for a year or more.[264] Such *superflare* events are predicted to occur about once every 2000 years.[265,266]

Magnetic Field Reversals: in Dense Interstellar Medium and Magnetic Field Substorms

The density of the interstellar medium is heterogeneous. If the solar system were to transit a region with higher density, enhanced rates of EP precipitation would be expected as the heliosphere contracts. It has been suggested that if the Earth experiences a magnetic field reversal while transiting such a region that biologically significant ozone depletion could result.[267] The coincidence of both situations seems highly improbable at first glance; however, a review of the expected frequencies and durations of these events provides the evidence to the contrary. The solar system has transited regions of enhanced density ($\geq$ 100 H atoms/cm^3 vs 0.3 H atoms/cm^3 currently) $\approx$ 135 times in the previous 4.5 Gy and the average duration of a transit was $\approx$ 1 My.[268] The Earth's magnetic field reverses stochastically, however on average once every 300 ky, the event itself lasting several thousand years.[269] A statistical treatment thus indicates that there may have been as many as 7 instances in the prior 250 My of a magnetic field reversal coinciding with the transit of the solar system through a region of enhanced density – and that EP fluxes would remain elevated for up to a period of thousands of years.[267]

Such 1000-year periods of enhanced GCR precipitation are projected to lead to widespread, longterm depletions of the stratospheric ozone layer. Pavlov et al. (2005) use a 2-D dynamical/chemical model to evaluate the new steady-state ozone solution following a 300-fold enhancement of GCR, finding that total column ozone decreases by 40% globally, and by up to 80% at high latitudes after a 5 – 10 year adjustment period.[267]

Transient, hours-long reconfigurations of the magnetic field are known as substorms and can induce enhancements in EPP and occur thousands of times each year. Substorm-induced electron energies are low, ranging between 20 – 300 keV, producing NO_x and HO_x between 60 – 90 km.[270] Seppälä et al. (2015) quantify the direct effect of such storms, finding that mesospheric partial ozone columns vary by as much as 50% as a result of intense substorm activity.[271] They do not calculate indirect effects of substorm EPP on stratospheric ozone; however, they do find NO_x enhancements between 200 – 300 %.

Supernovae and Gamma-Ray Bursts

Gamma-ray bursts (GRBs) and supernovae are associated phenomena characterized by the emission of gamma radiation. Supernovae are believed to occur following the abrupt collapse of a massive star's core due to gravitational forces and produce a high fluence of γ radiation and GCRs. Supernovae emissions are typically spherically symmetric and approximate 10^{40} J γ radiation delivered over a period of about 100 days.[272] Significant fluxes of GCRs and particulate matter from all but the closest supernovae (15 – 100 pc) are screened from the solar system by solar wind pressure.[273] If a supernova is within this distance, enhancements in GCR flux by an order of magnitude or more can be expected for a decade or longer.[272] Gamma-Ray Bursts are much more energetic than a supernovae, producing columnated γ radiation beams of $\approx 10^{44}$ J.[274] All observed GRBs are believed to originate from extragalactic supernovae or binary mergers, typically billions of light-years from the Earth. Because of the great distances between the Earth and a GRB [*], associated GCR fluxes are as-

[*] the closest GRB recorded, GRB980425, was 43 Mpc away[275]

sumed to be absent; however, if a GRB were to occur within the Milky Way galaxy, this assumption might not hold.

In contrast to supernovae, which may emit γ radiation over a period of weeks-to-months, the majority of GRBs are of very short duration (< 10 s). The differential temporal profiles of the two phenomena result in very different effects on atmospheric chemistry. NO_x production from GRBs will be localized only on the illuminated portion of the planet and the subsequent chemical implications will be dependent on transport. Contrastingly, NO_x resultant from γ radiation emission from a supernovae will be rotationally symmetric about the Earth.

Despite fluxional differences in the energetic and temporal profile of supernovae and GRBs, both events share similar mechanisms of atmospheric perturbation. Initially, γ radiation will interact with the top layers of the atmosphere producing nitrogen radicals from direct interaction of molecular nitrogen and γ radiation and interaction of molecular nitrogen with secondary electrons and UV produced from scattering processes. Subsequent production of NO_x will mirror closely equations 7.3 – 7.13 in both cases, the major difference between supernovae and GRBs being the rate of NO_x production.

Modeling studies of the atmospheric impacts of supernovaes and GRBs typically parameterize ozone depletion as a function of event proximity. Galante and Horvath (2007) provide such an analysis in terms of D_{10}^{ion} for *E. coli* and *D. radiodurans*, the ionizing radiation dosage resulting in 90% lethality for a population,[276] determining that an Earth-facing GRB must occur within 12 kpc (e.g., within the Milky Way galaxy – diameter 30 kpc) to produce significant ozone depletion on Earth. Other workers using more sophisticated methods find that the GRB must be much closer to

the Earth to have such an effect (e.g., Melott et al. (2005) provide a distance of 2-3 kpc).[277] Piran and Jimenez (2014) state that the Earth is fortunately situated at 8 kpc from the galactic center as the frequency of lethal GRB events increases dramatically with stellar density.[278]

The distance envelope, d_g (kpc), expected for the single closest GRB event to the Earth within a given time interval can be expressed according to equation 7.16, in which t_G is the interval between events in Gy.[279]

$$d_G = 1.9 \frac{\text{kpc}}{\text{Gy}} t_G^{-1/2} \tag{7.16}$$

or, rearranged for frequency

$$t_G = \left(\frac{1.9\text{kpc}}{d_G \text{Gy}} \right)^2 \tag{7.17}$$

The frequency then for an event at 2 kpc is about once per 1 Gy. Thomas et al. (2005) employ a 2-D dynamical/chemical model to evaluate a 2kpc GRB of 10 s duration and 5×10^{44} W power, providing 100 kJ m^{-2}. Though the event only lasts 10 s, NO_x production is so great that the stratospheric ozone column is reduced on average by 10% over a five-year period, with a peak depletion of 35% during the first year.[280] If a similar Earth-directed GRB were to occur within 4 kpc, with 10 kJ m^{-2} fluence, column ozone is predicted to decline by 10% over a two-year period – and if the event were to occur within 600 pc, 68% depletion is predicted over an eight-year period.[280]

Model studies indicate that supernovae must occur much closer to the Earth to produce similar effects. Ruderman (1974) first used a 1-D photochemical model to find a years-long 80% ozone depletion following a supernova within 17 pc due to γ radiation and perhaps a century-long reduction of ozone by 40% – 90% due to GCR precipitation.[281] Using a more sophisticated model, Crutzen

and Brühl (1996) determine that a similar supernova at 17 pc would produce a much more attenuated effect – century-long depletions of 20% at the tropics.[282] Gehrels et al. (2003) employ a different model and state that a biologically-relevant (on a mass-extinction basis) must occur within 8 pc, which is an event occuring with a frequency of about once per 1.5 Gy.[272]

Anthropogenic Phenomena

Geoengineering by Planetary Albedo Modification

Shortly after the identification of carbon dioxide as a climate-altering greenhouse gas entered the mainstream conversation (e.g., references[283–287]), individuals began to propose mitigating technological innovations.[288–290] Perhaps most prescient among these was the idea that one might deliberately seed the atmosphere with albedo-enhancing particles to reflect incoming shortwave radiation.[289]

Those interested in this problem noted the perturbation of the radiation budget of the Earth following the 1964 eruption of Mount Agung.[291] Subsequent analysis of prior volcanic explosions of global relevance (e.g., Tambora – 1815, Krakatoa – 1883, El Chichón – 1984, Mount Pinatubo – 1991) validated this theory[91,116,292–294] and suggestions for a simulated volcanic aerosol veil to counteract greenhouse warming quickly followed.[295,296] These observations were nearly commensurate in time with the discovery of the role of heterogeneous catalysis in enhancing anthropogenic ozone depletion and it was noted that volcanic aerosols certainly carried the same chemical risk.[45,46,297–300] Observations of large-scale zonal losses of ozone following the 1991 eruption of Mount Pinatubo as

discussed in section 3.5 dampened the conversation.

Interest in Albedo Modification began anew following the release of the Second Assessement Report of the Intergovernmental Panel on Climate Change and the increasing public face of the dangers posed by carbon-mediated climate change[301]. Solar Radiation Management by means of Stratospheric Aerosol Injection (SRM-SAI) was identified as a practical method by which to accomplish AM early on and most subsequent work focuses on this technique.[302] Aerosol candidates with lower ozone depleting capability were proposed[303–305] and problems of economics, ethics, legislation, and logistics were outlined[306–314].

The ozone impact of SRM-SAI schemes can be understood in close analogy to Pinatubo-like volcanic eruptions. Surface area enhancement in the stratosphere perturbs the chemical partitioning of Cl_y and sinks NO_x, increasing the rate of ozone loss in the lower stratosphere. Such an effect is expected so long as suitably reactive aerosols are injected and stratospheric inventories of anthropogenic halogens remains elevated. Explosive volcanism and SRM-SAI differ in that a volcanic eruption typically deposits volcanic gases to the stratosphere in closely spaced-in-time impulses rather than a sustained input. This results in transient stratospheric aerosol loadings which peak and then decay in time. SRM-SAI schemes call for continuous deposition of aerosol of specified particle size distribution at prescribed altitudes, in specific regions to produce sustained and controlled optical depths. Continuous monitoring would allow for adjustments to the operation if peculiarities were observed.

Pitari et al. (2014) summarize the results of the Geoengineering Model-Intercomparison Project (GeoMIP), in which four different atmospheric models were evaluated in a two different SRM-

SAI scenarios employing sulfate aerosol as the scattering material in RCP 4.5 climate futures.[156] The ozone response to SRM-SAI is complicated. In the years 2040-2049 of the experiment, models agreed that column ozone will increase in the middle latitudes due to suppression of odd-nitrogen cycling. Column reductions are predicted in tropical and polar regions. Enhancements in the strength of the Brewer-Dobson circulation results in increased upwelling of tropospheric air in the tropics, producing this predicted deficit. In the polar regions this reduction is due to enhanced odd-chlorine cycling as a result of elevated aerosol loading. After the year 2050, as anthropogenic halogens decline, the models predict that lower stratospheric halogen chemistry will become less important than the aerosol-mediated suppression of NO_x.

Keith et al. (2016) propose chemically-tuned aerosols for use in SRM-SAI to prevent the activation of halogen reservoirs and simultaneously sink inorganic Cl.[305] Specifically, they propose seeding the stratosphere with alkaline salts such as Na_2CO_3 or $CaCO_3$. These aerosols are likely to act as sinks of stratospheric NO_x and ClO_x via ion exchange, as in the following motif for reactions of $CaCO_3$.

$$2HCl + CaCO_3 \rightarrow CaCl_2 + CO_2 + H_2O \tag{7.18}$$

$$2HBr + CaCO_3 \rightarrow CaBr_2 + CO_2 + H_2O \tag{7.19}$$

$$2HNO_3 + CaCO_3 \rightarrow Ca(NO_3)_2 + CO_2 + H_2O \tag{7.20}$$

$$H_2SO_4 + CaCO_3 \rightarrow CaSO_4 + CO_2 + H_2O \tag{7.21}$$

SRM by Solar Constant Reduction (SRM-SCR) is another AM scheme which invokes some sunlight scattering medium situated outside the atmosphere of the Earth.[302] Such schema, though they do not interact physically with the ozone layer, will perturb the radiative/photochemical structure of the stratosphere. This effect is similar to the perturbation caused by solar variation as discussed in section 7.2.3 but with perhaps less wavelength-dependent variation. An evaluation of the stratospheric chemical implications of this type of modification was performed within GeoMIP.[315] In the scenario, the solar constant was reduced by 49 W m^{-2} to offset surface temperature increases forced by a fourfold increase in carbon dioxide. In such a situation, the stratosphere is expected to cool significantly, both from the carbon dioxide loading and from the reduction in insolation. This cooling speeds up the termolecular production of ozone as described in section 1.4 and slows down bimolecular ozone loss reactions of the type discussed in section 1.5. Enhancements in column ozone are realized across all latitude zones by 10 – 20%. The authors note that the corresponding $\approx$ 15% decrease in surface UV-B radiation may result in adverse human health consequences with respect to vitamin D biosynthesis.

Space Launch Vehicles and Supersonic Stratospheric Transports

Traffic within (and through) the stratosphere was perhaps the first recognized anthropogenic force for stratospheric perturbation. In the early 1970's, a proposed fleet of 400 Supersonic Stratospheric

Transports (SSTs) – or equivalently, High-Speed Civil Transports (HSCTs) – was severely scrutinized to address concerns which included the impact of SST HO_x and NO_x emissions on stratospheric ozone. Initial 1-D photochemical model estimates of ozone loss arising from such a fleet frequently exceeded 50% or more and contributed to a moratorium on US development of SSTs.[316–318,318–325] Wuebbles, Kinnison, and Johnston revisited this problem using a 2-D model in the 1990's, finding that these early estimates were too large[326]. Importantly, if 500 SSTs flewdaily between 21 – 24 km using 1990's engine technology (in terms of NO_x emissions index (EI) – 15 g NO per 1 Kg fuel), predictions indicated that global ozone reductions of 20 % would result from NO_x alone.[327] When HO_x and NO_x are considered together, the ozone impact is reduced due to enhanced heterogeneous hydrolysis of NO_2.[328] If engines were redesigned to produce only one third the NO_x produced by 1990's era engines, the total column ozone reduction would fall to 3 % which, while much smaller than the previous estimate of 20 %, is still not trivial. The extent of ozone depletion may also be reduced by flying at lower altitudes; however, flight altitude and maximum Mach number are highly correlated, so this solution would result in a slower SST fleet. The study authors also note that NO_x and HO_x addition from SSTs will result in ozone depletion at all projections of future Cly. Only when Cly exceeds 8 ppbv, as discussed in section 7.3.4, will SST fleets reduce the total rate of ozone depletion via chlorine nitrate formation pathways.[327,329]

In light of contemporary efforts to revive global supersonic transit (e.g., reference[330,331]), it is helpful to note that these calculations are performed with a very optimistic emissions index, and that contemporary propulsion technologies produce more than twice the simulated NO_x EI.[332] Baughcum et al. (2003) provide sensitivity studies demonstrating that the Northern Hemispheric

ozone column decreases by 0.2 % for every increment in EI for a 500 member fleet of SSTs.[333]

2-D and 3-D model studies estimate negligible reductions in total column ozone resultant from a fleet of 500 SuperSonic Business Jets (SSBJs) flying at 17 – 20 km altitude.[334–337] SSBJs are a technology of increasing interest which, because they fly slower and lower than an SST, can maintain higher NO_x EI profile with lower ozone impact. Subsonic commercial air traffic has a much higher NO_x EI, frequently exceeding 30 g NO per Kg fuel;[338] however, model intercomparisons of this traffic indicates minimal impact on total column ozone if only subsonic fleets operate into the future.[339]

Space Launch Vehicles (SLVs) also perturb stratospheric trace gas inventories. Solid Rocket Motors (SRMs) employ ammonium perchlorate oxidizers (NH_4ClO_4) and alumina fuel, producing ozone depletion in their plume wakes from the direct emission of chlorine oxides.[340–345] Danilin et al. (2001) employ a 2-D model to evaluate the global effects of SRM plume chemistry, finding with late 1990's rates of launch that SRM chlorine emissions produce negligible total column impact.[346]

Contemporary rocket designs for medium and heavy lifting tend to shy away from SRM employment due to the low specific impulse imparted. Liquid Rocket Engines (LREs), such as liquid oxygen/kerosine or liquid oxygen/hydrogen motors, are increasingly used in these cases. LRE emissions are considerably "cleaner" than SRM emissions; however, they still produce marginal enhancements of NO_x and HO_x in their plume wake. Econometric projections of the space launch market indicate the possibility of orders-of-magnitude growth in payload mass delivered to space by the middle of the century as launch prices decline.[25] Ross and colleagues (2009) explore such scenarios and develop metrics of the payload per annum launch limitations for different rocket motor technologies to constrain global ozone depletion below 0.2%.[25] Particularly interesting is the possible

deposition of large quantities of black carbon to the stratosphere following the adoption of solid hydrocarbon fuels.[347] Voigt et al. (2013) conclude that perturbations ofstratospheric ozone by volcanoes, aviation, and meteoric deposition of material by bolides are far more significant that emissions by contemporary levels of space access.[348] In a simulation of the number of flights required to maintain a proposed end-century space-based solar power infrastructure (Skylon hydrogen-fueled/air-breathing space-plane, 10^5 flights per year), Larson and coworkers (2017) use WACCM to find 3 ppm increases in stratospheric water vapor burden, 3 ppbv increases in NO_x, and 1.4 DU decreases in total column ozone at steady state.[349]

Nuclear Warfare

About 10^{32} molecules of NO are produced for every megaton of explosive energy produced by an explosion in the atmosphere.[350–352] While much of this NO recombines to form N_2 and O_2 during a ground burst, a significant proportion, depending on the explosion size, is estimated convect rapidly to the stratosphere, potentially disrupting global ozone columns.[353] Ground bursts additionally convect dust and other material vaporized from the interaction of the fireball with the surface. A higher proportion of the generated NO partitions to the stratosphere following an air blast. Foley and Ruderman (1973) determine that the fireball of a 250 kt (or larger) blast will penetrate the tropical tropopause.[350]

Full-scale nuclear war, defined as a war in which more than 5 Gt explosives are delivered, was predicted by Johnston et al. (1973) to result in widespread ozone depletion of up to 7 % in the northern hemisphere.[354] In addition to NO_x-catalyzed ozone depletion, widespread fires would produce vast

quantities of ash and black carbon which would increase the optical depth of the atmosphere for up to a year or longer.[352] Bimolecular ozone loss mechanisms in this darker, warmer stratosphere would quickly deplete ozone.

More contemporary works focus on smaller nuclear wars, termed ”regional nuclear wars”. Robock et al. (2007) simulate a hypothetical war between Pakistan and India employing 100 Hiroshima-sized bombs, whose collective 1.5 Mt of explosive energy is far smaller than the cutoff for a full-scale nuclear war.[355] Such an exchange would produce 5 Tg ash and black carbon. The subsequent transport of ash and black carbon to the stratosphere is found by Mills et al. (2014) to produce significant surface cooling on a global scale lasting years to decades.[356] A more sophisticated aerosol treatment indicates that climate effects from a regional war may be more moderate than the decades-long disruption calculated by Mills above, though still years-long. A 10-year climate disruption following a regional nuclear war is calculated by Xia and coworkers to result in regional crop failures for a decade or longer, likely resulting in famine.[357,358] While not as severe as the nuclear winter scenarios presented by Crutzen following full-scale nuclear wars, the ash clouds produced by these regional nuclear wars are still capable of significant perturbations of column ozone of 20 % globally.[359] Stenke et al. (2013) use the SOCOL CCM to evaluate climate and ozone following the employment of 750 kt nuclear explosives determining that soot emissions following the simulated war lead to up to 50 % column ozone reduction in the northern high latitudes.[360]

Nearly all the energy produced from very high altitude nuclear explosions is manifest as X-ray radiation. In such cases, NO_x will be produced from processes similar to those expected following a solar storm as described in section 7.2.4 and will not be considered further.

The World (Mostly) Avoided: Massive Release of Ozone-Depleting Gases

The seemingly innocuous question, "what happens to CFCs in the atmosphere?"[361], presented Sherwood Rowland and Mario Molina a Pandora's Box. The discovery of a significant and new stratospheric chlorine source from CFCs prompted the dire realization that, if nothing was done to reign in industry, within several decades CFC emissions would jeopardize the existance of the ozone layer[362,363].

The notion that anthropogenic trace gas emissions could lead to catalytic depletion of stratospheric ozone represented the consensus of an emerging group of atmospheric specialists, but was not entirely novel: In 1971, Hal Johnston reported that nitrogen oxides produced in the emissions of SST craft might enhance rates of ozone destruction[316]. This theory was further elucidated by Paul Crutzen[317,318]. Citing the works of John Hampson and B.G. Hunt[364,365], Halstead Harrison proposed that water vapor emissions from SSTs[†] may also produce conditions in which ozone is catalytically destroyed and that increased rates of skin cancer may result[319] - and this concern was reinforced a year later by meteorological physicist James McDonald[367]. Contemporaneous reports and reviews on the subject of trace gas perturbations of the stratosphere and ozone recombination were produced at a very fast pace between 1970 and 1973, further solidifying concern and awareness of the subject matter[318,320–325].

Though the catalytic cycling of ozone by chlorine radicals was not a new concept[368], the idea that chlorine might act as a sink for stratospheric ozone elicited skepticism. This changed in 1973

[†]He relates the story of this research paper and how it cost him his career at Boeing Scientific Research Laboratories in an essay found on his University of Washington website[366].

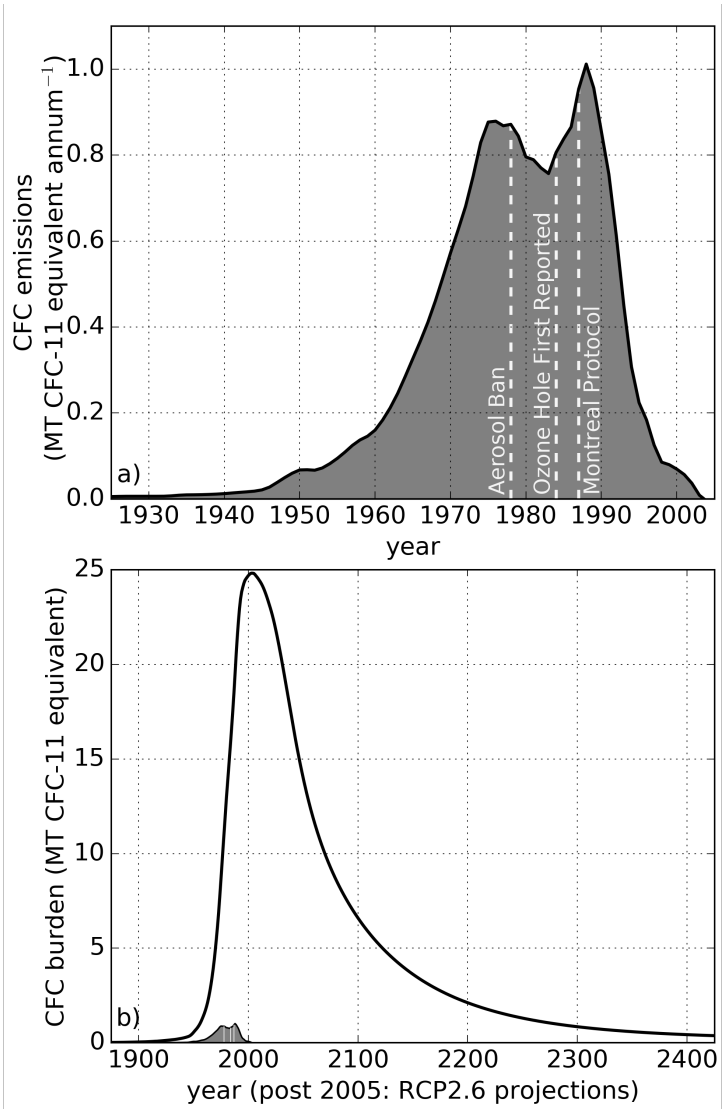

Figure 7.2: Emissions and global burden of CFCs. a) global emissions of CFCs regulated by the Montreal Protocol in MT CFC-11 equivalents. b) Total atmospheric burden of CFCs. Historical emissions are presented prior to the year 2005. Per annum emissions are overlaid, illustrating how quickly CFCs accumulated in the environment. Projections of CFC decay are presented within CMIP5 simulations of the RCP2.6 scenario. Data adapted from Meinshausen et al. (2011).[142]

when Steven Wofsy and Michael McElroy outlined the importance of chlorine as an ozone sink, citing stratospheric pertubations from volcanic and solid rocket sources of HCl[369]. Submitted two months later, and published in the same issue of the Canadian Journal of Chemistry, Richard Stolarski and Ralph Cicerone provided a similar analysis[370] echoing the findings of their 1973 NASA-contracted report on the Space Shuttle[371]. Crutzen published a review on the subject of ozone, including chlorine chemistry, also in the same issue[372]. An internal report by Hiro Hoshizaki and colleagues at Lockheed Martin reiterated the same concern that HCl originating from solid rocket motors may provide an avenue toward ozone destruction in the stratosphere[373]. Though the mechanism of chlorine-catalyzed ozone destruction was sound, the volcanic and rocket motor sources of chlorine were found to be much too small to contribute to any significant losses.

These findings, that trace gases might engage catalytic recombination cycles (and specifically chlorine radical precursors), set the stage for Rowland and Molina's hypothesis that stratospheric chlorine originating from a new and significant chlorine source, long-lived CFCs, posed a credible threat to stratospheric ozone inventories[362,363]. Environmental CFCs were molecular entities of very little interest except to those engaged in the study of atmospheric dynamics. James Lovelock wrote of their use as inert tracers solely of anthropogenic origin as "indicators of air masses which have recently been polluted by industrial effluents"[374] and that "the presence of these compounds constitutes no conceivable hazard"[375]. Thus, when Rowland and Molina conceived of an existential hazard originating from these compounds, that they decomposed in the stratosphere when exposed to ultraviolet radition < 230 nm and yielded a potent new source of stratospheric chlorine, the response was initially tepid.

Slowly, as the quantum yields and kinetics of CFC photolysis and oxidation were determined, vetted, and published[376–384] and sources of stratospheric chlorine from other halocarbons were sorted out[385–391], the greater scientific community began to appreciate the seriousness of the threat toward the ozone layer and produced many concretizing reviews on the subject[363,392–397] Meanwhile, Du Pont, the manufacturer of Freon® CFC gases, began to appreciate the seriousness of the threat to their financial bottom line and launched a highly-effective advertising campaign in which the science was questioned (see, for example, Figure 7.3, an advertisement in Science questioning the research[398] which prompted a response by Rowland and Molina[399]).

The direct detection of the chlorine monoxide radical (dubbed the "smoking gun" by the popular media[361,400]) was needed to prove the enhanced engagement of chlorine in the ozone recombination reaction as stratospheric mixing ratios of CFCs increased. Tentative detection of an increase in total column ClO by DOAS was first reported by Sherwood Rowland and Robert Carlson in 1976 at the AAAS meeting in Boston using a comparison of 1971 and 1975 spectra of the solar spectrometer at Kitt Peak National Observatory[400,401]; however, no further results were published due to dataset inconsistencies[402]. In 1976 and 1977, a team led by James G. Anderson definitively accomplished this using an atomic resonance fluorescence technique on a stratospheric balloon-borne instrument[403,404], finding mixing ratios maximized around 40 km, as predicted by prior modeling studies[394].

Despite this success and the subsequent prohibition of CFCs in certain under various regulatory actions (e.g., the so-called Aerosol ban[405]), the discovery of stratospheric chlorine nitrate, a chlorine reservoir, and refinements in relevant kinetics resulted in cartwheeling estimates of future steady-

You want the ozone question answered one way or the other. So does Du Pont.

And most scientists agree there is time to find the answer.

Fluorocarbons are liquids and gases used in refrigeration, for air conditioning, and as propellants in about half the aerosol spray cans sold in this country. Some say that these useful, normally safe compounds will cause a health hazard by attacking the earth's ozone layer. We believe this is an oversimplification.

The point is, to date there is no conclusive evidence to prove this statement. To understand, then, why there is a controversy, it is necessary to unsimplify the issue. We must treat the real world on its own terms, and they are complex.

The model that raised the question.

Ozone is continually created and destroyed by natural forces scientists are seeking to understand. The ozone depletion theory, based on a computer model of the stratosphere, was reported in 1974 by two chemists at the University of California.

This mathematical model calculates how fluorocarbons

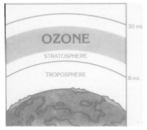

in the stratosphere behave under the influence of a series of variables (such as temperature, altitude, sunlight, chemical concentration) to affect the ozone layer.

In order to estimate hypothetical reactions, and because little is actually known about the real ones, the modelers made a number of assumptions about the way the upper atmosphere behaves.

The unmeasured yardstick.

Before any judgments can be made using this model as a stratospheric yardstick, its accuracy must be determined.

Does it describe the real, three-dimensional world? To find this out, the validity of the modeler's basic assumptions must be determined.

Turning assumptions into facts.

Before a valuable industry is hypothesized out of existence, more facts are needed. To get these facts Du Pont and the other fluorocarbon manufacturers are funding independent technological investigations in universities and research laboratories. Under the direction of acknowledged scientific experts, this research is designed to either prove or disprove the assumptions most important to the computer case against fluorocarbons.

Some research has been carried out since the model was first presented. Scientists now have a better idea of the accuracy of the assumptions in the model.

ASSUMPTION: The ozone-depleting reaction with chlorine from fluorocarbons takes place at a rate that demands an immediate decision on fluorocarbon use.

FACT: Recent determinations of reaction rates disclose that the ozone/chlorine reaction actually takes place at a slower rate than that assumed by the model. In addition, the same research has shown that the reaction of chlorine with stratospheric methane proceeds at a faster rate. Since this reaction tends to remove chlorine from the ozone layer, the net effect of both reactions is to lessen the originally-calculated impact of fluorocarbons. In fact, the impact was overstated by 300%.

RESEARCH: To guide future measurements of stratospheric reactions, a laboratory program has been funded to measure the reactions of chlorine compounds and ozone under simulated stratospheric conditions.

Most scientists agree there is time to conduct the research needed to settle the controversy one way or the other... before a final decision is made on fluorocarbon production and use.

ASSUMPTION: There is no other way to get fluorocarbons out of the atmosphere except by the ozone-depleting reaction.

FACT: One well-known class of chemical reactions not considered in the model is that of chlorine compounds in the atmosphere in heterogeneous reactions.

In an article in SCIENCE (Feb. 14, 1975), Professors S. C. Wofsy, M. B. McElroy, and N. D. Sze of Harvard University caution that "If additional removal processes could be identified... or if additional sinks could be identified for stratospheric odd chlorine, the atmospheric and biological impacts of [fluorocarbons] would be reduced accordingly."

RESEARCH: Atmospheric chemistry involving ion molecule reactions has been described in recent months by several investigators. Reaction rates with ion molecules are known to be extremely fast and are believed to occur primarily in the lower stratosphere.

Thus, ion molecules could react with fluorocarbons, allowing them to be removed from the atmosphere.

ASSUMPTION: Fluorocarbons are the only significant source of chlorine available for interaction with ozone in the stratosphere.

FACT: Many chlorine-containing materials are present in the atmosphere in varying concentrations. Of particular significance, large amounts of methyl chloride and carbon tetrachloride have been discovered in the troposphere and stratosphere.

In addition, new calculations on the injection of gaseous chlorine compounds into the stratosphere from volcanic eruptions have shown this as a significant contributor of chlorine not taken into account by the model.

RESEARCH: Scientists are completing an inventory of chlorine-containing compounds in the atmosphere. It must be determined how nature deals with chlorine from these natural sources, before it can be shown that chlorine from fluorocarbons might pose a threat to the ozone layer.

Additional research.

A fluorocarbon industry research program is funding the development of a computer model that will better reflect the complex chemistry of the stratosphere.

In addition, other studies are under way to broaden our understanding of the total ozone production/destruction balance. These will concern themselves with other stratospheric reactions affecting ozone.

A panel of highly qualified academic scientists will advise on the technical programs covering various facets of the problem. This panel of independent experts will review the projects, providing a critical opinion on the pertinence of each, the probability of their success, and the completeness of the overall investigation.

Conclusion.

Much more experimental evidence is needed to evaluate the ozone depletion theory. Fortunately, as most scientists agree, there is time to gather this evidence. Du Pont has joined with other fluorocarbon manufacturers to provide funds for work by independent university scientists. Governmental agencies are also conducting research to help in the assessment of the theory.

Should the theory be proven correct after all the evidence is in, Du Pont, as we have stated, will stop the manufacture and sale of the offending compounds.

In the meantime, we believe that to act without the facts—whether it be to alarm consumers, or to enact restrictive legislation—is irresponsible. Final decisions cannot be made with only the information at hand.

The independent research described above is presently being carried out by scientists at the following institutions:

Cambridge University—England
Environmental Research and Technology, Inc.
Massachusetts Institute of Technology
State University of New York
The Battelle Memorial Institute
The University of Reading—England
University of California
University of Denver
University of Illinois
University of Maryland
University of Michigan
Washington State University
York University—Canada
Xonics, Inc.

This is the second in a series of discussions by Du Pont to offer a perspective on an important subject. If you would like copies of either this or the first discussion, please write to: FREON®, Room 24517, Du Pont Company, Wilmington, DE 19898.

®Du Pont's trademark for fluorocarbon refrigerants and aerosol propellants.

DU PONT

Figure 7.3: A full-page DuPont advertisement in the Journal *Science*, 1975 casting doubt on the significance of stratospheric chlorine from CFC sources as an ozone sink[398].

state total ozone losses. The National Academy of Sciences produced specialist reports that, in 1976, provided a range of 2–20% depletion [406], 16.5% in 1979 [407], 5–9% in 1982 [408], and in 1984, 2–4% [409]. In the background, the CFC industry was booming, finding more and more applications for the now nearly ubiquitous product [410]. Figure 7.2a presents global emissions of CFCs (in megatons of CFC-11 equivalents). Although emissions were reduced following the Aerosol Bans of 1978, alternative markets were identified and capitalized upon in 1983.

As CFC production ramped back up, a report from an unexpected place caught the community by surprise. While the conversation had focused on the ozone column over mid-latitides (e.g, densely populated areas), Joe Farman and his team at the British Antarctic Survey had quietly noted an abrupt seasonal decline in column ozone since 1982. [411] His report was the first detail of what is now known as the *ozone hole* and it presented an unusual picture that elicited some doubt– NASA's Nimbus 7 solar backscatter ultraviolet instrument should have already identified such a trend if it were real. In fact, Nimbus 7 had imaged the Antarctic ozone hole, but in a data science gaffe of horrific proportions, engineers postprocessed data prior to ever reviewing it: an automated algorithm overwrote all columns recorded below 180 *Dobson units* as they were assumed to be in error. [412] A subsequent reanalysis of Nimbus 7 data was published, documenting the extreme scale of seasonal Antarctic ozone depletion. [413].

Theories regarding the origin of the ozone hole were produced relatively soon afterward, citing dynamical [414], solar variational [256], and heterogeneous chemical [45,415,416] causes. Results from the quickly-dispatched 1986 National Ozone Expedition to Antarctica did not establish a clear cause. This cause was definitively assigned in 1987 when the NASA ER-2 flew through the Antarctic vortex

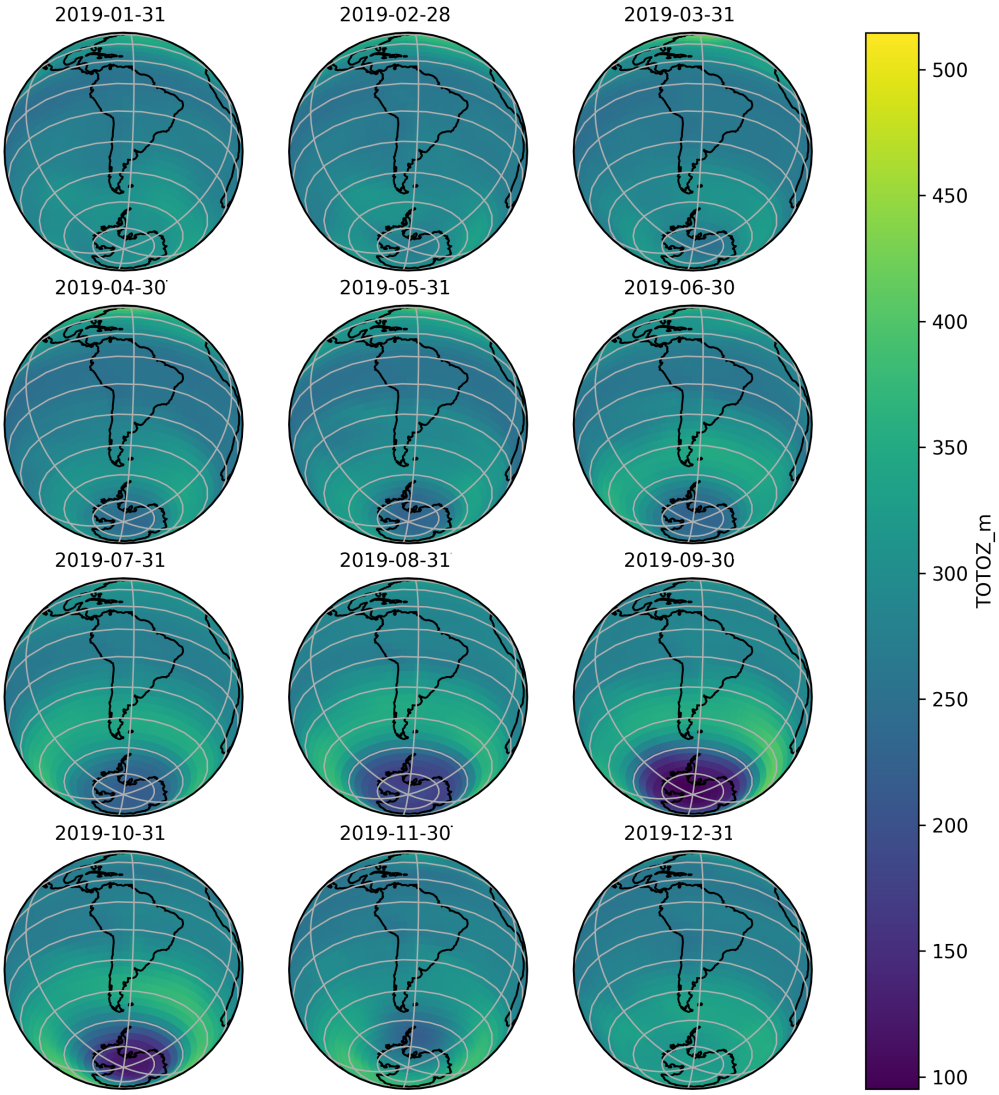

Figure 7.4: Temporal variation of column ozone (in Dobson Units) as a function of month. Profile generated for the year 2019 within the SOCOL-AER model. Despite high tropical insolation leading to high rates of production, poleward transport and subsequent reduction in photochemical loss rates due to variation in the solar zenith angle leads to an accumulation of column ozone at higher latitudes. During Austral spring, an ozone hole develops due to the wintertime isolation and denitrification of the Antarctic polar vortex air mass.

and recorded the so-called, again, ”smoking gun”: anti-correlated ozone and chlorine monoxide within the polar ozone vortex.[417]

Public, political, and industry sentiment quickly turned toward CFC alternatives. Figure 7.2a demonstrates the very fast phase-out of CFC materials as *hydrochlorofluorocarbons* (HCFCs) and *hydrofluorocarbons* (HFCs) were adapted to existing industrial needs following the adoption of the Montreal Protocol in 1987 and its subsequent amendments. The residual effect of sixty years of CFC release to the environment will last for hundreds of years, as indicated in figure 7.2b.

Humans emitted approximately 25 Mt of chlorofluorocarbons to the atmosphere between the period of their discovery in 1928 and their regulatory prohibition and phase out toward the end of the 20th century. The temporal trend in emissions is depicted in figure 7.2a. The slow decay of the atmospheric burden of CFCs is presented in figure 7.2b. Despite the very brief period of significant human production and emission of CFCs to the atmosphere, the atmospheric CFC burden will remain elevated for centuries due to the extremely long atmospheric lifetimes of the chlorofluorocarbons and the seasonal Antarctic ozone hole will remain for many years. Figure 7.4 provides a climate model illustration of the seasonality of the ozone hole, simulated in the year 2019. Despite continuous transport of ozone-rich air from the equator, the wintertime polar vortex seals off Antarctic air masses, resulting in the accumulation of ozone-rich air around the vortex boundaries. Heterogeneous processing and denitrification on polar stratospheric clouds inside the vortex produces a large enrichment in Cl_x, which rapidly destroys ozone when the solar terminator ascends back to higher latitude.

Scenarios of atmospheric chemistry and climate if the Montreal Protocol and subsequent amend-

ments had not been enacted are commonly referred to as "the world avoided".[418–422] Morgenstern et al. (2008) were the first to explore such a situation using a 3-D climate model.[418] In a situation in which stratospheric EESC has increased to 9 ppbv by the year 2025, they find profound reductions in the global ozone distribution. Tropical columns are reduced by 5 %, mid-latitude regions by 10 – 15 %, and greater than 30 % in the polar regions during the spring relative to 3.5 ppbv ("the world realized") simulations. These ozone deficits produce massive changes in the thermal structure of the stratosphere, which cools by more than 6 K while the surface temperature increases by 1 – 2 K. Newman et al. (2009) explore a similar scenario, but include projections to the late-middle 21st century.[419] For simulations in the year 2020, their results largely confirm the magnitude of ozone depletion predicted by Morgenstern and colleagues; however, they find that if the CFC emission continued at 1980's levels, the global ozone column would be reduced by 67 % of its 1980 levels by the year 2065. Cooling induced by ozone loss gradually increases the latitudinal domain of stratospheric cloud formation toward the equator. By the year 2053, their simulations indicate the temperature threshold for forming "polar" stratospheric clouds is acheived in the tropical lower stratosphere, resulting in massive increases of surface UV flux to near top-of-atmosphere levels. A similar work by Chipperfield et al. (2015) finds that deep boreal spring ozone holes would have appeared around the year 2011 if human emissions of CFCs had not been regulated while northern midlatitude ozone columns would have declined by a further 15 %.[420] Garcia et al. (2012) further quantify climate changes toward the end of the century in a scenario in which humanity continues emitting at 1980's rates and then corrects course in the year 2050, projecting that Antarctic surface temperatures would increase by more than 4 K.[421]

The Stratospheric Threat Matrix in Context

A graphic depiction of the relative threats each of the above scenarios poses to ozone, in terms of % loss years, is presented in figure 7.5. Natural events are plotted as a function of their recurrence interval and anthropogenic threats are plotted as a function of probability, which I have taken the liberty to estimate.

The most severe threats to stratospheric ozone are grouped along three categories: (a) injections of stratospheric soot, (b) long-term enhancements in the production rates of NO_x, and (c) the direct addition of halogen species to the stratosphere. Minor threats originate from either (a) transient high-magnitude perturbations in ozone-loss processing rates or (b) long-term, low-magnitude perturbations in ozone-loss processing rates.

Stratospheric injections of soot produce extreme heating of up to several hundred degrees in the immediate environment, depending on the magnitude of soot injected. Such heating events speed up bimolecular processes and suppress the recombination of ozone. Exchanges of nuclear weapons constituting a "full-scale" nuclear war – a war in which 10 MT of nuclear explosives are detonated – are expected to produce devastating nuclear winters in which soot and ash from widespread fires convectively loft into the stratosphere. Such an event is optimistically plotted with a very low probability. Regional events, in which less than 2 MT of nuclear explosives are exchanged, are more likely to occur and are also predicted to constitute a radical threat to ozone, though less than a full-scale nuclear war.

Comet and asteroid impacts on land produce tremendous injections of stratospheric soot in a

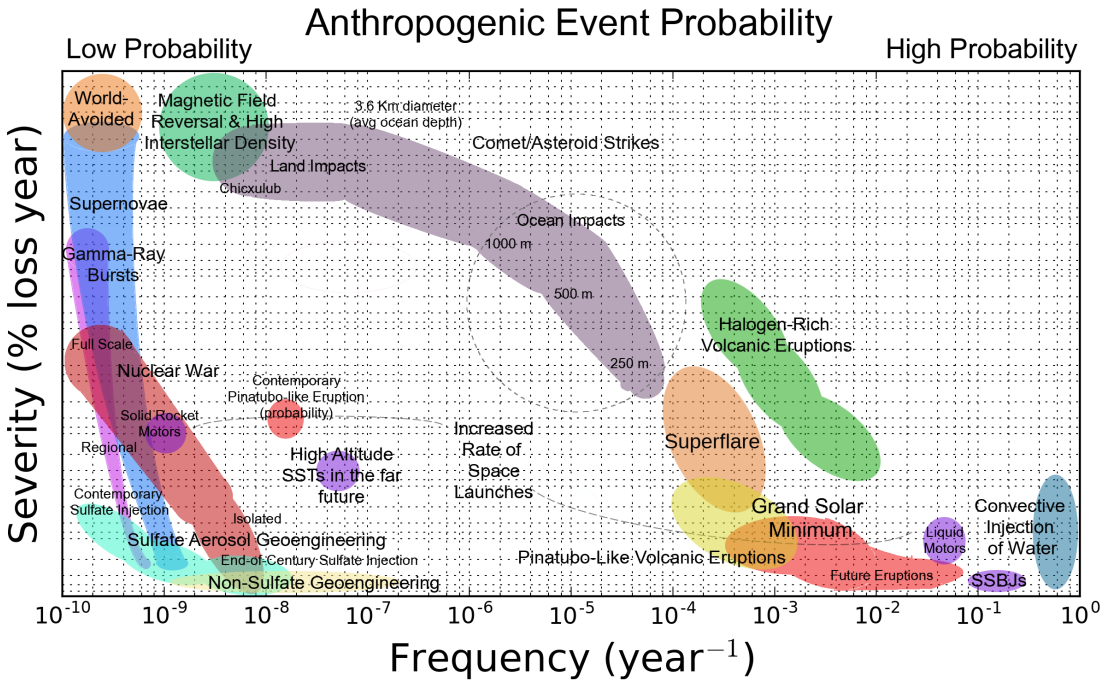

Figure 7.5: Severity of ozone response (in terms of % column loss years) for the different stratospheric perturbation scenarios discussed in this chapter. Natural events are plotted according to their expected recurrence frequency. Anthropogenic phenomena are plotted according to the author's estimate of probability of actualization. Estimates of severity and probability are qualitative.

manner similar to an exchange of nuclear weaponry. A 250 m asteroid impacting at the average impact velocity of 17.8 km / s possesses the same kinetic energy as energy that would be released by 800 MT of nuclear explosives (assuming dense rock equivalent of 2500 kg / m^3) and will efficiently loft soot into the mesosphere. Years-long ozone depletion is expected as a result of radiative heating of the stratosphere, though those on the surface would not likely be at risk of sunburn due to the lack of insolation. Such events occur infrequently – on multiple tens-of-thousands to hundreds-of-thousands of year timescales – and recovery is very quick in comparison to the recurrence interval.

Perturbations in stratospheric NO_x through energetic particle precipitation processes, especially in the GCR wake of a nearby supernova might also efficiently destroy ozone for long time periods. Supernovae and gamma ray bursts are both expected to produce large changes in total ozone, however, recovery from gamma ray bursts is expected to be quite fast while supernovae may suppress ozone columns for millenia or longer. Thankfully, both events are expected to occur very rarely, on the scale of the age of the universe. More frequently, surprisingly, are expected thousand-year reductions in column ozone resultant from the superposition of magnetic field reversal events with solar transits through regions of high interstellar density, expected to occur perhaps once every 50 million years.

More frequent, but less severe, superflares occur once every several hundred years and can perturb ozone via NO_x production severely at midlatitudes for a year or longer but have maximal impact at the relatively unpopulated high-latitude regions. Small enhancements in NO_x and HO_x are expected from increasing trans-stratospheric traffic from rocket launches and passenger transports. Assessments of their ozone impact indicate that they will have minimal effect on column ozone, but

the impact is expected to persist indefinitely as these markets develop.

Two perturbative forces which may directly increase the stratospheric burden of halogen gases are also plotted in figure 7.5. Comet and asteroid impacts, especially 250 – 3600 m oceanic impactors, are expected to engage ozone loss processes tremendously; however, even the most frequent (and least severe) events occur on timescales of 25 ky or more. Halogen-r Halogen-rich volcanic eruptions, on the other hand, pose an out-sized threat to stratospheric ozone. Mazama-scale volcanic injections of halogens are at least as destructive to stratospheric ozone as oceanic CAI, but occur on timescales of 10 ky or less at the greatest severity constrained by the ice-core record. Smaller, more frequent volcanic injections of halogen gases are likely to pose a threat to stratospheric ozone in perpetuity at possibly century-scale recurrence intervals.

This figure illustrates that, though a contemporary Pinatubo-like eruption (plotted in probability space) is likely to pose a large threat to ozone, future Pinatubo-like eruption (plotted in recurrence interval space) are likely to pose as large a threat as sulfate-injection geoengineering. The threat in these scenarios is minimal in the far future due to the overwhelming power of EESC in dictating the severity of the ozone response. Perturbations in the partitioning of halogen chemical inventories are expected to decline in significance as anthropogenic long-lived halocarbons decay; however, in the immediate future, which is the time period which should most concern emergency responders, events forcing such a change in the partitioning of halogens will have a significant impact on column ozone. These events are frequent: Large, explosive volcanic eruptions are expected to occur on decadal time scales and seasonal injections of water into the stratosphere from strongly convecting monsoonal storms are expected every year, with perhaps increasing magnitude and frequency as the

climate changes.

Figure 7.5 provides two important points: (a) halogen-rich volcanic eruptions pose the greatest natural risk to stratospheric ozone in terms of frequency of recurrance and magnitude of effect, and (b) in the immediate future the repartitioning of halogen inventories by stratospheric pertubations via volcanic eruption, convective injection, or SRM-SAI provide the highest likelihood of significant ozone depletion.

8

Conclusions and Future Directions

The work discussed in the prior chapters indicates that the evolution of the ozone layer's response to the a large perturbation in reactive stratospheric surface area couples dynamically with both the chemical inventory and physical state of the stratosphere. For Pinatubo-like volcanism, the impact of enhanced surface area on ozone declines. The chemical reactions responsible for ozone loss processing slow down as the stratosphere cools while the number density of inorganic halogens declines.

Though the focus of this thesis is volcanism, Pinatubo-like eruptions closely resemble the proposed climate intervention of planetary albedo modification by stratospheric aerosol injection – and similar to the scenarios explored in chapter 5, the response of the stratospheric ozone layer to such a mitigation will diminish as long-lived anthropogenic halocarbons decay and the stratosphere cools. Prior works assessing the ozone impact of this technique are based on the CMIP5 4.1 scenario and are resultantly burdened with accelerated anthropogenic halocarbon decay as was discussed in chapters 4 and 5.[156] Due to this, it is likely that projections of the date at which the ozone layer response mode switches from depletionary to accretionary following albedo modification are optimistic. Given that the likelihood of the implementation of this technology will increase as policymakers are increasingly confronted with the broader economic costs of a changing climate, future works must be conducted to assess ozone response within the WMO A1 halocarbon trajectory constraints.

Furthermore, it was revealed in chapter 6 that the efficiency by which volcanic halogens partition to the stratosphere within an eruption column is largely unconstrained. It is likely that the different halogen components partition to the stratosphere with different injection efficiencies – and engage ozone with alpha efficiency factors which will differ from contemporary values. Because bromine and iodine are 60 – 250 times more effective at destroying ozone than chlorine, even small changes in these efficiency factors may produce outsized impacts on global ozone response.

It is also likely that geographical considerations may further tune halogen injection efficiency – especially as tropopause heights increase with the changing climate. While high-latitude volcanic eruptions have been explored in the context of their climate effects, the literature provides no quantitative assessment on expected contemporary or future impacts of high-latitude volcanism on strato-

spheric ozone. Additionally, as the tropics expand poleward, regions in which volcanism may have less effectively produced global aerosol veils may in the future inject gases into the ascending branch of the Brewer-Dobson circulation.[9] That is to say, a larger fraction of worldwide volcanic eruptions will be expected to exert global impacts on stratospheric chemistry and climate.

These topics elicit several exciting research possibilities which will be discussed in the following:

- Will the halogen alpha efficiency factors evolve with the climate?
- What are the volcanic halogen alpha efficiency factors?
- To what degree does the latitude of a volcanic eruption influence the halogen injection efficiency of a given eruption?
- What is the ozone impact of a high-latitude Pinatubo-like volcanic eruption?
- What is the ozone impact of a high-latitude halogen-rich volcanic eruption?
- How much more ozone depletion is expected if bromine and/or iodine are injected into the stratosphere vs chlorine alone?
- To what extent does intraplume chemistry modulate the halogen injection efficiency of a given eruption?

Alpha Factors: Changing Climate and Volcanic Injection

As discussed in chapter 1, alpha factors are quantifications of the efficiency by which a single atom of bromine or iodine will process ozone normalized to the efficiency of chlorine within the same chemical environment. Established alpha values were determined using 2-D models in the late 20th century.[44,51,54,423] These alpha factors are not constant in latitude or vertical profile and are highly dependent on the chemicophysical environment.

Alpha factors have only been quantified for 20th century atmospheres with high anthropogenic halogen loading. As stratospheric chlorine produced from the decay of long-lived anthropogenic halogens declines, interhalogen ozone-loss processing cycles will become increasingly less important, as indicated in comparison of panels (b) and (e) of figure 5.6. If equal-sized impulses of chlorine and bromine were to occur in a far-future stratosphere, it is expected that a larger portion of the chlorine impulse would be lost to reservoir formation due to increased availability of reservoir-promoting reaction partners (OH, NO_2, CH_4. Because the analogous bromine reservoirs are more photo/thermolabile, the resultant alpha factor is likely to be greater than in the present day.

As discussed in the previous section, the alpha efficiency factor of a halogen is a function of its chemicophysical environment. Alpha factors are frequently related as a single global average value, or a range of values, usually computed near the tropopause. For bromine and iodine originating from short-lived sources, this is an appropriate region from which to obtain the metric – this is where stratospheric bromine exists in the highest mixing ratio. A halogen-rich volcanic eruption is likely to distribute large quantities of halogens to much higher levels of the atmosphere than where they maximize from source-gas aging processes. If such an injection of halogens were to occur, ozone loss projections produced on the basis of enhanced EESC considerations alone may suffer; the alpha values for middle-stratospheric bromine and iodine are likely to differ from their lower stratospheric values.

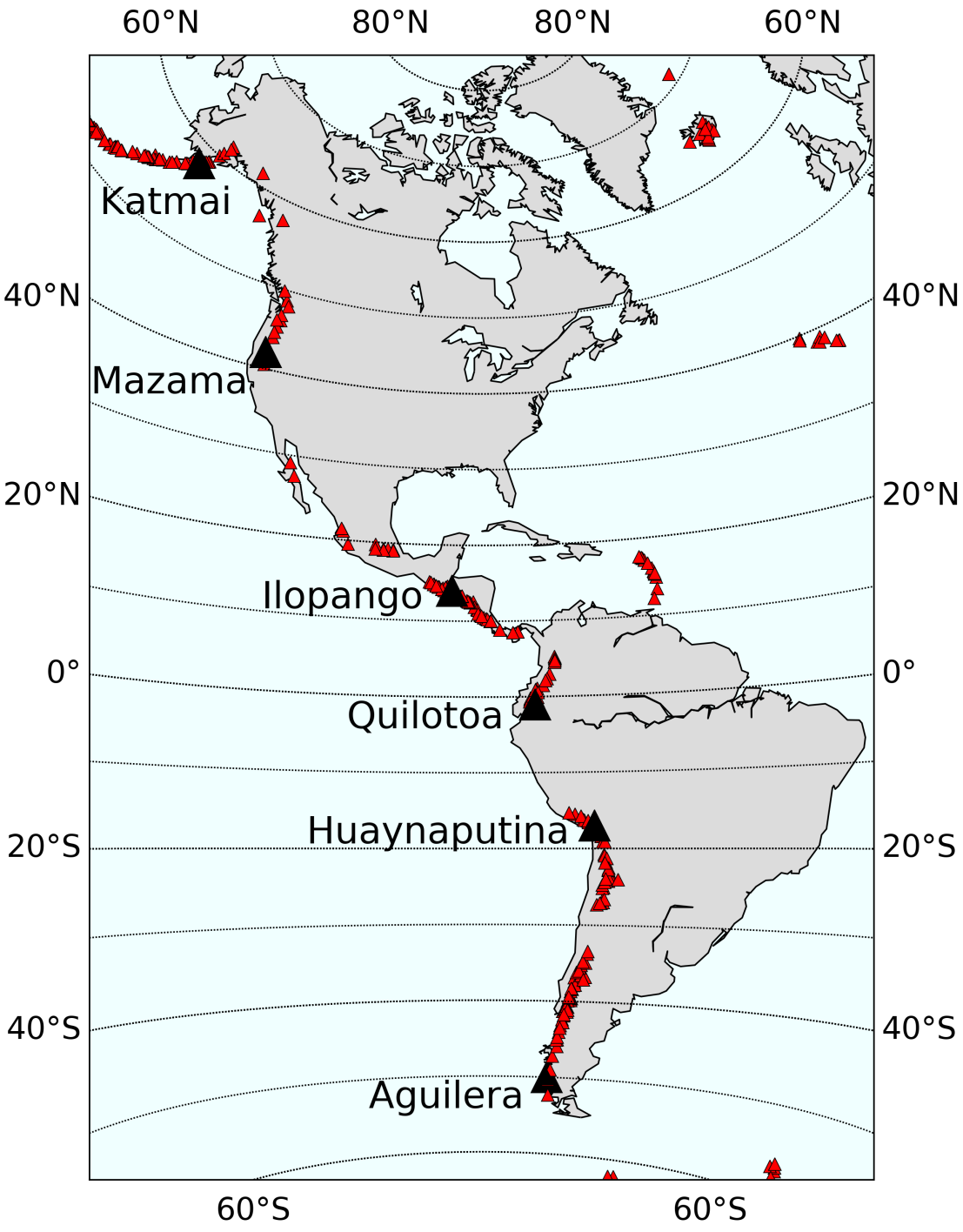

Figure 8.1: Locations of 314 stratovolcanoes known to have erupted in the western hemisphere during the Holocene era (red triangles).[85] Representative volcanoes distributed between 60°N – 50°S which have erupted within the previous 10 ky with magnitudes of 6 or greater are indicated with black triangles.

Volcanic Eruption Latitude and Evolution of the Volcanic Aerosol Veil

The latitude and seasonality of a volcanic eruption may significantly impact its influence on regional and global ozone columns. It is known that the radiative impact of a volcanic eruption on climate is highly dependent on the latitude of the volcano[117,118,424; –429]; however, to date, the latitudinal dependence of ozone response following a volcanic eruption has never been systematically quantified. The height of the tropopause and the humidity of the eruption column entrainment volume are the primary meteorological factors governing the magnitude of the volcanic injection efficiency of halogen species into the stratosphere.

While ratios and quantities of the halogen species in volcanic gases at the crater rim are not correlated with volcanic latitude, latitudinal effects on meteorology are likely to impact the efficiency of stratospheric injection. Whereas a tropical eruption is likely to feature enhanced halogen scavenging,[147,176] wintertime eruptions at higher latitudes may result in substantial halogen partitioning to the stratosphere; indeed, up to 70% of the February 26, 2000 Hekla (64°N) total halogen emission was detected in the stratosphere following the interception of the volcanic cloud by the DC-8 during the NASA SOLVE mission.[184–186] A combination of drier entrainment air volumes and reduced tropopause heights at higher latitudes provide for a longer tropospheric chemical lifetime for halogen species within the eruption column, which increases the probability that a significant portion of emitted halogen species survive transport to the stratosphere. These factors almost certainly contributed to the extraordinary prehistoric Antarctic ozone hole resultant from a series of halogen-rich eruptions of Mt. Takahe (76°S) 17.7 kya as well.[11]

The seasonality of an eruption may further modulate ozone response to extratropical eruptions. Air masses entrained into the eruption column are subject to seasonal variation in humidity, likely dampening halogen injection efficiency during moist summertime months. Additionally, aerosol distribution patterns are expected to be dependent on seasonal large-scale circulation patterns. For example, past simulations of a very large northern mid-latitude eruption in summertime showed production of more globally-dispersed volcanic aerosol clouds than in boreal winter, where the dominance of the Aleutian high pressure system resulted in cloud confinement to the northern hemisphere.[430] In another study, this seasonal effect was found to be mass-dependent.[426]

During the holocene era, 713 stratovolcanoes are known to have erupted. As shown in figure 8.3 for the western hemisphere, these volcanoes are distributed broadly across latitudinal zones. Although the majority of the most recent large, explosive volcanic eruptions (e.g., Mount Agung, El Chichón, Mount Pinatubo, Mount Merapi) have been tropical, the largest volcanic eruption of the 20th century was the June 1912 eruption of Mount Katmai (indicated in figure 8.3), which is situated in the Aleutian range at 58°N. Figure 8.2 provides the frequency of explosivity of eruptions occuring since the year 1800 as a function of latitude. It is apparent that large explosive eruptions are not only tropical phenomena.

Preliminary results from the 2-dimensional AER model with offline climatology, shown in 8.3, provide strong motivation to further explore the impact of eruption latitude in a 3-dimensional climate model with full climatology. Two contemporary volcanic eruption scenarios are presented for three volcanic eruption latitudes. A tropical eruption is simulated in the leftmost column, a northern midlatitude eruption is simulated in the center column, and an Arctic eruption is simulated in

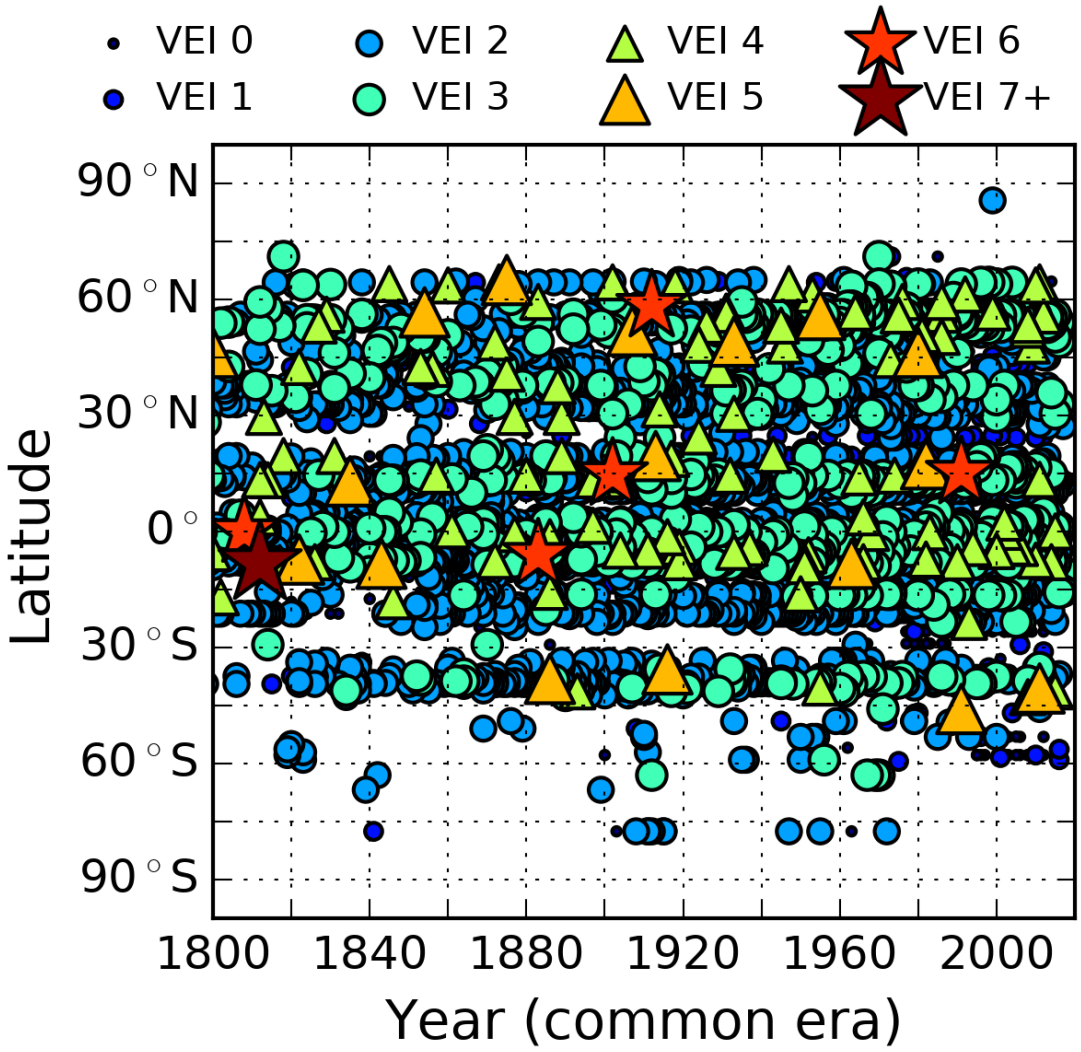

Figure 8.2: Explosive eruptions occurring between 1800 – January 2018 are plotted as a function of date, latitude, and explosivity index. Data provided by the World Volcanism Project.[85]

the rightmost column. 8.3(a-c), corresponds to a Pinatubo-like eruption and 8.3(d-f) corresponds to an eruption with 0.3 ppbv EESC enhancement (matching recent Aura/MLS HCl:SO2 ratios, but scaled to a Pinatubo-sized eruption). Hydrogen chloride is the only halogen simulated in the volcanic halogen injection scenarios. Above each panel is presented temporally-averaged column ozone deviations from the non-volcanic case. Latitudinal average ozone deviations are indicated to the right of each panel. The top right box corresponds to a 4-year global-temporal average ozone deviation. Though the model does not have interactive climatology, historical average transport fields demonstrate the enhancement in hemispheric asymmetry of ozone chemistry as the volcanic latitude tends poleward. Likewise, global-temporal ozone anomalies decrease due to decreased aerosol lifetime as eruption latitude increases; however, regional effects intensify. When quantities of hydrogen chloride are co-injected, 8.3(d-f), prolonged ozone losses of 15% or more begin to develop over the northern midlatitudes.

The results presented in figure 8.3 are a compelling first estimate of the sensitivity of column ozone to the latitude of a volcanic eruption; however, the AER-2D model does not compute changes in circulation patterns as a result of enhanced aerosol loading and this effect can significantly alter quantitative estimates of column ozone following an eruption.[125,146,153] For this and other reasons, a future analysis using a 3-D climate model with aerosol microphysics to properly quantify column ozone response as a function of eruption latitude is of interest. Preliminary results for such an analysis are presented in figures 8.4 – 8.9. For each figure, total column ozone is presented along the top map projections, colored according to the topmost colorscale. time-averaged column ozone deviations are presented on the extreme sides of these projections. The lowermost projections indi-

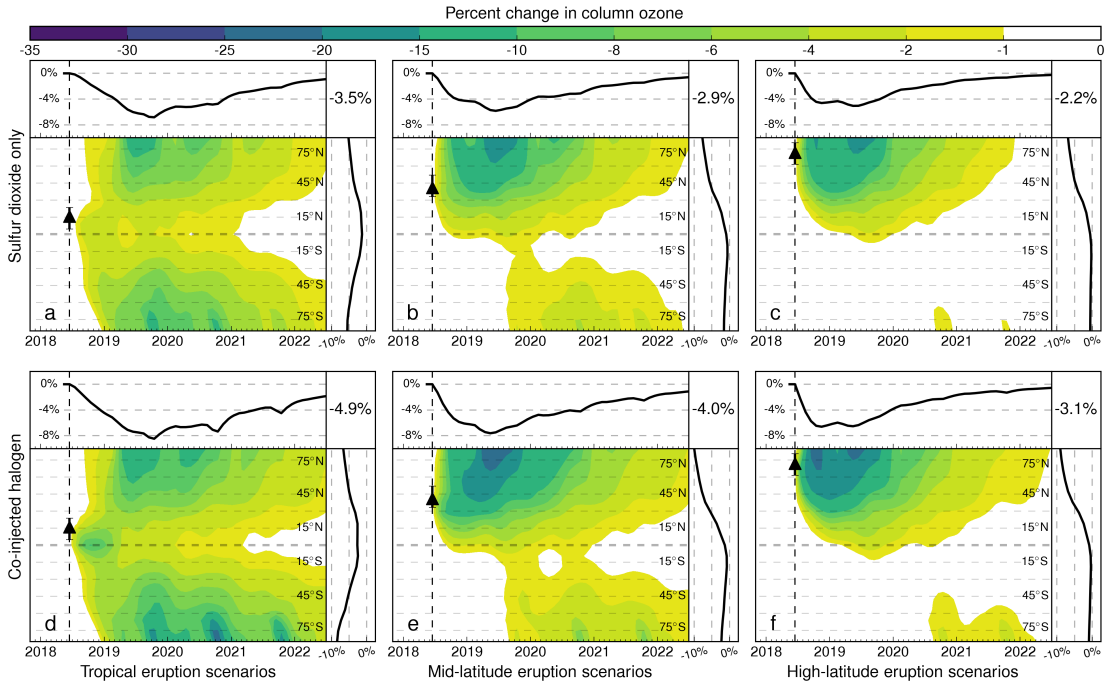

Figure 8.3: 2-dimensional model output depicting the column ozone response to a volcanic eruption of (a-c) 7 Tg SO2 and (d-f) 7 Tg SO2 and 0.1 Tg HCl. Eruption latitudes: left (15°N), center (40°N), right (70°N). As latitude increases poleward, hemispheric asymmetry and regional severity also increase.

cate stratospheric aerosol burden, logarithmically colored according to the bottom colorbar. The left panels present a tropical eruption of 3.5 Tg SO_2 on June 19th 2019. The right panels represent an eruption of equivalent mass at high northern latitudes – the eruption locations indicated in figure 8.4, a snapshot two days after the initial SO_2 injection. Figure 8.5, 20 days after the eruption, demonstrates the zonal mixing of stratospheric aerosol. Ozone perturbations are not yet evident. Significant ozone differences appear in figure 8.6, half a year after the eruption. Notably, sulfate aerosol, mixed into the Austral polar vortex, has significantly increased the magnitude of ozone processing in the southern hemisphere – especially for the case of the tropical eruption. Much less enhancement is observed following the sub-polar eruption, as the bulk of the injected aerosol is retained in the northern hemisphere. Interesting interhemispheric impacts are observed one year after the eruption, in figure 8.7. Stratospheric aerosol is well-mixed and nearly homogeneous in the tropical case, while the high-latitude eruption still demonstrates hemispheric asymmetry. Chemical ozone response also varies. In the high-latitude eruption scenario, monotonic ozone loss trends are apparent in the northern hemisphere. The tropical eruption is observed to produce enhancements in between the Hadley and Ferrel cells due to acceleration in downwelling air fractions. At high latitudes, heterogeneous chemical reactions reduce the thickness of the ozone layer. Two years after the eruption, figure 8.8, the stratospheric aerosol loading has decayed significantly. Ozone depletion trends are similar to the case in figure 8.7. Finally, four years after the eruption, aerosol background has decayed to nearly the pre-eruption background, as presented in figure 8.9. Time-averaged deviations in column ozone are declining, though the net deviation remains negative.

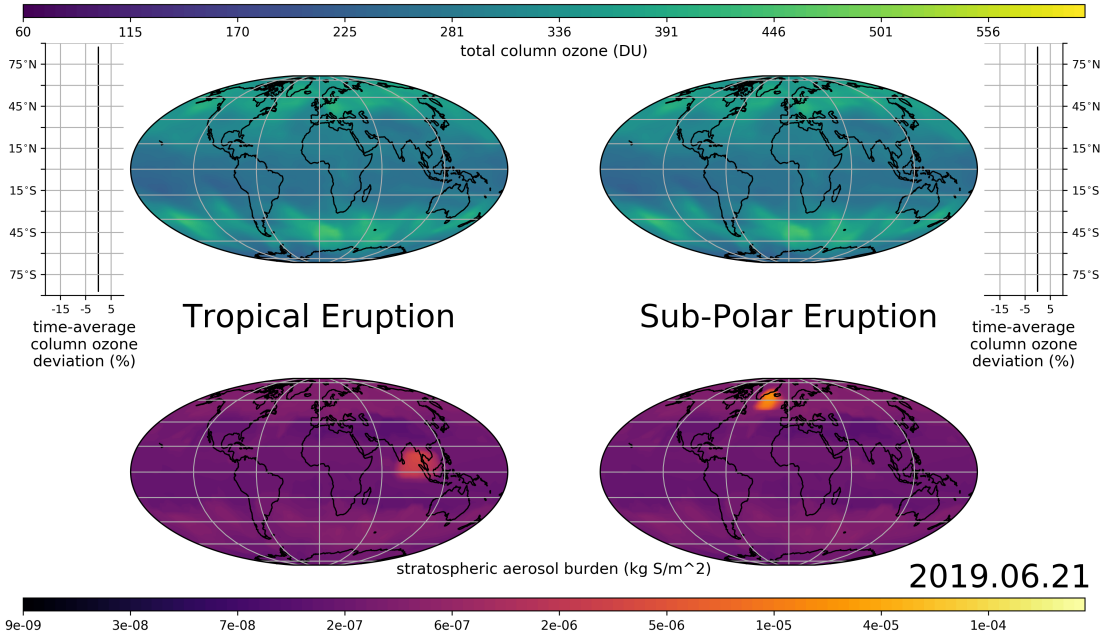

Figure 8.4: 3-dimensional model output depicting the column ozone response to a volcanic eruption of 3.5 Tg SO_2, 2 days after an eruption on June 17th, 2019 (date bottom right). Eruption latitudes: left (15°N), right (70°N). Topmost projections provide total ozone layer thickness. Bottommost projections indicate stratospheric aerosol burden. Extreme axes demonstrate running-average zonal column ozone deviations versus the non-volcanic case.

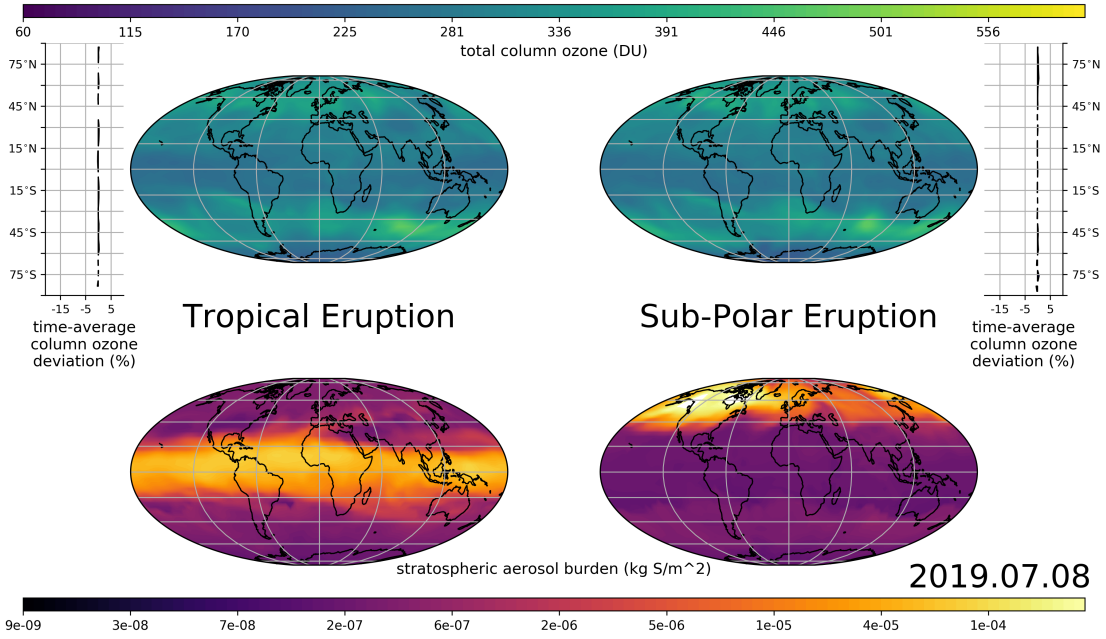

Figure 8.5: 3-dimensional model output depicting the column ozone response to a volcanic eruption of 3.5 Tg SO_2, 20 days after an eruption on June 17th, 2019 (date bottom right). Eruption latitudes: left (15°N), right (70°N). Top-most projections provide total ozone layer thickness. Bottommost projections indicate stratospheric aerosol burden. Extreme axes demonstrate running-average zonal column ozone deviations versus the non-volcanic case.

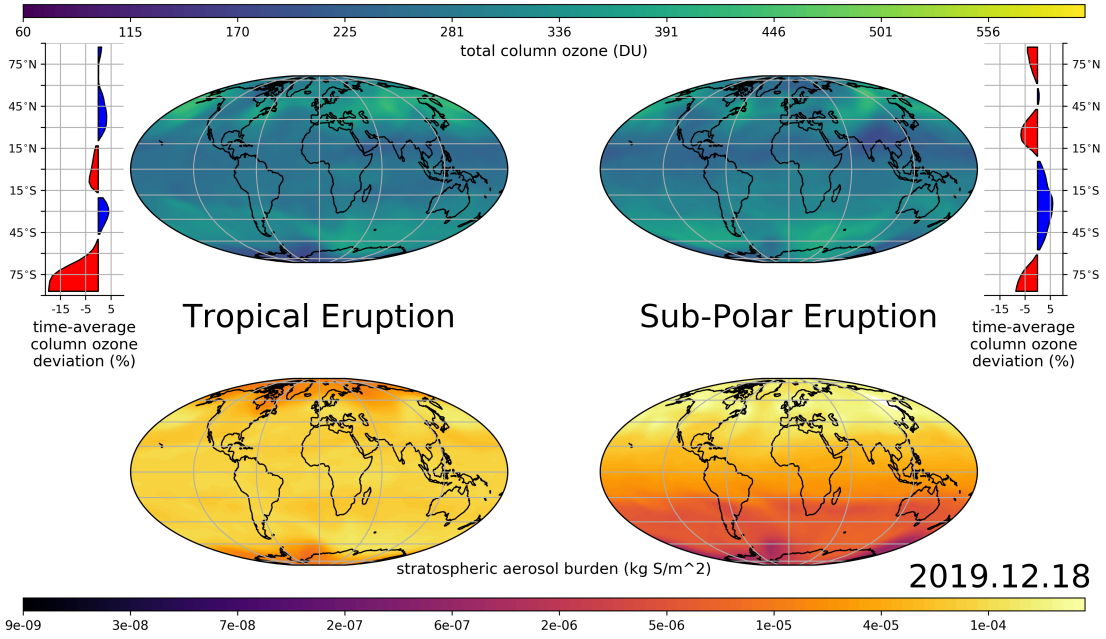

Figure 8.6: 3-dimensional model output depicting the column ozone response to a volcanic eruption of 3.5 Tg SO_2, a half year after an eruption on June 17th, 2019 (date bottom right). Eruption latitudes: left (15°N), right (70°N). Top-most projections provide total ozone layer thickness. Bottommost projections indicate stratospheric aerosol burden. Extreme axes demonstrate running-average zonal column ozone deviations versus the non-volcanic case.

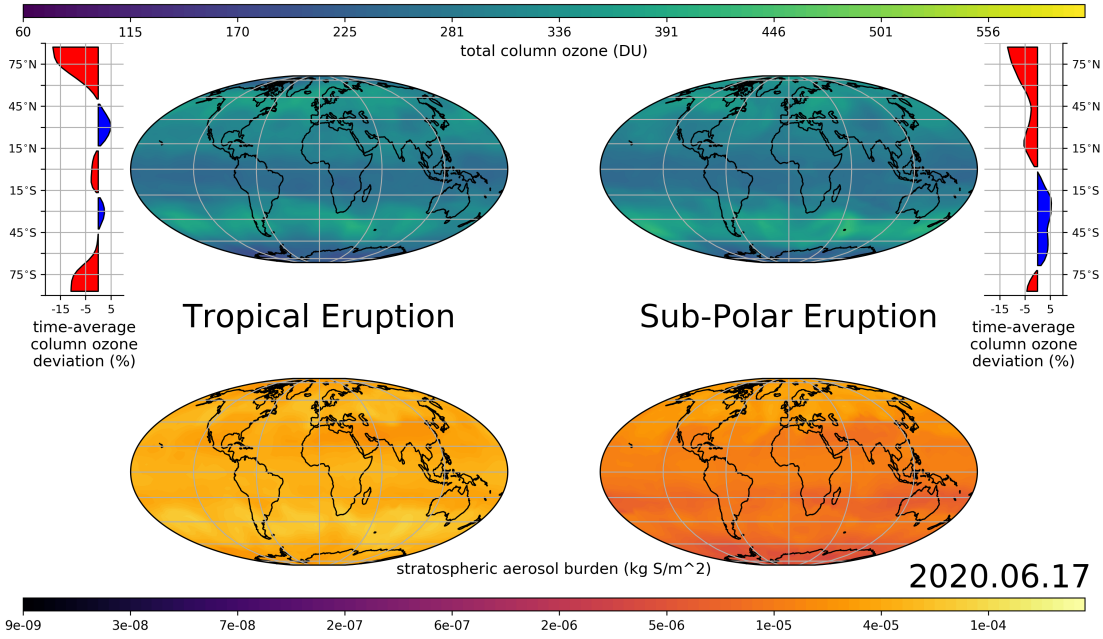

Figure 8.7: 3-dimensional model output depicting the column ozone response to a volcanic eruption of 3.5 Tg SO_2, 1 year after an eruption on June 17th, 2019 (date bottom right). Eruption latitudes: left (15°N), right (70°N). Topmost projections provide total ozone layer thickness. Bottommost projections indicate stratospheric aerosol burden. Extreme axes demonstrate running-average zonal column ozone deviations versus the non-volcanic case.

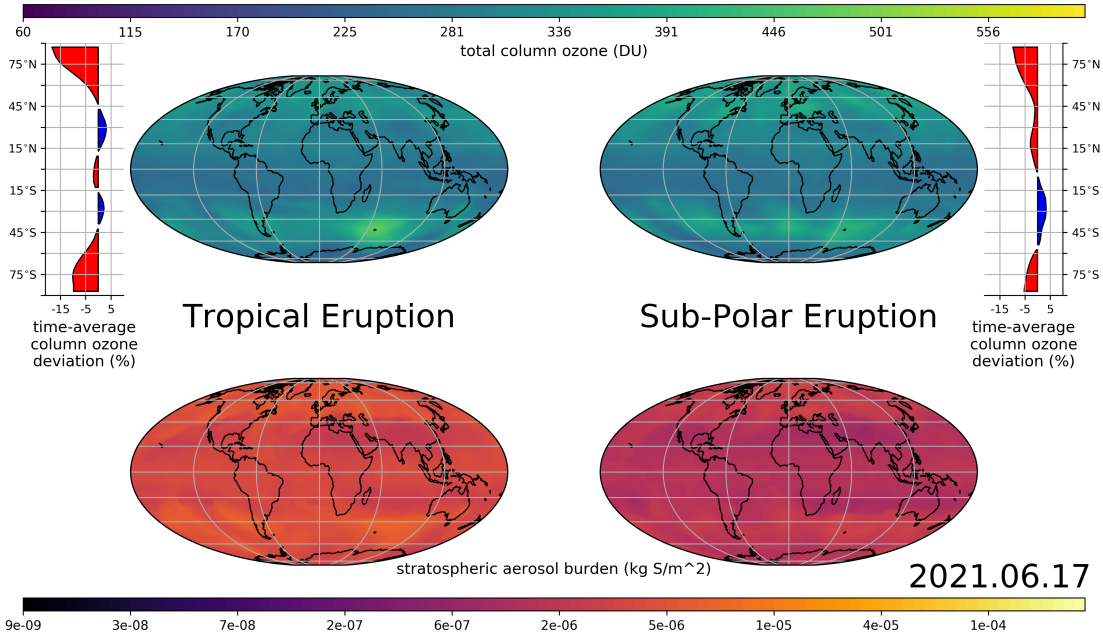

Figure 8.8: 3-dimensional model output depicting the column ozone response to a volcanic eruption of 3.5 Tg SO_2, 2 years after an eruption on June 17th, 2019 (date bottom right). Eruption latitudes: left (15°N), right (70°N). Topmost projections provide total ozone layer thickness. Bottommost projections indicate stratospheric aerosol burden. Extreme axes demonstrate running-average zonal column ozone deviations versus the non-volcanic case.

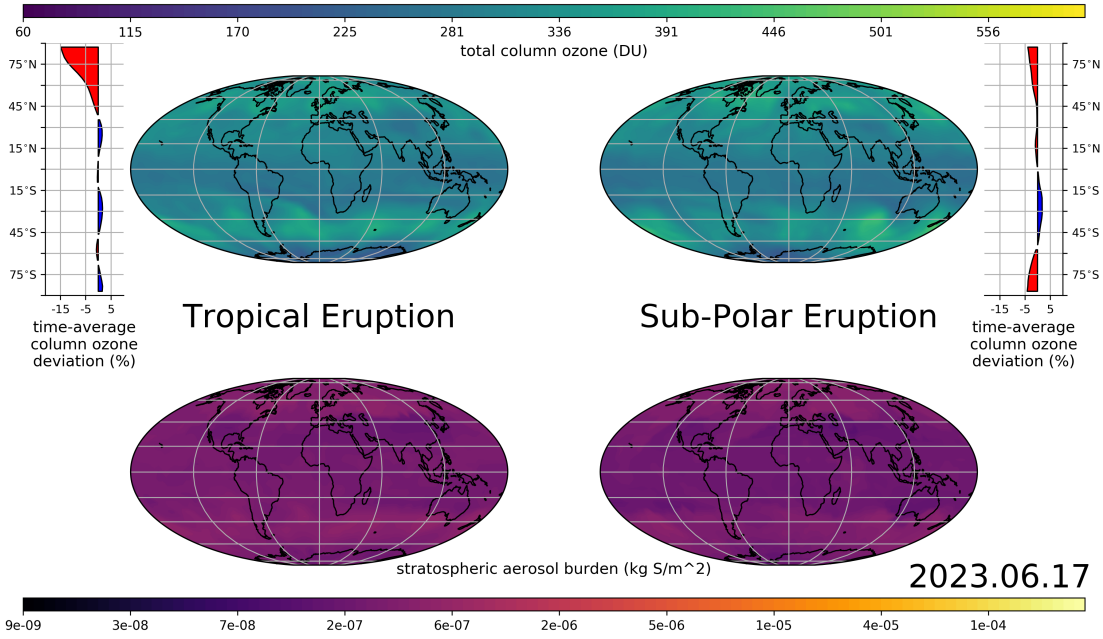

Figure 8.9: 3-dimensional model output depicting the column ozone response to a volcanic eruption of 3.5 Tg SO_2, 4 days after an eruption on June 17th, 2019 (date bottom right). Eruption latitudes: left (15°N), right (70°N). Topmost projections provide total ozone layer thickness. Bottommost projections indicate stratospheric aerosol burden. Extreme axes demonstrate running-average zonal column ozone deviations versus the non-volcanic case.

Injections of Volcanic Bromine and Iodine

In chapter 6, it was found that the ozone layer remained vulnerable following an eruption in which significant quantities of hydrogen chloride are partitioned to the stratosphere until at least the end of the century, and likely in perpetuity. To date, there has been no quantification of the additional risk to the ozone layer that would occur if volcanic bromine and iodine were to be co-injected with hydrogen chloride to the stratosphere. Iodine and bromine atoms have a large alpha factor; that is, they engage the catalytic processing of ozone much more efficiently than chlorine.[44,47,50,51,54,423,431] Numerous recent works explicitly express the need to evaluate future stratospheric ozone response to a volcanic eruption that is rich not only in chlorine, but in bromine and/or iodine.[90,98,157,177,178,182,209,432,433]

This is especially relevant given recent findings of complex halogen oxidation chemistry within the volcanic eruption column.[207] The partitioning of bromine and iodine to oxidized forms is very likely to impact the stratospheric injection efficiency of these species. Chlorine chemistry within the eruption column is largely suppressed and most chlorine remains bound as HCl with observations of reactive chlorine oxides in plumes being sparse.[69,180,196–198] Conversely, volcanic emissions of bromine are frequently observed as bromine monoxide resultant from autocatalytic bromine explosion chemistry analogous to polar tropospheric bromine processing.[69,180–182,190,194–205]

In 2017, a highly important finding was reported: Volcanic IO had been observed in a volcanic eruption column for the first time.[182] The observed IO was present within the 2008 Kasatochi (52°N) plume in 3 pptv (10 Mg) quantities, as detected in measurements made by both SCHIAMACHY and GOME-2. Within the same eruption column, BrO was quantified to be an order

of magnitude more prevalent (100 Mg) than IO.[181,182] The majority of this BrO and IO are believed to have partitioned to the lower stratosphere. An interdiction of the aged 2008 Kasatochi volcanic cloud during the CONCERT campaign indicated a 20% enhancement in local stratospheric HCl,[208] and an extrapolation of Aura MLS HCl:SO2 ratios in the UTLS indicates a total additional stratospheric burden of about 10,000 Mg HCl from the eruption.[179] This relative halogen loading for stratospheric I: Br: Cl of 1: 16: 3611 matches well with expected volcanic halogen emission ratios, although it should be noted that uncertainties arising from differences in magma composition, degassing environment, and temporal evolution of the eruption in addition to meteorological perturbation of the stratospheric injection efficiency may significantly alter these values following a future eruption.[96]

Bromine and chlorine emission budgets for dozens of large Central American Volcanic Arc (CAVA) eruptions spanning the past 70 ka establish that tremendous quantities of halogens are periodically released to the atmosphere, averaging 130 Gg Br and 56,000 Gg. Cl.[177,178] Though iodine quantities were not reported, extrapolation using the halogen ratio estimated above for the eruption of Kasatochi provides an estimate of a CAVA emission of 8 Gg I on average.[182] If 10% of the above quantities were to penetrate the tropopause, the enhancement in EESC would be 6326 pptv (α_{Br} = 60, α_{I} = 150).

A preliminary exploration of the additional effect on ozone of co-injected sulfur dioxide (7 Tg), chlorine (1 Tg), and bromine (2 Gg) is presented in figure 8.10and indicates that these scenarios need to be explored further. Figure 6.22(a) demonstrates the enhancement in the processing of ozone by halogen reaction families and odd nitrogen in the summertime midlatitudes one year following a

tropical Pinatubo-like eruption of 7 Tg SO2 in the year 2100 within the RCP 2.6 scenario. Chlorine-only reactions are colored green, odd-nitrogen reactions are colored blue, and bromine-only and interhalogen reactions are colored red. For each case, the dotted line represents the baseline non-volcanic ozone loss rate and the solid line depicts the ozone loss rate after the volcanic perturbation. As described in the preceding chapters, the elevated aerosol loading results in the enhanced activation of inorganic halogen reservoirs, mainly increasing the rate of ClOx and interhalogen reaction cycles. Additionally, the rate of NOx processing of ozone is suppressed via reactive hydrolysis/uptake on aerosol surfaces, resulting in a net increase in ozone in the middle stratosphere. When comparatively small quantities (relative to the CAVA estimates) of bromine and chlorine are also injected into the stratosphere, as in figure 6.22(b), ozone loss rates increase tremendously at all pressure levels within the volcanic cloud. Figure 6.22(c) illustrates the additive effect each additional perturbation has on the vertical profile of ozone number density. Note that suppression of NOx processing in the future Pinatubo-like eruption (SO2 injection only) results in a positive ozone anomaly in the middle stratosphere. For The enhancement in ozone loss attributable volcanic Brx, as opposed to volcanic Clx, is displayed in figure 6.22(d). This enhancement is outsized relative to the quantity of bromine injected (injection mole ratio of 1130:1 Cl:Br with expected EESC ratio of 19:1 Cl:Br), indicating that quantities of bromine directly injected to the lower and middle stratosphere may engage ozone loss catalysis with higher sensitivity than the globally-averaged alpha factor of 60 belies.

The ozone loss numbers shown in figure 8.10 are large but consistent with prior calculations and estimates of extreme reductions in column ozone from historic, large volcanic eruptions that injected HCl into the stratosphere in preindustrial atmospheres.[90,98,177,178,187] These modeled re-

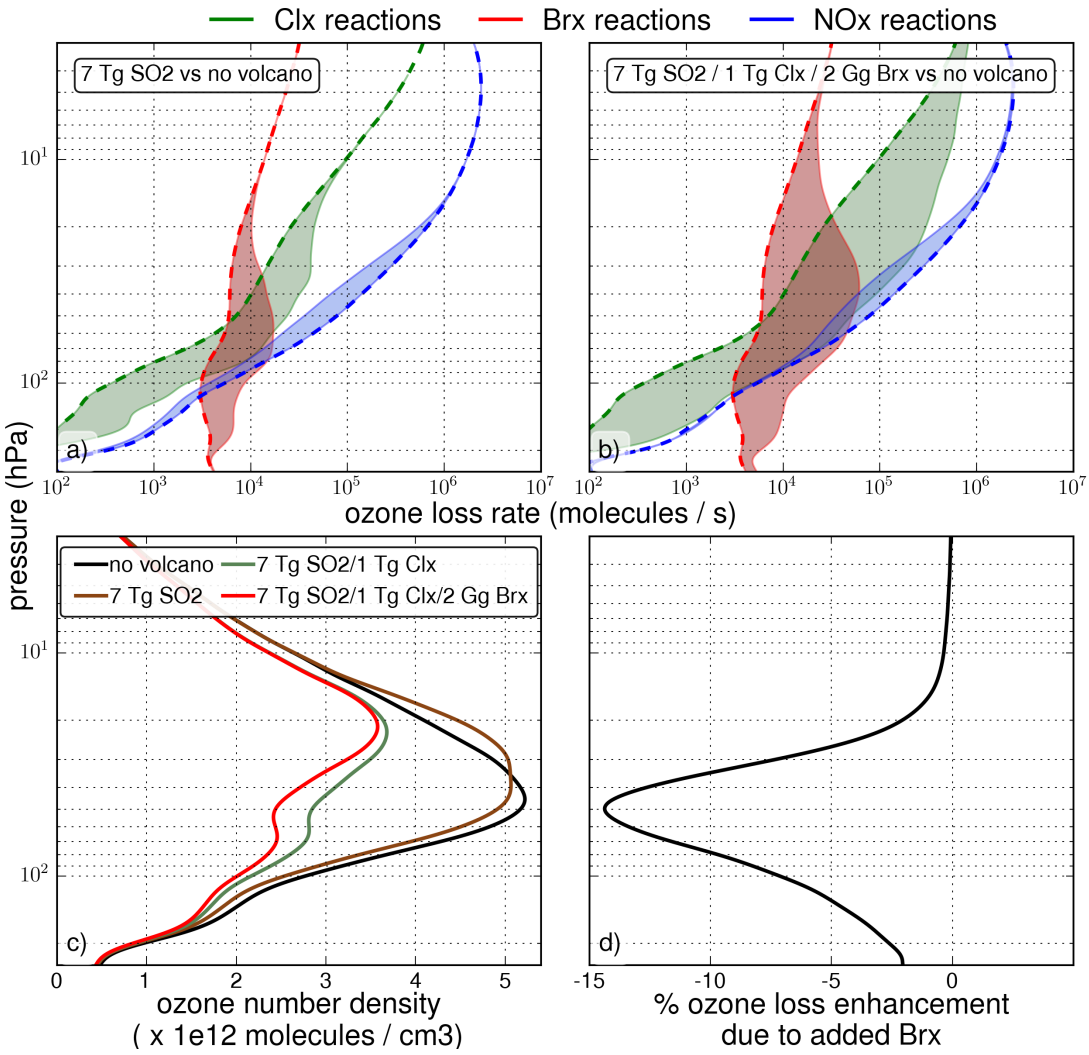

Figure 8.10: (a,b) Northern midlatitude vertical profiles of chemical family loss processing rates for eruptions occuring in the year 2018 within the RCP 6.0 greenhouse gas emissions trajectory storyline one year after eruption. Dashed lines indicate the processing rate for each respective chemical family in the non-volcanic scenario. Shaded regions indicate the change experienced by each chemical family following the indicated volcanic perturbation. Pinatubo-like eruptions (a) demonstrate minor enhancements in halogen processing rates, especially in the lower stratosphere. Halogen-rich eruptions, including bromine, (b) are demonstrated to rapidly accelerate halogen processing rates and the domain in which halogen processing occurs. (c) Ozone number density corresponding to the indicated volcanic perturbations at the same latitude and date as (a,b). (d) % of ozone loss due to addition of bromine to eruption column.

sults will vary significantly with size of the volcanic eruption, chemical composition of the eruption column, year of eruption, modeled RCP/SSP scenario, and a variety of other factors specific to geography, geology, and meteorology. It is evident from figure 8.10 that even the small 54 pptv global enhancement in EESC from this 2 Gg bromine injection ($\alpha_{\mathrm{Br}} = 60$) may result in significant ozone reduction relative to the chlorine injection scenario alone as a result of enhanced interhalogen reaction rates. Additionally, one must note that iodine family reactions ($\alpha_{\mathrm{I}} = 150$ - 300) have not been included in this precursory survey and are expected to provide further ozone losses when injected to the stratosphere in realistic quantities.

The implications of volcanic halogen injection are compelling: there exists the possibility that eruptions much smaller than the 1991 eruption of Mount Pinatubo may significantly reduce the ozone layer's thickness, even after anthropogenic halogen species have decayed to preindustrial levels. Clearly, there exists room for more exploration of this parameter space. Especially interesting would be the implementation of a crater-rim–to–stratosphere model of reactive volcanic halogen chemistry with microphysics coupled to a chemistry and climate model. It is very likely that very trace halogen species partition more efficiently than chlorine to the stratosphere and that the role of volcanic halogens in stratospheric ozone processing is greater than currently believed.

Implications for Other (Non-Volcanic) Stratospheric Perturbations

The work described in this thesis quantifies a coupling between the ozone layer and the changing climate in the context of a gross perturbation of the stratosphere. Though large, explosive volcan-

ism was the topic, the implication of a dynamic ozone layer response as the climate evolves can be applied to many of the stratospheric perturbations discussed in chapter 7. For example: the space launch market is expected to grow by orders of magnitude throughout the 21st century – though ozone layer response to such an enhancement in space access has been quantified for the present-day stratosphere, how might the response change as the climate evolves? Despite the fact that the stability of the ozone layer is expected to change significantly with the climate, remarkably few studies have explored how a future stratospheric ozone layer might respond to direct external forcing.

This may seem immaterial on first glance, but the extraordinary dynamic range of ozone response exhibited by Pinatubo-like volcanic eruptions as a function of year, as plotted in figure 5.16 – bridging net production of ozone in the past, net depletion in the present, and an uncertain result dependent on the exact climate emissions pathway realized in the far future – demonstrates how sensitive the stratospheric ozone layer is to seemingly small variations in its chemical and physical environment. This result emerged as a surprise – it was expected that all 22nd century scenarios would lead to a thickening of the ozone layer when the experiment was designed – and, given the complicated and interconnected nature of the stratospheric chemical cycles dictating the ozone steady state, it seems probable that similar surprises might emerge when considering perturbations other than volcanism in future climate change situations.

Hazard response is limited by the capability of the responder to describe the nature of the hazard. For this reason, it is imperative that further investigation of potentially significant pertubations of the stratosphere include a sensitivity analysis of the ozone layer to the effects of the same perturbation in a changing climate. Surprises will undoubtedly manifest; in some cases the effect of the

external forcing will be attenuated, but in others, amplification may belie what intuition implied.

References

[1] R Hossaini, MP Chipperfield, S Dhomse, C Ordonez, A Saiz-Lopez, NL Abraham, A Archibald, P Braesicke, P Telford, N Warwick, et al. Modelling future changes to the stratospheric source gas injection of biogenic bromocarbons. *Geophysical Research Letters*, 39(20), 2012.

[2] EC Leedham, C Hughes, FSL Keng, S-M Phang, G Malin, and WT Sturges. Emission of atmospherically significant halocarbons by naturally occurring and farmed tropical macroalgae. *Biogeosciences*, 10(6):3615–3633, 2013.

[3] Helmke Hepach, Birgit Quack, Franziska Ziska, Steffen Fuhlbruegge, EL Atlas, K Krüger, Ilka Peeken, and Douglas WR Wallace. Drivers of diel and regional variations of halocarbon emissions from the tropical north east atlantic. *Atmospheric Chemistry and Physics*, 14(3): 1255, 2014.

[4] R Hossaini, MP Chipperfield, SA Montzka, A Rap, S Dhomse, and W Feng. Efficiency of short-lived halogens at influencing climate through depletion of stratospheric ozone. *Nature Geoscience*, 8(3):186–190, 2015.

[5] Daniel B Kirk-Davidoff, Eric J Hintsa, James G Anderson, and David W Keith. The effect of climate change on ozone depletion through changes in stratospheric water vapour. *Nature*, 402(6760):399–401, 1999.

[6] AE Dessler, MR Schoeberl, T Wang, SM Davis, and KH Rosenlof. Stratospheric water vapor feedback. *Proceedings of the National Academy of Sciences*, 110(45):18087–18091, 2013.

[7] James G Anderson, David M Wilmouth, Jessica B Smith, and David S Sayres. Uv dosage levels in summer: Increased risk of ozone loss from convectively injected water vapor. *Science*, page 1222978, 2012.

[8] James G Anderson, Debra K Weisenstein, Kenneth P Bowman, Cameron R Homeyer, Jessica B Smith, David M Wilmouth, David S Sayres, J Eric Klobas, Stephen S Leroy, John A Dykema, and Steven C. Wofsy. Stratospheric ozone over the united states in summer linked

to observations of convection and temperature via chlorine and bromine catalysis. *Proceedings of the National Academy of Sciences*, page 201619318, 2017.

[9] Dian J Seidel, Qiang Fu, William J Randel, and Thomas J Reichler. Widening of the tropical belt in a changing climate. *Nature geoscience*, 1(1):21–24, 2008.

[10] Daniela Kracher, Christian H Reick, Elisa Manzini, Martin G Schultz, and Olaf Stein. Climate change reduces warming potential of nitrous oxide by an enhanced brewer-dobson circulation. *Geophysical Research Letters*, 43(11):5851–5859, 2016.

[11] Joseph R McConnell, Andrea Burke, Nelia W Dunbar, Peter Köhler, Jennie L Thomas, Monica M Arienzo, Nathan J Chellman, Olivia J Maselli, Michael Sigl, Jess F Adkins, et al. Synchronous volcanic eruptions and abrupt climate change 17.7 ka plausibly linked by stratospheric ozone depletion. *Proceedings of the National Academy of Sciences*, page 201705595, 2017.

[12] F Li, RS Stolarski, and PA Newman. Stratospheric ozone in the post-cfc era. *Atmospheric Chemistry and Physics*, 9(6):2207–2213, 2009.

[13] DW Waugh, L Oman, SR Kawa, RS Stolarski, S Pawson, AR Douglass, PA Newman, and JE Nielsen. Impacts of climate change on stratospheric ozone recovery. *Geophysical Research Letters*, 36(3), 2009.

[14] Daniel J Lunt, Tom Dunkley Jones, Malte Heinemann, Matthew Huber, Allegra LeGrande, Arne Winguth, Claire Loptson, Jochem Marotzke, CD Roberts, J Tindall, et al. A model–data comparison for a multi-model ensemble of early eocene atmosphere–ocean simulations: Eomip. *Climate of the Past*, 8:1717–1736, 2012.

[15] Eric J Barron. Eocene equator-to-pole surface ocean temperatures: A significant climate problem? *Paleoceanography*, 2(6):729–739, 1987.

[16] L Cirbus Sloan and DK Rea. Atmospheric carbon dioxide and early eocene climate: A general circulation modeling sensitivity study. *Palaeogeography, Palaeoclimatology, Palaeoecology*, 119(3-4):275–292, 1996.

[17] Max Popp, Hauke Schmidt, and Jochem Marotzke. Transition to a moist greenhouse with co 2 and solar forcing. *Nature communications*, 7:10627, 2016.

[18] A Serdyuchenko, V Gorshelev, M Weber, W Chehade, and JP Burrows. High spectral resolution ozone absorption cross-sections. *Atmospheric Measurement Techniques*, 7(2):625, 2014.

[19] James F Kasting and David Catling. Evolution of a habitable planet. *Annual Review of Astronomy and Astrophysics*, 41(1):429–463, 2003.

[20] Antígona Segura, Kara Krelove, James F Kasting, Darrell Sommerlatt, Victoria Meadows, David Crisp, Martin Cohen, and Eli Mlawer. Ozone concentrations and ultraviolet fluxes on earth-like planets around other stars. *Astrobiology*, 3(4):689–708, 2003.

[21] Gerd P Pfeifer and Ahmad Besaratinia. Uv wavelength-dependent dna damage and human non-melanoma and melanoma skin cancer. *Photochemical & photobiological sciences*, 11(1): 90–97, 2012.

[22] FR De Gruijl and JC Van der Leun. Estimate of the wavelength dependency of ultraviolet carcinogenesis in humans and its relevance to the risk assessment of a stratospheric ozone depletion. *Health physics*, 67(4):319–325, 1994.

[23] Deevya L Narayanan, Rao N Saladi, and Joshua L Fox. Ultraviolet radiation and skin cancer. *International journal of dermatology*, 49(9):978–986, 2010.

[24] National Research Council (US). Climatic Impact Committee. *Environmental impact of stratospheric flight: Biological and climatic effects of aircraft emissions in the stratosphere*. National Academies, 1975.

[25] Martin Ross, Darin Toohey, Manfred Peinemann, and Patrick Ross. Limits on the space launch market related to stratospheric ozone depletion. *Astropolitics*, 7(1):50–82, 2009.

[26] E Pierazzo, RR Garcia, DE Kinnison, DR Marsh, Julia Lee-Taylor, and PJ Crutzen. Ozone perturbation from medium-size asteroid impacts in the ocean. *Earth and Planetary Science Letters*, 299(3-4):263–272, 2010.

[27] XueXi Tie and Guy Brasseur. The response of stratospheric ozone to volcanic eruptions: Sensitivity to atmospheric chlorine loading. *Geophysical research letters*, 22(22):3035–3038, 1995.

[28] Joan E Rosenfield. Effects of volcanic eruptions on stratospheric ozone recovery. *Volcanism and the Earth's Atmosphere*, pages 227–236, 2003.

[29] World Meteorological Organization (WMO). *Scientific Assessment of Ozone Depletion: 2014, World Meteorological Organization, Global Ozone Research and Monitoring Project - Report No. 55*. WMO, Geneva, 2014.

[30] William T Hyde and Thomas J Crowley. Probability of future climatically significant volcanic eruptions. *Journal of climate*, 13(9):1445–1450, 2000.

[31] John Austin and R John Wilson. Ensemble simulations of the decline and recovery of stratospheric ozone. *Journal of Geophysical Research: Atmospheres*, 111(D16), 2006.

[32] AR Ravishankara, S Solomon, AA Turnipseed, and RF Warren. Atmospheric lifetimes of long-lived halogenated species. *SCIENCE-NEW YORK THEN WASHINGTON-*, 259: 194–194, 1993.

[33] Eric A Ray, Fred L Moore, James W Elkins, Karen H Rosenlof, Johannes C Laube, Thomas Röckmann, Daniel R Marsh, and Arlyn E Andrews. Quantification of the sf6 lifetime based on mesospheric loss measured in the stratospheric polar vortex. *Journal of Geophysical Research: Atmospheres*, 122(8):4626–4638, 2017.

[34] Richard Peer Wayne, I Barnes, P Biggs, JP Burrows, CE Canosa-Mas, J Hjorth, G Le Bras, GK Moortgat, D Perner, G Poulet, et al. The nitrate radical: Physics, chemistry, and the atmosphere. *Atmospheric Environment. Part A. General Topics*, 25(1):1–203, 1991.

[35] M Rigby, RG Prinn, S O'Doherty, SA Montzka, A McCulloch, CM Harth, J Mühle, PK Salameh, RF Weiss, D Young, et al. Re-evaluation of the lifetimes of the major cfcs and ch 3 ccl 3 using atmospheric trends. *Atmospheric Chemistry and Physics*, 13(5):2691–2702, 2013.

[36] SG Love and DE Brownlee. A direct measurement of the terrestrial mass accretion rate of cosmic dust. *SCIENCE-NEW YORK THEN WASHINGTON-*, 262:550–550, 1993.

[37] K Mohanakumar. *Stratosphere troposphere interactions: an introduction*. Springer Science & Business Media, 2008.

[38] Neal Butchart. The brewer-dobson circulation. *Reviews of geophysics*, 52(2):157–184, 2014.

[39] KK Tung and H Yang. Global qbo in circulation and ozone. part i: Reexamination of observational evidence. *Journal of the Atmospheric Sciences*, 51(19):2699–2707, 1994.

[40] Martyn M Caldwell, Lars Olof Björn, Janet F Bornman, Stephan D Flint, G Kulandaivelu, Alan H Teramura, and Manfred Tevini. Effects of increased solar ultraviolet radiation on terrestrial ecosystems. *Journal of Photochemistry and Photobiology B: Biology*, 46(1):40–52, 1998.

[41] M Norval, AP Cullen, FR De Gruijl, J Longstreth, Y Takizawa, RM Lucas, FP Noonan, and JC Van der Leun. The effects on human health from stratospheric ozone depletion and its interactions with climate change. *Photochemical & Photobiological Sciences*, 6(3):232–251, 2007.

[42] AL Andrady, A Torikai, HH Redhwi, KK Pandey, and Peter Gies. Consequences of stratospheric ozone depletion and climate change on the use of materials. *Photochemical & Photobiological Sciences*, 14(1):170–184, 2015.

[43] Vladimir L Orkin, James B Burkholder, SP Sander, JPD Abbatt D Abbatt, JR Barker, Robert E Huie, C E Kolb, Michael J Kurylo III, David M Wilmouth, and PH Wine. Chemical kinetics and photochemical data for use in atmospheric studies, evaluation no. 18. *JPL Publication 15-10*, 2015.

[44] Susan Solomon, Rolando R Garcia, and AR Ravishankara. On the role of iodine in ozone depletion. *Journal of Geophysical Research: Atmospheres*, 99(D10):20491–20499, 1994.

[45] Susan Solomon, Rolando R Garcia, F Sherwood Rowland, and Donald J Wuebbles. On the depletion of antarctic ozone. *Nature*, 321(6072):755–758, 1986.

[46] Guy P Brasseur, Claire Granier, and Stacy Walters. Future changes in stratospheric ozone and the role of heterogeneous chemistry. *Nature*, 348(6302):626–628, 1990.

[47] Steven C Wofsy, Michael B McElroy, and Yuk Ling Yung. The chemistry of atmospheric bromine. *Geophysical Research Letters*, 2(6):215–218, 1975.

[48] John S Daniel, Susan Solomon, and Daniel L Albritton. On the evaluation of halocarbon radiative forcing and global warming potentials. *Journal of Geophysical Research: Atmospheres*, 100(D1):1271–1285, 1995.

[49] PA Newman, JS Daniel, DW Waugh, and ER Nash. A new formulation of equivalent effective stratospheric chlorine (eesc). *Atmospheric Chemistry and Physics*, 7(17):4537–4552, 2007.

[50] S Solomon, M Mills, LE Heidt, WH Pollock, and AF Tuck. On the evaluation of ozone depletion potentials. *Journal of Geophysical Research: Atmospheres*, 97(D1):825–842, 1992.

[51] Michael Y Danilin, Nien-Dak Sze, Malcolm KW Ko, Jose M Rodriguez, and Michael J Prather. Bromine-chlorine coupling in the antarctic ozone hole. *Geophysical research letters*, 23(2):153–156, 1996.

[52] LJ Carpenter, S Reimann, JB Burkholder, C Clerbaux, BD Hall, R Hossaini, JC Laube, and S Yvon-Lewis. Scientific assessment of ozone depletion: 2014, global ozone research and monitoring project–report no. 55. *World Meteorological Organization*, pages 1–1, 2014.

[53] Susan Solomon, James B Burkholder, AR Ravishankara, and Rolando R Garcia. Ozone depletion and global warming potentials of cf3i. *Journal of Geophysical Research: Atmospheres*, 99(D10):20929–20935, 1994.

[54] Malcolm KW Ko, Nien Dak Sze, Courtney Scott, José M Rodríguez, Debra K Weisenstein, and Stanley P Sander. Ozone depletion potential of ch3br. *Journal of Geophysical Research: Atmospheres*, 103(D21):28187–28195, 1998.

[55] Christian E Junge, Charles W Chagnon, and James E Manson. Stratospheric aerosols. *Journal of Meteorology*, 18(1):81–108, 1961.

[56] James M Rosen, David J Hofmann, and Jean Laby. Stratospheric aerosol measurements ii: The worldwide distribution. *Journal of the Atmospheric Sciences*, 32(7):1457–1462, 1975.

[57] DJ Hofmann and JM Rosen. Antarctic observations of stratospheric aerosol and high altitude condensation nuclei following the el chichon eruption. *Geophysical Research Letters*, 12 (1):13–16, 1985.

[58] Patrick Hamill, Eric J Jensen, PB Russell, and Jill J Bauman. The life cycle of stratospheric aerosol particles. *Bulletin of the American Meteorological Society*, 78(7):1395–1410, 1997.

[59] Stefanie Kremser, Larry W Thomason, Marc Hobe, Markus Hermann, Terry Deshler, Claudia Timmreck, Matthew Toohey, Andrea Stenke, Joshua P Schwarz, Ralf Weigel, et al. Stratospheric aerosol—observations, processes, and impact on climate. *Reviews of Geophysics*, 54(2): 278–335, 2016.

[60] Larry W Thomason, Sharon P Burton, B-P Luo, and Thomas Peter. Sage ii measurements of stratospheric aerosol properties at non-volcanic levels. *Atmospheric Chemistry and Physics*, 8 (4):983–995, 2008.

[61] Paul J Crutzen and Frank Arnold. Nitric acid cloud formation in the cold antarctic stratosphere: a major cause for the springtime 'ozone hole'. *Nature*, 324(6098):651–655, 1986.

[62] Owen B Toon, Patrick Hamill, Richard P Turco, and Joseph Pinto. Condensation of hno3 and hcl in the winter polar stratospheres. *Geophysical Research Letters*, 13(12):1284–1287, 1986.

[63] Mark A Zondlo, Paula K Hudson, Anthony J Prenni, and Margaret A Tolbert. Chemistry and microphysics of polar stratospheric clouds and cirrus clouds. *Annual review of physical chemistry*, 51(1):473–499, 2000.

[64] Owen B Toon, EV Browell, S Kinne, and J Jordan. An analysis of lidar observations of polar stratospheric clouds. *Geophysical Research Letters*, 17(4):393–396, 1990.

[65] EV Browell, CF Butler, S Ismail, PA Robinette, AF Carter, NS Higdon, OB Toon, MR Schoeberl, and AF Tuck. Airborne lidar observations in the wintertime arctic stratosphere: Polar stratospheric clouds. *Geophysical Research Letters*, 17(4):385–388, 1990.

[66] B Stein, C Wedekind, H Wille, Franz Immler, Marion Müller, L Wöste, M Del Guasta, M Morandi, L Stefanutti, A Antonelli, et al. Optical classification, existence temperatures, and coexistence of different polar stratospheric cloud types. *Journal of Geophysical Research: Atmospheres*, 104(D19):23983–23993, 1999.

[67] Claire S Witham, Clive Oppenheimer, and Claire J Horwell. Volcanic ash-leachates: a review and recommendations for sampling methods. *Journal of volcanology and Geothermal Research*, 141(3):299–326, 2005.

[68] U Niemeier, C Timmreck, H-F Graf, S Kinne, S Rast, and S Self. Initial fate of fine ash and sulfur from large volcanic eruptions. *Atmospheric Chemistry and Physics*, 9(22):9043–9057, 2009.

[69] Nicole Bobrowski, R Von Glasow, A Aiuppa, S Inguaggiato, I Louban, OW Ibrahim, and U Platt. Reactive halogen chemistry in volcanic plumes. *Journal of Geophysical Research: Atmospheres*, 112(D6), 2007.

[70] Xochilt Gutiérrez, Federica Schiavi, and Hans Keppler. The adsorption of hcl on volcanic ash. *Earth and Planetary Science Letters*, 438:66–74, 2016.

[71] Song Guo, William I Rose, Gregg JS Bluth, and I Matthew Watson. Particles in the great pinatubo volcanic cloud of june 1991: The role of ice. *Geochemistry, Geophysics, Geosystems*, 5(5), 2004.

[72] KD Froyd, DM Murphy, TJ Sanford, DS Thomson, JC Wilson, Leonhard Pfister, and L Lait. Aerosol composition of the tropical upper troposphere. *Atmospheric Chemistry and Physics*, 9(13):4363–4385, 2009.

[73] Paula K Hudson, Daniel M Murphy, Daniel J Cziczo, David S Thomson, Joost A De Gouw, Carsten Warneke, John Holloway, Hans-Jürg Jost, and Gerd Hübler. Biomass-burning particle measurements: Characteristic composition and chemical processing. *Journal of Geophysical Research: Atmospheres*, 109(D23), 2004.

[74] J Hendricks, B Kärcher, A Döpelheuer, Johann Feichter, Ulrike Lohmann, and D Baumgardner. Simulating the global atmospheric black carbon cycle: a revisit to the contribution of aircraft emissions. *Atmospheric Chemistry and Physics*, 4(11/12):2521–2541, 2004.

[75] John MC Plane. Cosmic dust in the earth's atmosphere. *Chemical Society Reviews*, 41(19): 6507–6518, 2012.

[76] JD Carrillo-Sánchez, D Nesvornỳ, P Pokornỳ, D Janches, and JMC Plane. Sources of cosmic dust in the earth's atmosphere. *Geophysical Research Letters*, 43(23), 2016.

[77] JD Carrillo-Sánchez, JMC Plane, W Feng, D Nesvornỳ, and D Janches. On the size and velocity distribution of cosmic dust particles entering the atmosphere. *Geophysical research letters*, 42(15):6518–6525, 2015.

[78] John MC Plane, Wuhu Feng, and Erin CM Dawkins. The mesosphere and metals: Chemistry and changes. *Chemical reviews*, 115(10):4497–4541, 2015.

[79] Yu M Gorbanev, IA Stogneeva, VA Shestopalov, EF Knyazkova, II Kimakovskaya, SR Kimakovsky, and AV Golubaev. The effect of major meteor streams on the total ozone in the earth's atmosphere. 2017.

[80] DJ Cziczo, DS Thomson, and DM Murphy. Ablation, flux, and atmospheric implications of meteors inferred from stratospheric aerosol. *Science*, 291(5509):1772–1775, 2001.

[81] J Eric Klobas, Martin Schmid, Cynthia M Friend, and Robert J Madix. The dissociation-induced displacement of chemisorbed o 2 by mobile o atoms and the autocatalytic recombination of o due to chain fragmentation on ag (110). *Surface Science*, 630:187–194, 2014.

[82] Matthew M Montemore, Ekin D Cubuk, J Eric Klobas, Martin Schmid, Robert J Madix, Cynthia M Friend, and Efthimios Kaxiras. Controlling o coverage and stability by alloying au and ag. *Physical Chemistry Chemical Physics*, 18(38):26844–26853, 2016.

[83] DR Hanson. Reactivity of brono2 and hobr on sulfuric acid solutions at low temperatures. *Journal of Geophysical Research: Atmospheres*, 108(D8), 2003.

[84] Nicholas S Holmes, Jonathan W Adams, and John N Crowley. Uptake and reaction of hoi and iono 2 on frozen and dry nacl/nabr surfaces and h 2 so 4. *Physical Chemistry Chemical Physics*, 3(9):1679–1687, 2001.

[85] Lee Siebert, Tom Simkin, and Paul Kimberly. *Volcanoes of the World*. Univ of California Press, 2011.

[86] Christoph Helo, Marc-Antoine Longpré, Nobumichi Shimizu, David A Clague, and John Stix. Explosive eruptions at mid-ocean ridges driven by co2-rich magmas. *Nature Geoscience*, 4(4):260–263, 2011.

[87] Clive Oppenheimer. Climatic, environmental and human consequences of the largest known historic eruption: Tambora volcano (indonesia) 1815. *Progress in physical geography*, 27(2): 230–259, 2003.

[88] Franck Lavigne, Jean-Philippe Degeai, Jean-Christophe Komorowski, Sébastien Guillet, Vincent Robert, Pierre Lahitte, Clive Oppenheimer, Markus Stoffel, Céline M Vidal, Indyo Pratomo, et al. Source of the great ad 1257 mystery eruption unveiled, samalas volcano, rinjani volcanic complex, indonesia. *Proceedings of the National Academy of Sciences*, 110(42): 16742–16747, 2013.

[89] Céline M Vidal, Jean-Christophe Komorowski, Nicole Métrich, Indyo Pratomo, Nugraha Kartadinata, Oktory Prambada, Agnès Michel, Guillaume Carazzo, Franck Lavigne, Jessica Rodysill, et al. Dynamics of the major plinian eruption of samalas in 1257 ad (lombok, indonesia). *Bulletin of Volcanology*, 77(9):73, 2015.

[90] Céline M Vidal, Nicole Métrich, Jean-Christophe Komorowski, Indyo Pratomo, Agnès Michel, Nugraha Kartadinata, Vincent Robert, and Franck Lavigne. The 1257 samalas eruption (lombok, indonesia): the single greatest stratospheric gas release of the common era. *Scientific reports*, 6:34868, 2016.

[91] Michael R Rampino and Stephen Self. Historic eruptions of tambora (1815), krakatau (1883), and agung (1963), their stratospheric aerosols, and climatic impact. *Quaternary Research*, 18 (2):127–143, 1982.

[92] Stephen Self and Alan J King. Petrology and sulfur and chlorine emissions of the 1963 eruption of gunung agung, bali, indonesia. *Bulletin of Volcanology*, 58(4):263–285, 1996.

[93] Christopher G Newhall and Stephen Self. The volcanic explosivity index (vei) an estimate of explosive magnitude for historical volcanism. *Journal of Geophysical Research: Oceans*, 87 (C2):1231–1238, 1982.

[94] David M Pyle. Sizes of volcanic eruptions. In *The Encyclopedia of Volcanoes (Second Edition)*, pages 257–264. Elsevier, 2015.

[95] Clive Oppenheimer. *Eruptions that shook the world*. Cambridge University Press, 2011.

[96] Alessandro Aiuppa, DR Baker, and JD Webster. Halogens in volcanic systems. *Chemical Geology*, 263(1):1–18, 2009.

[97] Paul J Wallace and Marie Edmonds. The sulfur budget in magmas: evidence from melt inclusions, submarine glasses, and volcanic gas emissions. *Reviews in Mineralogy and Geochemistry*, 73(1):215–246, 2011.

[98] Anita Cadoux, Bruno Scaillet, Slimane Bekki, Clive Oppenheimer, and Timothy H Druitt. Stratospheric ozone destruction by the bronze-age minoan eruption (santorini volcano, greece). *Scientific reports*, 5, 2015.

[99] Thomas J Aubry, A Mark Jellinek, Wim Degruyter, Costanza Bonadonna, Valentina Radić, Margot Clyne, and Adjoa Quainoo. Impact of global warming on the rise of volcanic plumes and implications for future volcanic aerosol forcing. *Journal of Geophysical Research: Atmospheres*, 121(22), 2016.

[100] M Patrick McCormick, Larry W Thomason, and Charles R Trepte. Atmospheric effects of the mt pinatubo eruption. *Nature*, 373(6513):399–404, 1995.

[101] Andrew Tupper, J Scott Oswalt, and Daniel Rosenfeld. Satellite and radar analysis of the volcanic-cumulonimbi at mount pinatubo, philippines, 1991. *Journal of Geophysical Research: Atmospheres*, 110(D9), 2005.

[102] JE Hammer, KV Cashman, RP Hoblitt, and S Newman. Degassing and microlite crystallization during pre-climactic events of the 1991 eruption of mt. pinatubo, philippines. *Bulletin of Volcanology*, 60(5):355–380, 1999.

[103] David H Harlow, John A Power, Eduardo P Laguerta, Gemme Ambubuyog, Randall A White, and Richard P Hoblitt. Precursory seismicity and forecasting of the june 15, 1991, eruption of mount pinatubo. *Fire and Mud: eruptions and lahars of Mount Pinatubo, Philippines*, pages 223–247, 1996.

[104] Christopher G Newhall, James W Hendley II, and Peter H Stauffer. The cataclysmic 1991 eruption of mount pinatubo, philippines. Technical report, Geological Survey (US), 1997.

[105] HR Westrich and TM Gerlach. Magmatic gas source for the stratospheric so2 cloud from the june 15, 1991, eruption of mount pinatubo. *Geology*, 20(10):867–870, 1992.

[106] F Arfeuille, BP Luo, P Heckendorn, D Weisenstein, JX Sheng, E Rozanov, M Schraner, Stefan Brönnimann, LW Thomason, and T Peter. Modeling the stratospheric warming following the mt. pinatubo eruption: uncertainties in aerosol extinctions. *Atmospheric chemistry and physics*, 13(22):11221–11234, 2013.

[107] SS Dhomse, KM Emmerson, GW Mann, N Bellouin, KS Carslaw, MP Chipperfield, R Hommel, NL Abraham, P Telford, P Braesicke, et al. Aerosol microphysics simulations of the mt. pinatubo eruption with the um-ukca composition-climate model. *Atmospheric Chemistry and Physics*, 14(20):11221–11246, 2014.

[108] J-X Sheng, DK Weisenstein, B-P Luo, E Rozanov, F Arfeuille, and T Peter. A perturbed parameter model ensemble to investigate mt. pinatubo's 1991 initial sulfur mass emission. *Atmospheric chemistry and physics*, 15(20):11501–11512, 2015.

[109] Douglas E Kinnison, Keith E Grant, Peter S Connell, Douglas A Rotman, and Donald J Wuebbles. The chemical and radiative effects of the mount pinatubo eruption. *Journal of Geophysical Research: Atmospheres*, 99(D12):25705–25731, 1994.

[110] CP Rinsland, GK Yue, MR Gunson, Rodolphe Zander, and MC Abrams. Mid-infrared extinction by sulfate aerosols from the mt pinatubo eruption. *Journal of Quantitative Spectroscopy and Radiative Transfer*, 52(3-4):241–252, 1994.

[111] Makiko Sato, James E Hansen, M Patrick McCormick, and James B Pollack. Stratospheric aerosol optical depths, 1850–1990. *Journal of Geophysical Research: Atmospheres*, 98(D12): 22987–22994, 1993.

[112] Makiko Sato. Forcings in giss climate model: Stratospheric aerosol optical thickness. https://data.giss.nasa.gov/modelforce/strataer/. Accessed: 2017-12-05.

[113] Andrew Lacis, James Hansen, and Makiko Sato. Climate forcing by stratospheric aerosols. *Geophysical Research Letters*, 19(15):1607–1610, 1992.

[114] Roger Saunders. Radiative properties of mount pinatubo volcanic aerosols over the tropical atlantic. *Geophysical research letters*, 20(2):137–140, 1993.

[115] PB Russell, JM Livingston, EG Dutton, RF Pueschel, JA Reagan, TE Defoor, MA Box, D Allen, P Pilewskie, BM Herman, et al. Pinatubo and pre-pinatubo optical-depth spectra: Mauna loa measurements, comparisons, inferred particle size distributions, radiative effects, and relationship to lidar data. *Journal of Geophysical Research: Atmospheres*, 98(D12): 22969–22985, 1993.

[116] Alan Robock. Volcanic eruptions and climate. *Reviews of Geophysics*, 38(2):191–219, 2000.

[117] Luke Oman, Alan Robock, Georgiy Stenchikov, Gavin A Schmidt, and Reto Ruedy. Climatic response to high-latitude volcanic eruptions. *Journal of Geophysical Research: Atmospheres*, 110(D13), 2005.

[118] Luke Oman, Alan Robock, Georgiy L Stenchikov, and Thorvaldur Thordarson. High-latitude eruptions cast shadow over the african monsoon and the flow of the nile. *Geophysical Research Letters*, 33(18), 2006.

[119] Ross J Salawitch, Debra K Weisenstein, Laurie J Kovalenko, Chris E Sioris, Paul O Wennberg, Kelly Chance, Malcolm KW Ko, and Chris A McLinden. Sensitivity of ozone to bromine in the lower stratosphere. *Geophysical research letters*, 32(5), 2005.

[120] Susan Solomon, RW Portmann, RR Garcia, LW Thomason, LR Poole, and MP McCormick. The role of aerosol variations in anthropogenic ozone depletion at northern midlatitudes. *Journal of Geophysical Research: Atmospheres*, 101(D3):6713–6727, 1996.

[121] S Solomon, RW Portmann, RR Garcia, W Randel, F Wu, R Nagatani, J Gleason, L Thomason, LR Poole, and MP McCormick. Ozone depletion at mid-latitudes: Coupling of volcanic

aerosols and temperature variability to anthropogenic chlorine. *Geophysical research letters*, 25(11):1871–1874, 1998.

[122] Lori M Perliski and Susan Solomon. Radiative influences of pinatubo volcanic aerosols on twilight observations of no2 column abundances. *Geophysical research letters*, 19(19):1923–1926, 1992.

[123] DJ Hofmann, SJ Oltmans, WD Komhyr, JM Harris, JA Lathrop, AO Langford, T Deshler, BJ Johnson, A Torres, and WA Matthews. Ozone loss in the lower stratosphere over the united states in 1992–1993: Evidence for heterogeneous chemistry on the pinatubo aerosol. *Geophysical Research Letters*, 21(1):65–68, 1994.

[124] James K Angell. Estimated impact of agung, el chichón and pinatubo volcanic eruptions on global and regional total ozone after adjustment for the qbo. *Geophysical research letters*, 24 (6):647–650, 1997.

[125] Stefan Muthers, Florian Arfeuille, Christoph C Raible, and Eugene Rozanov. The impacts of volcanic aerosol on stratospheric ozone and the northern hemisphere polar vortex: separating radiative-dynamical changes from direct effects due to enhanced aerosol heterogeneous chemistry. *Atmospheric chemistry and physics*, 15(20):11461–11476, 2015.

[126] S Kinne, OB Toon, and MJ Prather. Buffering of stratospheric circulation by changing amounts of tropical ozone a pinatubo case study. *Geophysical research letters*, 19(19):1927–1930, 1992.

[127] W.G. Mankin, M.T. Coffey, and A. Goldman. Airborne observations of SO2, HCl, and O3 in the stratospheric plume of the Pinatubo volcano in July 1991. *Geophysical Research Letters*, 19(2):179–182, 1992.

[128] Peter J Linstrom and WG Mallard. *NIST Chemistry webbook; NIST standard reference database No. 69*. 2001.

[129] Thomas F Stocker, Dahe Qin, Gian-Kasper Plattner, Melinda Tignor, Simon K Allen, Judith Boschung, Alexander Nauels, Yu Xia, B Bex, and BM Midgley. Ipcc, 2013: climate change 2013: the physical science basis. contribution of working group i to the fifth assessment report of the intergovernmental panel on climate change, 2013.

[130] David Archer, Michael Eby, Victor Brovkin, Andy Ridgwell, Long Cao, Uwe Mikolajewicz, Ken Caldeira, Katsumi Matsumoto, Guy Munhoven, Alvaro Montenegro, et al. Atmospheric lifetime of fossil fuel carbon dioxide. *Annual Review of Earth and Planetary Sciences*, 37, 2009.

[131] Isaac M Held and Brian J Soden. Water vapor feedback and global warming. *Annual review of energy and the environment*, 25(1):441–475, 2000.

[132] Ryan Hossaini, Martyn P Chipperfield, Alfonso Saiz-Lopez, Jeremy J Harrison, R von Glasow, Roberto Sommariva, Elliot Atlas, M Navarro, Stephen A Montzka, Wuhu Feng, et al. Growth in stratospheric chlorine from short-lived chemicals not controlled by the montreal protocol. *Geophysical research letters*, 42(11):4573–4580, 2015.

[133] Deqiang Zhang, Jinxian Zhong, and Lianxiong Qiu. Kinetics of the reaction of hydroxyl radicals with ch 2 br 2 and its implications in the atmosphere. *Journal of atmospheric chemistry*, 27(2):209–215, 1997.

[134] Keith P Shine, Jan S Fuglestvedt, Kinfe Hailemariam, and Nicola Stuber. Alternatives to the global warming potential for comparing climate impacts of emissions of greenhouse gases. *Climatic Change*, 68(3):281–302, 2005.

[135] Detlef P Van Vuuren, Jae Edmonds, Mikiko Kainuma, Keywan Riahi, Allison Thomson, Kathy Hibbard, George C Hurtt, Tom Kram, Volker Krey, Jean-Francois Lamarque, et al. The representative concentration pathways: an overview. *Climatic change*, 109(1-2):5, 2011.

[136] Detlef P Vuuren, Elke Stehfest, Michel GJ Elzen, Tom Kram, Jasper Vliet, Sebastiaan Deetman, Morna Isaac, Kees Klein Goldewijk, Andries Hof, Angelica Mendoza Beltran, et al. Rcp2. 6: exploring the possibility to keep global mean temperature increase below 2 c. *Climatic Change*, 109(1-2):95–116, 2011.

[137] Allison M Thomson, Katherine V Calvin, Steven J Smith, G Page Kyle, April Volke, Pralit Patel, Sabrina Delgado-Arias, Ben Bond-Lamberty, Marshall A Wise, Leon E Clarke, et al. Rcp4. 5: a pathway for stabilization of radiative forcing by 2100. *Climatic change*, 109(1-2): 77, 2011.

[138] Toshihiko Masui, Kenichi Matsumoto, Yasuaki Hijioka, Tsuguki Kinoshita, Toru Nozawa, Sawako Ishiwatari, Etsushi Kato, PR Shukla, Yoshiki Yamagata, and Mikiko Kainuma. An

emission pathway for stabilization at 6 wm- 2 radiative forcing. *Climatic Change*, 109(1-2): 59–76, 2011.

[139] Keywan Riahi, Shilpa Rao, Volker Krey, Cheolhung Cho, Vadim Chirkov, Guenther Fischer, Georg Kindermann, Nebojsa Nakicenovic, and Peter Rafaj. Rcp 8.5—a scenario of comparatively high greenhouse gas emissions. *Climatic Change*, 109(1-2):33, 2011.

[140] S Watanabe, T Hajima, K Sudo, T Nagashima, T Takemura, H Okajima, T Nozawa, H Kawase, M Abe, T Yokohata, et al. Miroc-esm 2010: Model description and basic results of cmip5-20c3m experiments. *Geoscientific Model Development*, 4(4):845, 2011.

[141] Eric L Fleming, Charles H Jackman, Richard S Stolarski, and David B Considine. Simulation of stratospheric tracers using an improved empirically based two-dimensional model transport formulation. *Journal of Geophysical Research: Atmospheres*, 104(D19):23911–23934, 1999.

[142] Malte Meinshausen, Steven J Smith, K Calvin, John S Daniel, MLT Kainuma, Jean-Francois Lamarque, Km Matsumoto, SA Montzka, SCB Raper, K Riahi, et al. The rcp greenhouse gas concentrations and their extensions from 1765 to 2300. *Climatic change*, 109(1-2):213, 2011.

[143] Veronika Eyring, DW Waugh, GE Bodeker, E Cordero, H Akiyoshi, J Austin, SR Beagley, BA Boville, P Braesicke, C Brühl, et al. Multimodel projections of stratospheric ozone in the 21st century. *Journal of Geophysical Research: Atmospheres*, 112(D16), 2007.

[144] Robert W Portmann and Susan Solomon. Indirect radiative forcing of the ozone layer during the 21st century. *Geophysical research letters*, 34(2), 2007.

[145] H Akiyoshi, Y Yamashita, K Sakamoto, LB Zhou, and T Imamura. Recovery of stratospheric ozone in calculations by the center for climate system research/national institute for environmental studies chemistry-climate model under the ccmval-ref2 scenario and a no-climate-change run. *Journal of Geophysical Research: Atmospheres*, 115(D19), 2010.

[146] Theodore G Shepherd. Dynamics, stratospheric ozone, and climate change. *Atmosphere-Ocean*, 46(1):117–138, 2008.

[147] Christiane Textor, Hans-F Graf, Michael Herzog, and JM Oberhuber. Injection of gases into the stratosphere by explosive volcanic eruptions. *Journal of Geophysical Research: Atmospheres*, 108(D19), 2003.

[148] RG Grainger and EJ Highwood. Changes in stratospheric composition, chemistry, radiation and climate caused by volcanic eruptions. *Geological Society, London, Special Publications*, 213(1):329–347, 2003.

[149] P Minnis, EF Harrison, LL Stowe, GG Gibson, FM Denn, DR Doelling, and WL Smith. Radiative climate forcing by the mount pinatubo eruption. *Science*, 259(5100):1411–1415, 1993.

[150] Giovanni Pitari and Vincenzo Rizi. An estimate of the chemical and radiative perturbation of stratospheric ozone following the eruption of mt. pinatubo. *Journal of the atmospheric sciences*, 50(19):3260–3276, 1993.

[151] TG Shepherd, DA Plummer, JF Scinocca, MI Hegglin, VE Fioletov, MC Reader, E Remsberg, T Von Clarmann, and HJ Wang. Reconciliation of halogen-induced ozone loss with the total-column ozone record. *Nature Geoscience*, 7(6):443–449, 2014.

[152] SS Dhomse, MP Chipperfield, W Feng, Ryan Hossaini, GW Mann, and ML Santee. Revisiting the hemispheric asymmetry in midlatitude ozone changes following the mount pinatubo eruption: A 3-d model study. *Geophysical research letters*, 42(8):3038–3047, 2015.

[153] Jassim A Al-Saadi, R Bradley Pierce, T Duncan Fairlie, Mary M Kleb, Richard S Eckman, William L Grose, Murali Natarajan, and Jennifer R Olson. Response of middle atmosphere chemistry and dynamics to volcanically elevated sulfate aerosol: Three-dimensional coupled model simulations. *Journal of Geophysical Research: Atmospheres*, 106(D21):27255–27275, 2001.

[154] Valentina Aquila, Luke D Oman, R Stolarski, Anne R Douglass, and Paul A Newman. The response of ozone and nitrogen dioxide to the eruption of mt. pinatubo at southern and northern midlatitudes. *Journal of the Atmospheric Sciences*, 70(3):894–900, 2013.

[155] Gwenaël Berthet, Fabrice Jégou, Valéry Catoire, Gisèle Krysztofiak, Jean-Baptiste Renard, Adam E Bourassa, Doug A Degenstein, Colette Brogniez, Marcel Dorf, Sebastian Kreycy, et al. Impact of a moderate volcanic eruption on chemistry in the lower stratosphere: balloon-borne observations and model calculations. *Atmospheric Chemistry and Physics*, 17(3):2229–2253, 2017.

[156] Giovanni Pitari, Valentina Aquila, Ben Kravitz, Alan Robock, Shingo Watanabe, Irene Cionni, Natalia De Luca, Glauco Di Genova, Eva Mancini, and Simone Tilmes. Strato-

spheric ozone response to sulfate geoengineering: Results from the geoengineering model intercomparison project (geomip). *Journal of Geophysical Research: Atmospheres*, 119(5): 2629–2653, 2014.

[157] J. Eric Klobas, David M Wilmouth, Debra K Weisenstein, James G Anderson, and Ross J Salawitch. Ozone depletion following future volcanic eruptions. *Geophysical Research Letters*, 44(14):7490–7499, 2017.

[158] M Dorf, A Butz, C Camy-Peyret, MP Chipperfield, L Kritten, and K Pfeilsticker. Bromine in the tropical troposphere and stratosphere as derived from balloon-borne bro observations. *Atmospheric Chemistry and Physics*, 8(23):7265–7271, 2008.

[159] Bodo Werner, Jochen Stutz, Max Spolaor, Lisa Scalone, Rasmus Raecke, James Festa, Santo Fedele Colosimo, Ross Cheung, Catalina Tsai, Ryan Hossaini, et al. Probing the subtropical lowermost stratosphere and the tropical upper troposphere and tropopause layer for inorganic bromine. *Atmospheric Chemistry and Physics*, 17(2):1161–1186, 2017.

[160] X Yang, NL Abraham, AT Archibald, P Braesicke, J Keeble, PJ Telford, NJ Warwick, and JA Pyle. How sensitive is the recovery of stratospheric ozone to changes in concentrations of very short-lived bromocarbons? *Atmospheric Chemistry and Physics*, 14(19):10431–10438, 2014.

[161] Rafael P Fernandez, Douglas E Kinnison, Jean-Francois Lamarque, Simone Tilmes, and Alfonso Saiz-Lopez. Impact of biogenic very short-lived bromine on the antarctic ozone hole during the 21st century. *Atmospheric Chemistry and Physics*, 17(3):1673–1688, 2017.

[162] YK Lim, SM Phang, N Abdul Rahman, WT Sturges, and G Malin. Halocarbon emissions from marine phytoplankton and climate change. *International Journal of Environmental Science and Technology*, pages 1–16, 2017.

[163] Franziska Ziska, Birgit Quack, Susann Tegtmeier, Irene Stemmler, and Kirstin Krüger. Future emissions of marine halogenated very-short lived substances under climate change. *Journal of Atmospheric Chemistry*, 74(2):245–260, 2017.

[164] Alison L Webb, Frances E Hopkins, Lennart T Bach, Corina PD Brussaard, and Peter S Liss. Effect of ocean acidification and elevated fco 2 on trace gas production by a baltic sea summer phytoplankton community. *Biogeosciences*, 13(15):4595, 2016.

[165] Olivier Dessens, Guang Zeng, Nicola Warwick, and John Pyle. Short-lived bromine compounds in the lower stratosphere; impact of climate change on ozone. *Atmospheric Science Letters*, 10(3):201–206, 2009.

[166] Alfonso Saiz-Lopez, Sunil Baidar, Carlos A Cuevas, TK Koenig, Rafael P Fernandez, Barbara Dix, Douglas E Kinnison, J-F Lamarque, Xavier Rodriguez-Lloveras, Teresa L Campos, et al. Injection of iodine to the stratosphere. *Geophysical Research Letters*, 42(16):6852–6859, 2015.

[167] Debra K Weisenstein, Glenn K Yue, Malcolm KW Ko, Nien-Dak Sze, Jose M Rodriguez, and Courtney J Scott. A two-dimensional model of sulfur species and aerosols. *Journal of Geophysical Research: Atmospheres*, 102(D11):13019–13035, 1997.

[168] DK Weisenstein, JE Penner, M Herzog, and Xiaohong Liu. Global 2-d intercomparison of sectional and modal aerosol modules. *Atmospheric Chemistry and Physics*, 7(9):2339–2355, 2007.

[169] L Thomason and Th Peter. Sparc assessment of stratospheric aerosol properties, wcrp-124, wmo/td-no. 1295. Technical report, SPARC Report, 2006.

[170] EV Rozanov, ME Schlesinger, NG Andronova, F Yang, SL Malyshev, VA Zubov, TA Egorova, and B Li. Climate/chemistry effects of the pinatubo volcanic eruption simulated by the uiuc stratosphere/troposphere gcm with interactive photochemistry. *Journal of Geophysical Research: Atmospheres*, 107(D21), 2002.

[171] P Telford, P Braesicke, O Morgenstern, and J Pyle. Reassessment of causes of ozone column variability following the eruption of mount pinatubo using a nudged ccm. *Atmospheric Chemistry and Physics*, 9(13):4251–4260, 2009.

[172] Drew T Shindell, Gavin A Schmidt, Ron L Miller, and Michael E Mann. Volcanic and solar forcing of climate change during the preindustrial era. *Journal of Climate*, 16(24):4094–4107, 2003.

[173] RJ Salawitch, Tim Canty, Thomas Kurosu, Kelly Chance, Qing Liang, Arlindo da Silva, Steven Pawson, JE Nielsen, JM Rodriguez, PK Bhartia, et al. A new interpretation of total column bro during arctic spring. *Geophysical Research Letters*, 37(21), 2010.

[174] Qing Liang, Elliot Atlas, Donald Blake, Marcel Dorf, Klaus Pfeilsticker, and Sue Schauffler. Convective transport of very short lived bromocarbons to the stratosphere. *Atmospheric Chemistry and Physics*, 14(11):5781–5792, 2014.

[175] Lin Song, Peter Langfelder, and Steve Horvath. Random generalized linear model: a highly accurate and interpretable ensemble predictor. *BMC bioinformatics*, 14(1):5, 2013.

[176] A Tabazadeh and RP Turco. Stratospheric chlorine injection by volcanic eruptions: Hcl scavenging and implications for ozone. *Science*, 260(5111):1082–1086, 1993.

[177] Steffen Kutterolf, TH Hansteen, K Appel, Armin Freundt, Kirstin Krüger, Wendy Perez, and Heidi Wehrmann. Combined bromine and chlorine release from large explosive volcanic eruptions: A threat to stratospheric ozone? *Geology*, 41(6):707–710, 2013.

[178] Steffen Kutterolf, Thor H Hansteen, Armin Freundt, Heidi Wehrmann, Karen Appel, Kirstin Krüger, and Wendy Perez. Bromine and chlorine emissions from plinian eruptions along the central american volcanic arc: From source to atmosphere. *Earth and planetary science letters*, 429:234–246, 2015.

[179] SA Carn, L Clarisse, and AJ Prata. Multi-decadal satellite measurements of global volcanic degassing. *Journal of Volcanology and Geothermal Research*, 311:99–134, 2016.

[180] Nicolas Theys, Isabelle De Smedt, Michel Van Roozendael, Lucien Froidevaux, Lieven Clarisse, and François Hendrick. First satellite detection of volcanic oclo after the eruption of puyehue-cordón caulle. *Geophysical Research Letters*, 41(2):667–672, 2014.

[181] Nicolas Theys, M Van Roozendael, B Dils, F Hendrick, Nan Hao, and M De Maziere. First satellite detection of volcanic bromine monoxide emission after the kasatochi eruption. *Geophysical Research Letters*, 36(3), 2009.

[182] Anja Schönhardt, Andreas Richter, Nicolas Theys, and John P Burrows. Space-based observation of volcanic iodine monoxide. *Atmospheric Chemistry and Physics*, 17(7):4857–4870, 2017.

[183] William G Mankin and MT Coffey. Increased stratospheric hydrogen chloride in the el chichon cloud. *Science*, 226:170–173, 1984.

[184] DE Hunton, AA Viggiano, TM Miller, JO Ballenthin, JM Reeves, JC Wilson, Shan-Hu Lee, BE Anderson, WH Brune, H Harder, et al. In-situ aircraft observations of the 2000 mt. hekla

volcanic cloud: Composition and chemical evolution in the arctic lower stratosphere. *Journal of Volcanology and Geothermal Research*, 145(1):23–34, 2005.

[185] William I Rose, Genevieve A Millard, Tamsin A Mather, Donald E Hunton, Bruce Anderson, Clive Oppenheimer, Brett F Thornton, Terrence M Gerlach, Albert A Viggiano, Yutaka Kondo, et al. Atmospheric chemistry of a 33–34 hour old volcanic cloud from hekla volcano (iceland): Insights from direct sampling and the application of chemical box modeling. *Journal of Geophysical Research: Atmospheres*, 111(D20), 2006.

[186] GA Millard, TA Mather, DM Pyle, William I Rose, and B Thornton. Halogen emissions from a small volcanic eruption: Modeling the peak concentrations, dispersion, and volcanically induced ozone loss in the stratosphere. *Geophysical Research Letters*, 33(19), 2006.

[187] Chris M Zdanowicz, Gregory A Zielinski, and Mark S Germani. Mount mazama eruption: Calendrical age verified and atmospheric impact assessed. *Geology*, 27(7):621–624, 1999.

[188] M De Angelis, J Simoes, H Bonnaveira, J-D Taupin, and RJ Delmas. Volcanic eruptions recorded in the illimani ice core (bolivia): 1918–1998 and tambora periods. *Atmospheric Chemistry and Physics*, 3(5):1725–1741, 2003.

[189] Charles R Bacon. Eruptive history of mount mazama and crater lake caldera, cascade range, usa. *Journal of Volcanology and Geothermal Research*, 18(1-4):57–115, 1983.

[190] Clive Oppenheimer, Vitchko I Tsanev, Christine F Braban, Richard A Cox, Jonathan W Adams, Alessandro Aiuppa, Nicole Bobrowski, Pierre Delmelle, Jenni Barclay, and Andrew JS McGonigle. Bro formation in volcanic plumes. *Geochimica et Cosmochimica Acta*, 70(12):2935–2941, 2006.

[191] Roland von Glasow, Nicole Bobrowski, and Christoph Kern. The effects of volcanic eruptions on atmospheric chemistry. *Chemical Geology*, 263(1):131–142, 2009.

[192] TJ Roberts, CF Braban, RS Martin, C Oppenheimer, JW Adams, RA Cox, RL Jones, and PT Griffiths. Modelling reactive halogen formation and ozone depletion in volcanic plumes. *Chemical Geology*, 263(1):151–163, 2009.

[193] RS Martin and E Ilyinskaya. Volcanic lightning as a source of reactive radical species in eruption plumes. *Geochemistry, Geophysics, Geosystems*, 12(3), 2011.

[194] Peter J Kelly, Christoph Kern, Tjarda J Roberts, Taryn Lopez, Cynthia Werner, and Alessandro Aiuppa. Rapid chemical evolution of tropospheric volcanic emissions from redoubt volcano, alaska, based on observations of ozone and halogen-containing gases. *Journal of Volcanology and Geothermal Research*, 259:317–333, 2013.

[195] TJ Roberts, RS Martin, and L Jourdain. Reactive bromine chemistry in mount etna's volcanic plume: the influence of total br, high-temperature processing, aerosol loading and plume–air mixing. *Atmospheric Chemistry and Physics*, 14(20):11201–11219, 2014.

[196] Chulkyu Lee, Young J Kim, Hiroshi Tanimoto, Nicole Bobrowski, Ulrich Platt, Toshiya Mori, Keigo Yamamoto, and Chun S Hong. High clo and ozone depletion observed in the plume of sakurajima volcano, japan. *Geophysical Research Letters*, 32(21), 2005.

[197] Michael Zelenski and Yuri Taran. Volcanic emissions of molecular chlorine. *Geochimica et Cosmochimica Acta*, 87:210–226, 2012.

[198] Jonas Gliss, Nicole Bobrowski, Leif Vogel, D Pöhler, and U Platt. Oclo and bro observations in the volcanic plume of mt. etna–implications on the chemistry of chlorine and bromine species in volcanic plumes. *Atmospheric Chemistry and Physics*, 15(10):5659–5681, 2015.

[199] N Bobrowski, G Hönninger, B Galle, and U Platt. Detection of bromine monoxide in a volcanic plume. *Nature*, 423(6937):273–276, 2003.

[200] G Hönninger, N Bobrowski, ER Palenque, R Torrez, and U Platt. Reactive bromine and sulfur emissions at salar de uyuni, bolivia. *Geophysical research letters*, 31(4), 2004.

[201] N Bobrowski and U Platt. So 2/bro ratios studied in five volcanic plumes. *Journal of Volcanology and Geothermal Research*, 166(3):147–160, 2007.

[202] Philipson Bani, Clive Oppenheimer, Vitchko I Tsanev, Simon A Carn, Shane J Cronin, Rachel Crimp, Julie A Calkins, Douglas Charley, Michel Lardy, and Tjarda R Roberts. Surge in sulphur and halogen degassing from ambrym volcano, vanuatu. *Bulletin of Volcanology*, 71 (10):1159, 2009.

[203] Christoph Kern, Holger Sihler, Leif Vogel, Claudia Rivera, Martha Herrera, and Ulrich Platt. Halogen oxide measurements at masaya volcano, nicaragua using active long path differential optical absorption spectroscopy. *Bulletin of Volcanology*, 71(6):659–670, 2009.

[204] K-P Heue, CAM Brenninkmeijer, AK Baker, A Rauthe-Schöch, D Walter, T Wagner, C Hörmann, H Sihler, B Dix, U Frieß, et al. So 2 and bro observation in the plume of the eyjafjallajökull volcano 2010: Caribic and gome-2 retrievals. *Atmospheric Chemistry and Physics*, 11 (6):2973–2989, 2011.

[205] C Hörmann, H Sihler, N Bobrowski, S Beirle, M Penning de Vries, U Platt, and T Wagner. Systematic investigation of bromine monoxide in volcanic plumes from space by using the gome-2 instrument. *Atmospheric Chemistry and Physics*, 13(9):4749, 2013.

[206] Rolf Sander. Compilation of henry's law constants (version 4.0) for water as solvent. *Atmospheric Chemistry & Physics*, 15(8), 2015.

[207] N Bobrowski, GB Giuffrida, S Arellano, M Yalire, M Liotta, L Brusca, S Calabrese, S Scaglione, J Rüdiger, JM Castro, et al. Plume composition and volatile flux of nyamulagira volcano, democratic republic of congo, during birth and evolution of the lava lake, 2014–2015. *Bulletin of Volcanology*, 79(12):90, 2017.

[208] Tina Jurkat, Christiane Voigt, Frank Arnold, Hans Schlager, Heinfried Aufmhoff, Julia Schmale, Johannes Schneider, Michael Lichtenstern, and Andreas Dörnbrack. Airborne stratospheric itcims measurements of so2, hcl, and hno3 in the aged plume of volcano kasatochi. *Journal of Geophysical Research: Atmospheres*, 115(D2), 2010.

[209] Hélène Bureau, Hans Keppler, and Nicole Métrich. Volcanic degassing of bromine and iodine: experimental fluid/melt partitioning data and applications to stratospheric chemistry. *Earth and Planetary Science Letters*, 183(1):51–60, 2000.

[210] Glen T Snyder and Udo Fehn. Origin of iodine in volcanic fluids: 129i results from the central american volcanic arc. *Geochimica et Cosmochimica Acta*, 66(21):3827–3838, 2002.

[211] Florin Caldararu, Stefan Patrascu, Mira Caldararu, Anca Paraschiv, and Dan Nicolaescu. The far to equilibrium time evolution of the ozone layer: steady-state and critical behaviour. *Atmospheric environment*, 33(26):4243–4254, 1999.

[212] Institute for Defense Analyses. Science, Technology Division, and Elmar R Reiter. *The natural stratosphere of 1974*. Department of Transportation, Climatic Impact Assessment Program, 1975.

[213] TF Hanisco, EJ Lanzendorf, PO Wennberg, KK Perkins, RM Stimpfle, PB Voss, JG Anderson, RC Cohen, DW Fahey, RS Gao, E. J. Hintsa, R. J. Salawitch, J. J. Margitan, C. T. McElroy, and C. Midwinter. Sources, sinks, and the distribution of oh in the lower stratosphere. *The Journal of Physical Chemistry A*, 105(9):1543–1553, 2001.

[214] Felix Ploeger, Gebhard Günther, Paul Konopka, Stephan Fueglistaler, Ro Müller, Christiane Hoppe, Anne Kunz, Reinhold Spang, J-U Grooß, and Martin Riese. Horizontal water vapor transport in the lower stratosphere from subtropics to high latitudes during boreal summer. *Journal of Geophysical Research: Atmospheres*, 118(14):8111–8127, 2013.

[215] B Vogel, G Günther, Rolf Müller, J-U Grooß, P Hoor, M Krämer, S Müller, A Zahn, and M Riese. Fast transport from southeast asia boundary layer sources to northern europe: rapid uplift in typhoons and eastward eddy shedding of the asian monsoon anticyclone. *Atmospheric Chemistry and Physics*, 14(23):12745–12762, 2014.

[216] R Spang, G Günther, M Riese, L Hoffmann, R Müller, and S Griessbach. Satellite observations of cirrus clouds in the northern hemisphere lowermost stratosphere. *Atmospheric chemistry and physics*, 15(2):927–950, 2015.

[217] Jessica B Smith, David M Wilmouth, Kristopher M Bedka, Kenneth P Bowman, Cameron R Homeyer, John A Dykema, Maryann R Sargent, Corey E Clapp, Stephen S Leroy, David S Sayres, Jonathan M. Dean-Day, T. Paul Bui, and James G. Anderson. A case study of convectively sourced water vapor observed in the overworld stratosphere over the united states. *Journal of Geophysical Research: Atmospheres*, 122(17):9529–9554, 2017.

[218] Robert L Herman, Eric A Ray, Karen H Rosenlof, Kristopher M Bedka, Michael J Schwartz, William G Read, Robert F Troy, Keith Chin, Lance E Christensen, Dejian Fu, et al. Enhanced stratospheric water vapor over the summertime continental united states and the role of overshooting convection. *Atmospheric Chemistry and Physics*, 17(9):6113, 2017.

[219] Q Shi, JT Jayne, CE Kolb, DR Worsnop, and P Davidovits. Kinetic model for reaction of clono2 with h2o and hcl and hocl with hcl in sulfuric acid solutions. *Journal of Geophysical Research: Atmospheres*, 106(D20):24259–24274, 2001.

[220] TF Hanisco, JB Smith, RM Stimpfle, DM Wilmouth, KK Perkins, JR Spackman, JG Anderson, D Baumgardner, B Gandrud, CR Webster, S. Dhaniyala, K. A. Mckinney, and T. P. Bui. Quantifying the rate of heterogeneous processing in the arctic polar vortex with in situ observations of oh. *Journal of Geophysical Research: Atmospheres*, 107(D20), 2002.

[221] K Drdla and R Müller. Temperature thresholds for chlorine activation and ozone loss in the polar stratosphere. In *Annales geophysicae*, volume 30, pages 1055–1073. Copernicus GmbH, 2012.

[222] John William Cooney. *Ten-Year Analysis of Tropopause-Overshooting Convection over the Eastern United States using NEXRAD Data*. PhD thesis, Texas A&M, 2016.

[223] LW Alvarez, W Alvarez, F Asaro, and HV Michel. Extraterrestrial cause for the cretaceous-tertiary extinction: Experiment and theory. *Science*, 1979.

[224] Kenneth J Hsü. Terrestrial catastrophe caused by cometary impact at the end of cretaceous. *Nature*, 285(5762):201–203, 1980.

[225] Thomas J Ahrens and John D O'Keefe. Impact of an asteroid or comet in the ocean and extinction of terrestrial life. *Journal of Geophysical Research: Solid Earth*, 88(S02), 1983.

[226] Marc Davis, Piet Hut, and Richard A Muller. Extinction of species by periodic comet showers. *Nature*, 308(5961):715–717, 1984.

[227] Piet Hut, Walter Alvarez, William P Elder, Thor Hansen, Erle G Kauffman, Gerta Keller, Eugene M Shoemaker, and Paul R Weissman. Comet showers as a cause of mass extinctions. *Nature*, 329(6135):118–126, 1987.

[228] Alan R Hildebrand, Glen T Penfield, David A Kring, Mark Pilkington, Antonio Camargo, Stein B Jacobsen, and William V Boynton. Chicxulub crater: a possible cretaceous/tertiary boundary impact crater on the yucatan peninsula, mexico. *Geology*, 19(9):867–871, 1991.

[229] Charles G Bardeen, Rolando R Garcia, Owen B Toon, and Andrew J Conley. On transient climate change at the cretaceous- paleogene boundary due to atmospheric soot injections. *Proceedings of the National Academy of Sciences*, page 201708980, 2017.

[230] Clark R Chapman. The hazard of near-earth asteroid impacts on earth. *Earth and Planetary Science Letters*, 222(1):1–15, 2004.

[231] John W Birks, Paul J Crutzen, and Raymond G Roble. Frequent ozone depletion resulting from impacts of asteroids and comets. *Comet/Asteroid Impacts and Human Society: An Interdisciplinary Approach. Springer, Berlin*, pages 225–245, 2007.

[232] Richard P Binzel. The torino impact hazard scale. *Planetary and Space Science*, 48(4):297–303, 2000.

[233] HJ Melosh. The mechanics of large meteoroid impacts in the earth's oceans. *Geological Society of America Special Papers*, 190:121–128, 1982.

[234] Eric M Jones and John W Kodis. Atmospheric effects of large body impacts: The first few minutes. *Geological Society of America Special Papers*, 190:175–186, 1982.

[235] Owen B Toon, Charles Bardeen, and Rolando Garcia. Designing global climate and atmospheric chemistry simulations for 1 and 10 km diameter asteroid impacts using the properties of ejecta from the k-pg impact. *Atmospheric Chemistry and Physics*, 16(20):13185–13212, 2016.

[236] Guy P Brasseur. Natural and anthropogenic perturbations of the stratospheric ozone layer. *Planetary and space science*, 40(2-3):403–412, 1992.

[237] Guy Brasseur. The response of the middle atmosphere to long-term and short-term solar variability: A two-dimensional model. *Journal of Geophysical Research: Atmospheres*, 98 (D12):23079–23090, 1993.

[238] Eric L Fleming, Sushil Chandra, Charles H Jackman, David B Considine, and Anne R Douglass. The middle atmospheric response to short and long term solar uv variations: Analysis of observations and 2d model results. *Journal of Atmospheric and Terrestrial Physics*, 57(4): 333–365, 1995.

[239] LL Hood. The solar cycle variation of total ozone: Dynamical forcing in the lower stratosphere. *Journal of Geophysical Research: Atmospheres*, 102(D1):1355–1370, 1997.

[240] T Egorova, E Rozanov, E Manzini, M Haberreiter, W Schmutz, V Zubov, and Th Peter. Chemical and dynamical response to the 11-year variability of the solar irradiance simulated with a chemistry-climate model. *Geophysical Research Letters*, 31(6), 2004.

[241] Kunihiko Kodera and Yuhji Kuroda. Dynamical response to the solar cycle. *Journal of Geophysical Research: Atmospheres*, 107(D24), 2002.

[242] V Williams, J Austin, and JD Haigh. Model simulations of the impact of the 27-day solar rotation period on stratospheric ozone and temperature. *Advances in Space Research*, 27(12): 1933–1942, 2001.

[243] A.V. Shapiro, E. Rozanov, T. Egorova, A.I. Shapiro, Th. Peter, and W. Schmutz. Sensitivity of the earth's middle atmosphere to short-term solar variability and its dependence on the

choice of solar irradiance data set. *Journal of Atmospheric and Solar-Terrestrial Physics*, 73(2): 348 – 355, 2011. ISSN 1364-6826. doi: https://doi.org/10.1016/j.jastp.2010.02.011. URL http://www.sciencedirect.com/science/article/pii/S1364682610000593. Space Climate.

[244] JG Anet, EV Rozanov, Stefan Muthers, T Peter, Stefan Brönnimann, F Arfeuille, J Beer, AI Shapiro, CC Raible, F Steinhilber, et al. Impact of a potential 21st century "grand solar minimum" on surface temperatures and stratospheric ozone. *Geophysical Research Letters*, 40(16):4420–4425, 2013.

[245] Eugene V Rozanov, Tatiana A Egorova, Alexander I Shapiro, and Werner K Schmutz. Modeling of the atmospheric response to a strong decrease of the solar activity. *Proceedings of the International Astronomical Union*, 7(S286):215–224, 2011.

[246] Irina A Mironova, Karen L Aplin, Frank Arnold, Galina A Bazilevskaya, R Giles Harrison, Alexei A Krivolutsky, Keri A Nicoll, Eugene V Rozanov, Esa Turunen, and Ilya G Usoskin. Energetic particle influence on the earth's atmosphere. *Space Science Reviews*, 194(1-4):1–96, 2015.

[247] HS Porter, CH Jackman, and AES Green. Efficiencies for production of atomic nitrogen and oxygen by relativistic proton impact in air. *The Journal of Chemical Physics*, 65(1):154–167, 1976.

[248] Susan Solomon and Paul J Crutzen. Analysis of the august 1972 solar proton event including chlorine chemistry. *Journal of Geophysical Research: Oceans*, 86(C2):1140–1146, 1981.

[249] M Sinnhuber, H Nieder, and N Wieters. Energetic particle precipitation and the chemistry of the mesosphere/lower thermosphere. *Surveys in Geophysics*, 33(6):1281–1334, 2012.

[250] S Solomon, DW Rusch, Jean-Claude Gérard, GC Reid, and PJ Crutzen. The effect of particle precipitation events on the neutral and ion chemistry of the middle atmosphere: Ii. odd hydrogen. *Planetary and Space Science*, 29(8):885–893, 1981.

[251] T Egorova, E Rozanov, Y Ozolin, A Shapiro, M Calisto, Th Peter, and W Schmutz. The atmospheric effects of october 2003 solar proton event simulated with the chemistry–climate model socol using complete and parameterized ion chemistry. *Journal of Atmospheric and Solar-Terrestrial Physics*, 73(2):356–365, 2011.

[252] LH Weeks, RS Cuikay, and JR Corbin. Ozone measurements in the mesosphere during the solar proton event of 2 november 1969. *Journal of the Atmospheric Sciences*, 29(6):1138–1142, 1972.

[253] Leonty Miroshnichenko. *Solar Cosmic Rays: Fundamentals and Applications*. Springer, 2015.

[254] Donald F Heath, Arlin J Krueger, and Paul J Crutzen. Solar proton event: Influence on stratospheric ozone. *Science*, 197(4306):886–889, 1977.

[255] Arseniy Karagodin, Irina Mironova, Anton Artamonov, and Natalia Konstantinova. Response of the total ozone to energetic electron precipitation events. *Journal of Atmospheric and Solar-Terrestrial Physics*, 2017.

[256] Linwood B Callis and Murali Natarajan. Ozone and nitrogen dioxide changes in the stratosphere during 1979–84. *Nature*, 323(6091):772–777, 1986.

[257] E Rozanov, M Calisto, T Egorova, T Peter, and W Schmutz. Influence of the precipitating energetic particles on atmospheric chemistry and climate. *Surveys in geophysics*, 33(3-4):483–501, 2012.

[258] Alessandro Damiani, Bernd Funke, Manuel López Puertas, Michelle L Santee, Raul R Cordero, and Shingo Watanabe. Energetic particle precipitation: A major driver of the ozone budget in the antarctic upper stratosphere. *Geophysical Research Letters*, 43(7):3554–3562, 2016.

[259] MH Denton, R Kivi, T Ulich, CJ Rodger, MA Clilverd, RB Horne, and AJ Kavanagh. Solar proton events and stratospheric ozone depletion over northern finland. *Journal of Atmospheric and Solar-Terrestrial Physics*, 2017.

[260] CE Randall, VL Harvey, GL Manney, Y Orsolini, M Codrescu, C Sioris, Samuel Brohede, CS Haley, LL Gordley, JM Zawodny, et al. Stratospheric effects of energetic particle precipitation in 2003–2004. *Geophysical Research Letters*, 32(5), 2005.

[261] Charles H Jackman, Eric L Fleming, and Francis M Vitt. Influence of extremely large solar proton events in a changing stratosphere. *Journal of Geophysical Research: Atmospheres*, 105 (D9):11659–11670, 2000.

[262] Katharina Meraner and Hauke Schmidt. Climate impact of idealized winter polar mesospheric and stratospheric ozone losses as caused by energetic particle precipitation. *Atmospheric Chemistry and Physics*, 18(2):1079–1089, 2018.

[263] ME Andersson, PT Verronen, DR Marsh, A Seppälä, S-M Päivärinta, CJ Rodger, MA Clilverd, N Kalakoski, and M van de Kamp. Polar ozone response to energetic particle precipitation over decadal time scales: the role of medium-energy electrons. *Journal of Geophysical Research: Atmospheres*.

[264] Brian C Thomas, Charles H Jackman, and Adrian L Melott. Modeling atmospheric effects of the september 1859 solar flare. *Geophysical research letters*, 34(6), 2007.

[265] Takuya Shibayama, Hiroyuki Maehara, Shota Notsu, Yuta Notsu, Takashi Nagao, Satoshi Honda, Takako T Ishii, Daisaku Nogami, and Kazunari Shibata. Superflares on solar-type stars observed with kepler. i. statistical properties of superflares. *The Astrophysical Journal Supplement Series*, 209(1):5, 2013.

[266] Manasvi Lingam and Abraham Loeb. Risks for life on habitable planets from superflares of their host stars. *The Astrophysical Journal*, 848(1):41, 2017.

[267] Alexander A Pavlov, Anatoli K Pavlov, Michael J Mills, Valery M Ostryakov, Gennadiy I Vasilyev, and Owen B Toon. Catastrophic ozone loss during passage of the solar system through an interstellar cloud. *Geophysical research letters*, 32(1), 2005.

[268] RJ Talbot Jr and MJ Newman. Encounters between stars and dense interstellar clouds. *The Astrophysical Journal Supplement Series*, 34:295–308, 1977.

[269] Steven C Cande and Dennis V Kent. Revised calibration of the geomagnetic polarity timescale for the late cretaceous and cenozoic. *Journal of Geophysical Research: Solid Earth*, 100(B4):6093–6095, 1995.

[270] MJ Beharrell, Farideh Honary, Craig J Rodger, and Mark A Clilverd. Substorm-induced energetic electron precipitation: Morphology and prediction. *Journal of Geophysical Research: Space Physics*, 120(4):2993–3008, 2015.

[271] A Seppälä, Mark A Clilverd, Mathew James Beharrell, Craig J Rodger, PT Verronen, ME Andersson, and DA Newnham. Substorm-induced energetic electron precipitation: Impact on atmospheric chemistry. *Geophysical Research Letters*, 42(19):8172–8176, 2015.

[272] Neil Gehrels, Claude M Laird, Charles H Jackman, John K Cannizzo, Barbara J Mattson, and Wan Chen. Ozone depletion from nearby supernovae. *The Astrophysical Journal*, 585(2): 1169, 2003.

[273] John Ellis, Brian D Fields, and David N Schramm. Geological isotope anomalies as signatures of nearby supernovae. *arXiv preprint astro-ph/9605128*, 1996.

[274] SE Thorsett. Terrestrial implications of cosmological gamma-ray burst models. *arXiv preprint astro-ph/9501019*, 1995.

[275] AM Soderberg, SR Kulkarni, E Berger, DW Fox, M Sako, DA Frail, A Gal-Yam, DS Moon, SB Cenko, SA Yost, et al. The sub-energetic γ-ray burst grb 031203 as a cosmic analogue to the nearby grb 980425. *Nature*, 430(7000):648–650, 2004.

[276] Douglas Galante and Jorge Ernesto Horvath. Biological effects of gamma-ray bursts: distances for severe damage on the biota. *International Journal of Astrobiology*, 6(1):19–26, 2007.

[277] Adrian L Melott, Brian C Thomas, Daniel P Hogan, Larissa M Ejzak, and Charles H Jackman. Climatic and biogeochemical effects of a galactic gamma ray burst. *Geophysical research letters*, 32(14), 2005.

[278] Tsvi Piran and Raul Jimenez. Possible role of gamma ray bursts on life extinction in the universe. *Physical review letters*, 113(23):231102, 2014.

[279] Adrian L Melott, Bruce S Lieberman, Claude M Laird, Larry D Martin, Mikhail V Medvedev, Brian C Thomas, JK Cannizzo, Neil Gehrels, and CH Jackman. Did a gamma-ray burst initiate the late ordovician mass extinction? *International Journal of Astrobiology*, 3 (1):55–61, 2004.

[280] Brian C Thomas and Adrian L Melott. Gamma-ray bursts and terrestrial planetary atmospheres. *New Journal of Physics*, 8(7):120, 2006.

[281] Malvin A Ruderman. Possible consequences of nearby supernova explosions for atmospheric ozone and terrestrial life. *Science*, 184(4141):1079–1081, 1974.

[282] Paul J Crutzen and Christoph Brühl. Mass extinctions and supernova explosions. *Proceedings of the National Academy of Sciences*, 93(4):1582–1584, 1996.

[283] JW Tukey, M Alexander, HS Bennett, NC Brady, JC Calhoun Jr, JC Geyer, AJ Haagen-Smit, N Hackerman, JB Hartgering, D Pimentel, et al. Restoring the quality of our environment. *Report of the environmental pollution panel, President's Science Advisory Committee, The White House*, 1965.

[284] Wallace S Broecker. Climatic change: Are we on the brink of a pronounced global warming? *Science*, 189:460–463, 1975.

[285] Stephen H Schneider. On the carbon dioxide–climate confusion. *Journal of the Atmospheric Sciences*, 32(11):2060–2066, 1975.

[286] Stephen H Schneider and Roger D Dennett. Climatic barriers to long-term energy growth. *Ambio*, pages 65–74, 1975.

[287] James Hansen, Donald Johnson, Andrew Lacis, Sergej Lebedeff, Pius Lee, David Rind, and Gary Russell. Climate impact of increasing atmospheric carbon dioxide. *Science*, 213(4511): 957–966, 1981.

[288] National Research Council (US). Committee on Atmospheric Sciences. *Weather and climate modification problems and prospects: final report of the Panel on Weather and Climate Modification*. National Academies, 1966.

[289] Robert A McCormick and John H Ludwig. Climate modification by atmospheric aerosols. *Science*, 156(3780):1358–1359, 1967.

[290] Cesare Marchetti. On geoengineering and the co_2 problem. *Climatic change*, 1(1):59–68, 1977.

[291] James E Hansen, Wei-Chyung Wang, and Andrew A Lacis. Mount agung eruption provides test of a global climatic perturbation. *Science*, 199(4333):1065–1068, 1978.

[292] Stephen Self, Michael R Rampino, and James J Barbera. The possible effects of large 19th and 20th century volcanic eruptions on zonal and hemispheric surface temperatures. *Journal of Volcanology and Geothermal Research*, 11(1):41–60, 1981.

[293] Michael R Rampino, Stephen Self, and Richard B Stothers. Volcanic winters. *Annual Review of Earth and Planetary Sciences*, 16(1):73–99, 1988.

[294] Stephen Self, Jing-Xia Zhao, Rick E Holasek, Ronnie C Torres, and Alan J King. The atmospheric impact of the 1991 mount pinatubo eruption. *Fire and Mud*, 1993.

[295] Mikhail I Budyko. On present-day climatic changes. *Tellus*, 29(3):193–204, 1977.

[296] Mikhail Ivanovich Budyko. *The earth's climate: past and future*. New York, NY (USA) Academic Press, 1982.

[297] Richard D Cadle, Paul Crutzen, and Dieter Ehhalt. Heterogeneous chemical reactions in the stratosphere. *Journal of Geophysical Research*, 80(24):3381–3385, 1975.

[298] SA McKeen, SC Liu, and CS Kiang. On the chemistry of stratospheric so2 from volcanic eruptions. *Journal of Geophysical Research: Atmospheres*, 89(D3):4873–4881, 1984.

[299] David J Hofmann and Susan Solomon. Ozone destruction through heterogeneous chemistry following the eruption of el chichon. *Journal of Geophysical Research: Atmospheres*, 94(D4): 5029–5041, 1989.

[300] F Arnold, Th Bührke, and S Qiu. Evidence for stratospheric ozone-depleting heterogeneous chemistry on volcanic aerosols from el chichón. *Nature*, 348(6296):49–50, 1990.

[301] Robert T Watson, Marufu C Zinyowera, and Richard H Moss. *Climate change 1995. Impacts, adaptations and mitigation of climate change: Scientific-technical analyses*. 1996.

[302] David W Keith. Geoengineering the climate: History and prospect. *Annual review of energy and the environment*, 25(1):245–284, 2000.

[303] Edward Teller, Lowell Wood, and Roderick Hyde. Global warming and ice ages: I. prospects for physics based modulation of global change. Technical report, Lawrence Livermore National Lab., CA (United States), 1996.

[304] K Caldeira, G Caravan, B Govindasamy, A Grossman, R Hyde, M Ishikawa, A Ledebuhr, C Leith, C Molenkamp, E Teller, et al. Long-range weather prediction and prevention of climate catastrophes: A status report. Technical report, Lawrence Livermore National Lab., CA (US), 1999.

[305] David W Keith, Debra K Weisenstein, John A Dykema, and Frank N Keutsch. Stratospheric solar geoengineering without ozone loss. *Proceedings of the National Academy of Sciences*, 113(52):14910–14914, 2016.

[306] Scott Barrett. The incredible economics of geoengineering. *Environmental and resource economics*, 39(1):45–54, 2008.

[307] David G Victor. On the regulation of geoengineering. *Oxford Review of Economic Policy*, 24 (2):322–336, 2008.

[308] Philip W Boyd. Geopolitics of geoengineering. *Nature Geoscience*, 2(12):812–812, 2009.

[309] Martin Bunzl. Researching geoengineering: should not or could not? *Environmental Research Letters*, 4(4):045104, 2009.

[310] Stephen Gardiner. Is' arming the future'with geoengineering really the lesser evil? some doubts about the ethics of intentionally manipulating the climate system. 2009.

[311] Stephen M Gardiner. Some early ethics of geoengineering the climate: a commentary on the values of the royal society report. *Environmental Values*, 20(2):163–188, 2011.

[312] Marlos Goes, Nancy Tuana, and Klaus Keller. The economics (or lack thereof) of aerosol geoengineering. *Climatic change*, 109(3-4):719–744, 2011.

[313] Alexander Proelss. Geoengineering and international law. *Sicherheit und Frieden (S+F)/Security and Peace*, pages 205–211, 2012.

[314] Dane Scott. Geoengineering and environmental ethics. *Nature Education Knowledge*, 3(10): 10, 2012.

[315] Peer Johannes Nowack, Nathan Luke Abraham, Peter Braesicke, and John Adrian Pyle. Stratospheric ozone changes under solar geoengineering: implications for uv exposure and air quality. *Atmospheric Chemistry and Physics*, 16(6):4191–4203, 2016.

[316] Harold Johnston. Reduction of stratospheric ozone by nitrogen oxide catalysts from supersonic transport exhaust. *Science*, 173(3996):517–522, 1971.

[317] Paul J Crutzen. Ozone production rates in an oxygen-hydrogen-nitrogen oxide atmosphere. *Journal of Geophysical Research*, 76(30):7311–7327, 1971.

[318] Paul J. Crutzen. SST's: A threat to the Earth's ozone shield. *Ambio*, 1(2):41–51, 1972. ISSN 00447447, 16547209.

[319] Halstead Harrison. Stratospheric ozone with added water vapor: influence of high-altitude aircraft. *Science*, 170(3959):734–736, 1970.

[320] P. J. Crutzen. The influence of nitrogen oxides on the atmospheric ozone content. *Quarterly Journal of the Royal Meteorological Society*, 96(408):320–325, 1970. ISSN 1477-870X. doi: 10.1002/qj.49709640815.

[321] Michael B McElroy and John C McConnell. Nitrous oxide: A natural source of stratospheric NO. *Journal of the Atmospheric Sciences*, 28(6):1095–1098, 1971.

[322] Francis S. Johnson. Ozone and SSTs. *Biological Conservation*, 4(3):220 – 222, 1972. ISSN 0006-3207. doi: http://dx.doi.org/10.1016/0006-3207(72)90175-9.

[323] Paul Crutzen. A discussion of the chemistry of some minor constituents in the stratosphere and troposphere. *Pure and Applied Geophysics*, 106(1):1385–1399, 1973.

[324] John C McConnell and Michael B McElroy. Odd nitrogen in the atmosphere. *Journal of the Atmospheric Sciences*, 30(8):1465–1480, 1973.

[325] Michael B McElroy, Steven C Wofsy, Joyce E Penner, and John C McConnell. Atmospheric ozone: Possible impact of stratospheric aviation. *Journal of the atmospheric sciences*, 31(1): 287–304, 1974.

[326] Harold S Johnston, Douglas E Kinnison, and Donald J Wuebbles. Nitrogen oxides from high-altitude aircraft: An update of potential effects on ozone. *Journal of Geophysical Research: Atmospheres*, 94(D13):16351–16363, 1989.

[327] Donald J Wuebbles and Douglas E Kinnison. Sensitivity of stratospheric ozone to present and possible future aircraft emissions. In *Air Traffic and the Environment—Background, Tendencies and Potential Global Atmospheric Effects*, pages 107–123. Springer, 1990.

[328] Harold S Johnston. Atmospheric ozone. *Annual review of physical chemistry*, 43(1):1–31, 1992.

[329] Harold S Johnston, Michael John Prather, and RT Watson. The atmospheric effects of stratospheric aircraft: A topical review. 1991.

[330] Yicheng Sun and Howard Smith. Review and prospect of supersonic business jet design. *Progress in Aerospace Sciences*, 2016.

[331] Michelle Ruiz. 3-hour supersonic flights from new york to london are just around the corner. *NYmag.com*, December 2016.

[332] Volker Grewe, Martin Plohr, G Cerino, M Di Muzio, Yann Deremaux, M Galerneau, P de Saint Martin, T Chaika, A Hasselrot, Ulf Tengzelius, et al. Estimates of the climate impact of future small-scale supersonic transport aircraft–results from the hisac eu-project. *The Aeronautical Journal*, 114(1153):199–206, 2010.

[333] S Baughcum, IC Plumb, and PF Vohralik. Stratospheric ozone sensitivity to aircraft cruise altitudes and nox emissions. In *Proceedings of the AAC-Conference*, volume 30, 2003.

[334] S Randolph Kawa, James G Anderson, Steven L Baughcum, Charles A Brock, William H Brune, Ronald C Cohen, Douglas E Kinnison, Paul A Newman, Jose M Rodriguez, Richard S Stolarski, et al. Assessment of the effects of high-speed aircraft in the stratosphere: 1998. 1999.

[335] DE Kinnison, PS Connell, JM Rodriguez, DA Rotman, DB Considine, J Tannahill, R Ramaroson, PJ Rasch, AR Douglass, SL Baughcum, et al. The global modeling initiative assessment model: Application to high-speed civil transport perturbation. *Journal of Geophysical Research: Atmospheres*, 106(D2):1693–1711, 2001.

[336] Debra K Weisenstein, Malcolm KW Ko, Igor G Dyominov, Giovanni Pitari, Lucrezia Ricciardulli, Guido Visconti, and Slimane Bekki. The effects of sulfur emissions from hsct aircraft: A 2-d model intercomparison. *Journal of Geophysical Research: Atmospheres*, 103(D1):1527–1547, 1998.

[337] Chowen Wey, M Dutta, K Patten, and D Wuebbles. Parametric analyses of potential effects on stratospheric and tropospheric ozone chemistry by a fleet of supersonic business jets projected in a 2020 atmosphere. 2004.

[338] Volker Grewe, Lisa Bock, Ulrike Burkhardt, Katrin Dahlmann, Klaus Martin Gierens, Ludwig Hüttenhofer, Simon Unterstrasser, Arvind Rao, Abhishek Bhat, Feijia Yin, et al. Assessing the climate impact of the ahead multi-fuel blended wing body. *Meteorologische Zeitschrift*, pages 1–15, 2016.

[339] DS Lee, Giovanni Pitari, Volker Grewe, K Gierens, JE Penner, A Petzold, MJ Prather, U Schumann, A Bais, T Berntsen, et al. Transport impacts on atmosphere and climate: Aviation. *Atmospheric Environment*, 44(37):4678–4734, 2010.

[340] Martin Ross. Local effects of solid rocket motor exhaust on stratospheric ozone. *Journal of spacecraft and rockets*, 33(1):144–153, 1996.

[341] MN Ross, JR Benbrook, WR Sheldon, Paul F Zittel, and DL McKenzie. Observation of stratospheric ozone depletion in rocket exhaust plumes. *Nature*, 390(6655):62–64, 1997.

[342] MN Ross, JO Ballenthin, RB Gosselin, RF Meads, PF Zittel, JR Benbrook, and WR Sheldon. In-situ measurement of cl2 and o3 in a stratospheric solid rocket motor exhaust plume. *Geophysical research letters*, 24(14):1755–1758, 1997.

[343] Martin N Ross, Philip D Whitefield, Donald E Hagen, and Alfred R Hopkins. In situ measurement of the aerosol size distribution in stratospheric solid rocket motor exhaust plumes. *Geophysical research letters*, 26(7):819–822, 1999.

[344] Martin N Ross, Darin W Toohey, WT Rawlins, EC Richard, KK Kelly, AF Tuck, MH Proffitt, Donald E Hagen, Alfred R Hopkins, Philip D Whitefield, et al. Observation of stratospheric ozone depletion associated with delta ii rocket emissions. *Geophysical research letters*, 27(15):2209–2212, 2000.

[345] DJ Cziczo, DM Murphy, DS Thomson, and MN Ross. Composition of individual particles in the wakes of an athena ii rocket and the space shuttle. *Geophysical research letters*, 29(21), 2002.

[346] Michael Y Danilin, Malcolm KW Ko, and Debra K Weisenstein. Global implications of ozone loss in a space shuttle wake. *Journal of Geophysical Research: Atmospheres*, 106(D4): 3591–3601, 2001.

[347] Martin Ross, Michael Mills, and Darin Toohey. Potential climate impact of black carbon emitted by rockets. *Geophysical Research Letters*, 37(24), 2010.

[348] Christiane Voigt, Ulrich Schumann, Kaspar Graf, and Klaus-Dirk Gottschaldt. Impact of rocket exhaust plumes on atmospheric composition and climate–an overview. *EUCASS Proceedings Series–Advances in Aerospace Sciences*, 4:657–670, 2013.

[349] Erik JL Larson, Robert W Portmann, Karen H Rosenlof, David W Fahey, John S Daniel, and Martin N Ross. Global atmospheric response to emissions from a proposed reusable space launch system. *Earth's Future*, 5(1):37–48, 2017.

[350] Henry M Foley and Malvin A Ruderman. Stratospheric no production from past nuclear explosions. *Journal of Geophysical Research*, 78(21):4441–4450, 1973.

[351] Forrest R Gilmore. The production of nitrogen oxides by low-altitude nuclear explosions. *Journal of Geophysical Research*, 80(33):4553–4554, 1975.

[352] Paul J Crutzen, Ian E Galbally, and Christoph Brühl. Atmospheric effects from post-nuclear fires. *Climatic Change*, 6(4):323–364, 1984.

[353] John Hampson. Photochemical war on the atmosphere. *Nature*, 250(5463):189–191, 1974.

[354] Harold Johnston, Gary Whitten, and John Birks. Effect of nuclear explosions on stratospheric nitric oxide and ozone. *Journal of geophysical research*, 78(27):6107–6135, 1973.

[355] Alan Robock, Luke Oman, Georgiy L Stenchikov, Owen B Toon, Charles Bardeen, and Richard P Turco. Climatic consequences of regional nuclear conflicts. *Atmospheric Chemistry and Physics*, 7(8):2003–2012, 2007.

[356] Michael J Mills, Owen B Toon, Julia Lee-Taylor, and Alan Robock. Multidecadal global cooling and unprecedented ozone loss following a regional nuclear conflict. *Earth's Future*, 2 (4):161–176, 2014.

[357] Lili Xia and Alan Robock. Impacts of a nuclear war in south asia on rice production in mainland china. *Climatic Change*, 116(2):357–372, 2013.

[358] Lili Xia, Alan Robock, Michael Mills, Andrea Stenke, and Ira Helfand. Decadal reduction of chinese agriculture after a regional nuclear war. *Earth's Future*, 3(2):37–48, 2015.

[359] Michael J Mills, Owen B Toon, Richard P Turco, Douglas E Kinnison, and Rolando R Garcia. Massive global ozone loss predicted following regional nuclear conflict. *Proceedings of the National Academy of Sciences*, 105(14):5307–5312, 2008.

[360] Andrea Stenke, CR Hoyle, B Luo, E Rozanov, J Gröbner, L Maag, Stefan Brönnimann, and T Peter. Climate and chemistry effects of a regional scale nuclear conflict. *Atmospheric chemistry and physics*, 13(19):9713–9729, 2013.

[361] Sharon L. Roan. *Ozone Crisis*. John Wiley& Sons, 605 Third Avenue, New York City, 1990.

[362] Mario J Molina and F. Sherwood Rowland. Stratospheric sink for chlorofluoromethanes: chlorine atom-catalysed destruction of ozone. *Nature*, 249(28):810–812, 1974.

[363] F. S. Rowland and Mario J. Molina. Chlorofluoromethanes in the environment. *Reviews of Geophysics*, 13(1):1–35, 1975. ISSN 1944-9208. doi: 10.1029/RG013i001p00001.

[364] John Hampson. *Photochemical behaviour of the ozone layer*. Canadian Armament Research and Development Establishment, 1964.

[365] Barrie. G. Hunt. Photochemistry of ozone in a moist atmosphere. *Journal of Geophysical Research*, 71(5):1385–1398, 1966. ISSN 2156-2202. doi: 10.1029/JZ071i005p01385.

[366] Halstead Harrison. Boeing adventures, with digressions. http://www.atmos.washington.edu/ harrison/reports/b2707.pdf; archived at http://archive.is/auQtL, March 2003.

[367] J. E. McDonald. Congressional record S3904, 12 March. *Record of the 92nd Congress of the United States of America*, 1971.

[368] Ronald GW Norrish and George HJ Neville. The decomposition of ozone photosensitised by chlorine. *Journal of the Chemical Society*, pages 1864–1872, 1934.

[369] Steven C Wofsy and Michael B McElroy. HOx, NOx, and ClOx: Their role in atmospheric photochemistry. *Canadian Journal of Chemistry*, 52(8):1582–1591, 1974.

[370] Richard S Stolarski and Ralph J Cicerone. Stratospheric chlorine: a possible sink for ozone. *Canadian journal of Chemistry*, 52(8):1610–1615, 1974.

[371] R. J. Cicerone, D. H. Stedman, R. S. Stolarski, A. N. Dingle, and R. A. Cellarius. Assessment of possible environmental effects of space shuttle operations. *NASA Contractor Report CR-129003*, 1973.

[372] Paul Crutzen. A review of upper atmospheric photochemistry. *Canadian Journal of Chemistry*, 52(8):1569–1581, 1974.

[373] H Hoshizaki, JW Meyer, and KO Redler. Study of high altitude aircraft wake dynamics, Interim Report, Task VII: Problem definition advanced aircraft and fuels, Section 4: Potential destruction of ozone by HCl in rocket exhausts. *Report LMSCD354204, Lockheed, Palo Alto, CA*, 1973.

[374] James E Lovelock. Atmospheric fluorine compounds as indicators of air movements. *Nature*, 230(5293):379–379, 1971.

[375] James E Lovelock, RJ Maggs, and RJ Wade. Halogenated hydrocarbons in and over the atlantic. *Nature*, 241(5386):194–196, 1973.

[376] DA Armstrong and JL Holmes. Decomposition of halides and derivatives. *Comprehensive Chemical Kinetics*, 4:143–195, 1972.

[377] KF Preston and RJ Cvetanovlć. The decomposition of inorganic oxides and sulphides. *Comprehensive Chemical Kinetics*, 4:47–141, 1972.

[378] JN Pitts, HL Sandoval, and R Atkinson. Relative rate constants for the reaction of O(1D) atoms with fluorocarbons and n2o. *Chemical Physics Letters*, 29(1):31–34, 1974.

[379] HL Sandoval, R Atkinson, and JN Pitts. Reactions of electronically excited O(1D) atoms with fluorocarbons. *Journal of Photochemistry*, 3(2):325–327, 1974.

[380] R Atkinson, DA Hansen, and JN Pitts Jr. Rate constants for the reaction of OH radicals with CHF2Cl, CF2Cl2, CFCl3, and H2 over the temperature range 297–434° k. *The Journal of Chemical Physics*, 63(5):1703–1706, 1975.

[381] R.K.M. Jayanty, R. Simonaitis, and Julian Heicklen. The photolysis of chlorofluoromethanes in the presence of O2 or O3 at 213.9 nm and their reactions with O(1D). *Journal of Photochemistry*, 4(5):381 – 398, 1975. ISSN 0047-2670. doi: http://dx.doi.org/10.1016/0047-2670(75)85020-9.

[382] Mario J Molina and FS Rowland. Some unmeasured chlorine atom reaction rates important for stratospheric modeling of atom catalyzed removal of ozone. *The Journal of Physical Chemistry*, 79(6):667–669, 1975.

[383] Richard Milstein and F Rowland. Quantum yield for the photolysis of CF2Cl2 in O2. *The Journal of Physical Chemistry*, 79(6):669–670, 1975.

[384] R Atkinson, GM Breuer, JN Pitts, and HL Sandoval. Tropospheric and stratospheric sinks for halocarbons: photooxidation, O(1D) atom, and OH radical reactions. *Journal of Geophysical Research*, 81(33):5765–5770, 1976.

[385] J. A. Ryan and N. R. Mukherjee. Sources of stratospheric gaseous chlorine. *Reviews of Geophysics*, 13(5):650–658, 1975. ISSN 1944-9208. doi: 10.1029/RG013i005p00650.

[386] Mario J. Molina and F. S. Rowland. Predicted present stratospheric abundances of chlorine species from photodissociation of carbon tetrachloride. *Geophysical Research Letters*, 1(7):309–312, 1974. ISSN 1944-8007. doi: 10.1029/GL001i007p00309.

[387] James E Lovelock. Atmospheric halocarbons and stratospheric ozone. *Nature*, 252:292–294, 1974.

[388] FS Rowland, Mario J Molina, and CC Chou. Natural halocarbons in air and sea. *Nature*, 258 (5537):775–776, 1975.

[389] JE Lovelock. Natural halocarbons in the air and in the sea. *Nature*, 256(5514):193–194, 1975.

[390] R. J. Cicerone, D. H. Stedman, and R. S. Stolarski. Estimate of late 1974 stratospheric concentration of gaseous chlorine compounds (ClX). *Geophysical Research Letters*, 2(6):219–222, 1975. ISSN 1944-8007. doi: 10.1029/GL002i006p00219.

[391] Yuk Ling Yung, Michael B. McElroy, and Steven C. Wofsy. Atmospheric halocarbons: A discussion with emphasis on chloroform. *Geophysical Research Letters*, 2(9):397–399, 1975. ISSN 1944-8007. doi: 10.1029/GL002i009p00397.

[392] RT Watson. Chemical kinetics data survey viii. *Rate Constants of C10 of Atmospheric Interest. NBSIR74-516, National Bureau of Standards, Washington, DC*, 1974.

[393] Ralph J Cicerone, Richard S Stolarski, and Stacy Walters. Stratospheric ozone destruction by man-made chlorofluoromethanes. *Science*, 185(4157):1165–1167, 1974.

[394] Paul J. Crutzen. Estimates of possible variations in total ozone due to natural causes and human activities. *Ambio*, 3(6):201–210, 1974. ISSN 00447447, 16547209.

[395] R P Turco and RC Whitten. Chlorofluoromethanes in the stratosphere and some possible consequences for ozone. *Atmospheric Environment (1967)*, 9(12):1045–1061, 1975.

[396] Harold S Johnston. Pollution of the stratosphere. *Annual Review of Physical Chemistry*, 26 (1):315–338, 1975.

[397] Paul J. Crutzen, Ivar S. A. Isaksen, and John R. McAfee. The impact of the chlorocarbon industry on the ozone layer. *Journal of Geophysical Research: Oceans*, 83(C1):345–363, 1978. ISSN 2156-2202. doi: 10.1029/JC083iC01p00345.

[398] Du Pont. You want the ozone question answered one way or the other. so does Du Pont. *Science*, 190(4209):8–9.

[399] FS Rowland and Mario J Molina. The ozone question. *Science*, 190(4219):1038–1040, 1975.

[400] George Alexander. On the trail of ozone culprit: USC physicist may have detected 'suspect'. *Los Angeles Times*, 23, February 1976.

[401] *General program of the eighth Philadelphia meeting; the 143rd meeting of the Association.* AAAS, [New York], 1976.

[402] Robert W. Carlson. personal communication.

[403] JG Anderson, JJ Margitan, and DH Stedman. Atomic chlorine and the chlorine monoxide radical in the stratosphere: Three in situ observations. *Science*, 198(4316):501–503, 1977.

[404] JG Anderson, HJ Grassl, RE Shetter, and JJ Margitan. Stratospheric free chlorine measured by balloon-borne in situ resonance fluorescence. *Journal of Geophysical Research: Oceans*, 85 (C5):2869–2887, 1980.

[405] *Title 21 §2.125*. 2017.

[406] National Research Council et al. *Halocarbons, Effects on Stratospheric Ozone*. National Academies, 1976.

[407] National Research Council (US). Panel on Stratospheric Chemistry, Assembly of Mathematical, and Physical Sciences (US). Committee on Impacts of Stratospheric Change. *Stratospheric ozone depletion by halocarbons: Chemistry and transport*. National Academies, 1979.

[408] Environmental Studies Board, National Research Council, et al. *Causes and effects of stratospheric ozone reduction: an update*. National Academies Press, 1982.

[409] National Research Council et al. Causes and effects of changes in stratospheric ozone: update 1983. *Update*, pages 101–110, 1984.

[410] James K Hammitt, Kathleen A Wolf, Frank Camm, William E Mooz, Timothy H Quinn, and Anil Bamezai. Product uses and market trends for potential ozone-depleting substances, 1985-2000. 1986.

[411] JC Farman, BG Gardiner, and JD Shanklin. Large losses of total ozone in antarctica reveal seasonal clox/nox interaction. *Nature*, 315(6016):207–210, 1985.

[412] Arthur P Cracknell. Climate change—the background. In *Remote Sensing and Global Climate Change*, pages 1–33. Springer, 1994.

[413] Richard S Stolarski, Arlin J Krueger, Mark R Schoeberl, Richard D McPeters, Patricia A Newman, and JC Alpert. Nimbus 7 satellite measurements of the springtime antarctic ozone decrease. *Nature*, 322(6082):808–811, 1986.

[414] Ka-Kit Tung, Malcolm KW Ko, José M Rodriguez, and Nien Dak Sze. Are antarctic ozone variations a manifestation of dynamics or chemistry? *Nature*, 322(6082):811–814, 1986.

[415] Michael B McElroy, Ross J Salawitch, Steven C Wofsy, and Jennifer A Logan. Reductions of antarctic ozone due to synergistic interactions of chlorine and bromine. *Nature*, 321(6072): 759–762, 1986.

[416] Mario J Molina, Tai-Ly Tso, Luisa T Molina, and Frank C-Y Wang. Antarctic stratospheric chemistry of chlorine nitrate, hydrogen chloride, and ice: release of active chlorine. *Science*, 238(4831):1253–1257, 1987.

[417] James G Anderson, William H Brune, and Michael H Proffitt. Ozone destruction by chlorine radicals within the antarctic vortex: The spatial and temporal evolution of clo-o3 anticorrelation based on in situ er-2 data. *Journal of Geophysical Research: Atmospheres*, 94(D9): 11465–11479, 1989.

[418] Olaf Morgenstern, Peter Braesicke, Margaret M Hurwitz, Fiona M O'Connor, Andrew C Bushell, Colin E Johnson, and John A Pyle. The world avoided by the montreal protocol. *Geophysical Research Letters*, 35(16), 2008.

[419] PA Newman, LD Oman, AR Douglass, EL Fleming, SM Frith, MM Hurwitz, SR Kawa, CH Jackman, NA Krotkov, ER Nash, et al. What would have happened to the ozone layer if chlorofluorocarbons (cfcs) had not been regulated? *Atmospheric Chemistry and Physics*, 9(6): 2113–2128, 2009.

[420] Martyn P Chipperfield, SS Dhomse, W Feng, RL McKenzie, GJM Velders, and JA Pyle. Quantifying the ozone and ultraviolet benefits already achieved by the montreal protocol. *Nature communications*, 6, 2015.

[421] Rolando R Garcia, Douglas E Kinnison, and Daniel R Marsh. "world avoided" simulations with the whole atmosphere community climate model. *Journal of Geophysical Research: Atmospheres*, 117(D23), 2012.

[422] T Egorova, E Rozanov, J Gröbner, M Hauser, and W Schmutz. Montreal protocol benefits simulated with ccm socol. *Atmospheric Chemistry and Physics*, 13(7):3811–3823, 2013.

[423] JS Daniel, S Solomon, RW Portmann, and RR Garcia. Stratospheric ozone destruction: The importance of bromine relative to chlorine. *Journal of Geophysical Research: Atmospheres*, 104(D19):23871–23880, 1999.

[424] David P Schneider, Caspar M Ammann, Bette L Otto-Bliesner, and Darrell S Kaufman. Climate response to large, high-latitude and low-latitude volcanic eruptions in the community climate system model. *Journal of Geophysical Research: Atmospheres*, 114(D15), 2009.

[425] Morgan B Yarker, Debasish PaiMazumder, Catherine F Cahill, Jonathan Dehn, Anupma Prakash, Nicole Mölders, et al. Theoretical investigations on potential impacts of high-latitude volcanic emissions of heat, aerosols and water vapor and their interactions on clouds and precipitation. *The Open Atmospheric Science Journal*, 4:24–44, 2010.

[426] Ben Kravitz and Alan Robock. Climate effects of high-latitude volcanic eruptions: Role of the time of year. *Journal of Geophysical Research: Atmospheres*, 116(D1), 2011.

[427] Francesco SR Pausata, Leon Chafik, Rodrigo Caballero, and David S Battisti. Impacts of high-latitude volcanic eruptions on enso and amoc. *Proceedings of the National Academy of Sciences*, 112(45):13784–13788, 2015.

[428] Francesco SR Pausata, Alf Grini, Rodrigo Caballero, Abdel Hannachi, and Øyvind Seland. High-latitude volcanic eruptions in the norwegian earth system model: the effect of different initial conditions and of the ensemble size. *Tellus B: Chemical and Physical Meteorology*, 67 (1):26728, 2015.

[429] Francesco SR Pausata, Christina Karamperidou, Rodrigo Caballero, and David S Battisti. Enso response to high-latitude volcanic eruptions in the northern hemisphere: The role of the initial conditions. *Geophysical Research Letters*, 43(16):8694–8702, 2016.

[430] C Timmreck and H-F Graf. The initial dispersal and radiative forcing of a northern hemisphere mid-latitude super volcano: a model study. *Atmospheric Chemistry and Physics*, 6(1): 35–49, 2006.

[431] B-M Sinnhuber, N Sheode, M Sinnhuber, MP Chipperfield, and W Feng. The contribution of anthropogenic bromine emissions to past stratospheric ozone trends: a modelling study. *Atmospheric Chemistry and Physics*, 9(8):2863–2871, 2009.

[432] Martina M Halmer. Have volcanoes already passed their zenith influencing the ozone layer? *Terra Nova*, 17(6):500–502, 2005.

[433] H Bureau, A-L Auzende, M Marocchi, C Raepsaet, P Munsch, D Testemale, M Mézouar, S Kubsky, M Carrière, A Ricolleau, et al. Modern and past volcanic degassing of iodine. *Geochimica et Cosmochimica Acta*, 173:114–125, 2016.